



UNIVERSITÀ
DEGLI STUDI
DI PADOVA

Sede Amministrativa: Università degli Studi di Padova

Dipartimento di Ingegneria Civile, Edile ed Ambientale

CORSO DI DOTTORATO DI RICERCA IN SCIENZE DELL'INGEGNERIA CIVILE ED AMBIENTALE

CICLO XXIX

INNOVATIVE CONNECTION SYSTEMS FOR TIMBER STRUCTURES

Coordinatore: Ch.mo Prof. Stefano Lanzoni
Supervisore: Ch.mo Prof. Roberto Scotta
Controrelatori: Ch.mo Prof. Jan Hofmann
Ch.ma Prof.ssa. Carmen Sandhaas

Dottorando: Luca Marchi

Gennaio 2018

Summary

Connections and fasteners play an essential role in the determination of strength and stability, ductility and robustness, i.e., the overall behaviour of timber structures. In particular, connections subjected to static loads are to be investigated in terms of strength and stiffness, whereas the ones designed to withstand cyclic (e.g., seismic) loads need also the definition of their complete hysteretic response. This Ph.D. dissertation focuses on the behaviour of modern connections being developed and employed in timber engineering.

An initial overview on mechanical connections employed in timber structures and their evolution is reported in the introductory section of this thesis. Advantages as well as critical issues of traditional connections are the motivations for the evolution and the improvements brought by innovative connections. Two different applications of innovative timber connections are analysed and hereby discussed, each one facing different issues. The first one claims to give an insight into modern screws employed in Timber-concrete composite (TCC) structures, where the major objective is to achieve maximum strength and above all stiffness. The second is directly focused on the cyclic performance of modern connections employed in Cross Laminated Timber (CLT) structures where dissipative capacity and structural damping are of utmost importance. Consequently, the present manuscript is subdivided into two main parts.

The first part deals with TCC joints realized with modern screws. The key-point to guarantee adequate mechanical performance to these composite structures is the use of connectors that demonstrate sufficient shear strength and stiffness at the interface between timber beam and concrete slab independently of the presence of an intermediate layer. Modern cylindrical connectors, such as self-tapping screws, are rising interest because they combine remarkable performance, when their withdrawal capacity is exploited, and quickness of execution especially in case of onsite installation. In this paper, a theoretical approach to calculate shear strength and stiffness of TCC joints made with inclined screws is discussed and compared to current design procedures. Furthermore, a report on short-term push-out tests of TCC joints realized with inclined self-tapping screws carried out varying fastener arrangement, diameter and concrete type is given. Consequently, a comparison between the results obtained with the theoretical method and experimental tests is reported and critically discussed in terms of both strength and stiffness.

The last section of the first part present the design of an innovative connector that combines the use of self-tapping screws and a glass-fibre reinforced polymer (GFRP) element as components to realize structural TCC joints. FRP is being used in civil engineering since decades, but most of these applications utilize pre-impregnated thermosetting composites, the most common of which is carbon fibre-reinforced polymer (CFRP). On the contrary, injection moulded thermoplastic materials are relatively new and lack of history of their use in civil infrastructures. The aim is to develop a connection that solves typical installation issues of inclined screws and avoids stress concentration issues that may occur in the concrete layer. Numerical simulations, carried out to design this

particular joint and exploiting a hybrid approach, are described in detail. Then, results from the experimental tests conducted to investigate the behaviour of the device subjected to shear loading conditions are compared with the analytical predictions valid for inclined screws previously described.

The second part of this work focuses on the developing of an innovative earthquake-resistant connections employed for CLT structures. The seismic performance of CLT buildings is mainly related to the capability of joints to perform plastic work, since timber elements have limited capability to deform inelastically. Nowadays, the use of hold-down and angle bracket connections, which were originally developed for platform-frame constructions, has been extended also to CLT buildings. Nevertheless, the dissipative capacity of light-frame buildings is mainly diffused in nailing between frames and panels while, in CLT walls, the dissipative contribution is exclusively assured by ductile joints connecting the panels. The need of more reliable connections that provides well predictable and stable hysteretic behaviour, reduced pinching phenomenon (caused by the wood embedment) and strength degradation, justifies the continuous development of “innovative” connections. In this work, a newly developed connection element that overcomes the aforementioned issues and works for both tensile or shear loads is designed and assessed, and various significant aspects are discussed.

Initially, the design procedure of the connection element and preliminary experimental tests that validates the numerical predictions are illustrated. Then, improved versions of the device are illustrated and their experimental results reported with particular attention in describing their hysteretic response and coupled shear-tension strength domain. In this work, an important role is also given to the application of the capacity design criteria applied at the joint level in order to guarantee the best exploitation of the connection’s dissipative capacity. Therefore, theoretical concepts, which describe the overstrength of traditional and innovative connections, confirmed by experimental tests of the brackets anchored to a CLT panel, are also given. In the last chapter is presented a numerical model that, following a macro-element approach, reproduces the actual cyclic response of the investigated device when subjected to combined shear-tension loads. Finally, the results of Non-Linear Dynamic Analyses of a case study CLT building realized which such model are reported and the seismic capacity of the case study building is evaluated.

With these two examples, this thesis aims to give an original contribution in the evaluation of performance of innovative connection systems for timber structures, combining the use of theoretical, numerical and experimental models, and highlighting the emerging differences with respect to the use of traditional fasteners and connections.

Keywords: timber engineering, timber-concrete connections, self-tapping screws, analytical model, Glass-fibre-reinforced polymers, injection moulding, Cross Laminated Timber, dissipative connections, hysteretic model, viscous damping, shear-tensile strength domain, seismic design, macro-element model, behaviour factor.

Sommario

Le connessioni e gli elementi di fissaggio svolgono un ruolo essenziale nella determinazione della resistenza, stabilità e solidità, ovvero nella risposta globale delle strutture del legno. In particolare, le connessioni soggette a carichi statici devono essere studiate in termini di resistenza e rigidità, mentre quelle progettate per resistere a carichi ciclici (ad es. sismici), necessitano anche della completa definizione della loro risposta isteretica. Questa tesi si concentra sul comportamento dei collegamenti moderni sviluppati e impiegati nell'ingegneria del legno.

Una prima panoramica sulle connessioni meccaniche impiegate nelle strutture del legno e la loro evoluzione è riportata nella sezione introduttiva di questa tesi. Vantaggi e criticità delle connessioni tradizionali sono le motivazioni dell'evoluzione e dei miglioramenti prodotti dalle connessioni innovative. Vengono analizzate e discusse due diverse applicazioni di connessioni per strutture in legno, ognuna delle quali espone aspetti e problematiche diverse. Il primo afferma di dare una panoramica delle moderne viti utilizzate nelle strutture composte legno-calcestruzzo (TCC), dove l'obiettivo principale è ottenere massima resistenza e ancor più rigidità. Il secondo, è incentrato direttamente nell'analisi delle prestazioni cicliche delle connessioni moderne utilizzate nelle strutture in CrossLam (CLT) in cui la capacità dissipativa e lo smorzamento strutturale sono della massima importanza. Di conseguenza, il presente manoscritto è suddiviso in due parti principali.

La prima parte riguarda le giunzioni legno-calcestruzzo realizzate con viti moderne. Il punto chiave per garantire prestazioni meccaniche adeguate a queste strutture composite è l'utilizzo di connettori caratterizzati da un'adeguata resistenza e rigidità tra trave di legno e soletta di calcestruzzo, indipendentemente dalla presenza di uno strato intermedio. I connettori cilindrici moderni, come le viti autofilettanti, possiedono un crescente interesse perché combinano elevate prestazioni, se è sfruttata la loro elevata capacità ad estrazione, e rapidità di esecuzione. In questo lavoro viene proposto un approccio teorico semplificato per calcolare la resistenza al taglio e la rigidità dei giunti TCC realizzati con viti inclinate e poi confrontato con le attuali procedure di progettazione. Inoltre, viene fornito un rapporto sulle prove di push-out a breve termine di giunti TCC realizzati con viti autofilettanti inclinate, effettuate con vari tipi di fissaggio, diametro e tipo di calcestruzzo. Di conseguenza, viene anche riportato un confronto tra i risultati ottenuti con il metodo teorico e le prove sperimentali e viene discusso criticamente in termini di forza e rigidità.

L'ultima sezione della prima parte comprende la progettazione di un connettore innovativo che combina l'utilizzo di viti autofilettanti e polimero termoplastico rinforzato con fibra di vetro (GFRP) per realizzare giunti TCC strutturali. Gli FRP vengono utilizzati nell'ingegneria civile da decenni, ma la maggior parte di queste applicazioni utilizza compositi termoindurenti pre-impregnati, il più comune dei quali è il polimero rinforzato in fibra di carbonio (CFRP). Al contrario, i materiali termoplastici sono relativamente nuovi e mancano di storia nell'utilizzo nell'infrastruttura civile. Le simulazioni numeriche, effettuate per progettare questo giunto, sono descritte in dettaglio. Quindi, i

risultati delle prove sperimentali condotte per esaminare il comportamento del dispositivo sottoposto a condizioni di carico di taglio sono confrontati con le previsioni analitiche descritte.

La seconda parte di questo lavoro si concentra sullo sviluppo di collegamenti innovativi impiegati per le strutture in CLT. La prestazione sismica degli edifici CLT è principalmente legata alla capacità dei collegamenti di plasticizzarsi, poiché gli elementi del legno hanno una capacità limitata di deformazione inelastica. Oggi, l'utilizzo di connessioni quali hold-down e angolari, originariamente sviluppati per costruzioni tipo platform-frame, è stato esteso anche agli edifici CLT. Tuttavia, la capacità di dissipazione degli edifici a telaio è diffusa soprattutto nella connessione telaio-pannello, mentre nelle strutture in CLT il contributo dissipativo è assicurato esclusivamente da connessioni duttili che collegano i pannelli. La necessità di una connessione più affidabile che fornisca un comportamento isteretico prevedibile ed affidabile, un fenomeno ridotto di "pinching" (causato dal rifollamento del legno) e una degrado di resistenza giustifica lo sviluppo continuo di connessioni "innovative". In questo lavoro è stato progettato e valutato un elemento di connessione che sormonti i problemi sopradescritti e che lavora sia per i carichi di trazione che per taglio, e ne vengono discussi gli aspetti più significativi.

Inizialmente viene illustrata la procedura di progettazione dell'elemento di connessione e dei test sperimentali preliminari che convalidano le previsioni numeriche. Successivamente vengono descritte le fasi di progettazione e test di ulteriori versioni migliorate delle staffe dissipative e sono riportati i loro risultati sperimentali facendo particolare attenzione nel descrivere la loro risposta isteretica e il dominio di resistenza tensione-taglio. Un ruolo importante in questo lavoro è dato all'applicazione dei criteri di gerarchia delle resistenze (progettazione in capacità) a livello di connessione al fine di garantire il miglior sfruttamento della capacità dissipativa della connessione. Di conseguenza, vengono forniti concetti teorici che descrivono l'applicazione di tali concetti a connessioni tradizionali e innovative, e confermate da prove sperimentali delle staffe oggetto di studio ancorate a un pannello CLT. Infine, i risultati di simulazioni numeriche dettagliate e prove cicliche quasi-statiche sono state utilizzate per sviluppare un modello di macro-elemento implementato in un codice numerico che ha permesso di determinare le prestazioni sismiche di un edificio caso studio in CLT realizzato con tali connessioni.

Con questi due esempi la presente tesi mira a definire un originale procedura di valutazione delle performance delle connessioni innovative per legno, combinando l'uso di modelli teorici, numerici ed analisi sperimentali e mettendone in evidenza le differenze emergenti rispetto all'impiego di sistemi di connessioni tradizionali.

Parole chiave: ingegneria del legno, connessioni legno-calcestruzzo, viti autofilettanti, modelli analitici, polimeri fibrorinforzati, stampaggio per iniezione, connessioni per CrossLam, connessioni dissipative, modello isteretico, smorzamento viscoso equivalente, dominio di resistenza taglio-trazione, modello a macro-elementi, fattore di struttura.

Acknowledgments

I am personally grateful to my supervisor Prof. Roberto Scotta for being constantly present during my Ph.D. experience. His precious suggestions demonstrated to be always helpful for the continuation and completion of my work. He taught me how operate in the field of civil engineering with a confident and practical attitude though always supported by a solid scientific background.

I wish to thank the company fischer Italia Srl for funding this research project, in particular Eng. Massimo Fioraso for being promoter of this project. In this context I am very grateful to Eng. Enrico Crivellaro and, with him, to the whole engineering office of fischer Italia and the constant support of Elena, Mansur, Luca, Alberto, which helped me during these years.

On this occasion, I would like to thank my Ph.D. teammates at the university of Padova, Davide, Luca, Lorenzo, Laura, Giovanni, Sara, Valentina for sharing excellent discussion ideas and having gladden all the moments spent together.

I extend my appreciation to Dr. Joachim Schätzle of fischer Germany and to Prof. Jan Hofmann of the University of Stuttgart for the excellent cooperation developed within these years. A gratifying thank also to Dr. Carmen Sandhaas for her valuable suggestions, which further enhanced my final work.

My very deepest gratitude to my nearest: my parents, brother and grandparents who supported me during all my studies, and to my friends who were always there when I strongly needed their presence. Finally, I would like to express my thanks to my dearest Maddalena, for her incredible love, patience, her constant encouragement that I appreciated during difficult times, and for her smile that permanently accompanies my life.

Table of contents

Introduction	1
I.1 Development of connections in timber structures	1
I.1.1 Connections in static loading conditions: the case of TCC structures joints	2
I.1.1.1 Standards and experimental evidence	3
I.1.2 Connections in seismic loading conditions: the case of connections for earthquake-resistant CLT structures	4
I.1.1.1 Standards and experimental evidences	4
I.2 Objectives and scope of this dissertation.....	5
References - Introduction.....	7
Part I INNOVATIVE CONNECTIONS FOR TIMBER-CONCRETE COMPOSITE STRUCTURES	11
Chapter 1 Timber-concrete composite joints with modern self-tapping screws.....	13
1.1 Introduction and state of the art.....	14
1.1.1 Design of TCC structures	15
1.1.2 Connections for TCC structures	16
1.1.3 Parameters influencing TCC connection's mechanical performance	18
1.1.4 TCC connections with inclined screws	19
1.2 Analytical methods of calculation.....	20
1.2.1 Load bearing capacity	20
1.2.2 Stiffness	26
1.3 Experimental tests.....	27
1.3.1 Specimen geometry	27
1.3.2 Materials and test setup	28
1.3.3 Test results	29
1.4 Comparison between experimental and analytical results	33
1.4.1 Load bearing capacity	35
1.4.2 Stiffness	35
1.5 Conclusions	36
Acknowledgments.....	37
References – Chapter 1	37
Chapter 2 Development of an innovative TCC system using GFRP and modern screws.....	43
2.1 Introduction and aims of the present work	44
2.1.1 State of the art of TCC joints realized with screws.....	44

2.1.2	Issues of TCC connections with screws	45
2.1.3	Thermoplastic materials in civil engineering	47
2.1.4	Aim of this work	48
2.2	Design process assisted by FEM analyses.....	49
2.2.1	Details on the numerical modelling of the TCC joint	49
2.2.2	Modelling of materials	51
2.2.3	Calibration of the numerical model	55
2.2.4	Design of the GFRP element.....	56
2.3	Experimental tests.....	60
2.3.1	Specimen geometry	60
2.3.2	Material and test setup	62
2.3.3	Test results	63
2.3.4	Comparison with analytical calculations	68
2.3.5	Comparison with the screw only configuration.....	71
2.3.6	FE model results and considerations on the creep phenomena.....	71
2.4	Conclusions.....	73
	Acknowledgments.....	74
	References – Chapter 2.....	74
Part II INNOVATIVE EARTHQUAKE-RESISTANT DISSIPATIVE DEVICE FOR CLT		
STRUCTURES.....		79
Chapter 3 Development of an innovative high-dissipative device for CLT structures.....		81
3.1	Introduction	82
3.1.1	State of the art on innovative connections for CLT buildings	84
3.1.2	Capacity design of connections for CLT structures.....	87
3.1.3	Aim of this work.....	91
3.2	Design, testing and mechanical characterization of an innovative dissipative connection.....	92
3.2.1	Design Criteria	92
3.2.2	Version 1.....	94
3.2.3	Version 2.....	100
3.2.4	Version 3.....	110
3.2.5	Comparison between the investigated versions.....	119
3.3	Conclusions.....	122
	Acknowledgments.....	123
	References – Chapter 3.....	123

Chapter 4 Development of a Macro-element model to simulate the hysteretic behaviour of the dissipative device.....	129
4.1 Introduction	130
4.1.1 Numerical approaches to simulate CLT structures	130
4.1.2 Aim of this work.....	131
4.2 Definition of the strength domain.....	132
4.2.1 Abacus of strength	134
4.3 Macro-element model.....	138
4.3.1 Calibration of the MEM model	140
4.4 MEM application to Case-study CLT shear walls.....	141
4.4.1 Detailed model	142
4.4.2 Macro-element model.....	143
4.4.3 Main results.....	144
4.4.4 Prediction of the mechanical properties.....	146
4.5 MEM application to a Case-study CLT building and computation of q-factor	147
4.5.1 Assumed design hypotheses and building specifications	147
4.6 Conclusions	151
References – Chapter 4.....	151
Chapter 5 Conclusions and future works.....	155
Appendix A Macro-element model detail.....	159
A.1 Numerical code of the MEM	159
A.2 Detailed results of case-study CLT shear walls	162
A.2.1 Wall A	162
A.2.2 Wall B	163
A.2.3 Wall C	164
A.2.4 Wall D	165
List of Figures	167
List of Tables	171
List of Publications	173

List of notations

<i>CLT</i>	<i>Cross-laminated timber</i>
<i>COV</i>	<i>Coefficient of variation</i>
<i>CP</i>	<i>Connection point</i>
<i>DLS</i>	<i>Damage Limitation State</i>
<i>EEEEP</i>	<i>Equivalent Elastic-Plastic Energy method</i>
$F_{ax,Rk,cone}$	<i>Characteristic concrete cone strength of fastener</i>
$F_{ax,Rk}$	<i>Characteristic withdrawal strength of fastener</i>
F_{ax}	<i>Axial strength of fastener</i>
F_d	<i>Design shear strength</i>
<i>FE</i>	<i>Finite Element</i>
F_{HD}	<i>Resistance of connection working in tension</i>
F_{SH}	<i>Resistance of connection working in shear</i>
F_{lat}	<i>Lateral load bearing capacity of fastener</i>
F_{max}	<i>Maximum load bearing capacity</i>
$F_{v,est}$	<i>Estimated shear load bearing capacity of the joint</i>
$F_{v,Rk,exp}$	<i>Characteristic experimental shear load bearing capacity of joint</i>
$F_{v,Rk,th}$	<i>Characteristic theoretical shear load bearing capacity of joint</i>
$F_{v,Rk}$	<i>Characteristic shear load bearing capacity of joint</i>
$F_{v,Rk}^c$	<i>Characteristic shear load bearing capacity of a shear-compression loaded screw</i>
$F_{v,Rk}^t$	<i>Characteristic shear load bearing capacity of a shear-tension loaded screw</i>
$F_{v,y}$	<i>Yielding shear load bearing capacity of the joint</i>
F_y	<i>Yielding load bearing capacity</i>
K_e	<i>Elastic stiffness of bi-linear response</i>
K_{pl}	<i>Post-elastic stiffness of bi-linear response</i>
K_{ser}	<i>Slip modulus of fastener</i>
$K_{ser, }$	<i>Slip modulus of the fastener axially loaded</i>
$K_{ser,\perp}$	<i>Slip modulus to the fastener laterally loaded</i>
$K_{ser,exp}$	<i>Experimental slip modulus of fastener</i>
$K_{ser,th}$	<i>Theoretical slip modulus of fastener</i>
$M_{y,Rk}$	<i>Characteristic yield moment of fastener</i>
<i>NLDA</i>	<i>Non-linear dynamic analysis</i>
<i>NLSA</i>	<i>Non-linear static analysis</i>
<i>PGA</i>	<i>Peak ground acceleration</i>
PGA_d	<i>Design peak ground acceleration</i>
PGA_u	<i>Near-collapse peak ground acceleration</i>
PGA_y	<i>Yielding peak ground acceleration</i>
$R_{ax,k}$	<i>Characteristic axial load-carrying capacity of fastener</i>
R_d	<i>Design resistance</i>
R_k	<i>Characteristic resistance</i>
<i>SD</i>	<i>Standard deviation</i>
<i>TCC</i>	<i>Timber-Concrete composite</i>
<i>ULS</i>	<i>Ultimate Limit State</i>
<i>X-Lam</i>	<i>Cross-laminated timber</i>

d	<i>Diameter of fastener</i>
d_{head}	<i>Head diameter of fastener</i>
d_{nom}	<i>Nominal fastener diameter</i>
d_u	<i>Ultimate displacement</i>
d_y	<i>Yielding displacement</i>
$f_{ax,k}$	<i>Characteristic withdrawal strength of fastener</i>
f_{ck}	<i>Characteristic compressive cylinder strength of concrete</i>
$f_{h,k}$	<i>Characteristic wood embedment strength of fastener</i>
h_{eff}	<i>Concrete cover of the screw's head</i>
k_1	<i>Concrete cone failure coefficient</i>
k_{mod}	<i>Modification factor for influences of duration of loading and moisture</i>
l_{eff}	<i>Threaded length of fastener</i>
q	<i>Behaviour factor</i>
q_0	<i>Intrinsic behaviour factor</i>
t	<i>Penetration of fastener perpendicular to the shear plane</i>
t_1	<i>Depth of penetration of fastener into timber member</i>
α	<i>Screw inclination with respect to the orthogonal line to the shear plane</i>
β_{Sd}	<i>Strength degradation due to cyclic loading factor</i>
γ_m	<i>Partial coefficient of material</i>
γ_{Rd}	<i>Overstrength factor in the capacity design</i>
γ_{an}	<i>Analytical overstrength</i>
γ_{sc}	<i>Scattering of peak strength</i>
δ_y	<i>Slip of connection at yielding of the connection</i>
λ	<i>Form factor</i>
μ	<i>Friction coefficient</i>
μ_d	<i>Ductility ratio</i>
$v_{0.1}$	<i>Slip of connection at 10% of $F_{v,est}$</i>
$v_{0.4}$	<i>Slip of connection at 40% of $F_{v,est}$</i>
ρ_k	<i>Characteristic wood density</i>
ρ_m	<i>Mean wood density</i>
$\Delta F_{v,Rk}$	<i>Shear load-carrying capacity relative difference of the connection</i>
ΔK_{Rk}	<i>Stiffness relative difference of the connection</i>
Ω	<i>Design overstrength</i>

Superscripts

-	<i>5th percentile of resistance</i>
+	<i>95th percentile of resistance</i>
mean	<i>Mean value</i>

Subscripts

s	<i>Screw</i>
y	<i>Yielding value</i>
u	<i>Ultimate value</i>
peak	<i>Peak value</i>
D	<i>Ductile element</i>
B	<i>Brittle element</i>

Introduction

I.1 Development of connections in timber structures

The well-known statement “A *structure is a constructed assembly of joints separated by members*” [I.1] highlights the attention that is to be given to connections in timber engineering. Assessments of timber buildings damaged after extreme wind or earthquake events often point to inadequate connections as the primary cause of damage [I.2]. Therefore, the joints are particularly important, since those used in timber construction tend to be weaker than the members being joined [I.3] and as a result, condition the behaviour of the entire structure. Consequently, they need to be treated with particular care by the designer of timber structures.

The evolution of the technology of timber joints and of the base material, i.e. structural timber, are strictly correlated one to another. Nowadays, the rapid increasing interests of timber at both research level and construction level made this development gain more and more momentum. In this context, it is possible to distinguish three different typologies of timber connections: carpentry joints, glued joints and mechanical joints.

Carpentry joints express the most fascinating technique to be used in joining members. In this case, loads are transferred by means of perpendicular compression stresses and friction without needing additional mechanical components. In the past years, the application of this method produced exceptional examples of state-of-the-art timber engineering and allowed raising impressive monumental structures even in high seismic countries like Japan [I.4]. On the contrary, this technique still requires time-demanding operations and extremely high woodworking skills to be owned by the carpenters. Even if the introduction of CNC technology helped to recover part of this knowledge, carpentry joints are often being preferred by the two other typologies.

Glued joints are known to be the most efficient in terms of strength and stiffness than the other two typologies. However, the research in gluing technology have been producing more results in the realization of products realized by processed or sawn wood (e.g., glued-laminated timber, laminated-veneer lumber, etc.), than in the field of connections. As proof of that, no recognized international standards and rules are available yet concerning the design of glued joints. Nevertheless, progress in gluing technology led to the development of cross-laminated timber (CLT), and through it, carried out important “collateral” consequences in the field of mechanical joints that will be deeply discussed in this thesis.

The last typology, *mechanical joints* are by far the most used connecting method in timber engineering. They are represented by *dowel-type fasteners*, i.e. nails, staples, bolts, screws, dowels and threaded rods and *surface-type fasteners*, like split-rings and toothed plate connectors. In both categories, forces are transmitted by bending and tensile stresses in the fasteners as well as embedment and shear stresses in the wood along the shank [1.3]. Progress in this field have been the most conspicuous. The most evident case are self-tapping screws, which are now produced at lengths of up to 1.5 m and have substantially changed jointing and reinforcement technology [1.5].

As anticipated, this thesis will directly focus on the development of mechanical fasteners. However, the point-of-view from which connections are studied highly depends on the intended application. For example, a very stiff joint designed to withstand static loads may unpredictably fail or be incapable to work well if subjected to repeated cyclic loads, and vice versa. Hence, connections subjected to static loading conditions will be addressed differently from the ones design for seismic loading conditions. The next paragraphs will briefly introduce the argument to help the reader understand the choice of splitting the manuscript into two distinct parts.

1.1.1 Connections in static loading conditions: the case of TCC structures joints

Progress at the joint level allowed attaining further enhancement in the field of hybrid constructions. In particular, the studies on mechanically jointed members such as timber-concrete composite (TCC) structures have been again taking high consideration as balanced solution between costs and structural efficiency. TCC joints are an easy example of the direct consequence that a well-designed joint produces on a structure. It is worth noting, that this evidence can easily be extended to every timber structure. As an example, moment-resisting joints require the prediction of the rotational stiffness achieved by the shear joints in order to assess the overall deflection performed by the structure. Consequently, stiffness can be as important as the load bearing capacity and cannot be analysed separately.

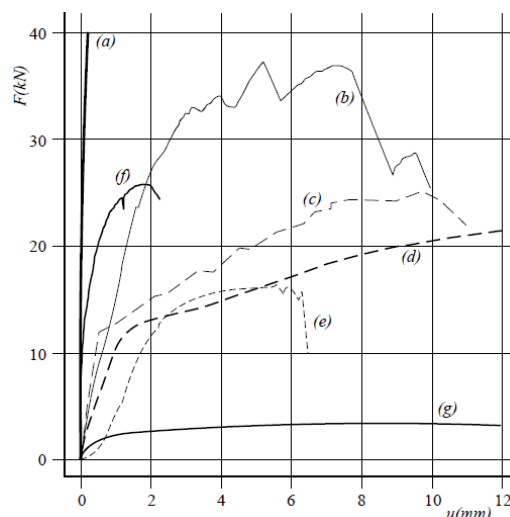


Fig. 1.1 – Comparison of the inelastic behaviour of several type of joints [1.3]. The stiffest joint is glued joint (a) followed by punched metal plate fastener (f), split ring (b), double-sided toothed-plate (c), 14-mm dowel (d), 14-mm bolt (e), 4.4 mm nail (g).

The variety of mechanical connections available for structural purposes, have been analysed also when applied to the case of TCC structures (see state of the art in following section 1.1.2). Fig 1.1 compares the inelastic behaviour of various types of mechanical connections. It clearly emerges that

these types of connections demonstrate a semi-rigid behaviour with respect to glued joints but, depending on the stiffness level to be reached, each of them can be considered valid. However, due to the highly dissimilar behaviour obtained within each type, experimental characterization and possible development of analytical formulations are two fundamental steps to make easier and reliable the design of these joints. In fact, the lack of information regarding the use of modern self-tapping screws as TCC joints is one of the motivations that led to this thesis work.

1.1.1.1 Standards and experimental evidence

Before analysing the behaviour of a connection applied to a timber element, the connection itself has to be experimentally characterized with the aim to evaluate its main mechanical properties. For example, in Europe dowel-type fasteners like self-tapping screws are to be tested according to EN 14592 [I.6] in order to define geometry, withdrawal strength, tensile strength, pull-through parameter, etc. If a CE marking procedure is needed than, the same screw should follow the European Assessment Document procedure [I.7]. Consequently, the static behaviour of a joint involving one or multiple fasteners should be addressed according to specific standards like the European EN 26891 protocol [I.6] in order to obtain the monotonic load vs. slip curve, which is then analysed to obtain the necessary parameters to design it accordingly. Not to forget that also the timber properties must be assured by applying appropriate standards like [I.9]. EN 26891 protocol [I.6] allows analysing the joint' behaviour at different load levels. Once that the estimated total force F_{est} is known (e.g., by means of a monotonic test) the range between 10 and 40% of this load determine the serviceability limit state (SLS) conditions, which is expressed by the slip modulus K_{ser} . Valuable information of near collapse stiffness are then derived by calculating the secant stiffness at $0.6F_{max}$ and $0.8F_{max}$, where F_{max} is the maximum force (or peak force) demonstrated in tests. Finally, statistical analysis according to [I.10] are to be used to derive characteristic values of the yielding force, the peak and ultimate load bearing capacity according to a normal or log-normal distribution.

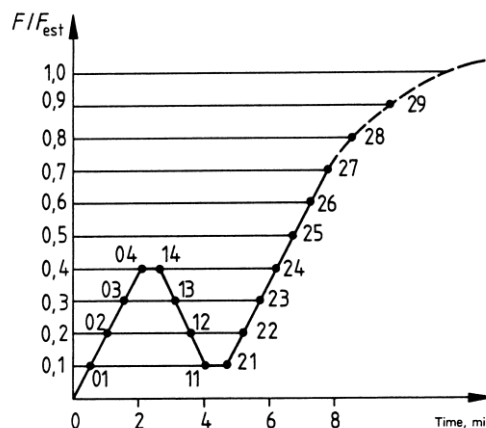


Fig. 1.2 – Loading procedure according to EN 26891 [I.6]

Analytical methods to derive the load bearing capacity of timber joints subjected to static loads are already available in literature. They are based on well-founded hypotheses, which have been validated during years throughout intensive experimental characterization and are now taken as valid by the whole engineering practice. This work will take them as reference and will try to enhance or redefine part of these analytical methods, which were derived from traditional mechanical joints, by adapting them to the capabilities obtainable with modern connections.

1.1.2 Connections in seismic loading conditions: the case of connections for earthquake-resistant CLT structures

The introduction in the market of cross-laminated timber (CLT) helped timber to widespread all over the world and allowed to re-invent the structure's architecture in the countries that embrace this technology. The characteristics of lightness and strength possessed by CLT, took the attraction of countries characterized by high seismicity. Immediately, connections employed in traditional, platform-frame or balloon-frame buildings were adapted to be used with this technique.. However, it has been demonstrated that particular care had to be given to the connection as it turned out that, unlike to traditional shear walls, quite all the seismic energy developed by the structure had to be withstood by the mechanical joints ([1.11];[1.12]). Research work concentrated more in solving installation issues of CLT structures [1.13]. However, the result is that a new generation of high performance mechanical connections is strongly needed.

In traditional joints, the energy dissipation and ductility is assured by the hysteretic behaviour, during shear deformation, of dowel-type fasteners that connect the steel element to the timber panel. Two mechanisms concur simultaneously: formation of one or two plastic hinges in the connector and wood embedment near fasteners ([1.14]-[1.16]). Fig. 1.3 clearly explains these phenomena. Depending on the slenderness of the fastener, intended as ratio between fastener diameter and penetration in the timber member, the cyclic behaviour can change significantly. Fig. 1.3a shows the hysteretic response of a correctly designed joint where slender fasteners allow to obtain both by plastic deformation of steel and wood embedment. On the contrary, Fig 1.3b shows that large-diameter connectors are too stiff to deform plastically, total deformation is given only by wood embedment and the amplified pinching phenomenon reduces energy dissipation capacity for repeated loading cycles. The best solution in terms of energy dissipation, which is being carried out by *innovative* connections can be obtained ensuring the localization of deformations in steel plates, limiting deformation on the wooden side (see Fig. 1.3c).

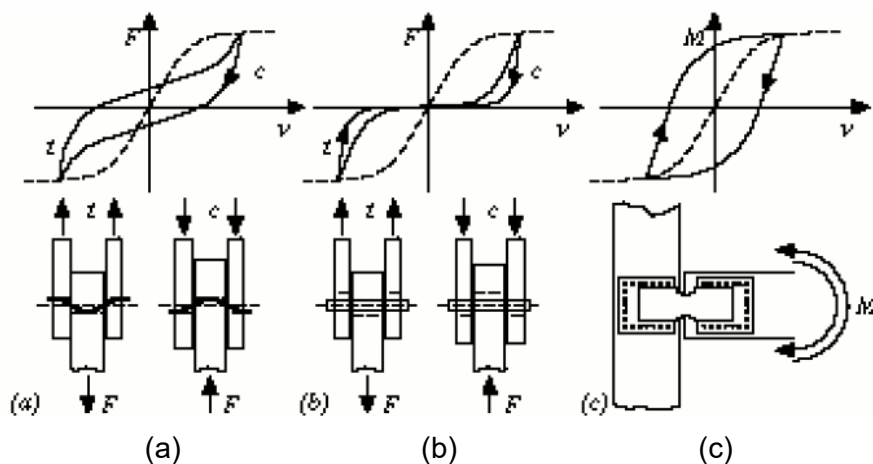


Fig. 1.3 – Typical hysteresis behaviour of a connection with metal fasteners [1.17].

1.1.1.1 Standards and experimental evidences

The aforementioned connection properties and cyclic response affect the whole seismic behaviour of a seismic-resistant timber structure. In Europe, Eurocode 8 [1.18] requires the evaluation of the mechanical performance of timber connections according to a cyclic loading procedure (recalling EN 12512 [1.19]). This protocol requires a preliminary estimation of the yielding displacement V_y of the

connection. Then, adopting a displacement cyclic procedure with maximum amplitude defined by progressive multiples of V_y (Fig I.4) it allows to determine the maximum ductility, as ratio between ultimate and yielding displacement V_u / V_y , and the equivalent viscous damping ratio v_{eq} . The latter gives important information of the energy dissipating capacity demonstrated by the connection.

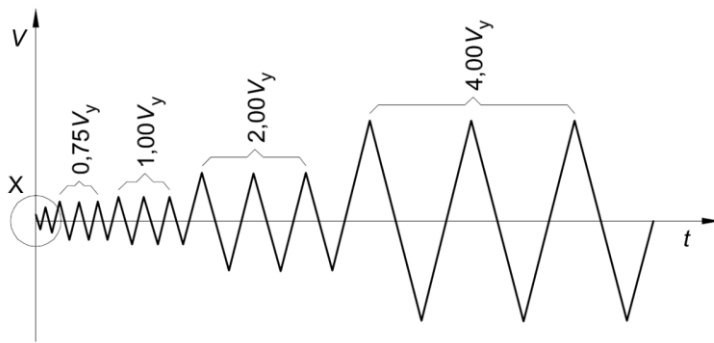


Fig. I.4 – Loading procedure according to EN 12512 [I.19]

This procedure have been assessed when *traditional* connections made use of the cyclic dissipative behaviour of dowel-type fasteners (see Fig. I.3a) and research of *innovative* systems had not yet been addressed. However, the question whether this protocol should be applied or substituted with other protocols have always been a delicate question ([I.20];[I.21]). Actually, several different procedures are available and may be applicable [I.22]. Innovative connections may require further different loading protocol. In fact, rather than pinching phenomenon, these devices may be more susceptible to oligo-cyclic fatigue that reduce the ultimate conditions. Nevertheless, a protocol that simulates the actual randomness of a seismic shock is still under investigation.

In this context, analytical and experimental methods used describe the monotonic behaviour are substituted with numerical simulations that help the designer to predict the effect of the joint when applied to a structure. In fact, the second aim of this thesis is to demonstrate the easiness in predicting via numerical simulations, the hysteretic behaviour of these connections with respect to traditional connections.

I.2 Objectives and scope of this dissertation

The main scope of this thesis work is to give a contribution to international scientific research and current design practice about the design of innovative connections for timber structures, with particular focus to timber-concrete composite (TCC) system and high energy-dissipating earthquake-resistant devices. The initial objective is to clarify the actual behaviour of connections employed in timber engineering, on two different case studies: modern connections designed for static loading conditions, and connections designed to withstand cyclic forces, due to high seismic shock. Henceforth, the present work addresses multiple aspects of research:

1. The first aspect focus on the use of modern self-tapping screws as connections in TCC structures. In detail, existing theoretical approaches that describes the behaviour of these fasteners are illustrated and, at the occasion, adapted accordingly. The modifications to the analytical models are supported by means of experimental tests.
2. In the same context, an innovative connection element, which combines inclined self-tapping screws and a glass-fibre reinforced polymer produced by injection moulding, is designed and tested. To this aim, numerical simulations and experimental tests are reported in order to

define and predict its mechanical behaviour and to introduce GFRP injection moulding products into the field of timber engineering.

3. The second part claims to provide useful instruments to design innovative high-dissipative connection for timber structures. In particular, the design process of a new steel device is accurately described, together with its experimental investigation. This connection is also exploited to give a deep analysis on the capacity design criteria applied to joints in timber structures.
4. Lastly, the impact of its high dissipative capacity and its coupled shear-tension response are analysed by means of non-linear dynamic simulations of a case-study CLT structure. A macro-element approach has proven to be successful to analyse the potential improvements on the seismic response of the CLT buildings that uses such innovative connections and to compare the resulting behaviour factor with respect to more traditional solutions.

The main tools used to obtain the results presented in this dissertation are:

1. Experimental data from monotonic and cyclic-loading tests of connecting devices and full-scale complete connection assemblies;
2. Analytical methods based on code provisions or on actual literature;
3. Numerical dynamic simulations of linear and non-linear models calibrated on results from tests or on code provisions.

This thesis presents original data, results and conclusions based both on novel research activities, which started in the period between 2014 and 2017, and on the continuation of existing research activities presented in ([1.23];[1.24]).

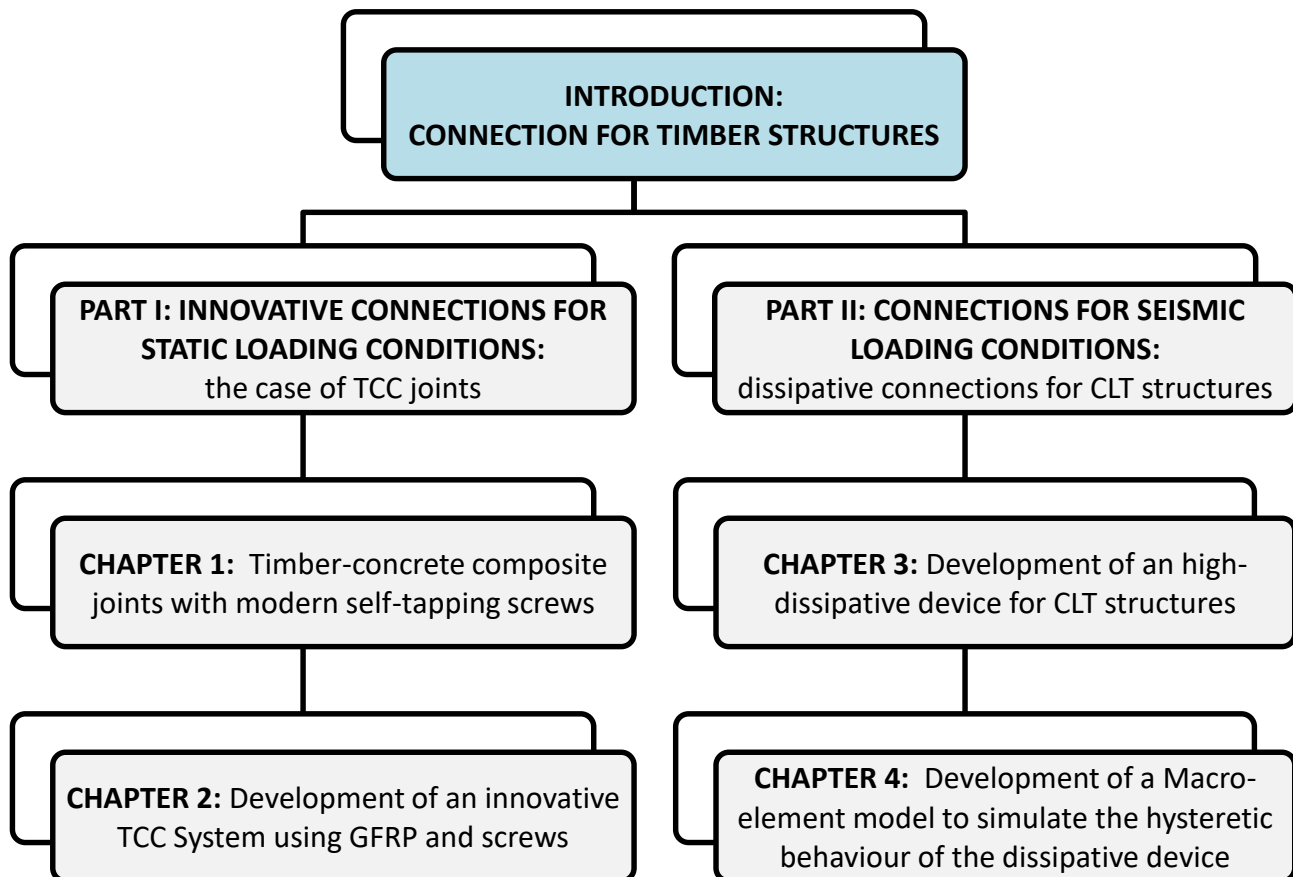


Fig. 1.5 – Organization of the present work

References - Introduction

- [I.1] McLain, T. E. (1984). "Mechanical fastening of structural wood members—Design and research status". In *Structural wood research: State-of-the-art and research needs* (pp. 33-68). ASCE.
- [I.2] Smith, I., and Foliente, G. (2002). "Load and resistance factor design of timber joints: International practice and future direction". *Journal of structural engineering*. ASCE. DOI: 10.1061/(ASCE)0733-9445(2002)128:1(48).
- [I.3] Racher, P. (1995). Mechanical timber joints-general. Timber Engineering-STEP lecture C, 1, 1-10.
- [I.4] Sakamoto I., Fujita K. (2000). "Structural analyses on traditional timber buildings in Japan". Proceeding of Conservation of the ancient timber load bearing structures meeting, March 2000, Florence, Italy.
- [I.5] Aicher, S., Reinhardt, H. W., and Garrecht, H. (2013). *Materials and Joints in Timber Structures: Recent Developments of Technology (Vol.9)* (preface). Springer. Dordrecht, Netherlands.
- [I.6] EN 14592 (2012). "Timber structures - Dowel-type fasteners – Requirements". CEN. Brussels, Belgium.
- [I.7] EAD 130118-00-0603 (2016). "Screws for use in timber constructions". EOTA, Brussels, Belgium.
- [I.8] EN 26891 (1991). "Joints made with mechanical fasteners. General principle for the determination of strength and deformation characteristics". CEN. Brussels, Belgium.
- [I.9] EN ISO 8970 (2010). "Timber structures - Testing of joints made with mechanical fasteners - Requirements for wood density". CEN. Brussels, Belgium.
- [I.10] EN 14358 (2016). "Timber structures - Calculation and verification of characteristic values". CEN. Brussels, Belgium.
- [I.11] Piazza, M., Polastri, A., and Tomasi, R. (2011). "Ductility of Joints in Timber Structures". Proceedings of the ICE – Structures and Buildings, **164(2)**:79–90.
- [I.12] Pozza, L., Scotta, R., Trutalli, D., Ceccotti, A., and Polastri, A. (2013). "Analytical formulation based on extensive numerical simulations of behavior factor q for CLT buildings". In Proceedings of the Meeting 46 of the Working Commission W18-Timber Structures, CIB, Vancouver, BC, Canada, paper CIB-W18/46-15-5.
- [I.13] Scotta, R., Marchi, L., Trutalli, D., and Pozza, L. (2017). "Engineered aluminium beams for anchoring timber buildings to foundation". *Structural Engineering International*, **27(2)**:158-164. IABSE. DOI: 10.2749/101686617X14881932435736.
- [I.14] Ceccotti, A., Follesa, M., and Lauriola, M.P. (2007). "Le strutture di legno in zona sismica. Criteri e regole per la progettazione ed il restauro". C.L.U.T. Editrice, Torino, Italy.
- [I.15] Johansen, K.W. (1949). "Theory of timber connections". *International Association of bridge and structural Engineering*, Bern, p. 249-262.
- [I.16] EN 1995-1-1 Eurocode 5 (2004). "Design of timber structures, Part 1-1, General: Common rules and rules for buildings". CEN. Brussels, Belgium.
- [I.17] Ceccotti, A. (2003). "Il manuale del legno strutturale Vol. II". Mancosu Editore, Roma.
- [I.18] EN 1998-1-1 Eurocode 8 (2004). "Design of structures for earthquake resistance, part 1: general rules, seismic actions and rules for buildings". CEN. Brussels, Belgium.
- [I.19] EN 12512 (2001). "Timber structures - test methods - cyclic testing of joints made with mechanical fasteners". CEN. Brussels, Belgium.

- [1.20] Foliente, G. C., Karacabeyli, E., and Yasumura, M. (1998). "International test standards for joints in timber structures under earthquake and wind loads". In Proceedings of Structural Engineers World Congress (SEWC), July 19-23, San Francisco, California, USA.
- [1.21] Karacabeyli, E., Yasumura, M., Foliente, G.C., and Ceccotti, A., (2005). "Background Information on ISO Standard 16670 for Cyclic Testing of Connections". In Proceedings of the Meeting 38 of the Working Commission W18-Timber Structures, CIB, Karlsruhe, Germany, paper CIB-W18/38-15-1
- [1.22] Kirkham, W. J., Gupta, R., & Miller, T. H. (2013). "State of the art: Seismic behavior of wood-frame residential structures". *Journal of Structural Engineering*, **140**(4), 04013097.
- [1.23] Pozza, L. (2013). "Ductility and behaviour factor of wood structural systems". Ph.D. Thesis, University of Padova, Italy.
- [1.24] Trutalli, D. (2016). "Insight into seismic behaviour of timber shear-wall systems". Ph.D. Thesis, University of Padova, Italy.

PART I

INNOVATIVE CONNECTIONS FOR TIMBER-CONCRETE COMPOSITE STRUCTURES

Chapter 1 Timber-concrete composite joints with modern self-tapping screws

Abstract

Timber-concrete composite structures have become a widespread technique to realize new composite floors or improve existing ones. The key-point to guarantee adequate mechanical performance to these composite structures is the use of connectors characterized by adequate resistance and stiffness between timber beam and concrete slab. Modern cylindrical connectors, such as self-tapping screws, are rising interest because they combine high performance mechanical properties and quickness of execution. In this paper, a simplified theoretical approach to calculate shear load carrying capacity and stiffness of timber-concrete composite (TCC) joints made with inclined screws is suggested and compared to available design procedures. Furthermore, a report on short-term push-out tests of TCC joints realized with inclined self-tapping screws carried out varying fastener arrangement, diameter and concrete type is given. A comparison between the results obtained with the theoretical method and experimental tests is reported and critically discussed in terms of both load carrying capacity and stiffness.

Research results presented in this section are partially available at Springer via <http://dx.doi.org/10.1617/s11527-017-1047-1>. Journal Materials and Structures is acknowledged as the original source of publication.

1.1 Introduction and state of the art

Timber-concrete-composite (TCC) systems have gradually been introduced in structural engineering since the last century, and yet have been wide spreading thanks to its simple conceptual technology: combining two materials with different mechanical properties and exploiting their technical advantages to create highly efficient composite structures.

TCC technology was appeared due to the shortage of steel between the two world wars of last century [1.1] and was initially developed to refurbish historical floors of buildings in Europe [1.2]. In this case, existing timber floors realized with massive timber beams and a single orthogonal layer of boards nailed to the beams had to be renovated in order to improve their mechanical performance. In particular, the main purpose of these interventions was to enhance the load-bearing capacity and increase the bending stiffness (i.e. reduce deflections) to adapt this existing structures to the new demands and be suitable to the new, more severe and safer regulations. This technique gradually expanded thanks to other implicit advantages such as, reduced vibrational issues, acoustic damping, increased thermal mass and structural fire rating.

The success of this building system widened its use by extending it to the construction of medium-span (7-15m) horizontal structures [1.3]. Its interests led to the employment of this solution also for bridge decks [1.4] and complete bridges [1.5]. In this case, the saving of permanent mass is the main advantage. More recently, TCC prefabricated systems have been developed ([1.6];[1.7]) to realize economically competitive solutions overcoming some drawbacks such as the time needed for the concrete curing, the lower stiffness and higher creep during the concrete curing. Recent extensive literature works on TCC systems can be found in ([1.8];[1.9]).



Fig. 1.1 – TCC bridge deck in Finland on the right [1.5] and TCC prefabricated floor on the left [1.6].

Apart from the improvement of floors on static loading conditions, this solution has proven to be a viable technique to create a theoretically infinitely rigid floor [1.10]-[1.12], which is able to transmit uniformly the horizontal forces during a seismic event among the vertical earthquake-resisting structures. Consequently, TCC system have been increasing also in seismic prone countries (e.g., the Mediterranean area) characterized by a large number of buildings to be renewed and made suitable to the new and more severe seismic regulations. For this reason, the mechanical behaviour of TCC structures is continuously investigate, now with particular care to the onsite realization of such structures.



Fig. 1.2 – Renovation of existing timber floors with mechanical connectors before realization of the concrete slab.

1.1.1 Design of TCC structures

Design procedures of TCC structures is not covered by many timber standards and specific provision appears only in Eurocode 5 – Annex B [1.13] and Eurocode 5 – Part 2 [1.14]. In this case, the commonly adopted theory is the linear elastic theory, proposed by Newmark [1.15] and Mohler [1.16] and endorsed by Ceccotti [1.17] on which the main hypotheses are: a) all materials (concrete, timber, and connection) remain within the linear-elastic range until failure of the beam; b) equality between vertical deflection and curvature; c) plane cross-sections; d) load applied with a sinusoidal distribution; e) joints equally spaced.

Natterer et al. [1.18] tried to find solutions for different load distributions and effective widths of the concrete beam. There is also an elastoplastic design approach, proposed by Frangi and Fontana [1.19], in which a rigid perfectly plastic behaviour of the connection is assumed and the failure of the beam is reached after subsequent plasticization of the joints among the beam. This method, best suited for high-ductility connections, is not as widely known as the first one.

The first approach (known as γ -method) is based on the assumption that the TCC connection is actually a semi-rigid joint and the stresses between the two elements are dependent on the stiffness and the spacing of the connectors. The closed form formulations describes the effective stiffness of a wood-concrete structure EJ_{eff} as:

$$EJ_{eff} = E_c J_c + E_t J_t + \gamma_c E_c J_c a_c^2 + \gamma_t E_t J_t a_t^2 \quad (1.1)$$

where E , A and I are the modulus of elasticity, area and the second moment of area of the element (subscripts c and t are for concrete and timber respectively). Consequently, the structural efficiency of these structures highly depends on the resistance and stiffness demonstrated by the element connecting timber and concrete and described in the previous equation by the connection's reduction factor γ . Eq. (1.2) is a simple equation that describes the level of efficiency of a composite beam:

$$\eta = \frac{EJ_{eff} - EJ_0}{EJ_{\infty} - EJ_0} \quad (1.2)$$

where EJ_{∞} and EJ_0 are respectively the total bending stiffness of the composite structure in case of a fully rigid and fully deformable connection. EJ_{eff} is the effective bending stiffness reached by the structure with the defined connectors and from which results that η may vary between 0 and 1.

1.1.2 Connections for TCC structures

The development of TCC connections is progressing along with the continuous study of the composite system. The expansion of TCC structures on various applications, as previously described, lead to the realization of numerous types of connection systems. Each one having its intrinsic advantages and disadvantages.

The initial studies of TCC systems, in the first half of the last century, focused on the use of steel Z-profiles and I-profiles fastened to the timber beam and covered with the concrete layer [1.1]. Then, these “*rough*” mechanical connections were substituted by creating notches in the upper side of the timber beam in which the poured concrete acted as a “shear key”. This method can be considered as an adaptation from a technique that can be still found in ancient buildings to create timber-to-timber connections without mechanical fasteners. It exploits the same concept of the link usually realized between the rafter and the horizontal tie in a typical timber truss. Shape and definition of the notches are still being deeply investigated and, if necessary, reinforced with steel screws or dowel-type fasteners. Although this connection method have proven to be the one that reach the highest level of load carrying capacity and stiffness, it is also recognized as a not very economical when notches have to be cut manually [1.20].

In parallel, other connection elements have been studied to avoid or, at least, limit cutting and general woodworks in the timber beam. For example, by creating a single longitudinal cut on the upper side of the beam that is then used to place L-shaped metal plates glued in with epoxy resin. This solution provides also high levels of efficiency and reduced amount of works with respect to the notched system. It was investigated the use of punched metal plate fasteners to be fixed on both sides of the beam [1.21] avoiding any wood cutting operation. In this work, the procedure of cutting and gluing the L-shaped profiles was substituted by simply fastening the metal plate with nails to the top of the beam.

However, most of the effort was concentrated on solution that reduced the amount of handwork to be done on the timber beam by using distributed steel fasteners as the only mechanical connection system (see Fig. 1.3). One of the most examined technique is the recognized “Turrini-Piazza method” [1.22]: distributed connections are made with L-shaped steel rods glued into timber beams and used as dowel-type fasteners. The technique have been developed to refurbish historical timber floors and proved to achieve satisfactory results in terms of both load carrying capacity and stiffness. Failure of these connectors is due to combined wood embedment phenomenon and plastic hinges formation. In particular, the latter phenomenon is also the main aspect, which determine the stiffness demonstrated by the joint. However, some limitations arise when an interlayer is present, which forces the dowel to work as a standoff beam thus reducing considerably its overall stiffness [1.23]. From this concept, several fastening system that used dowel-type fasteners or cylindrical elements placed orthogonal to the sliding-plane have been studied in literature ([1.1];[1.21]-[1.31]). These fasteners, as previously reported, works in shear, consequently they must involve high core diameters to exhibit a rigid behaviour in the timber element while withstanding high loads. To apply correctly these fasteners, predrilling of the timber beam is always needed to avoid brittle failures due to possible crack propagation along the grain direction.

All these connections have been tested in research works (examples are referred above) and their performance compared by means of experimental tests and numerical simulations. Fig. 1.4a shows the load-slip curve obtained from a single test according to a standardized procedure [1.17], while Fig. 1.4b shows a comparison of the several connection typologies presented above. It is clear how notched solutions are stiffer and offer higher load carrying capacity with respect to dowel-type

connections which demonstrate lower stiffness and ultimate resistance but a much higher ductility level.

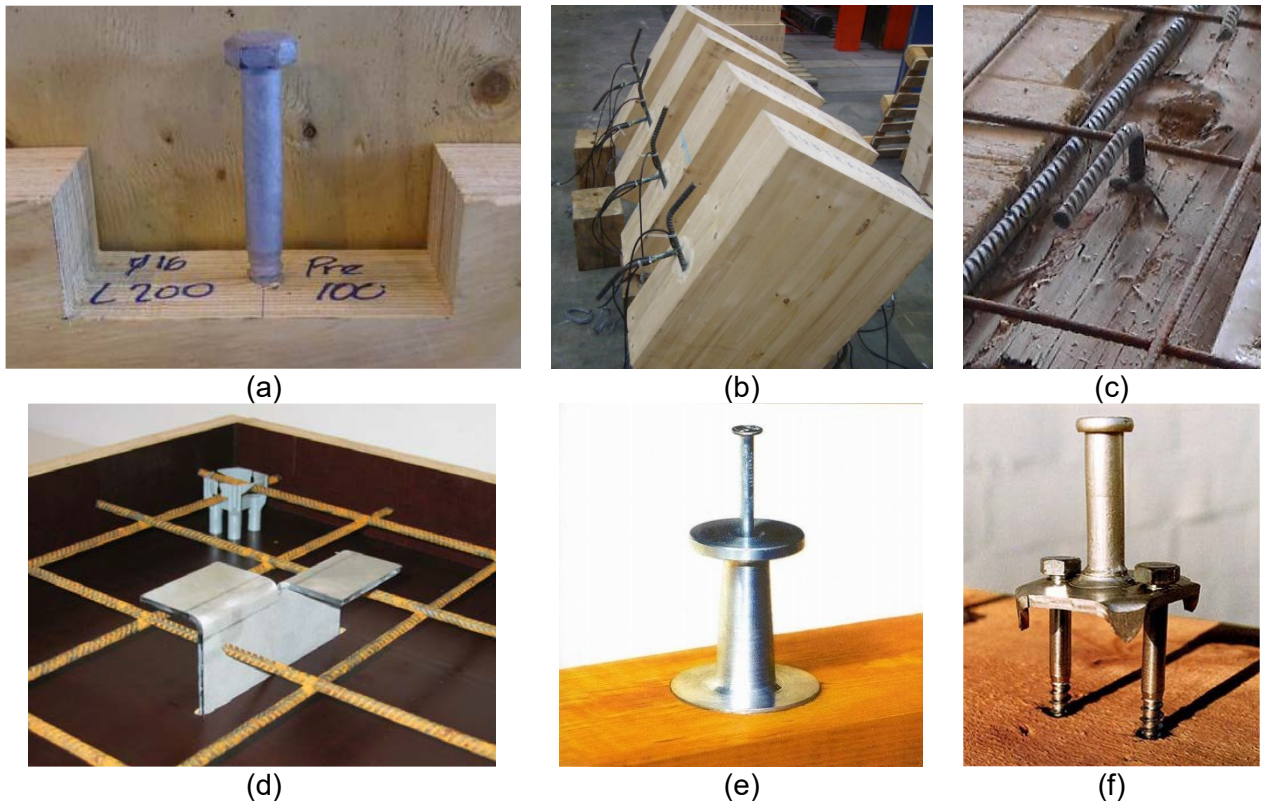


Fig. 1.3 – Example of TCC connections: (a) Notch with steel screw [1.2]; (b) Glued-in Rebar at 45° [1.30]; (c) Glued-in Rebar at 90°; (d) folded steel plate [1.29]; (e) HSB® connection [1.31]; f) Tecnaria connector [1.27].

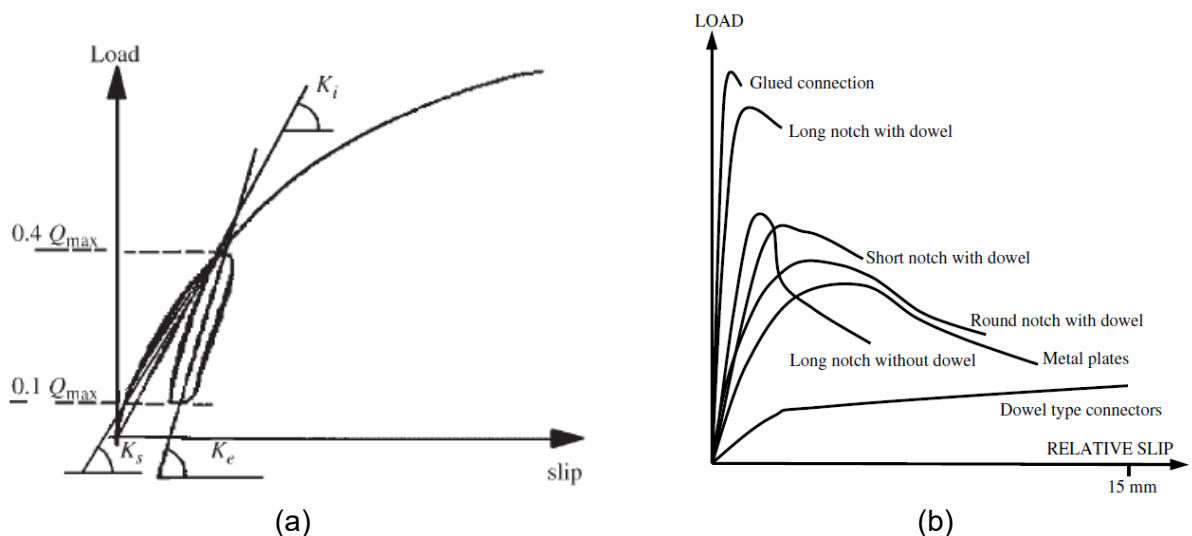


Fig. 1.4 – Load vs. slip behaviour of a connection: (a) according to standard procedure [1.17]; (b) comparison of different categories of connectors from Yeoh et al. [1.8].

The use of *traditional*, more ductile, dowel-type connectors that work in pure shear lead to structures with an efficiency ratio η comprised between 0.4-0.6 while *modern* high-performance fasteners (arranged at an angle with respect to the grain) may increase this value to a range of 0.7-0.8. Although, the highest efficiency is still reached only by notched and glued solutions.

In summary, it can be stated that there is not one solution prevailing over the others, but the choice of the connection type is strictly correlated to the use for which a TCC structure is going to be

designed. For example, notched connections are to be preferred for long span or precast TCC structures, where the realization costs can be economically withstood and justified by on-site time saving costs. On the contrary, for on-site construction of TCC assemblies, timesaving benefits will shift the choice to dowel-type fasteners that do not require particular woodworking of the timber beam.

1.1.3 Parameters influencing TCC connection's mechanical performance

The performance of a TCC connection is normally related to the connector's geometrical and mechanical properties and its behaviour in within the timber element only. However, several studies listed hereafter, aimed to study the possible changing of performance encountered by using different concrete types (e.g., concrete with light aggregates) and the impact of an interlayer between timber and concrete (normally employed to withstand the concrete pour during its curing time).

1.1.3.1 Concrete type

Normal concrete is an ordinary choice when designing new TCC structures and thanks to the higher elastic modulus compared to the timber (about three times), the connections are assumed as nearly infinitely stiff in the concrete layer. This is confirmed by the definition of specific K_{ser} for steel-to-timber and concrete-to timber connections, for which a multiplication factor of 2 is suggested, compared to a timber-to-timber connection.

Lightweight aggregate concrete (LWAC) is a structural concrete which, by containing lightweight aggregates, has a significantly reduced density. It is a feasible solution to decrease the dead load of concrete structures by partially sacrificing its mechanical performance mostly in terms of stiffness (according to EN 1992-1-1 [1.32]). Another advantage is the reduced nominal creep coefficient of LWAC, which reduces deflection of TCC beams against normal concrete solutions. For these reasons, LWAC is considered as a valuable solution [1.33] to realize even lighter, but still trustworthy, timber composite structures. Experimental test conducted by Steinberg et al. [1.34] with LWAC of density equal to 1.6 kN/m^3 confirmed that the reduced Young's modulus and a greater tendency to split when compared to normal weight concrete, reflects in a lower load carrying capacity and stiffness demonstrated by the connector. On the contrary, Fragiaco et al. [1.27] did not record significant differences between normal and lightweight concrete either in the long-term or in the short-term collapse tests because the failure took place in both cases in the timber. The influence of LWAC with inclined screw connections was also investigated by Jorge et al. [1.35] and Dias et al. [1.36] who observed a moderate reduction of the shear load carrying capacity (i.e., about 10%) and a more pronounced decrease of the slip modulus (i.e., approximately 30%).

1.1.3.2 Presence of an intermediate layer

The presence of an interlayer in timber-concrete composite cross-sections is an important topic, especially when considering the retrofitting of existing timber floor. In this case, the orthogonal layer of timber boards fastened to the main beams can be used as a formwork for the concrete slab. However, this topic was not accounted in the initial studies as the timber and concrete components were meant to be in direct contact neglecting any eccentricity effects. The interposition of an interlayer, translates into an unwanted load eccentricity on the dowel-type connector, which causes an important reduction of the shear load carrying capacity and in particular stiffness. The fact is that

even if the interlayer is realized with planks of higher strength, the force is acting orthogonal to the fibre direction and consequently manifesting a lower strength and stiffness [1.23]. The presence of an interlayer have been investigate also with TCC connections employing screws [1.35] resulting that the interlayer changes failure of the connection from a failure due to crushing of the aggregates near the screw heads to a ductile failure with withdrawal of screws and consequent plastic hinges formation.

1.1.4 TCC connections with inclined screws

Thanks to more than a few innovations in the shape of dowel-type fasteners characterized by withdrawal strength - annular-ring shank nails, self-tapping screws - their axial load-bearing capacity was greatly increased. In particular, the shape of modern screws are clearly different [1.37] from mainly laterally loaded screws according to DIN 571 [1.38]. Fig. 1.5 shows a traditional DIN 571 screw and a modern screw. The latter is characterized by a single core diameter for both the smooth shank and the threaded part. A larger pitch and sharper thread angle is the main responsible for the characteristic withdrawal parameter $f_{ax,k}$. The reduced screw-in torque during the installation is due to presence of additional shank ribs, at the end of the threaded part, and to particular lubricant coating treatments of the screw's surface. These features allow installing them without predrilling, while for traditional screw two pre-holes with different diameter are necessary to set the fastener correctly. These optimizations allow obtaining higher loads by positioning the screws inclined to fibre direction [1.37]. This evidence was obtained, with less evidence, on connections with timber screws inclined at 45° with respect to the shear plane.

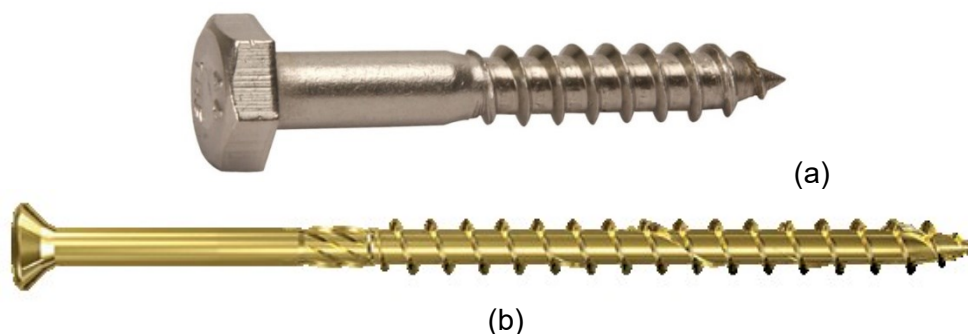


Fig. 1.5 – Timber screws: (a) traditional 16x120 mm DIN 571 screw; (b) 10x160 mm self-tapping screw.

Therefore, several studies are converging to the idea to exploit these fasteners as standalone TCC connections [1.39]-[1.43]. Research works have proven the reliability of these connectors, assessing that they can be an optimal solution particularly for short to medium span TCC structures. Actually, such connections are offering a balanced opportunity between rapidity of execution and mechanical performances. In particular:

- Apart from specific cases, when the floor to be refurbished is characterized by a big historical heritage and for which may require particular cares (i.e. predrilling, low amount of connections), the time for the realization of the connection is by far the shortest possible;
- These fasteners demonstrate high shear strength values especially when the fastener is placed at an angle with respect to the grain, thus being axially loaded as well as in bending;
- Presence of an interlayer marginally affects the shear strength and stiffness, contrary to traditional connections.

1.2 Analytical methods of calculation

This section presents a comparison between the analytical approach that can be used to calculate the shear load carrying capacity and stiffness of a TCC joint realized with inclined screws. According to Eurocode 5 [1.13] a quadratic combination of the axial and lateral loading ratios can be used to assess the connection capacity. As these conditions resulted to be quite restrictive for modern screws, starting from the Johansen's yielding theory model [1.44], analytical solutions to calculate mixed shear-tension or shear-compression capacity have been proposed and validated through experimental tests [1.45]-[1.48]. However, there is a lack of information regarding the behaviour of screws in crossed configuration and about the contribution of the screw loaded in shear and compression to the overall load carrying capacity of the CP.

The aim of this part of research is to investigate the mechanical behaviour of inclined self-tapping screws employed as timber-concrete connectors in both inclined and crossed configurations and define an analytical approach through modifications of existing theoretical propositions ([1.45];[1.46]). Concrete failure evaluations were added to the model as well as minor modifications to be able to apply it also in case of partial threaded screws.

1.2.1 Load bearing capacity

1.2.1.1 Analytical calculation with Johansen's theory (EC5 method)

Two different screw arrangements for a timber-concrete joint were analysed and detailed in Fig. 1.6. The first configuration of Fig. 1.6a, involves an inclined screw oriented in the same direction of the applied shear force (F_v) with an angle $\alpha = 45^\circ$ with respect to the vertical direction (i.e. perpendicular to grain direction). In the second configuration, plotted in Fig. 1.6b, a couple of crossed screws inclined at an angle $\alpha = \pm 45^\circ$ with respect to the vertical direction is placed to set up a single CP.

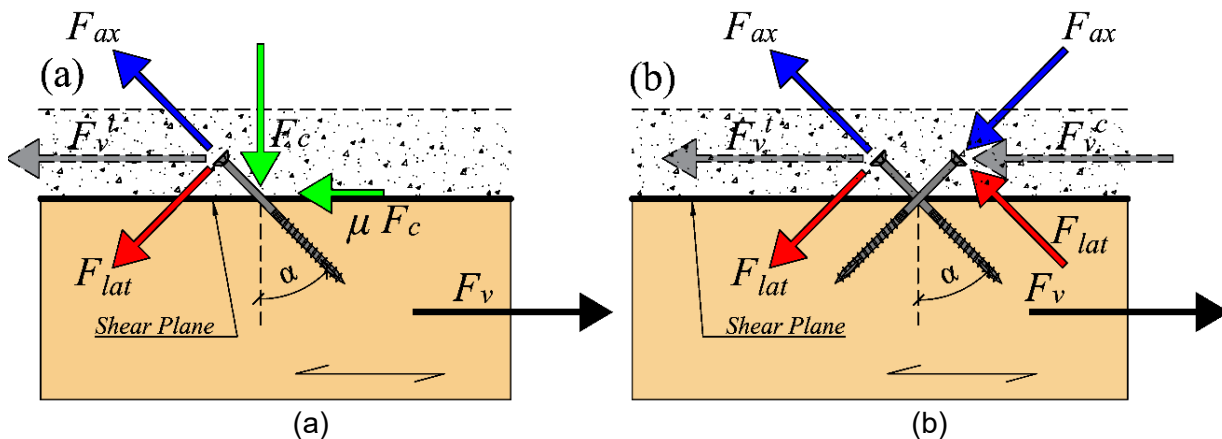


Fig. 1.6 – Loading models for screws according to Eurocode 5: (a) inclined screw; (b) couple of crossed screws. According to Fig. 1.6a, the force transmitted to the screw (F_v^t) acts parallel to the shear plane and can be split into an axial component (F_{ax}) and a lateral component (F_{lat}) according to the expressions:

$$\begin{aligned} F_{ax} &= F_v \cdot \sin \alpha \\ F_{lat} &= F_v \cdot \cos \alpha \end{aligned} \quad (1.3)$$

where α is the fastener inclination with respect to the vertical direction (i.e. perpendicular to grain direction). As the inclined screw is subjected to a combined shear-tension loading condition, actual design method disposed in Eurocode 5 [1.13] limits the maximum load bearing capacity of a screw with the following inequality representing the tension-shear resistance domain:

$$\left(\frac{F_{ax}}{F_{ax,Lim}}\right)^2 + \left(\frac{F_{lat}}{F_{lat,Lim}}\right)^2 \leq 1 \quad (1.4)$$

where F_{ax} and F_{lat} are respectively the applied axial and shear actions while $F_{ax,lim}$ and $F_{lat,lim}$ are the maximum load bearing capacity in axial and shear direction, respectively.

Similarly to timber-to-timber connections with inclined screws, as reported in [1.49], the load-bearing capacity parallel to the shear plane can be written combining Equations (1.3) and (1.4), providing:

$$F_v = \frac{1}{\sqrt{\left[\left(\frac{\sin \alpha}{F_{ax,Lim}}\right)^2 + \left(\frac{\cos \alpha}{F_{lat,Lim}}\right)^2\right]}} \quad (1.5)$$

The maximum load bearing capacity $F_{ax,lim}$ should be calculated according to Eurocode 5 [1.13] formulation if no other specifications are available for the adopted fastener (e.g., in the fastener homologation document). $F_{lat,lim}$ calculation are also provided by Eurocode 5 [1.13] according to the Johansen's Theory [1.44]. In detail, an increment of the shear component $F_{lat,lim}$ is allowed by including the so called "rope effect", which allows exploitation of the withdrawal capacity of a fastener. This additional shear capacity is computed as $\mu \cdot F_c$, where μ is a friction coefficient equal to 0.25 that multiply the force F_c acting orthogonal to the shear plane, and is suitable for wood-to-wood surfaces. No specific values are provided in standards for wood-to-concrete surfaces.

1.2.1.2 Advanced method for shear-tensile loaded screws

An extension to the original Johansen theory model was proposed by Bejtka and Blass [1.45] to evaluate the behaviour of joints loaded in shear, realized with inclined self-tapping screws. Kavaliauskas et al. [1.46] applied this model to inclined screws utilized as TCC connections by adding two hypotheses: a rigid behaviour of the screw part in the concrete layer and the axial withdrawal capacity due to the threaded part of the screws. Thus, the kinematical failures are reduced to three modes and the ultimate load-bearing capacity equations were extrapolated from equilibrium laws for each of the three modes (see Fig. 1.7). In this work, threaded part l_{eff} , responsible for the withdrawal strength, is distinguished from the penetration length t , accountable for the lateral strength, to extend this model also to partially threaded screws.

The failure modes according to ([1.45];[1.46]) and represented in Fig. 1.7 correspond to:

- *Mode I*: wood embedment with rigid translation of the screw;
- *Mode II*: wood embedment plus development of a single plastic hinge at the interface between timber and concrete;
- *Mode III*: wood embedment with development of two plastic hinges in the wood layer.

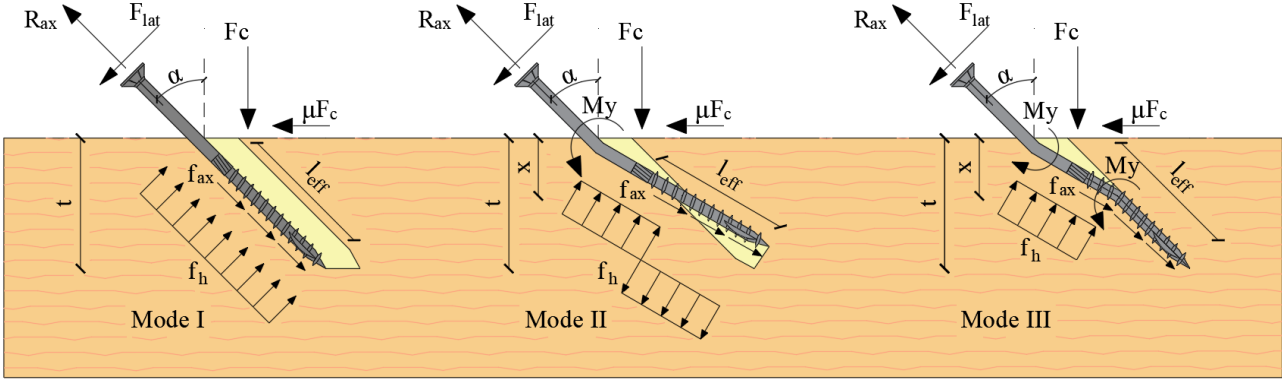


Fig. 1.7 – Mechanical models of the different failure modes for an inclined screw subjected to shear-tension stress extrapolated from [1.45] and adapted to the proposed modifications.

To obtain the *first failure mode* the axial and lateral load-carrying capacity R_{ax} and F_{lat} and the compression between timber and concrete F_c should be addressed as:

$$R_{ax} = f_{ax} \cdot d \cdot l_{eff} \quad (1.6)$$

$$F_{lat} = f_h \cdot d \cdot t_1 = f_h \cdot d \cdot t / \cos \alpha \quad (1.7)$$

$$F_c = R_{ax} \cdot \cos \alpha - F_{lat} \cdot \sin \alpha \quad (1.8)$$

Where f_{ax} is the withdrawal strength of fastener, d is the nominal fastener diameter, l_{eff} is the threaded length of the fastener inserted into the wood member, and t_1 is the depth of penetration of fastener into timber. The resulting shear force is the sum of each component parallel to the shear plane:

$$F_v^{It} = R_{ax} \cdot \sin \alpha + F_{lat} \cdot \cos \alpha + \mu F_c = R_{ax} \cdot (\sin \alpha + \mu \cos \alpha) + F_{lat} \cdot (\cos \alpha - \mu \cdot \sin \alpha) \quad (1.9)$$

$$F_v^{It} = f_{ax} \cdot d \cdot l_{eff} \cdot (\sin \alpha + \mu \cos \alpha) + f_h \cdot d \cdot t_1 \cdot (\cos \alpha - \mu \cdot \sin \alpha) \quad (1.10)$$

$$F_v^{It} = f_{ax} \cdot d \cdot l_{eff} \cdot (\sin \alpha + \mu \cos \alpha) + f_h \cdot d \cdot t \cdot (1 - \mu \cdot \tan \alpha) \quad (1.11)$$

The *second failure mode* is obtained through the evaluation of the maximum yielding moment M_y which enables the rigid rotation of the screw portion embedded in the wood layer. With reference to Fig. 1.7 equilibrium between internal and external forces yields to:

$$M_y = f_h \cdot d \cdot \left[\frac{x}{\cos \alpha} \cdot \frac{x}{2 \cos \alpha} - \frac{(t-x)}{\cos \alpha} \left(\frac{x}{\cos \alpha} + \frac{1}{2} \frac{(t-x)}{\cos \alpha} \right) \right] \quad (1.12)$$

$$M_y = f_h \cdot d \cdot \left[\frac{x^2 - 2(t-x)x - (t-x)^2}{2 \cos^2 \alpha} \right] \quad (1.13)$$

where x is the distance plotted in Fig. 1.7. From the latter expression, the value of x can be extrapolated:

$$x = \frac{t}{\sqrt{2}} \cdot \sqrt{\frac{2M_y}{f_h \cdot d \cdot t^2} \cdot \cos^2 \alpha + 1} \quad (1.14)$$

The resulting shear load acting on the screw is:

$$R_{lat} = f_h \cdot d \cdot \left(\frac{x}{\cos \alpha} - \frac{(t-x)}{\cos \alpha} \right) = \frac{f_h \cdot d}{\cos \alpha} \cdot (2x-t) = \frac{f_h \cdot d \cdot t}{\cos \alpha} \cdot \left(2 \frac{x}{t} - 1 \right) \quad (1.15)$$

Substituting Eq. (1.14) in Eq. (1.15) it is possible to write:

$$F_{lat} = \frac{f_h \cdot d \cdot t}{\cos \alpha} \cdot \left(\frac{2}{t} \frac{t}{\sqrt{2}} \cdot \sqrt{\frac{2M_y}{f_h \cdot d \cdot t^2} \cdot \cos^2 \alpha + 1} - 1 \right) \quad (1.16)$$

$$F_{lat} = \frac{f_h \cdot d \cdot t}{\cos \alpha} \cdot \left(\sqrt{\frac{4M_y}{f_h \cdot d \cdot t^2} \cdot \cos^2 \alpha + 1} - 1 \right) \quad (1.17)$$

The compression load F_c responsible for the frictional effect can be expressed again substituting Eqs. (1.6) and (1.17) in Eq. (1.8) obtaining:

$$F_c = f_{ax} \cdot d \cdot l_{eff} \cdot \cos \alpha - \frac{f_h \cdot d \cdot t}{\cos \alpha} \cdot \left(\sqrt{2} \sqrt{\frac{2M_y}{f_h \cdot d \cdot t^2} \cdot \cos^2 \alpha + 1} - 1 \right) \cdot \sin \alpha \quad (1.18)$$

Finally, the resulting shear force is the sum of each component parallel to the shear plane, can be obtained by placing Eqs. (1.17) and (1.18) in Eq. (1.9) thus obtaining:

$$F_v^{III} = f_{ax} \cdot d \cdot l_{eff} \cdot (\sin \alpha + \mu \cos \alpha) + (1 - \mu \cdot \tan \alpha) \cdot f_h \cdot d \cdot t \cdot \left(\sqrt{2} \sqrt{\frac{2M_y}{f_h \cdot d \cdot t^2} \cdot \cos^2 \alpha + 1} - 1 \right) \quad (1.19)$$

The *third failure mode* contemplates the formation of two plastic hinges in the fastener for which the maximum yielding moment can be calculated as function of x , and from which x can be explicated:

$$M_y = \frac{1}{2} f_h \cdot d \cdot \left(\frac{x}{\cos \alpha} \cdot \frac{x}{2 \cos \alpha} \right) = \frac{f_h \cdot d \cdot x^2}{4 \cos^2 \alpha} \Rightarrow x^2 = \frac{4M_y}{f_h \cdot d} \cdot \cos^2 \alpha \Rightarrow x = \sqrt{\frac{4M_y}{f_h \cdot d}} \cos \alpha \quad (1.20)$$

The resulting shear load acting on the screw and the compression component can be written as:

$$F_{lat} = f_h \cdot d \cdot \left(\frac{x}{\cos \alpha} \right) = f_h \cdot d \cdot \sqrt{\frac{4M_y}{f_h \cdot d}} = \sqrt{4M_y \cdot f_h \cdot d} = 2\sqrt{M_y \cdot f_h \cdot d} \quad (1.21)$$

$$F_c = R_{ax} \cdot \cos \alpha - R_l \cdot \sin \alpha = f_{ax} \cdot d \cdot l_{eff} \cdot \cos \alpha - 2\sqrt{M_y \cdot f_h \cdot d} \cdot \sin \alpha \quad (1.22)$$

The shear capacity corresponding to the third failure mode is:

$$F_v^{III} = R_{ax} \cdot \sin \alpha + R_l \cdot \cos \alpha + \mu F_c = R_{ax} \cdot (\sin \alpha + \mu \cos \alpha) + R_l \cdot (\cos \alpha - \mu \cdot \sin \alpha) \quad (1.23)$$

$$F_v^{III} = f_{ax} \cdot d \cdot l_{eff} \cdot (\sin \alpha + \mu \cos \alpha) + 2\sqrt{M_y \cdot f_h \cdot d} \cdot (\cos \alpha - \mu \cdot \sin \alpha) \quad (1.24)$$

These formulations, adapted to the more convenient definition of the screw inclination α , describe the failure modes I, II and III. Hereafter to facilitate the comprehension of all following equations apex t and c on each term are referred to the shear-tension loaded and shear-compression load screw respectively. The characteristic load-bearing capacity parallel to the shear plane for a screw subjected to a combined shear-tension load with the extended method can be written as:

$$F_{v,Rk,th}^t = \min(F_{v,Rk}^{II}; F_{v,Rk}^{III}; F_{v,Rk}^{III}) \quad (1.25)$$

Where the three failure modes are resumed through the following expressions:

$$F_{v,Rk}^{III} = R_{ax,k}^t \cdot (\sin \alpha + \mu \cos \alpha) + f_{h,k} \cdot d \cdot t \cdot (1 - \mu \cdot \tan \alpha) \quad (1.26)$$

$$F_{v,Rk}^{III} = R_{ax,k}^t \cdot (\sin \alpha + \mu \cos \alpha) + f_{h,k} \cdot d \cdot t \cdot (1 - \mu \cdot \tan \alpha) \cdot \left[\sqrt{2} \sqrt{\frac{2M_{y,Rk}}{f_{h,k} \cdot d \cdot t^2} \cdot \cos^2 \alpha + 1} - 1 \right] \quad (1.27)$$

$$F_{v,Rk}^{III} = R_{ax,k}^t \cdot (\sin \alpha + \mu \cdot \cos \alpha) + 2 \sqrt{M_{y,Rk} \cdot f_{h,k} \cdot d} \cdot (\cos \alpha - \mu \cdot \sin \alpha) \quad (1.28)$$

$M_{y,Rk}$ and $f_{h,k}$ are the characteristic yielding moment of the screw and wood embedment strength while $R_{ax,k}$ is the characteristic axial capacity of the screw.

With respect to the original propositions ([1.45];[1.46]) experimental evidences described in the next section confirm that the latter term, should take into account the possibility that failure might take place also the concrete layer. To this aim, Eq.(1.29) introduces this possibility in the evaluation of the axial screw capacity: $R_{ax,k}$ should be the minimum between the withdrawal capacity of the threaded part $F_{ax,Rk}$ and the pull-through capacity of the screw head into the concrete $F_{ax,Rk,cone}$, which might lead to an anticipated failure in the concrete layer.

$$R_{ax,k} = \min(F_{ax,Rk}; F_{ax,Rk,cone}) \quad (1.29)$$

The first term is calculated according either to EC5 formulation [1.13] or the relevant homologation document of the fastener. The second term $F_{ax,Rk,cone}$, could be evaluated assuming an analogy between the behaviour of the countersunk head screw into the concrete layer and the behaviour of headed stud anchors in concrete, for which formulations of axial capacity are already provided by various regulations [1.50]-[1.52]. Although concrete capacity design has been proved more accurate for standard anchors, the 45° concrete cone theory [1.50] could also fit this particular problem as this failure model includes the effective depth of the fastener into the concrete layer h_{eff} , its head diameter d_h and the concrete cylinder compressive strength f_{ck} resulting in:

$$F_{ax,Rk,cone} = 0,96 \sqrt{f_{ck}} \pi \cdot h_{eff} \cdot (h_{eff} + d_h) \quad (1.30)$$

where h_{eff} could be approximately taken as the mean concrete cover of the screw head centroid measured parallel to the screw axis. Moreover, as the cone failure might occur either in the upper or lower part of the concrete layer depending on the load direction, the h_{eff} was distinguished according to Fig. 1.8.

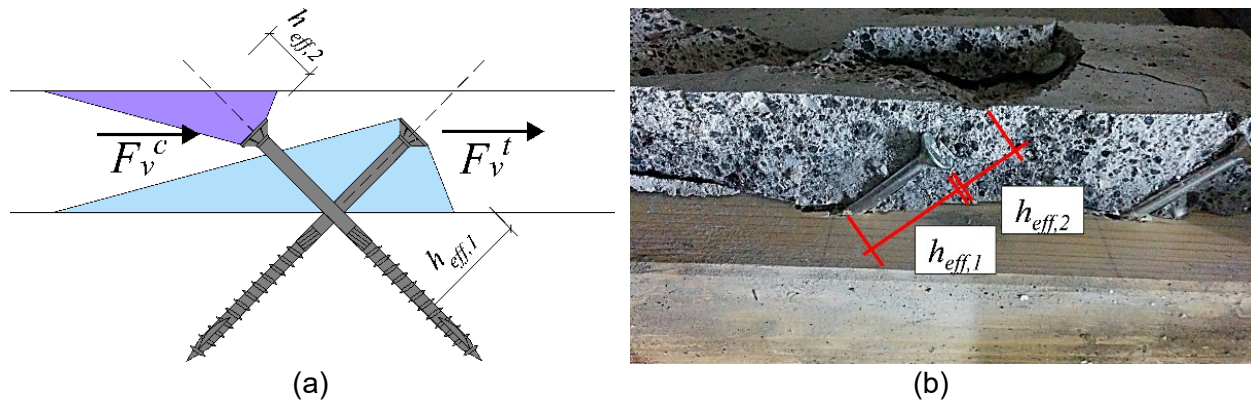


Fig. 1.8 – Failure models in the concrete layer for different loading conditions of an inclined screw subjected to shear-tension or shear-compression stress: (a) theoretical model; (b) experimental evidence.

Fig. 1.9 presents, as a preliminary analysis, a comparison between the analytical predictions of Eurocode 5 and the proposed approach. The ratio between the highest load bearing capacity $F_{v,th,max}$ (at 45°) calculated with both models and the current value $F_{v,th,\alpha}$ for an 8x160 mm self-tapping screw with 80 mm of effective length, is calculated and reported in Fig. 1.9a (values calculated with ductile failure of the connection, i.e. Failure mode III). For a screw placed perpendicular to the grain, the modified approach gives the same Eurocode 5 results in accordance with the Johansen’s theory, from which the model is extrapolated. The relative difference increases and reaches its peak at the 45° inclination as the axial contribution become predominant (see Fig. 1.9b).

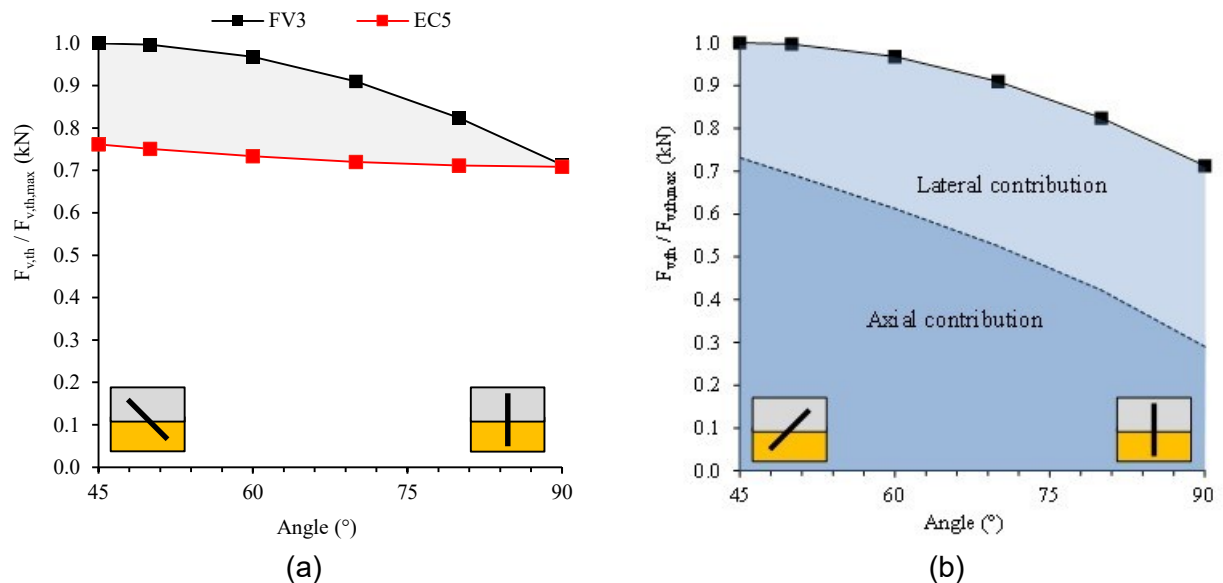


Fig. 1.9 – Analytical load bearing capacity of an inclined self-tapping screw varying the angle α with respect to the grain: (a) comparison between Eurocode 5 and the proposed approach; (b) axial and lateral contribution for failure mode 3, expressed by Eq.(1.28).

1.2.1.3 Couple of crossed screws

If a crossed screw configuration (Fig. 1.6b) is adopted, the design procedure of fasteners according to Eurocode 5 [1.13] provides Eq. (1.5) for both shear-tension and shear-compression loading conditions. The approach proposed in this work adopts the same theoretical model leading to Eq. (4) for each of the two screws, with the following differences:

- in Eq. (1.26) to (1.28), the frictional effects, represented by the terms including the μ coefficient, are neglected due to the absence of compression loads acting between timber

and concrete (see Fig. 1.6b). Such solution is also recommended for timber-to-timber connections with crossed screws in [1.49];

- in the evaluation of the axial strength $R_{ax,k}$, the concrete cone failure calculation is differentiated between the shear-tensile loaded screw and the shear-compression loaded screw (according to Fig. 1.8):

$$F_{ax,Rk,cone}^t = F(h_{eff,1}) \quad ; \quad F_{ax,Rk,cone}^c = F(h_{eff,2}) \quad (1.31)$$

The total strength of the couple of crossed screws should be:

$$F_{v,Rk,th}^{t+c} = \min(F_{v,Rk}^{I t+c}; F_{v,Rk}^{II t+c}; F_{v,Rk}^{III t+c}) \quad (1.32)$$

1.2.2 Stiffness

Since strength and stiffness are two mechanical properties strictly related to one another, investigations in the analytical definition of the stiffness of screws used as a timber-concrete connection were also taken. Eurocode 5 [1.13] does not contemplate specific rules for the estimation of the stiffness of inclined/crossed fasteners. Consequently, a cautelative approach might be to evaluate the instantaneous modulus K_{ser} of laterally loaded fasteners. Eq. (1.33) taken from Table 7.1 of Eurocode 5 [1.13] is valid for dowels, bolts, screws and predrilled nails loaded perpendicularly to the shear plane and depends exclusively from the timber properties, summarized by its mean density ρ_m in kg/m³, and fastener diameter d in mm:

$$K_{ser} = \rho_m^{1,5} \cdot d / 23 \quad (N/mm) \quad (1.33)$$

This formulation, valid for timber-to-timber connections shall be multiplied by a factor 2, to consider the higher stiffness of the concrete and implicitly assume no deformation on concrete [1.21]. Even Eurocode 5 [1.13] at point 7.1.c allows doubling the stiffness when a rigid element (i.e. steel or concrete) is fastened to a wooden member.

Similarly to the approach proposed for the load bearing capacity, the contribution of lateral and axial stiffness should be considered at the serviceability state, assuming a linear-elastic behaviour of the screw. Through equilibrium formulations imposed for an inclined screw, the stiffness parallel to the sliding plane has the same expression reported in [1.45]. The result is a linear combination of $K_{ser,||}$ and $K_{ser,\perp}$ which are the axial and lateral stiffness of the fastener respectively. While the lateral stiffness $K_{ser,\perp}$ could be expressed with Eq. (1.33) the axial contribution $K_{ser,||}$ should be evaluated experimentally or according to alternative approaches [1.53]. The proposed theoretical stiffness expression $K_{ser,th}$ alternative to Eurocode 5 provisions is the following:

$$K_{ser,th}^t = K_{ser,||} \cdot \sin \alpha \cdot (\sin \alpha + \mu \cdot \cos \alpha) + K_{ser,\perp} \cdot \cos \alpha \cdot (\cos \alpha - \mu \cdot \sin \alpha) \quad (1.34)$$

Assuming the standard screw inclination at 45°, Eq. (1.34) reduces to the following simplified expression where only the friction coefficient μ appears:

$$K_{ser,th}^t = \frac{K_{ser,||} \cdot (1 + \mu) + K_{ser,\perp} \cdot (1 - \mu)}{2} \quad (1.35)$$

1.3 Experimental tests

Short-term push-out tests were conducted on 12 series varying the screws diameters, connections arrangements and the concrete type adopted for the slab. Tests were repeated 4 times for each series for a total of 48 investigated specimens. Push-out tests are normally adopted to assess the overall behaviour, stiffness and strength of timber to concrete connections in hybrid T-shape beams.

1.3.1 Specimen geometry

Test samples consisted of two concrete elements connected through a central timber member connected with fasteners as depicted in Fig. 1.10. The timber beam and the concrete element were vertically shifted of about 4 cm to ease the load application in the event that unpredictably high displacements occurred. Due to symmetry of the test configuration, applied load is equally shared between the two wood-concrete interfaces. Concrete thickness s equal to 6 cm was chosen, as this is the slab thickness commonly adopted in these applications. The thickness t of the glulam timber element was set to 24 cm, in order to avoid interference between the threads of the inclined screws. The total height of the specimen h was 50 cm to allow enough spacing between screws. Details of the screw arrangement and spacing are reported in Table 1-1. Fasteners were screwed into timber until the counter-sunk head was positioned at half of the concrete thickness.

Two or three CPs per shear plane were realized. The adopted screw number was:

- 3 screws on each side (a total of six screws per specimen) for the inclined configuration (hereafter labelled as series AN and AL).
- 2 couple of screws on each side (a total of eight screws per specimen) for the crossed configuration (hereafter labelled as series XN and XL)

Screws spacing was set according to Eurocode 5 [1.1] and the screws homologation document ETA 11-0027 [1.54] (calculated with $d = d_{nom}$). Spacing of screws across the specimen width was arranged in order to avoid possible interferences and group effects (i.e. to ensure that the effective number of fasteners $n_{eff} = n$).

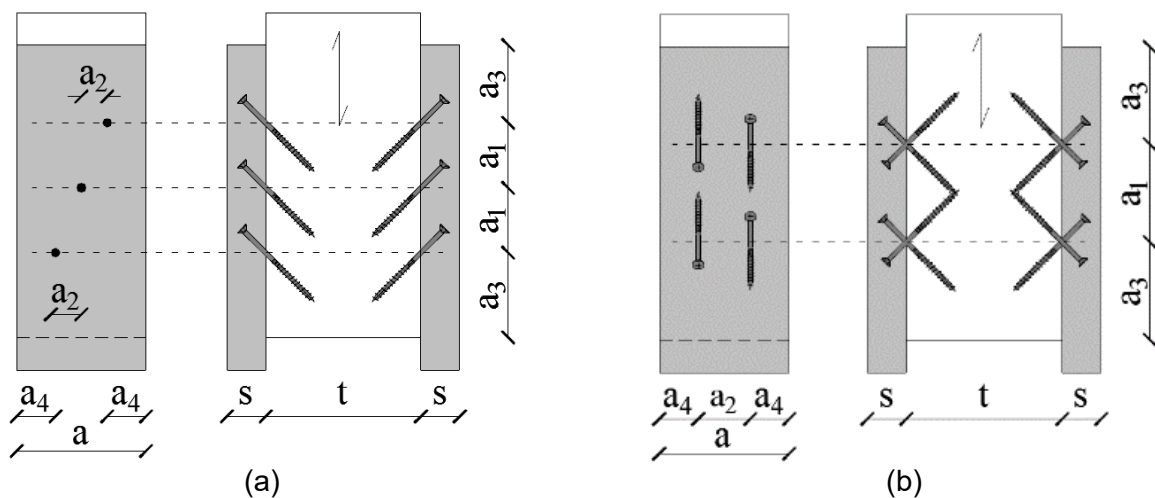


Fig. 1.10 – Specimen geometry: (a) AN and AL series; (b) XN and XL series.

Table 1-1 – Nomenclature and geometries of the specimens.

ID	Screws N° (-)	d (mm)	a ₁ (mm)	a ₁ /d (-)	a ₂ (mm)	a ₂ /d (-)	a ₃ (mm)	a ₃ /d (-)	a ₄ (mm)	a ₄ /d (-)	α (°)	Concrete Type	N° of tests (I)
AN-8		8	100	12.5	40	5.0	125	15.6	60	7.5			4
AN-10	6	10	100	10.0	40	4.0	125	12.5	60	6.0	+45	Normal	4
AN-12		12	100	8.4	40	3.5	120	10.0	60	5.0			4
AL-8		8	100	12.5	40	5.0	125	15.6	60	7.5			4
AL-10	6	10	100	10.0	40	4.0	125	12.5	60	6.0	+45	Light weight	4
AL-12		12	100	8.4	40	3.5	125	10.4	60	5.0			4
XN-8		8	150	18.8	80	10.0	150	18.8	60	7.5			4
XN-10	8	10	150	15.0	80	8.0	150	15.0	60	6.0	±45	Normal	4
XN-12		12	150	12.5	80	6.7	150	12.5	60	5.0			4
XL-8		8	150	18.8	80	10.0	150	18.8	60	7.5			4
XL-10	8	10	150	15.0	80	8.0	150	15.0	60	6.0	±45	Light weight	4
XL-12		12	150	12.5	80	6.7	150	12.5	60	5.0			4

1.3.2 Materials and test setup

The timber used for fabricating the test specimens is spruce (*Picea abies*) glued laminated timber of strength class GL24h according to EN 14080 [1.55] with nominal characteristic and mean density values of $\rho_k = 385 \text{ kg/m}^3$ and $\rho_m = 420 \text{ kg/m}^3$ respectively. Moisture content was determined on each series of specimen according to EN 13183-2 [1.56] with a mean value of 11.2%.

Self-tapping screws with counter-sunk head, the same threaded length l_{eff} of 80 mm and nominal diameters of 8, 10 and 12 mm were tested. Counter-sunk head support the hypothesis of screw rigidly embedded into the concrete slab. Characteristic withdrawal strength parameter $f_{ax,k}$ and bending moment formulation $M_{y,Rk}$ were derived directly from the homologation document ETA-11/0027 [1.54]:

$$f_{ax,k} = 10.0 \text{ MPa} \quad (1.36)$$

$$M_{y,Rk} = 0.15 \cdot 600 \cdot d^{2.6} \quad (1.37)$$

For the latter parameter, independency from the inclination angle α up to 45° is tolerated.

Concrete mechanical properties were evaluated by compressive tests on cubes for each of the four groups of specimens according to EN 12390-3 [1.57] and the corresponding mean elastic modulus E_{cm} was calculated following Eurocode 2 provisions. For normal concrete the measured mean uniaxial compressive strength was $f_{cm} = 35.62 \text{ MPa}$ and a corresponding elastic modulus of $E_{cm} = 31.256 \text{ GPa}$ was calculated. For lightweight aggregate concrete corresponding values were $f_{cm} = 32.73 \text{ MPa}$ and $E_{cm} = 16.072 \text{ GPa}$ respectively. Characterization tests on concretes were performed just before the start of push-out tests.

Short-term push-out tests were conducted following loading test protocol according to EN 26891 [1.58] on a universal machine with a load capacity up to 250 kN. Specimens were subjected to four different loading phases, each one characterized by a constant load-rate, following the specified imposed loading protocol. The load-rate was specifically calibrated for each specimen on the

respective ultimate shear load $F_{v,est}$, which was obtained by means of preliminary monotonic tests. A picture of the test setup is shown in Fig. 1.11. The applied forces were measured using a load cell placed between the actuator and the specimen. Relative displacement between sliding faces were measured with two linear variable differential transducers (LVDTs) placed along both shear planes.

Since EN 26891 [1.58] does not require specific measurements after peak load $F_{v,peak}$, tests were arbitrarily stopped after a sudden decrease in load capacity or when a slip of 15 mm was achieved.

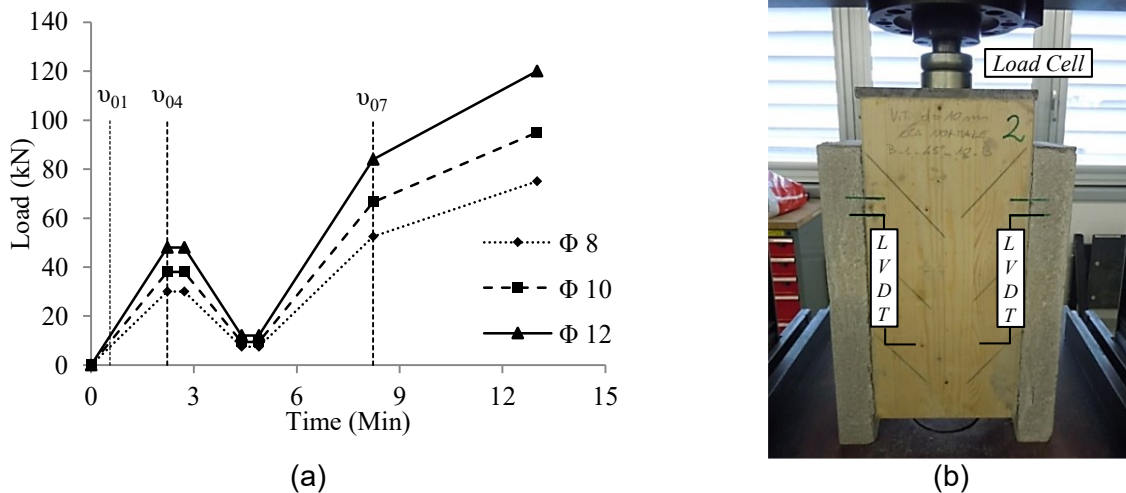


Fig. 1.11 – (a) Loading procedure according to EN 26891 calibrated on $F_{v,est}$ values; (b) clean specimen before tests.

1.3.3 Test results

Fig. 1.12 to Fig. 1.14 illustrate the force-displacement curves acquired from tests according to EN 26891 [1.58]. In order to have a clear view of the load capacity achieved by an inclined screw at 45° and its increment obtained with the addition of the second screw in the opposite direction, loads are divided by the number of CP comprised by each specimen whereas shown displacements are taken as the mean value measured by the couple of LVDTs.

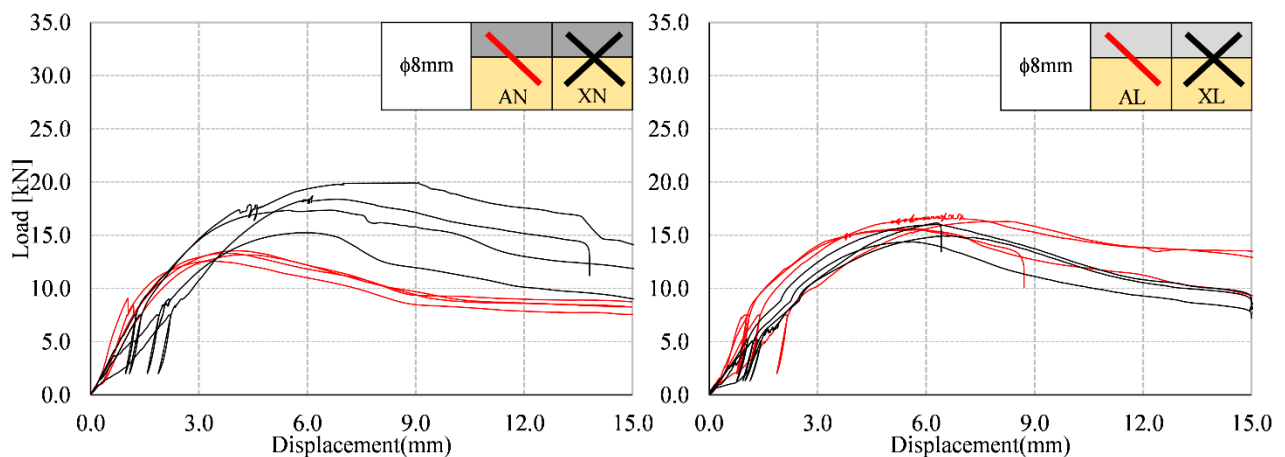


Fig. 1.12 – Experimental load vs. displacement curves for 8 mm screws. Symbols stay for: inclined screws (A series) or crossed screws (X series), normal (N) or lightweight (L) concrete.

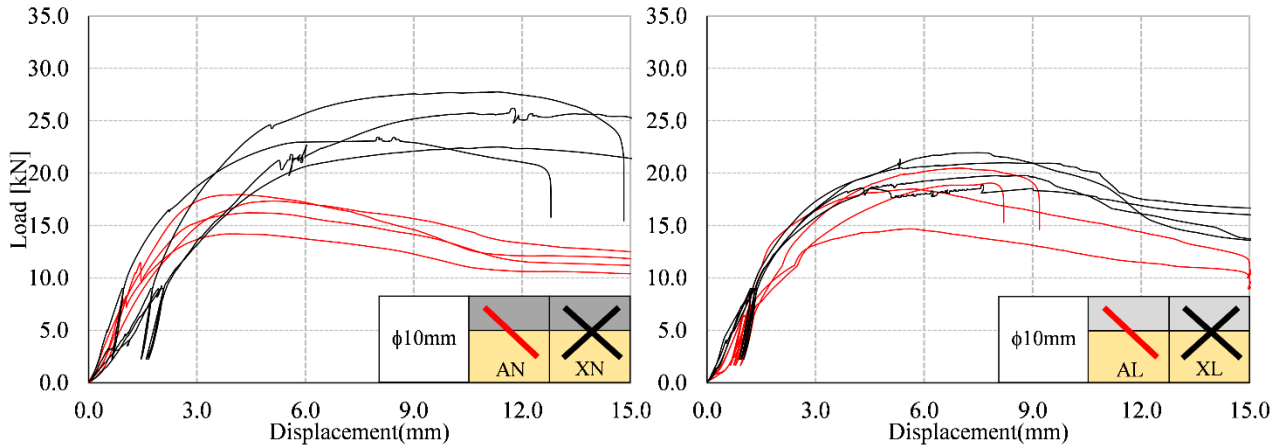


Fig. 1.13 – Experimental load vs. displacement curves for 10 mm screws. Symbols stay for: inclined screws (A series) or crossed screws (X series), normal (N) or lightweight (L) concrete.

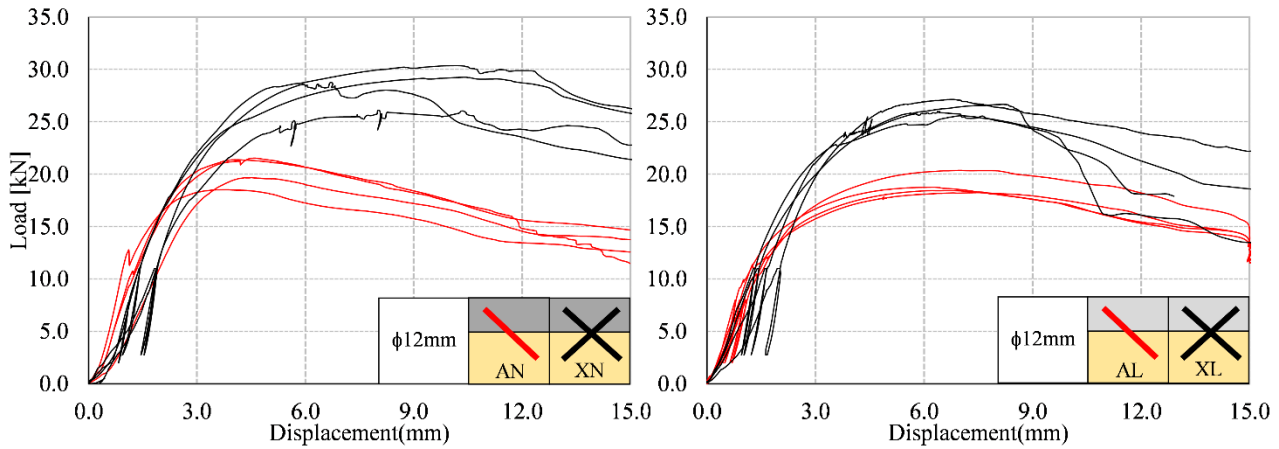


Fig. 1.14 – Experimental load vs. displacement curves for 12 mm screws. Symbols stay for: inclined screws (A series) or crossed screws (X series), normal (N) or lightweight (L) concrete.

Performed tests allow quantifying the experimental shear strength $F_{v,peak}$, i.e. the peak load applied, hereafter called $F_{v,exp}$. Moreover, the instantaneous slip modulus $K_{ser,exp}$ is determined from experimental load-displacement curves according to the formulation reported in EN 26891 [1.58]:

$$K_{ser,exp} = \frac{0.4 \cdot F_{v,est}}{v_{i,mod}} = \frac{0.4 \cdot F_{v,est}}{4/3 \cdot (v_{04} - v_{01})} = \frac{0.4F_{v,est} - 0.1F_{v,est}}{v_{04} - v_{01}} \quad (1.38)$$

where v_{01} and v_{04} correspond to the slip measured at $0.1 \cdot F_{v,est}$ and $0.4 \cdot F_{v,est}$ respectively.

In addition to the evaluation of $F_{v,exp}$ and $K_{ser,exp}$, serviceability conditions of the connections in terms of strength and displacement are useful parameters to be checked when designing TCC structures. Generally, in timber structures, these values could be identified as the yielding point shown by the connection. It is worth noting that the definition of the yielding point of dowel-type connections is still an open topic as the experimental curves usually exhibit an unclear change in the gradient of the load-deformation slope [1.59]-[1.61]. Several conventional methods are available in literature and summarized in [1.62]. In this work, the Forintek (FCC) method (see Karacabeyli and Ceccotti [1.63]) was adopted. The connection yielding strength and slip (defined by $F_{v,y}$ and δ_y respectively) is considered as the point on the load-deformation curve corresponding to 50% of the maximum experimental strength $F_{v,exp}$.

By analysing the experimental results in Fig. 1.12 to Fig. 1.14 it is possible to observe that all load-slip curves exhibit a uniform global trend for all specimens: shear strength $F_{v,exp}$ and service stiffness

$K_{ser,exp}$ increase with screws diameter increasing from 8 to 12 mm. Passing from normal to lightweight concrete, an increase in deformability without reduction of $F_{v,exp}$ can be observed as a consequence of the reduced elastic moduli of lightweight concrete. After the peak load $F_{v,exp}$ a constant smooth softening behaviour characterizes most single screw tests, while the concrete cone failure has been registered in both cases but especially in crossed screw specimens with consequent loss of capacity of the shear-compressed screw.

Table 1-2 lists for each specimen the measured peak shear capacity $F_{v,exp}$, the instantaneous slip modulus $K_{ser,exp}$ determined with Eq. (1.38) and the conventional yielding point coordinates ($F_{v,y}$, δ_y) determined according to [1.63], together with their mean values and variation coefficient (COV). For a better visual result, obtained mean values of $F_{v,exp}$ and $K_{ser,exp}$ are plotted in Fig. 1.16 on the assumption that the stiffness is equally distributed over all CPs.

For the inclined screw configuration scattering of results is quite limited: maximum COV is equal to 12.0% for $F_{v,exp}$ and equal to 18.3% for $K_{ser,exp}$. For the crossed screws configuration the limited COV of peak strength is confirmed, but results in terms of stiffness become quite variable and greater COVs have been obtained (up to 38.4% for the XN series with 12 mm screws).

On average, the increase of strength $F_{v,exp}$ and stiffness $K_{ser,exp}$ with the screw diameter is confirmed with all combination of other parameters.

Conversely, dependences on concrete type do not exhibit a clear trend. In terms of strength, specimens with 8 and 10 mm screws unexpectedly demonstrated a higher average strength when realized with lightweight concrete. Stiffness of connections was greater with NC, even if with small 8 mm screw diameters and crossed configuration some results with LC resulted to be greater than with NC.

However, the more interesting observations raised when comparing inclined screw configurations with crossed screws configurations (see Fig. 1.15), since means values were contrary to expectations. Introduction of the second screw:

- Uniformly resulted in a loss of stiffness for all screw diameters and concrete types;
- In case of normal concrete no differences were observed in term of mean strengths between AN and XN configurations;
- In case of lightweight concrete crossed configuration XL resulted to be on average less resistant than inclined screw configuration AL.

The diminishing of stiffness has been explained with the loss of friction contribution.

The worse performance in terms of load-carrying capacity (see Fig. 1.15), between two inclined screws (theoretical) and two crossed screws can be understood if the failure modes are considered. In the inclined screw configuration (A) failure mostly occurred on the wood side with the formation of a double plastic hinge in connectors coupled with wood embedment phenomenon (see Fig. 1.17a). While with crossed screws specimens (X), failure started with the formation of plastic hinges, then local failure due to concrete splitting and consequent expulsion ahead of the compressed screws (see Fig. 1.17b and c) impaired the shear capacity of the connection. Moreover, lightweight concrete is more prone to cone expulsion than normal concrete.

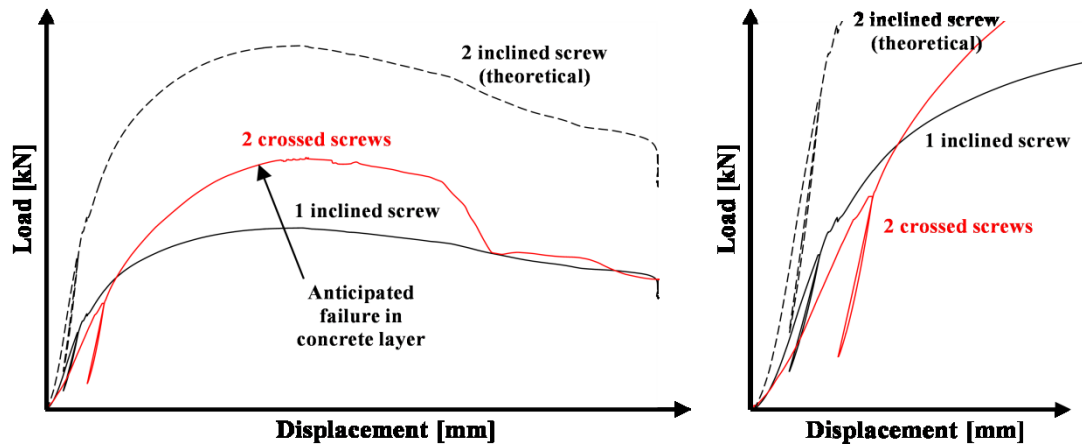


Fig. 1.15 – Qualitative comparison of the load–displacement for a CP realized with one or two screws for the same fastener diameter.

Table 1-2 – Experimental strength $F_{v,exp}$ and stiffness $K_{ser,exp}$ and yielding points ($F_{v,y}$; δ_y) for each specimen, average values and variation coefficient (COV). Values are referred to 6 CPs for A-series and to 4 CPs for X-series.

AN Series					AL Series					XN Series					XL Series				
Spec. ID	$F_{v,exp}$ (kN)	$K_{ser,exp}$ (kN/mm)	$F_{v,y}$ (kN)	δ_y (mm)	Spec. ID	$F_{v,exp}$ (kN)	$K_{ser,exp}$ (kN/mm)	$F_{v,y}$ (kN)	δ_y (mm)	Spec. ID	$F_{v,exp}$ (kN)	$K_{ser,exp}$ (kN/mm)	$F_{v,y}$ (kN)	δ_y (mm)	Spec. ID	$F_{v,exp}$ [kN]	$K_{ser,exp}$ [kN/mm]	$F_{v,y}$ (kN)	δ_y (mm)
8_1	75.4	60.2	37.7	0.7	8_1	89.6	36.3	44.8	2.0	8_1	69.4	24.2	34.7	1.4	8_1	68.2	23.6	34.1	1.5
8_2	78.9	40.9	39.4	1.2	8_2	96.0	34.5	48.0	1.7	8_2	82.3	22.8	41.1	1.9	8_2	62.4	38.7	31.2	1.1
8_3	81.2	54.0	40.6	0.9	8_3	86.3	43.5	43.1	1.8	8_3	68.0	21.0	34.0	2.2	8_3	65.2	17.2	32.6	2.3
8_4	79.8	53.3	39.9	1.0	8_4	96.9	44.1	48.4	2.2	8_4	76.8	20.1	38.4	2.7	8_4	62.0	31.0	31.0	1.1
Mean	78.8	52.1	39.4	1.0	Mean	92.2	39.6	46.1	1.9	Mean	76.2	22.4	38.1	2.0	Mean	64.4	31.1	32.2	1.5
COV	2.8%	13.7%	1.4%	19.9%	COV	4.9%	11.0%	2.4%	10.7%	COV	8.3%	7.5%	4.2%	24.2%	COV	4.0%	29.2%	2.0%	32.0%
10_1	85.2	63.2	42.6	0.9	10_1	88.1	45.9	44.1	1.2	10_1	98.2	41.5	49.1	1.4	10_1	79.1	28.4	39.5	1.5
10_2	104.1	60.1	52.0	1.5	10_2	114.3	51.9	57.2	2.0	10_2	111.0	23.2	55.5	2.3	10_2	87.8	31.3	43.9	1.6
10_3	97.3	53.3	48.7	1.1	10_3	110.9	48.1	55.4	1.3	10_3	104.7	44.4	52.4	2.9	10_3	85.0	27.8	42.5	1.5
10_4	107.7	51.1	53.8	1.2	10_4	122.9	44.5	61.4	1.9	10_4	90.0	20.3	45.0	2.5	10_4	83.9	31.2	42.0	1.4
Mean	98.6	56.9	49.3	1.1	Mean	109.0	47.6	54.5	1.6	Mean	101.0	32.4	50.5	2.3	Mean	83.9	29.7	42.0	1.5
COV	8.9%	8.8%	4.4%	19.3%	COV	12.0%	6.0%	6.0%	22.2%	COV	8.0%	34.1%	4.0%	25.5%	COV	3.9%	5.5%	1.9%	4.1%
12_1	128.2	70.5	64.1	1.2	12_1	122.2	55.6	61.1	1.3	12_1	117.0	65.7	58.5	1.8	12_1	104.5	34.2	52.2	1.6
12_2	129.2	65.5	64.6	1.3	12_2	110.6	46.5	55.3	1.2	12_2	121.5	47.5	60.7	1.9	12_2	102.3	38.0	51.2	1.5
12_3	111.1	66.2	55.5	0.8	12_3	112.5	62.4	56.3	0.9	12_3	115.0	30.3	57.5	2.2	12_3	108.5	34.6	54.2	2.3
12_4	118.0	42.4	59.0	1.8	12_4	109.5	56.3	54.7	1.0	12_4	105.5	25.8	52.8	2.1	12_4	106.6	30.4	53.3	1.9
Mean	121.6	61.1	60.8	1.3	Mean	113.7	55.2	56.8	1.1	Mean	114.7	42.3	57.4	2.0	Mean	105.5	34.3	52.7	1.8
COV	6.3%	18.3%	3.2%	27.7%	COV	4.5%	10.6%	2.3%	13.6%	COV	5.2%	38.4%	2.6%	8.0%	COV	2.3%	8.1%	1.1%	16.5%

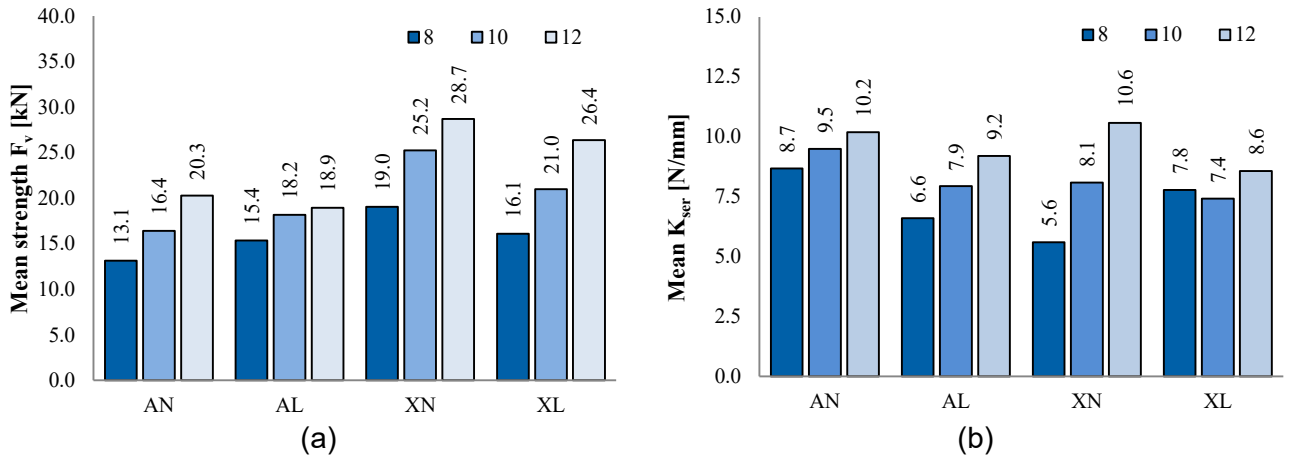


Fig. 1.16 – Experimental mean values of the shear capacity $F_{v,exp}$ (a) and service stiffness K_{ser} (b) varying screw diameter, screw configuration and concrete type (values are referred to a single CP).

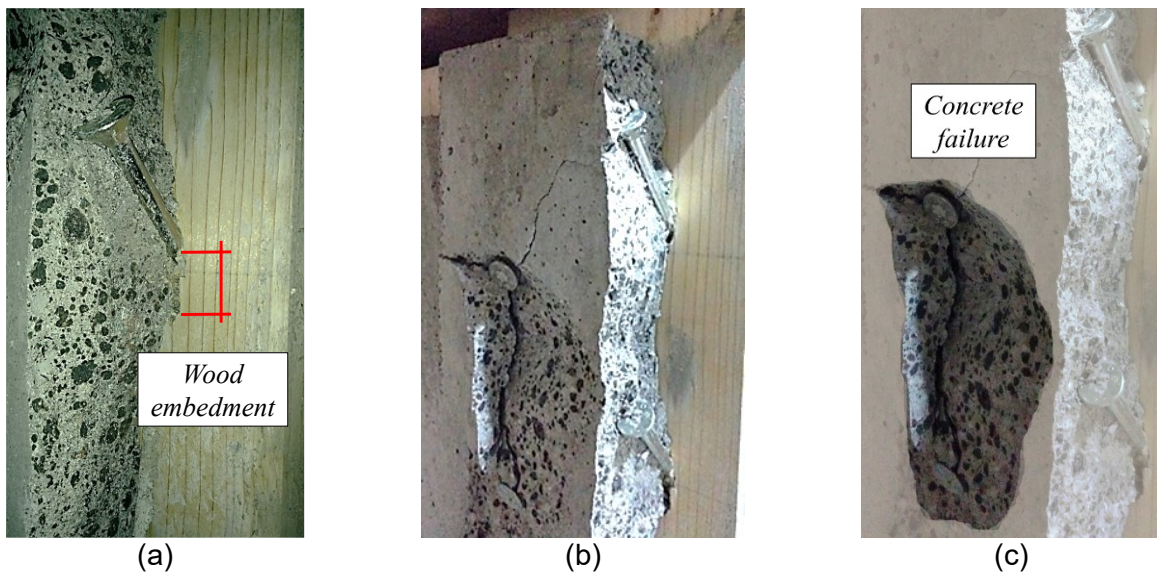


Fig. 1.17 – Failure mode of fasteners: (a) wood embedment for inclined screw configuration; (b) wood embedment with crossed screw configuration; (c) detail of concrete expulsion.

1.4 Comparison between experimental and analytical results

In this section the 5% characteristics values of load bearing shear strength $F_{v,exp}$ and stiffness $K_{ser,exp}$ derived from experimental tests are compared with analytical provisions. More specifically, the following parameters were adopted for the analytical calculation of strength with both the Eurocode 5 [1.13] method and the proposed approach described in section 1.2.1:

- Mean $\rho_m = 420 \text{ kg/m}^3$ and characteristic $\rho_k = 385 \text{ kg/m}^3$ wood density (see section 1.3.2);
- Friction coefficient $\mu = 0.25$ in compliance with the assumptions of Eurocode 5 [1.13];
- Characteristic yield moment $M_{y,Rk}$ and withdrawal strength $F_{ax,Rk}$ of screws calculated according their homologation certificate [1.54] with:

$$F_{ax,Rk} = f_{ax,k} \cdot l_{eff} \cdot (\rho_k / 350)^{0.8} \quad (1.39)$$

- Geometrical properties of screws like l_{eff} , d_{core} and head diameter d_h were also taken from homologation certificate [1.54];
- Characteristic wood embedment strength according to Eurocode 5 [1.13], with $d=1,1 d_{ef}$:

$$f_{h,k} = 0,082 \cdot (1 - 0,01 \cdot d) \cdot \rho_k \quad (1.40)$$

- Characteristic lateral strength $F_{lat,Rk}$ according to Eurocode 5 (i.e. Johansen's Theory model [1.44]) with the hypothesis of thick steel plate and with $d=1,1 d_{core}$;
- Lateral stiffness $K_{ser,\perp}$ of the screw calculated following Eq. (1.33) with $d=1,1 d_{ef}$, multiplied by a factor of 2;
- Axial stiffness $K_{ser,\parallel}$ of the screw calculated following recommendations reported in [1.54]:

$$K_{ser,\parallel} = 780 \cdot d^{0,2} \cdot l_{ef}^{0,4} \quad (1.41)$$

Table 1-3 summarizes the mean shear strength values $F_{v,exp}$, the 5% characteristic extrapolations $F_{v,Rk,exp}$ (obtained from statistical analysis of experimental results according to EN 14358 [1.64]) and the corresponding theoretical values calculated with both Eurocode 5 provisions [1.13] and the modified Johansen equations (Eqs. (1.25) and (1.32) – considering with $\mu = 0.25$). Table also includes the mean experimental instantaneous slip modulus $K_{ser,exp}$, and the corresponding theoretical values calculated with Eurocode 5 formulation and the modified approach.

Table 1-3 – Summary of experimental and theoretical results of F_v (with $\mu=0.25$) and K_{ser} , relative differences $\Delta F_{v,Rk}$ and ΔK_{ser} (calculated for each CP).

Series	Shear strength						Stiffness					
	Experimental		Theoretical				Experimental		Theoretical			
	Mean [kN]	k 5% [kN]	Eurocode 5		Eqs. 1.23, 1.30		Mean [kN/mm]	SD [N/mm]	Eurocode 5		Eq. 1.33	
		$F_{v,Rk}$ [kN]	$\Delta F_{v,Rk}$ [%]	$F_{v,Rk}$ [kN]	$\Delta F_{v,Rk}$ [%]			K_{ser} [kN/mm]	ΔK_{ser} [%]	K_{ser} [kN/mm]	ΔK_{ser} [%]	
AN-8	13.1	11.5	6.4	44.6%	8.3	27.2%	8.7	1.2	4.4	48.8%	5.9	31.7%
AN-10	16.4	12.8	8.4	34.4%	10.9	14.5%	9.5	0.8	5.3	44.5%	6.4	32.2%
AN-12	20.3	17.0	10.2	40.2%	13.3	22.1%	10.2	1.9	6.3	38.6%	7.0	31.6%
AL-8	15.4	13.4	6.4	52.7%	8.3	37.9%	6.6	0.7	4.4	32.7%	5.9	10.2%
AL-10	18.2	12.8	8.4	34.4%	10.9	14.5%	7.9	0.5	5.3	33.6%	6.4	18.9%
AL-12	18.9	16.5	10.2	38.4%	13.3	19.8%	9.2	1.0	6.3	32.0%	7.0	24.2%
Average values for A series			40.8%		22.7%				38.3%		24.8%	
XN-8	19.0	15.5	11.2	27.6%	13.9	10.2%	5.6	0.4	4.4	20.6%	5.6	-0.6%
XN-10	25.2	21.1	15.6	26.3%	18.4	12.9%	8.1	2.8	5.3	34.9%	6.2	23.3%
XN-12	28.7	25.0	19.1	23.8%	22.2	11.2%	10.6	4.1	6.3	40.9%	6.8	35.5%
XL-8	16.1	14.1	11.2	20.1%	13.8	2.1%	7.8	2.3	4.4	42.9%	5.6	27.6%
XL-10	21.0	18.3	15.6	15.1%	18.2	0.6%	7.4	0.4	5.3	29.0%	6.2	16.4%
XL-12	26.4	23.0	19.1	17.2%	22.0	4.4%	8.6	0.7	6.3	27.0%	6.8	20.4%
Average values for X series			21.7%		6.9%				32.5%		20.4%	

1.4.1 Load bearing capacity

Fig. 1.18 plot the experimental results for the obtained load bearing capacity and give a visual comparison between experimental and analytical predictions of both Eurocode 5 and modified approaches (dotted and dashed lines respectively).

With the inclined screw configurations the relative difference $\Delta F_{v,Rk} = 1 - (F_{v,Rk,th} / F_{v,Rk,exp})$ calculated with respect to theoretical provisions of Eurocode 5 varies between 34.4% and 52.7% with an average value of 40.8%. On the contrary, the modified approach proposed in section 2.1 for failure mode III provides better correspondence with experimental values as the mean relative difference $\Delta F_{v,Rk}$ is reduced to 22.7%. This confirms that contribution of the withdrawal capacity is relevant. If a friction value $\mu = 0.6$ is adopted, i.e. a value more appropriate for the case of direct contact between timber and concrete [1.65], such mean relative difference would further reduce to 11.0%.

The strength difference is less relevant in the crossed screws configurations: the adoption of a quadratic axial-shear strength domain for analytical evaluation allows for a mean $\Delta F_{v,Rk}$ of 21.7%. As the concrete expulsion leads to an early failure of the joint, usage of Eq. (1.25) also for shear-compression loaded screws leads to overestimating the total strength of the crossed screws. Only the inclusion of the concrete cone failure phenomenon (i.e. Eq. (1.31)) leads to a proper evaluation of the strength of the screws with inclination contrary to the load direction. The analytical approach proposed for crossed screws at 45° shows good fitting with experimental results (mean relative difference $\Delta F_{v,Rk} = 3.9\%$), thus demonstrating that neglecting frictional effects as well as the inclusion of concrete failure hypothesis are fundamental in the crossed screws configuration.

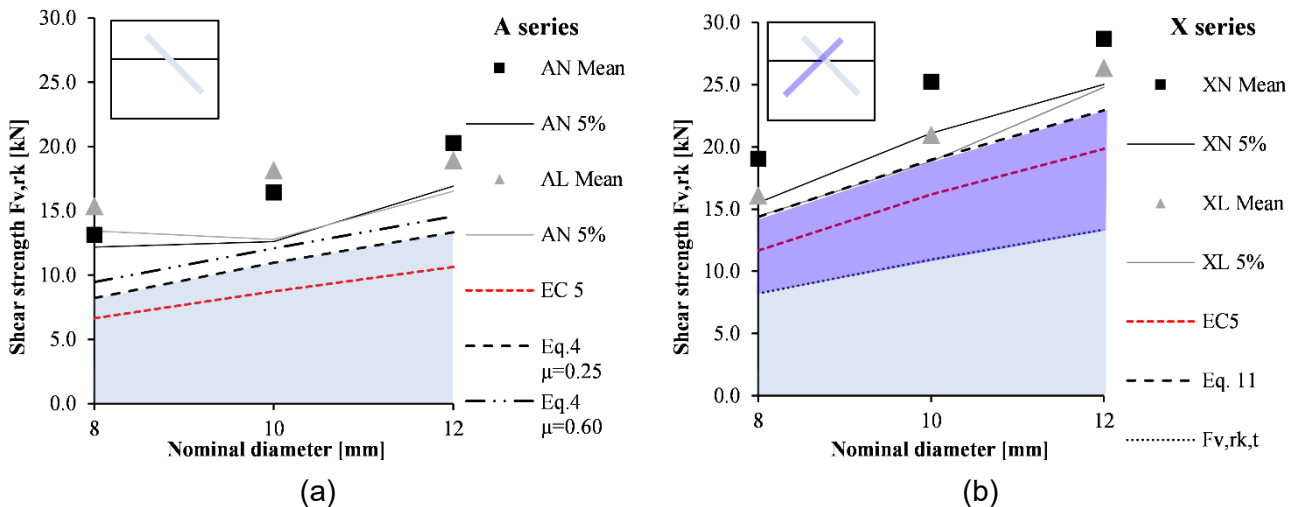


Fig. 1.18 – Experimental values of average shear strength $F_{v,exp}$ (dots) and 5% characteristic extrapolations (continuous lines) compared with theoretical predictions: (a) inclined screw series; (b) crossed screws series. Values are referred to a single CP. Filled area highlights the theoretical contribution of each screws in the global strength

1.4.2 Stiffness

The modified stiffness equations for K_{ser} proposed in Section 1.4.2 for the inclined screw at 45° - Eq. (1.35) - shows a finer matching with the experimental data than EC5 [1.13] predictions (see Fig. 1.19). The average relative difference $\Delta K_{ser} = 1 - (K_{ser,exp} / K_{ser,th})$ calculated with EC5 method is equal to 38.3%, while Eq. (1.35) does reduce this value to 24.8%. Additionally, in the proposed approach the concrete elastic modulus is not taken into account: further investigations would be needed to assess this phenomenon and eventually include this variable into the formulation.

Concerning the crossed screw configurations, it appears that the stiffness of the CP does not improve when a second inclined screw is added in the opposite direction. On the contrary, the second screw does decrease the CP stiffness in several circumstances. Calculating stiffness with Eurocode 5 recommendations considering only the shear-tensile loaded screw provides conservative results ($\Delta K_{ser} = 32.5\%$), but the modified approach (Eq. (1.35)) reduces such difference to 20.4%. This evidence demonstrates that the interaction between the two screws is indeed significant.

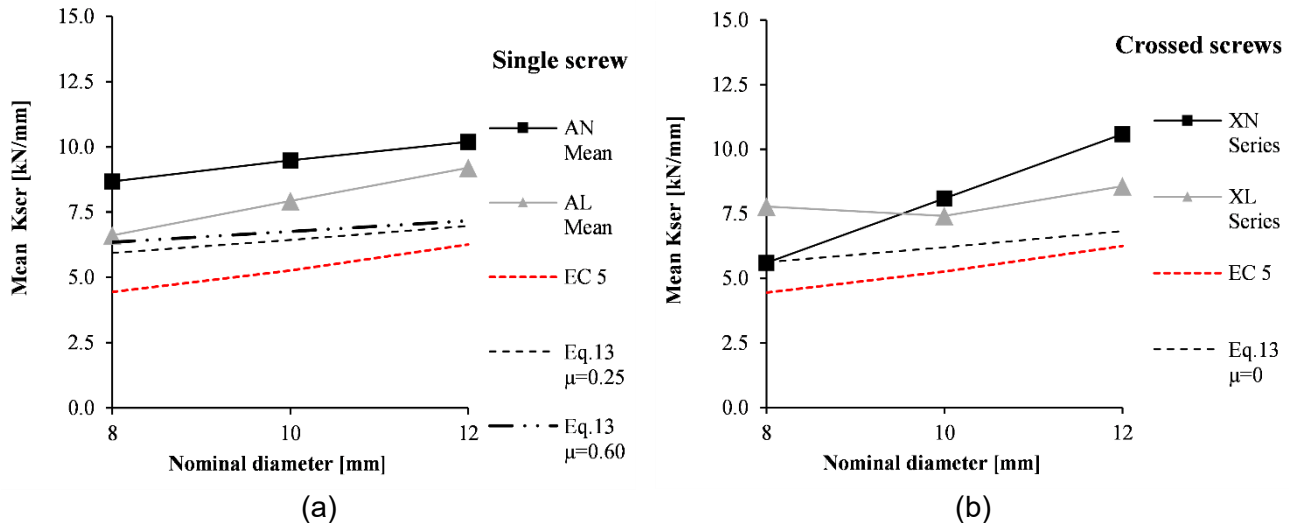


Fig. 1.19 – Experimental values of slip modulus K_{ser} compared with theoretical predictions: (a) inclined screws series; (b) crossed screws series. Values are referred to a single CP.

1.5 Conclusions

This chapter presented a detailed analysis on the behaviour of timber-concrete composite joints realized with self-tapping screws inclined at 45° . An analytical approach to calculate the load bearing capacity and stiffness of such connection was proposed as an extension of consistent literature models and reliable design rules.

Push-out tests were conducted and main mechanical properties were obtained by varying fastener diameter, installation configuration and concrete type.

The evaluation of the serviceability conditions of the connections in terms of load capacity and displacement were provided referring to the yielding condition of the experimental load-displacement curves according to the method proposed by Karacabeyli and Ceccotti. Regarding the evaluation of slip modulus, test showed limited scattering for the inclined screws connection and higher dispersion when a crossed screws configuration was adopted. A reduction in term of stiffness K_{ser} shifting from normal to lightweight concrete was also found in nearly all configurations, due to the expected lower concrete stiffness obtained with lightweight aggregates. Moreover, the contribution of the second screw is very limited when considering the overall stiffness of the CP and often leads to even lower values.

Outcomes from experimental tests were used to verify the reliability of the actual design method proposed by Eurocode 5 and to perform a preliminary validation of the proposed analytical approach.

Results showed that in the evaluation of the load bearing capacity, Eurocode 5 method underestimates strength of inclined screws at 45° resulting more reliable for crossed screw respect to inclined screws TCC joints. However, comparisons also shown that taking into account the screw

inclination and the contribution of the withdrawal capacity leads to a better correspondence with experimental behaviour from tests. According to the proposed approach, crossed screws in TCC connection might lead to a special failure condition with the expulsion of concrete cover, hence precautions when estimating the total shear-strength must be taken. Lastly, frictional effects could affect the resulting shear force obtained from push-out tests used to evaluate TCC connections performances in case of direct contact between timber and concrete.

As concerning the stiffness estimations, the comparison between the experimental results and the analytical estimation shows that Eurocode 5 method provide more conservative values respect to those provided by the proposed model. Moreover results demonstrate that the proposed formulation lead to more reliable estimation of the CP stiffness than simply neglecting the contribution of the shear-compressed screw as proposed by Eurocode 5.

However further researches are needed before the relationships proposed in this work could be incorporated in a code revision. They should focus on the evaluation of the actual contribute of friction and of a plausible μ value for timber-concrete connections. Finally, a more extensive and detailed experimental campaign should be conducted in order to better validate the proposed model and verify the reliability of the standard methods proposed by Eurocode 5.

Acknowledgments

The author would like to thank Fischer Italia s.r.l. for supplying materials and specimens for tests and Eng. Enrico Crivellaro for supervising tests.

References – Chapter 1

- [1.1] Van der Linden, M. (1999). "Timber concrete composite floors". Ph.D. Thesis Delft University of Technology, Netherlands.
- [1.2] Yeoh, D.E.C. (2010). "Behaviour and design of timber-concrete composite floor system". University of Canterbury, Christchurch, New Zealand.
- [1.3] Natterer, J., Hamm, J., and Favre, P. (1996). "Composite wood-concrete floors for multi-story buildings". In Proceedings of International Wood Engineering Conference, New Orleans, United States, Vol. 3, 431–435.
- [1.4] Mettem, C. (2003). "Structural timber-concrete composites - Advantages of a little known innovation". *The Structural Engineer*, **81(4)**:17-19.
- [1.5] Finnish Road Administration. (1999). "The Vihantasalmi Bridge— Mäntyharju, Finland 1997–1999." Available at: www.underwater.pg.gda.pl/didactics/ISPG/Mosty/Vihantasalmi%20bridge.htm.
- [1.6] Bathon, L., Bletz, O., and Schmidt, J. (2006). "Hurricane proof buildings - An innovative solution using prefabricated modular woodconcrete-composite elements". In Proceedings of the 9th World Conference on Timber Engineering (WCTE), 6-10 August 2006, Portland, Oregon, USA.
- [1.7] Lukaszewska, E., Fragiaco, M., and Johnsson, H. (2010). "Laboratory tests and numerical analyses of prefabricated timber-concrete composite floors". *Journal of Structural Engineering*, **136(1)**:46–55. ASCE.

- [1.8] Yeoh, D., Fragiaco, M., De Franceschi, M., and Heng Boon, K. (2011) "State of the art on timber-concrete composite structures: literature review". *Journal of Structural Engineering*, **137(10)**:1085–1095. ASCE.
- [1.9] Rodrigues, J.N., Dias, A. M., and Providência, P. (2013). "Timber-concrete composite bridges: State-of-the-art review". *BioResources*, **8(4)**:6630-6649.
- [1.10] Piazza, M., Baldessari, C., and Tomasi, R. (2008). "The role of in-plane floor stiffness in the seismic behaviour of traditional buildings". In *Proceedings of the 14th World Conference on Earthquake Engineering (WCTE)*, Beijing, China (pp. 12-17).
- [1.11] Baldessari, C. (2010). "In-plane behaviour of differently refurbished timber floors". Ph.D. Thesis, University of Trento, Italy.
- [1.12] Valluzzi, M. R., Garbin, E., Dalla Benetta, M., and Modena, C. (2010). "In-plane strengthening of timber floors for the seismic improvement of masonry buildings". In *Proceedings of the 11th World Conference on Timber Engineering WCTE*, Riva del Garda, Italy.
- [1.13] EN 1995-1-1 Eurocode 5 (2009). "Design of Timber Structures, Part 1-1, General: Common Rules and Rules for Buildings". CEN. Brussels, Belgium.
- [1.14] EN 1995-2 Eurocode 5 (2009) "Design of Timber Structures, Part 2, Bridges". CEN. Brussels, Belgium.
- [1.15] Newmark, N. M. (1951). "Tests and analysis of composite beams with incomplete interaction". *Proceedings of the Society for Experimental Stress Analysis*, **9(1)**, 75-92.
- [1.16] Möhler, K. (1956). "On the load carrying behavior of beams and columns of compound sections with flexible connections". Habilitation, Technical Univ. of Karlsruhe, Germany (in German).
- [1.17] Ceccotti, A. (2002). "Composite concrete-timber structures". *Progress in Structural Engineering and Materials*, **4(3)**:264-275.
- [1.18] Natterer, J., and Hoefl, M. (1987). "Zum Tragverhalten von Holz-Beton-Verbund-Konstruktionen" Forschungsbericht. (No. IBOIS-REPORT-1987-001).
- [1.19] Frangi, A., and Fontana, M. (2003). "Elasto-plastic model for timber-concrete composite beams with ductile connection". *Structural Engineering International: Journal of the International Association for Bridge and Structural Engineering (IABSE)*, **13(1)**:47-57.
- [1.20] Kuhlmann, U., and Schänzlin, J. (2001). "Grooves as shear connectors for timber-concrete composite decks". In *Proceedings of International RILEM Symposium on Joints in Timber Structures*. Stuttgart, Germany. pp.283–290.
- [1.21] Aicher S., Klöck, W., Dill-langer, G., and Radovic, B. (2003). "Nails and nailplates as shear connectors for timber-concrete composite constructions". *Otto-Graf-Journal*, **14**:189.
- [1.22] Turrini, G., and Piazza, M. (1983). "Una tecnica di recupero statico del solai in Legno". *Recuperare*, **5**:224-237 (in italian).
- [1.23] Gelfi, P., Giuriani, E., and Marini, A. (2002). "Stud shear connection design for composite concrete slab and wood beams". *Journal of Structural Engineering*, **128(12)**:1544-1550. ASCE.
- [1.24] Ceccotti, A. (1995). "Timber-concrete composite structures". *Timber engineering, Step*, **2(1)**.
- [1.25] Van der Linden, M. (1999). "Timber-concrete composite beams". *Heron*, **44(3)**: 215-239.
- [1.26] Gutkowski, R., Brown, K., Shigidi, A., and Natterer, J. (2008). "Laboratory tests of composite wood-concrete beams". *Construction and Building Materials*. DOI: 10.1016/j.conbuildmat.2007.03.013.
- [1.27] Fragiaco, M., Amadio, C., and Macorini, L. (2007). "Short and long-term performance of the "tecnaria" stud connector for timber-concrete composite beams". *Materials and Structures*. DOI:

10.1617/s11527-006-9200-2.

- [1.28] Dias, A.M.P. G., Lopes S.M.R., Van De Kuilen, J.W.G., and Cruz H.M.P. (2007). "Load-carrying capacity of timber-concrete joints with dowel-type fasteners". *Journal of Structural Engineering*, **133(5)**:720-727. ASCE.
- [1.29] Lukaszewska, E., Johnsson, H., and Fragiacom, M. (2008). "Performance of connections for prefabricated timber-concrete composite floors". *Materials and Structures*. DOI: 10.1617/s11527-007-9346-6.
- [1.30] Kuhlmann, U., and Aldi, P. (2008). "Fatigue of timber-concrete-composite beams: characterisation of the connection behaviour through push-out tests". In *Proceedings of the 10th World Conference on Timber Engineering (WCTE)*, 2-5 June 2008, Miyazaki, Japan.
- [1.31] Fernandez-Cabo, J. L., Arriaga, F., Majano-Majano, A., and Iñiguez-González, G. (2012). "Short-term performance of the HSB® shear plate-type connector for timber–concrete composite beams". *Construction and Building Materials*. **30**:455-462.
- [1.32] EN 1992-1-1 Eurocode 2 (2014). "Design of concrete structures, Part 1-1, General rules and rules for buildings". CEN. Brussels, Belgium.
- [1.33] Jorge, L.F., Schänzlin, J., Lopes, S.M.R., Cruz, H., and Kuhlmann, U. (2010). "Time-dependent behaviour of timber lightweight concrete composite floors". *Engineering structures*, **32(12)**:3966-3973.
- [1.34] Steinberg, E., Selle, R., and Faust, T. (2003). "Connectors for timber-lightweight concrete composite structures". *Journal of Structural Engineering*, **129(11)**:1538-1545. ASCE.
- [1.35] Jorge, L.F.C., Lopes, S.M.R., and Cruz, H.M.P. (2011). "Interlayer influence on timber-LWAC composite structures with screw connections". *Journal of Structural Engineering*. DOI: 10.1061/(ASCE)ST.1943-541X.0000299.
- [1.36] Dias, A.M.P.G., Cruz, H.M.P., Lopes, S.M.R., and van de Kuilen, J.W. (2010). "Stiffness of dowel-type fasteners in timber–concrete joints". *Proceedings of the Institution of Civil Engineers-Structures and Buildings*, **163(4)**:257-266.
- [1.37] Ringhofer, A., Brandner, R., and Schickhofer, G. (2015). "Withdrawal resistance of self-tapping screws in unidirectional and orthogonal layered timber products". *Materials and Structures*, **48(5)**:1435-1447.
- [1.38] DIN 571 "Hexagon head wood screws" Deutsches Institut für Normung, Germany.
- [1.39] Crocetti, R., Sartori, T., and Tomasi, R. (2015). "Innovative timber-concrete composite structures with prefabricated FRC slabs". *Journal of Structural Engineering*. DOI: 10.1061/(ASCE)ST.1943-541X.0001203.
- [1.40] Taazount, M., Amziane, S., and Molard, D. (2013). "Tangential behavior of nailed composite timber-concrete floor structures". *Construction and Building Materials*. DOI:10.1016/j.conbuildmat.2012.09.092.
- [1.41] Steinberg, E., Selle, R., and Faust, T. (2003) "Connectors for timber-lightweight concrete composite structures". *Journal of Structural Engineering*. **129(11)**:1538-1545.
- [1.42] Jorge, L.F.C., Lopes, S.M.R., and Cruz, H.M.P. (2011) "Interlayer influence on timber-LWAC composite structures with screw connections. *Journal of Structural Engineering*. DOI: 10.1061/(ASCE)ST.1943-541X.0000299.
- [1.43] Skinner, J., Bregulla, J., Harris, R., Paine, K., and Walker, P. (2014). "Screw connectors for thin topping, timberconcrete composites. *Materials and Structures*. DOI: 10.1617/s11527-013-0158-6.
- [1.44] Johansen, K.W. (1949). "Theory of timber connections". *International Association of bridge and structural Engineering*, Bern, p. 249-262.

- [1.45] Bejtka, I., and Blass, H.J., (2002). "Joints with inclined screws". In Proceedings of Meeting 35 of the Working Commission W18-Timber Structures, CIB, Kyoto, Japan. PAPER CIB-W18/35-7-4.
- [1.46] Kavaliauskas, S., Kvedaras, A. K., and Valiūnas, B. (2007). "Mechanical behaviour of timber-to-concrete connections with inclined screws". *Journal of Civil Engineering and Management*, **13(3)**:193-199.
- [1.47] Symons, D., Persaud, R., and Stanislaus, H. (2010). "Strength of inclined screw shear connections for timber and concrete composite construction". *Structural Engineer*, **88(1)**:25-32.
- [1.48] Moshiri, F., Shrestha, R., and Crews, K. (2014). "The Predictive Model for Stiffness of Inclined Screws as Shear Connection in Timber-Concrete Composite Floor". RILEM Bookseries. DOI: 10.1007/978-94-007-7811-5_40.
- [1.49] Tomasi, R., Crosatti, A., and Piazza, M. (2010). "Theoretical and experimental analysis of timber-to-timber joints connected with inclined screws". *Construction and Building Materials*. DOI:10.1016/j.conbuildmat.2010.03.007.
- [1.50] ACI 349-85 (1985). "Code Requirements for Nuclear Safety Related Concrete Structures". American Concrete Institute.
- [1.51] ACI 318-08 (2008). "Building Code Requirements for Structural Concrete and Commentary". American Concrete Institute.
- [1.52] European Organisation for Technical Assessment (EOTA) (2010). "ETAG 001: metal anchors for use in Concrete. Annex C: design methods for anchorages". Charlottenlund, Denmark.
- [1.53] Ringhofer, A., Brandner, R., and Schickhofer, G. (2015). "A universal approach for withdrawal properties of self-tapping screws in solid timber and laminated timber products". In Proceedings of International Network on Timber Engineering Research (INTER), meeting 48, 24-27 August 2015, Šibenik, Croatia. Paper INTER/48-7-1.
- [1.54] European Organisation for Technical Assessment (EOTA) (2016). "Self-tapping screws for use in timber structures". European Technical Approval ETA-11/0027. Charlottenlund, Denmark.
- [1.55] EN 14080 (2013). "Timber structures - Glued laminated timber and glued solid timber: Requirements". CEN. Brussels, Belgium.
- [1.56] EN 13183-2 (2002). "Moisture content of a piece of sawn timber - Estimation by electrical resistance method". CEN. Brussels, Belgium.
- [1.57] EN 12390-3 (2009). "Testing hardened concrete - Compressive strength of test specimens. CEN. Brussels, Belgium.
- [1.58] EN 26891 (1991). "Joints made with mechanical fasteners. General principle for the determination of strength and deformation characteristics". CEN. Brussels, Belgium.
- [1.59] Pozza, L., Scotta, R. (2015). "Influence of wall assembly on behaviour of cross-laminated timber buildings". *Proceedings of the ICE – Structures and Buildings*, **168(4)**:275-286.
- [1.60] Pozza, L., Scotta, R., Trutalli, D., and Polastri, A. (2015). "Behaviour factor for innovative massive timber shear walls". *Bulletin of Earthquake Engineering*. DOI:10.1007/s10518-015-9765-7.
- [1.61] Piazza, M., Polastri, A., and Tomasi, R. (2011). "Ductility of Joints in Timber Structures". *Proceedings of the ICE – Structures and Buildings*, **164(2)**:79–90.
- [1.62] Muñoz, W., Mohammad, M., Salenikovich, A., and Quenneville, P. (2008). "Need for a harmonized approach for calculations of ductility of timber assemblies". In Proceedings of Meeting 41 of the Working Commission W18-Timber Structures, St. Andrews, NB, Canada.
- [1.63] Karacabeyli, E., and Ceccotti, A. (1996). "Quasi-static reversed-cyclic testing of nailed joints". In

Proceedings of Meeting 29 of the Working Commission W18-Timber Structures, Universität Karlsruhe, Karlsruhe, Germany. PAPER CIB-W18/29-7-7.

- [1.64] EN 14358 (2016). "Timber structures - Calculation and verification of characteristic values". CEN. Brussels, Belgium.
- [1.65] Dias, A.M.P.G. (2004). "Experimental shear-friction tests on dowel-type fastener timber-concrete joints". In Proceedings of the 8th World conference on Timber Engineering (WCTE), 14-17 June 2004, Lahti, Finland.

Chapter 2 Development of an innovative TCC system using GFRP and modern screws

Abstract

An innovative connection system suitable for TCC structures is analysed in deep. The investigated connector combines the use of self-tapping screws and glass-fibre infilled thermoplastic polymer realized by injection moulding, introducing the latter material in the field of structural engineering. The aim is to enhance the use of inclined modern screws as TCC joints by solving installation issues typical of these connectors and avoid unwanted brittle failure that may develop in the concrete layer. Numerical simulations, carried out to design this joint, are described in detail. The results of experimental tests conducted to investigate the behaviour of the device subjected to shear loading conditions are reported. A comparison between numerical and experimental results and the analytical predictions described in the previous chapter is given.







2.1 Introduction and aims of the present work

2.1.1 State of the art of TCC joints realized with screws

The potential of employing modern screws as TCC connections have been analysed and carefully investigated in the academic world, as reported at the beginning of the previous chapter. The natural consequence of these research works was the introduction into the market of TCC connections, of several systems that exploit the respectable performance obtainable with modern timber screws. In the last two decades, several *dry* connection systems (i.e. systems that require only the mechanical work of installing the fasteners into the timber element) have been developed and successfully introduced. Table 2-1 lists the main TCC connections available in the Italian and part of European market that employ screws. Some solutions still make use of *traditional* fasteners (i.e. fasteners with a smooth shank and large diameter) placed orthogonal to the grain, but the actual market direction is the use of modern self-tapping screws placed at an angle of 30° to 45° with respect to the grain. Fastener nominal diameter d is normally comprised between 8 and 10 mm (higher diameters are to be preferably installed with a pre-drilling). The fastener length vary between a minimum of 100 mm to 160-200 mm or even more depending on the fastener withdrawal strength. The characteristic shear strength $F_{v,Rk}$, the serviceability stiffness K_{ser} and ultimate stiffness K_u are usually given separately in case of presence or absence of interlayer and for solid or glue-laminated timber.

These parameters are normally assessed via experimental tests according to the standards available for wood connections ([2.1]-[2.2]) once the material performance requirements and conditions have been guaranteed ([2.3]-[2.4]). Currently, no specific standards for timber-concrete composite connection exists. Alternatively, European Technical Assessments (ETAs) for the TCC specific application are provided, based on experimental proofs and analytical considerations in order to provide to the designer the necessary information on the connection's behaviour.

Table 2-1 – Examples of available products within the Italian market.

Connection system	Example	Characteristics	Fastener geometry
SFS VB Connector [2.5]		Pair of fasteners placed in crossed configuration (inclined at 45°)	d = 8.5 mm l = 100 ÷ 165 mm partial thread
LECA Centrostorico [2.6]		Single fastener inclined at 45° with a steel angular bracket	d = 10.0 mm l = 130 ÷ 150 mm partial thread
HECO PSV [2.7]		Three screws at 90° coupled with a plastic insert and an additional metal fixing	d = 8.0 mm l = 110 ÷ 145 mm partial thread
PETER COX® LPR [2.8]		Cold formed steel profile fastened with pairs of screws at 90°	d = 8.5mm l = 100 ÷ 135 mm partial thread
TECNARIA® Connettore Maxi [2.9]		Metal connector fastened with traditional screws at 90°	d = 10mm l = 100 ÷ 120 mm partial thread
WÜRTH® FT-Connector [2.10]		Inclined self-tapping screws at 30° with additional plastic element for precast systems	d = 8-10mm l = 150 ÷ 600mm full thread

2.1.2 Issues of TCC connections with screws

The advantages of TCC connections realized with inclined screws have been explicated in the previous sections however, this technique actually suffer from issues that are mostly related to the onsite installation. In particular, it must be recalled that these connections are rather fastened to the timber beam at the construction site without temporarily removing it from the structure, whereas in case of prefabricated solutions other typologies (e.g., notches, glued in steel plates) may be preferred. Additionally, the renovation of timber floors can mean setting up thousands of connectors per jobsite leading to a consequent increase of installation mistakes. The installation issues commonly arising for TCC connections with inclined screws can be summarized in:

- Incorrect application of the designed screw inclination (see Fig. 2.1a). This is the most important issue because increasing the inclination α with respect to the shear plane, for

example from 45° to 60° , does change the ratio between tensile and shear capacity and reduce significantly strength and stiffness ([2.11]-[2.12]);

- Incorrect penetration of the screw in the timber layer. A reduced penetration t into the timber side leads to a reduced load bearing capacity, especially in case of high-strength full threaded screws or with shorter screws employed with timber beams characterized by thin cross-sections;
- Insufficient anchoring to the concrete layer might involve a reduced load bearing capacity caused by anticipated concrete failure (short h_{eff} to develop the concrete cone). This concept, similar to the behaviour of metal anchors, is particularly critical with thin concrete layers. Additionally, stress concentrations are to be avoided with LWAC due to its greater tendency to split [2.13];
- High strength TCC joints realized with two screws in parallel may lead to incorrect spacing (see Fig. 2.1b) of the screws perpendicular to the beam (i.e. a_2 defined according to EC5 [2.14]). The result could be an unwanted group effect or anticipated brittle failures due to edge proximity.

In some cases, such issues have been partially overcome by providing to the workers specific accessories that accompany the insertion of the screw at the right angle and penetration ([2.6]; [2.10]). This *drilling template* is at times part of the connection system and is to be left in place after the screw is in position ([2.6];[2.7]). However, all these accessories have still some limitations/issues, for example: pre-installation is still delicate as they require to be glued or screwed to the timber beam before inserting the load-bearing screws in position; they are suitable for thick concrete layers [2.10], consequently cannot be adopted in high seismic prone areas where mass must be kept as low as possible.

The scope of this research is to develop and assess a system that overcome the aforementioned installation issues ensuring at the same times high strength and stiffness to the TCC joint. Differently from other connection systems, the self-tapping screws will be combined with a Glass Fibre Reinforced Polymer (GFRP) element realized by injection moulding. The choice of this material allows the realization of a “more engineered” shape of the connector than classic materials (see section 2.2.4), while ensuring great mechanical performance and a cost-efficient production.



Fig. 2.1 – Issues that might occur throughout the installation of many screws with an angle respect to the grain.

2.1.3 Thermoplastic materials in civil engineering

Composite materials are gaining more interests in the field of civil engineering due to their high performance, especially when comparing the strength/weight ratio with respect to traditional materials. Fibre reinforced polymers (FRP) have been deeply investigated in the past and are now often used in multiple structural engineering applications. They are mostly used as strengthening methods of existing structures and retrofitting interventions of buildings. They are available in the form of carbon fibre strips applied or in pultruded profiles. However, most of these applications utilize pre-impregnated thermosetting composites, the most common of which is carbon fibre-reinforced polymer (CFRP). On the contrary, thermoplastic materials are relatively new and lack the history of use in civil infrastructure [2.15]. Thermoplastic composites typically comprise a commodity matrix (e.g., polyethylene (PE), polyamide (PA)) reinforced with glass, carbon or aramid fibres. Generally, the matrix component affects the properties of the material when subjected to different environmental conditions (e.g., temperature and humidity) while the type and amount (percentage of filling) of fibres are mainly responsible for the overall mechanical performance. For example, the same Polyamide 6 with 15% of glass fibres has half of the strength and stiffness with respect to the same polymer reinforced with 50% of carbon fibres [2.15]. Several production methods are available to produce thermoplastic materials, however, the most common and used is the moulding process [2.16]. Injection moulding is a high efficiency process: once the injection moulds have been designed to the customer's specifications and the presses pre-programmed, the actual moulding process is very quick compared to other methods. Plastic injection moulding process hardly takes times and this allows more parts to be manufactured from a single mould. The high production output rate makes this method more cost effective and efficient. Furthermore, due to high pressure during the moulding process, complex and intricate shapes can easily be designed and manufactured which otherwise would have been too complicated and expensive to manufacture.

An important aspect to be accounted when complying with polyamides (PA) is that they are susceptible to environmental condition and their mechanical properties depend upon their moisture content. Therefore, the main mechanical parameters are usually defined on both *dry-as-moulded* (DAM) and *conditioned* state. DAM state correspond to the highest mechanical performance (e.g., in terms of elastic modulus, maximum tensile and bending stress, etc.) However, designers should always refer to the *conditioned* state, when the material have already reached its equilibrium with a specified temperature and relative humidity and, consequently, its actual performance. The rate of moisture absorption (i.e. the rate of conditioning) is a function of the temperature. For example, a 4 mm thick test specimen of PA66 requires more than a year to attain its equilibrium moisture content in standard atmosphere 23/50 [2.17]. To condition specimens in a relatively short period, higher temperatures are required, and most of the investigated materials have their properties evaluated after being accelerated ageing process of EN ISO 1110 [2.18]. As the loss in strength and elasticity can be conspicuous, high performance polymers nearly always include a significant amount of fibres, which normally vary between 10 and 60%. Lastly, GFRP are subjected to creep phenomena, which is also dependent of the percentage of filling.

Few research works that aims to use composite materials, in particular Glass Fibre Reinforced Polymers (GFRP), are known in Timber Engineering field. The only available works, presented by the University of Delft [2.19] and Bath ([2.20];[2.21]), concern the study of pultruded GFRP rods to realize dowel-type connections. Thermosetting polymers were used to realize dowel type fasteners subjected to shear loads with good results but Brandon et al. [2.22] found out that reaction to fire of the matrix made by polyester resin was not sufficient to guarantee reliable performance in case of fire.

2.1.4 Aim of this work

The scope of this research work is to develop and analyse a connection system for TCC structures realized by coupling modern steel self-tapping screws with a composite material element. The withdrawal of the screw is still entrusted for the load bearing capacity but the GFRP screw's socket is meant to undertake three purposes:

- To ensure the correctness of the screw insertion avoiding any installation-related issues;
- To provide a tight and secure pre-installation on the timber without additional screws or gluing operations;
- To avoid stress concentration at the fastener-concrete interface and consequent splitting failures that is to be expected especially in case of thin concrete layers and high-strength screws.

With regard to the third objective, thanks to the higher strength of GFRP materials with respect to concrete, the connector should act as a *cushion* element that distributes localized stress to larger areas. For example, this technique results of primary importance when high load-carrying capacity and stiffness are provided by screws with high withdrawal strength (e.g., full-threaded screws). In this case, the higher resistance provided on the timber side must be equalled (and exceeded, as ductile behaviours are to be preferred) by the resisting mechanism in the concrete layer (Fig. 2.2a). This translates into high stress concentration at the screw-concrete interface (i.e. the area in proximity to the shank and head of the screw), which must be limited, for example by increasing the contact area (Fig. 2.2b).

It is worth noting, that the modulus of elasticity E of a conditioned polyamide PA6 or PA66 with a percentage of filling near 50% vary between 10-12.5 GPa ([2.23];[2.24]) which is comparable the modulus parallel to the grain E_0 of a common solid timber. It is also roughly comparable to that of a LWAC. On the other hand, it has approximately seven times the ultimate stress than common timber and four times the strength of normal or lightweight concrete. Then, GFRP can be designed as an intermediate element between steel and concrete, which grant a smoother transition of stresses in the exchange of forces between fastener and concrete.

Consequently, it can be expected that once the mechanical behaviour of injection-moulded materials is more deeply comprehended, the local reinforcement of timber-to concrete or, more generally, all timber connections that suffer from high stress concentrations may be a promising field for future research works in structural engineering. In this context, this work could be an encouraging starting point from which to begin and develop new connections/devices in timber engineering adopting such innovative materials.

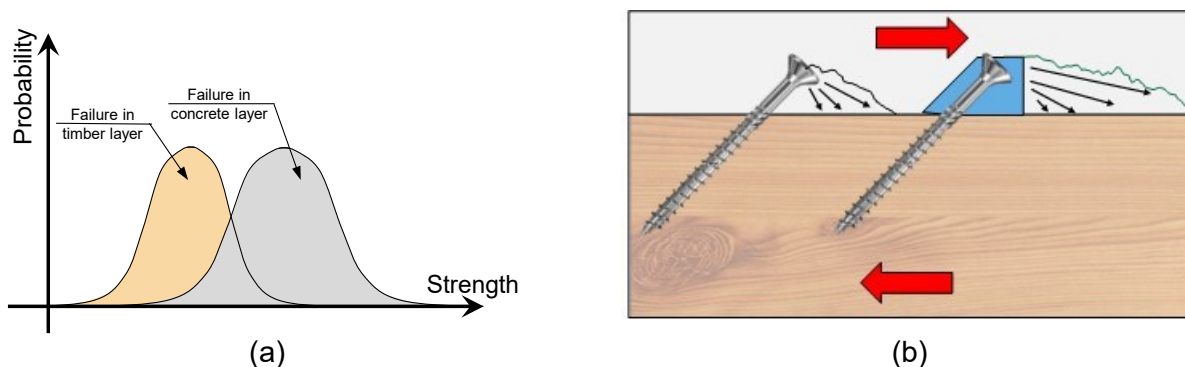


Fig. 2.2 – (a) capacity design applied to a TCC connection; (b) intended reinforcing effect of the GFRP element.

2.2 Design process assisted by FEM analyses

Assuming that the behaviour of TCC joints with inclined screws have been analytically derived and experimentally assessed, the design of the GFRP socket required the preliminary support of numerical simulations. The modelling technique presented in this work, was conceived to obtain sufficiently precise and realistic loading conditions in the GFRP component. The arising limitations that accompany the numerical model will be clarified in the next sections. The proposed finite element (FE) model followed a *hybrid* approach, i.e. a compromise between computational efficiency and reliability of results. The main hypotheses and features of the employed model were:

- The inelastic response of all the involved materials, i.e. isotropic plasticity was opted for steel and orthotropic plasticity for concrete and timber;
- Partial simplification of the screw-to-timber load transmission: withdrawal strength was modelled with an equivalent spring while lateral wood embedment was assured by contact elements;
- Splitting of timber due to tension stresses perpendicular to the grain was not included in the model. This simplification was supported by the analysis of the test results (see section 1.3.3), always confirming always a ductile failure (regarding the timber layer only);
- No damage model was taken into account for concrete, as the GFRP element shape must provide a geometry that assure a sufficient stress distribution to the concrete avoiding concrete splitting/crushing.

It must be emphasized that the last two hypotheses are consistent only for the investigated configurations and would need proper consideration in order to be applied in different circumstances.

As a brief summary, the modelling phase initially concentrated in the replication of the experimental tests conducted on screws presented in Chapter 1. Then, the GFRP component was added to the FE model to obtain important prediction particularly to the stress level for which the thermoplastic may be subjected. This, to avoid excessive stress concentration, optimize the shape and not less important, contain creep effects and consequently long-term deformations.

2.2.1 Details on the numerical modelling of the TCC joint

A three-dimensional FE model was developed with a commercial software [2.25] to reproduce the behaviour of the complete timber-to-concrete connection subjected to a monotonic load parallel to the shear plane.

Realizing a detailed model of a self-tapping screw fastened into the wood should be quite a straightforward task once the geometry is known and imported into the software to be *meshed* accordingly. However, it will almost certainly result into an high demanding problem due to the need of a high-order and refined mesh in order to simulate the load transmission occurring between the screw thread and the wood [2.26]. For this reason a simplified approach have been developed to obtain a balanced compromise between precision and computational effort.

Fig. 2.3 helps to clarify how the FE model was intended to work and to be calibrated. The self-tapping screw shape was simplified to a cylinder with diameter equal to 5.4 mm (i.e. the core diameter according to the tested screw geometry [2.27]). The transmission of the axial load component was obtained by means of a spring element, with stiffness equal to the axial stiffness K_{ser} calculated

according to Eq. (1.41) that connects the threaded part of the screw to the sides of the hole. The transmission of the lateral component was accounted through frictional contact elements (*CONTA174* and *TARGET170*) adopting an *augmented Lagrangian* formulation [2.27]. The orthogonal stiffness multiplier was set to 0.1 in order to help convergence and correctly allow the simultaneous crushing of the screw shank into the timber element and the detachment of the screw from timber at the opposite side of the fastener. With this model, the only necessary parameter to calibrate is the friction coefficient μ_s between screw and wood. This parameter govern the amount of load that translates into wood embedment. Lastly, the countersunk head shape was also modelled to account for the correct compression stress distribution that occurs in this area.

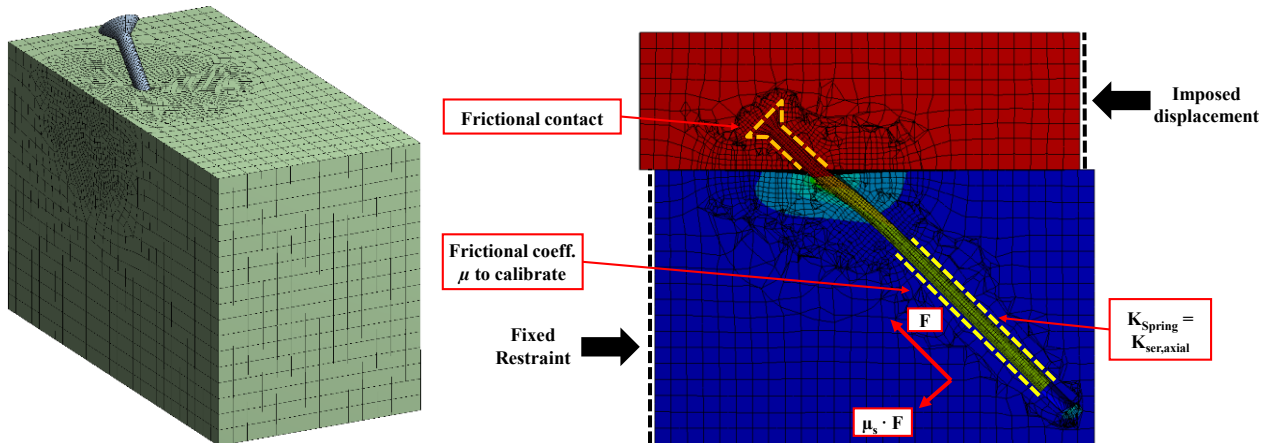


Fig. 2.3 – FE model: example of the 3D mesh (left) and load transmission model between screw and timber (right).

Additional contact formulations, available in the software library, were exploited to reproduce the interaction between the three materials. A *rough contact* formulation [2.27] was added between the screw head and the concrete. Friction between concrete and timber was assured by contact elements placed all along the sliding interface with a corresponding friction coefficient μ equal to 0.6, according to Dias et al. [2.29] and in agreement with the outcomes from the experimental tests (see Section 1.4.1). A distributed load was applied to the concrete layer on the side orthogonal to the loading direction. Lastly, boundary conditions were added to the timber element (see Fig. 2.3) thus forcing the correct displacements direction.

Yet, the numerical simulations were computationally demanding due to the multiple non-linearities included in the model and sufficient mesh refinement necessary to capture the wood embedment phenomenon. Therefore it was decided to split the analyses for SLS and ULS conditions:

- Analyses at service loading conditions (roughly 40-50% of the ultimate strength) where the connection is assumed to work mostly in the elastic field. In this case, material plasticity of concrete and timber was not required and the complete model was realized by means of high-order elements, in particular *SOLID186* and *SOLID285* elements (20-node *quadratic* elements and 4-node tetrahedral elements [2.30]) to evaluate stiffness and stress level on the GFRP element (to predict long-term phenomena). This model was mostly used in the initial calibration phase and for the prediction of possible creep deformations.
- Analyses at near collapse loading conditions where material orthotropic plasticity was activated but elements were necessary downgraded to low-order *SOLID45* elements [2.30]. Patch conforming meshing options combined with *automeshing* function implemented into the software were necessary to investigate the zones where plastic strains concentrates (i.e. near the plastic hinge of the connector and in the timber areas in which embedment should occur). This model was exploited to investigate the connection at higher loads where

deformation in the timber layer due to wood embedment are higher. It was used also for the design phase of the GFRP element.

2.2.2 Modelling of materials

Timber

Modelling timber material for numerical analyses of joints is a widely investigated topic ([2.31]-[2.39]) and due to the orthotropic nature of the raw material from which is obtained (i.e. sawn wood), several studies were conducted starting from experimental evidence. However, quite a few issues need to be overcome in order to obtain congruent results and sufficient precision when predicting the non-linear behaviour of timber, among which there is the material anisotropy.

In particular, timber is characterized by three orthogonal directions that behave differently: a longitudinal direction (or parallel to the grain) and a radial and a tangential direction, which are orthogonal to the first. Additionally, an elastic-plastic behaviour characterizes timber in all directions and the yielding limits, from which large strain occurs, are different in each direction. Lastly, the behaviour of timber under compression stresses can be described by an elastic-plastic law with hardening, while for tension stresses the material is essentially elastic and characterized by brittle failures.

In spite of these issues, some simplification have been demonstrated to be acceptable and overcome part of them. In particular, a common interpretation introduced in structural engineering is the equality of behaviour on the plane orthogonal to the fibres, thus switching from an orthotropic behaviour into an ideal transversal orthotropic one. Then, for preliminary work timber can be modelled assuming an orthotropic linear elastic constitutive law, however the definition of the main mechanical parameters (Modulus of elasticity E and Poisson's ratio ν may be difficult to determine [2.33]. It should be at least necessary to model the elastic-plastic behaviour of timber by neglecting the hardening effect of compression loads with an elastic – perfectly plastic law.

The yield criterion to be associated with the constitutive models is an important topic that is continuously discussed in literature ([2.31];[2.33]-[2.36]). The commonly adopted yielding criterion is the Hill's criterion [2.40], which is a generalized form of the Von Mises yield principle created to account for anisotropy of materials. Further studies aimed to find possible solutions to refine this model and take into account the inequality between compression and tension failures that characterizes timber. Tsai-Wu strength criterion [2.41] and Hoffman [2.42] were studied in ([2.35];[2.36]) with numerical analyses replicating experimental evidences finding that the combination of Hill and Hoffman method was suitable to replicate the non-linear behaviour of dowel-type joints in timber. It is worth noting that these models are suitable for monotonic loading as they work hardening is involved and therefore are not recommended for cyclic loading analyses.

In this work, the modified Hill criterion was used. Timber was modelled as an elastoplastic orthotropic material with mechanical properties obtained from EN 14080 [2.43] for a GL24h solid timber and indication contained in [2.44] for the Poisson's ratios (see Table 2-2). According to [2.32], no distinction was made between the radial (subscript r) and tangential (subscript t) direction with respect to fibre, even if in reality they vary by a factor of two. Yielding limit were assumed equal to the characteristic values reported in EN 14080 [2.43] and the tangent moduli were set equal to 0.01 times the Elastic values. It must be emphasized, that for dowel-type joints stressing timber orthogonally to the grain and causing brittle failures due to splitting, constitutive models that capture both ductile and fragile failures coupled with damage-based equations ([2.45]-[2.46]) can be used.

Table 2-2 – Orthotropic material properties chosen for GL24h.

Parameter	Notations	Notations	Value (MPa)	Parameter	Notations	Notations	Value (MPa)
Elastic Modulus	E_X	E_L	11500.00	Tensile yield stress	σ_X^t	σ_L^t	19.20
Elastic Modulus	$E_Y = E_Z$	$E_T = E_R$	300.00	Tensile yield stress	σ_Y^t	σ_T^t	2.50
Elastic Tangent modulus	$E_{X,t}$	$E_{L,t}$	115.00	Tensile yield stress	σ_Z^t	σ_R^t	2.50
Elastic Tangent modulus	$E_{Y,t} = E_{Z,t}$	$E_{T,t} = E_{R,t}$	3.00	Compressive yield stress	σ_X^c	σ_L^c	24.00
Shear Modulus	G_{XY}	G_{LT}	886.88	Compressive yield stress	σ_Y^c	σ_T^c	2.50
Shear Modulus	G_{ZY}	G_{RT}	125.94	Compressive yield stress	σ_Z^c	σ_R^c	2.50
Shear Tangent modulus	$G_{XY,t}$	$G_{LT,t}$	8.87	Shear yield stress	τ_{XY}	τ_{LT}	2.17
Shear Tangent modulus	$G_{ZY,t}$	$G_{RT,t}$	1.26	Shear yield stress	τ_{ZY}	τ_{RT}	0.82
Poisson's ratio	ν_{XY}	ν_{LT}	0.29				
Poisson's ratio	ν_{ZY}	ν_{RT}	0.38				
Poisson's ratio	ν_{YX}	ν_{TL}	0.01				

Steel

The steel of the screws used as connecting element between timber and concrete have been assumed as an elastoplastic material with a Modulus of Elasticity E equal to 210 GPa and Poisson ratio of $\nu = 0.25$. The yielding stress σ_y equal to 750 MPa was extrapolated from the yielding moment formulation of the screw and the screws geometrical properties included in the homologation document [2.27] and validated through a preliminary numerical simulation of the screw subjected to bending adopting the equivalent core diameter:

$$M_{y,Rk} = 0.15 \cdot 600 \cdot d^{2.6} \quad (2.1)$$

$$\sigma_y = M_{y,Rk} / W_{pl} = 750 \text{ MPa} \quad (2.2)$$

A tri-linear stress vs. strain curve (see Fig. 2.4b) was used by omitting horizontal yielding branch and assuming infinite yielding after the maximum stress is reached [2.33]. An isotropic behaviour was chosen for the constitutive law as well as for the yielding criterion.

Concrete

The concrete non-linear behaviour can be described according to section 3.1.2 of EN 1992-1-1 (Eurocode 2 [2.47]) with the following stress vs. strain relation:

$$\frac{\sigma_c}{f_{cm}} = \frac{k\eta - \eta^2}{1 + (k - 2)\eta} \quad (2.3)$$

where the compressive strength σ_c is correlated to the strain ε_c by the mean elastic modulus E_{cm} and the mean compressive strength F_{cm} with the following expressions:

$$\eta = \varepsilon_c / \varepsilon_{c1} \quad (2.4)$$

$$k = 1,05 E_{cm} \times |\varepsilon_{c1}| / f_{cm} \quad (2.5)$$

ε_{c1} is the nominal ultimate strain according to Eurocode 2 [2.47]. From the compressive tests of concrete cubes (see section 1.3.2), the following constitutive laws plotted in Fig. 2.4b were obtained for both normal and lightweight concrete. An ultimate strain ε_{c1} equal to 0.0035 was assumed for normal concrete and equal to 0.00178 for lightweight aggregate concrete. In this work, the concrete

material model used exploited a parabola-rectangle relationship, also included in Eurocode 2 [1.32]. The hypothesis that concrete failure should not occur with the investigated connection permitted to avoid using damage models to evaluate the concrete state of stress.

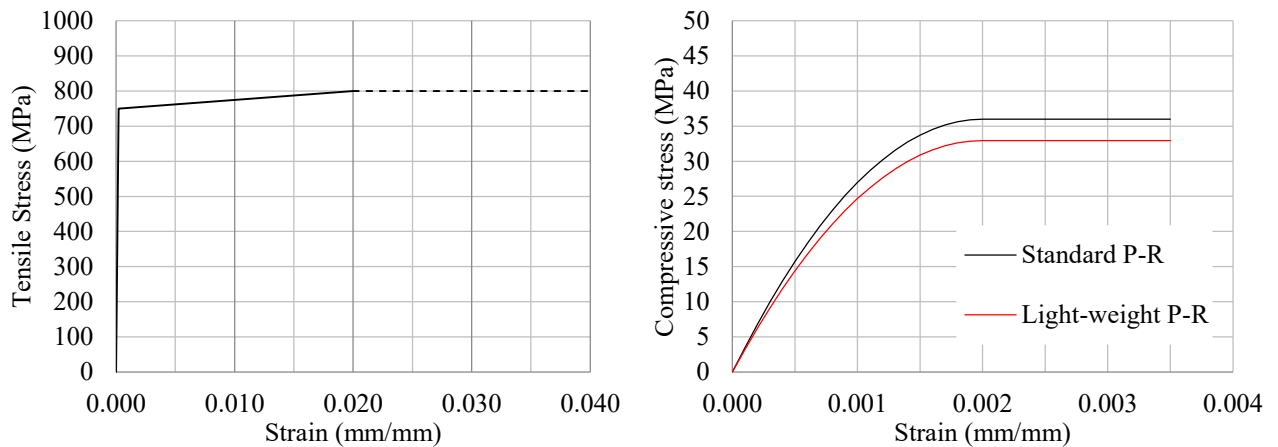


Fig. 2.4 – Stress vs. strain relations employed for the steel (left) and concrete (right).

Thermoplastic material

Modelling thermoplastic materials is still a discussed issue, in particular whether such materials are to be considered anisotropic or isotropic. In fact, fibre orientation induced by the injected material flowing into the mould causes localized anisotropy in the final product but from a macroscale perspective the material can be still considered as homogeneous and isotropic. The first hypothesis is often assumed in the design of the mould, where direction of flow, pressure and temperature gradients are all taken into account. The latter hypothesis is normally assumed in the engineering design process of a component, consequently will be acknowledged also in this work.

The thermoplastic material selected for the TCC joint is Domamid® 6G50 300 BK (A1-005-V50-B), a Polyamide 6 with a glass fibre filling of 50% and for which technical specifications extrapolated from [2.23]-[2.24] are reported in Fig. 2.5. In detail, it was chosen an inelastic isotropic constitutive law (see Fig. 2.6) with modulus E set equal to 11,000 MPa and the stress strain failure limits (σ_u, ϵ_u) were set to 145 MPa and 0.045 respectively. Additionally, the correctness of the stress-strain relationship was verified by replicating experimental tests of available non-structural components realized with the same material. The tested element, a bracket system used to support ventilated facades substructures, was tested monotonically until failure. An excerpt of one of the tested configuration and the comparison between experimental and numerical results are reported in Fig. 2.7.

Nylon based materials are susceptible to creep phenomenon and, consequently, an increase of long-term deformations which might reflect in a progressively reduced service stiffness K_{ser} of the connection system. A way to control this phenomenon is to limit the stress levels (at the serviceability conditions). According to [2.48] and to creep curves of GFRP materials with similar properties, the strain increments due to creep might be limited to acceptable values if the stress is under 80MPa. Isochronous curves are often made available by producers to help designers predicting long-term strains and therefore with their support more detailed consideration regarding the designed element are given in Section 2.3.6.

TYPICAL PROPERTIES	CONDITION	STANDARD	UNIT	VALUE
PHYSICAL				
Density		ISO 1183	[g/cm ³]	1,56
Moisture absorption	sat., 23°C, 50% RH	ISO 62	[%]	1,7
Mold shrinkage parallel	72 hrs, 23°C, 50% RH	ISO 2577	[%]	0,38
Mold shrinkage transverse	72 hrs, 23°C, 50% RH	ISO 2577	[%]	1,1
RHEOLOGICAL				
Melt Volume Rate (MVR)	275 °C - 5,0 kg	ISO 1133	[cm ³ /10 min]	22
Viscosity number		ISO 307	[ml/g]	145
MECHANICAL				
				dam / cond.*
Tensile modulus	1 mm/min	ISO 527	[MPa]	17000 / 11100
Tensile stress at break	5 mm/min	ISO 527	[MPa]	220 / 145
Tensile strain at break	5 mm/min	ISO 527	[%]	2,5 / 4,4
Tensile stress at yield	5 mm/min	ISO 527	[MPa]	215 / 145
Flexural modulus	5 mm/min	ISO 178	[MPa]	13300 / 8250
Flexural strength	5 mm/min	ISO 178	[MPa]	340 / 230
Charpy unnotched	+23 °C	ISO 179/1eU	[kJ/m ²]	100 / 100
Charpy notched	+23 °C	ISO 179/1eA	[kJ/m ²]	14 / 25
THERMAL				
Melting point		ISO 11357-1	[°C]	221
BURNING BEHAVIOUR				
Flammability	1,5 - 3,0 mm	UL 94	[Class]	HB

Fig. 2.5 – Domamid® A1-005-V50-B technical datasheet.

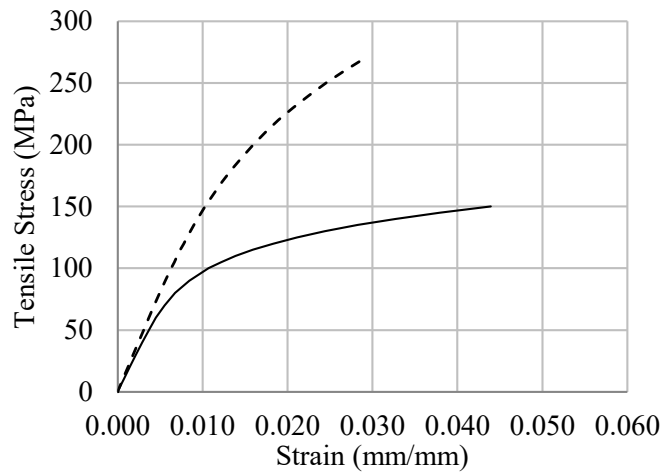


Fig. 2.6 – Stress vs. strain relations on DAM (dashed line) and conditioned state (continuous line) of GFRP.

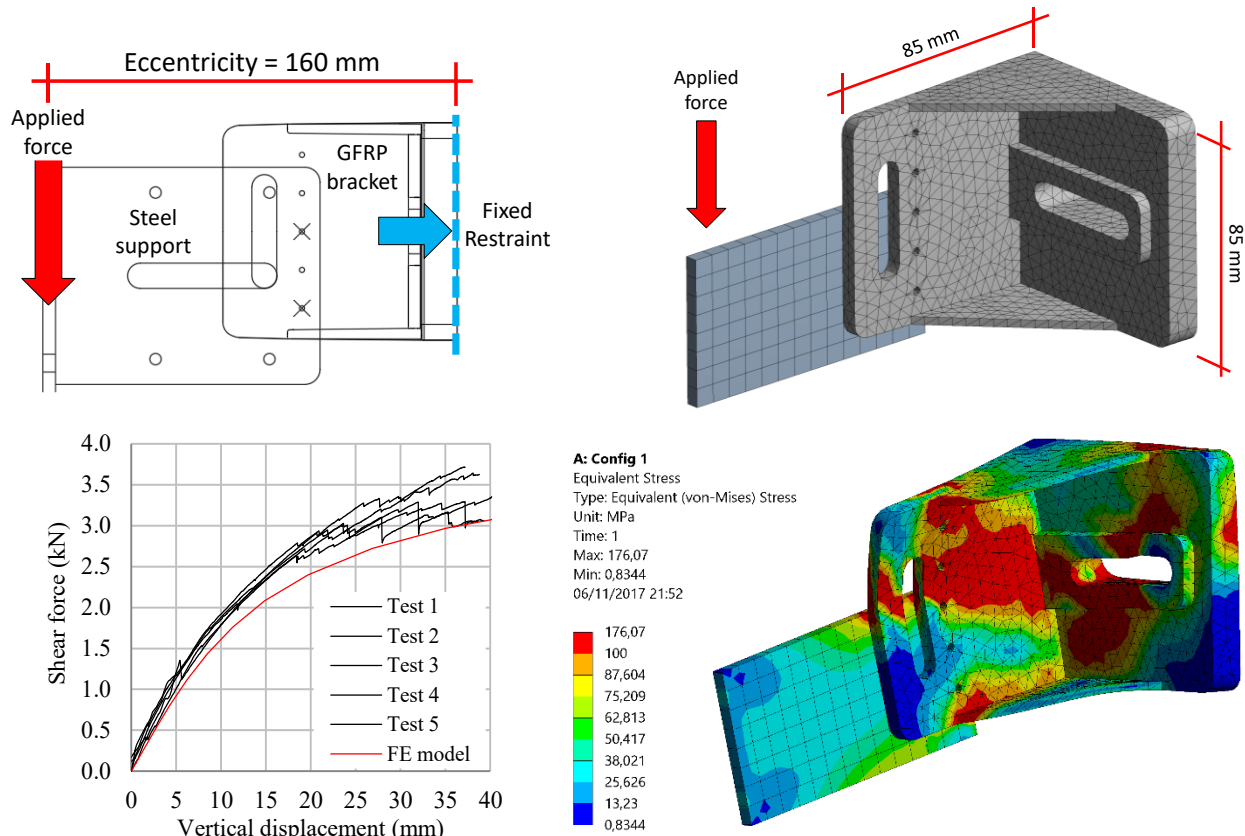


Fig. 2.7 – Excerpt of the material model calibration on the tested conditioned brackets made with GFRP.

2.2.3 Calibration of the numerical model

The numerical model was calibrated by replicating experimental tests of the inclined screws with normal concrete (AN series) and crossed screws with LWAC (XL series). Calibration consisted in finding a plausible friction value μ_s (reported in Table 2-3) of the contact area between screw and timber to match the stiffness experienced in tests $K_{ser,exp}$. Stiffness from FE model was calculated likely to the experimental test, namely between 0.1 and 0.4 of the estimated shear load $F_{v,est}$ (i.e. Eq. (1.38)). As calibration of the stiffness concerns only the initial branch of the force vs. displacement curve (in this case up to 2 mm) these analyses were mostly conducted with the SLS model. The ULS model, which included the Hill potential criterion, was used investigate the connection at higher displacements. However, due to the high demanding computational resources analyses at ULS were conducted only for the AN series. Fig. 2.8 and Fig. 2.9 show a visual comparison between the experimental and numerical force vs. displacement curves. A value of $\mu_s = 0.55$ resulted to be applicable for the case of shear-tension loaded screw.

Table 2-3 – Calibration of frictional parameter μ_s of the stiffness K_{ser} (in kN/mm) between experimental evidence and numerical simulations.

Screw configuration	Inclined screws		Crossed screws	
Concrete type	Normal concrete		Lightweight concrete	
$K_{ser,exp}$	8,68	-	7,75	-
$K_{ser,fem} (\mu_s=0.00)$ (kN/mm)	4,80	44.7%	6,51	16.0%
$K_{ser,fem} (\mu_s=0.15)$ (kN/mm)	5,19	40.2%	7,34	5.3%
$K_{ser,fem} (\mu_s=0.40)$ (kN/mm)	6,33	27.1%	8,50	-9.7%
$K_{ser,fem} (\mu_s=0.55)$ (kN/mm)	7,46	14.0%	8,73	-12.7%

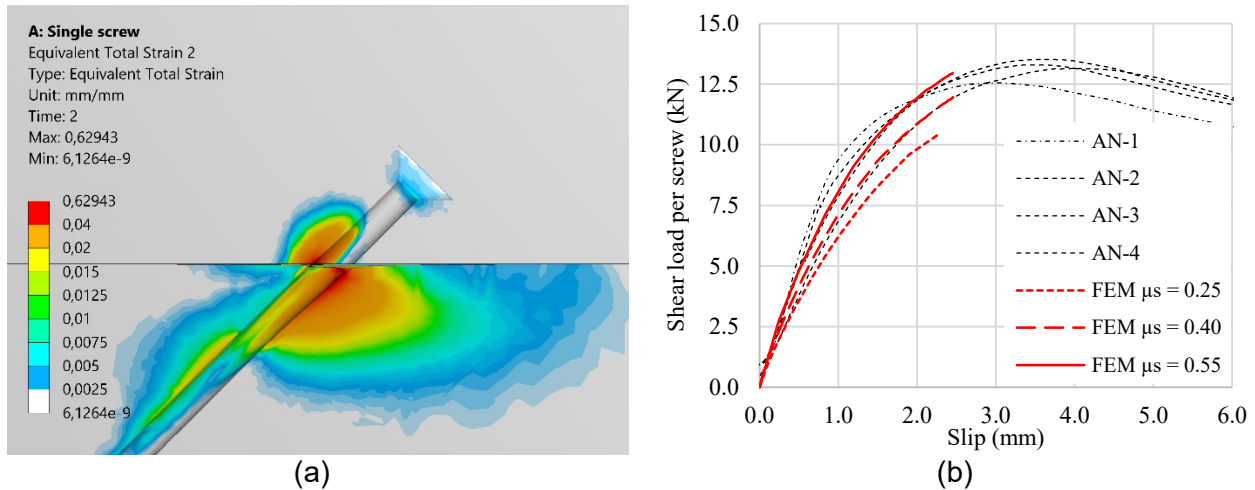


Fig. 2.8 – Inclined screw results: (a) total accumulated strains at 12.0 kN of shear load; (b) load vs. slip curves.

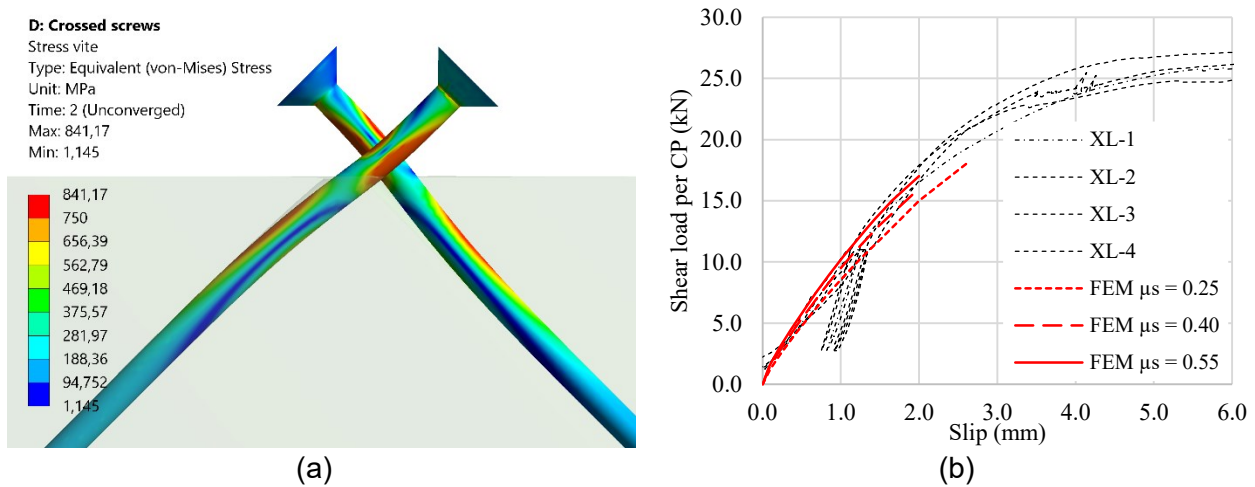


Fig. 2.9 – Crossed screws results: (a) double hinges development (displacement x5 times); (b) load vs. slip curves.

2.2.4 Design of the GFRP element

Although mechanical tests described in Chapter 1 confirmed an increase of shear strength and stiffness proportional to the fastener diameter, a nominal diameter of 8 mm was found to be suitable for this project. In particular, the main assumption was to use higher Connection Point (CP) spacing, by placing two screws in parallel for each CP and using a single GFRP connector for the couple of inclined screws. Consequently, screw spacing orthogonal to the grain direction ($a_2 \geq 4d$) and edge distance ($a_4 \geq 2.5d$) according to Eurocode 5 [2.14], had to be limited by using 8-mm timber screws. Additionally, the beams of timber floors subjected to strengthening are usually characterized by thin cross-sections, which makes more difficult the installation of large diameter fasteners and increase the risk of brittle failures for beams that may be prone to longitudinal cracking. Lastly, from a preliminary cost benefit analysis, the strength increase obtained from an 8-mm to a 10-mm screw was not justified by the increase of production costs from the first to the second diameter.

With the aim to solve the installation issues, improve easiness of use and realize a cost-efficient solution, the element:

- Should be used as a guide for the screw to be inserted at 45° and fix the screw at the correct depth in both concrete and timber layer;

- Should be also used as spacer for the steel mesh which is incorporated in the concrete layer;
- Should be pre-installed quickly without need of particular accessories or mechanical tools;
- Should be moulded from a two-part die in order to keep production costs low;
- Should have dimensions optimized for thin structures. Most of concrete slabs thickness vary from 5 to 6cm to keep weight as low, especially in the retrofitting of simple timber floors;

Preliminary experimental and numerical investigations were performed to define the gross-sections and element thicknesses. The final trapezoidal shape was refined with subsequent optimizations (see Fig. 2.10). During the refinement process, 3D prototypes were also realized by stereolithography (see Fig. 2.11). These prototypes proved to be very useful in the evaluation of the easiness of installation.

First samples (Rev_0 and Rev_1) incorporated squat teeth at the bottom shrill providing neither capacity to block the connector on the timber surface nor stability to for the screw insertion. These samples incorporate two orthogonal hollows placed at the bottom to block the steel mesh intersection. Subsequently, this feature was removed as it resulted to be inapplicable even with slight variations of the steel mesh arrangement.

In Rev_2, a feature to help longitudinal spacing along the beam was included in the zone between the two screws. The *undercut* shape given to the three sides opposing to the concrete compression was considerably improved. This to obtain an efficient clamping effect whilst simplifying the overall shape and adapting it to the needs of moulding process.

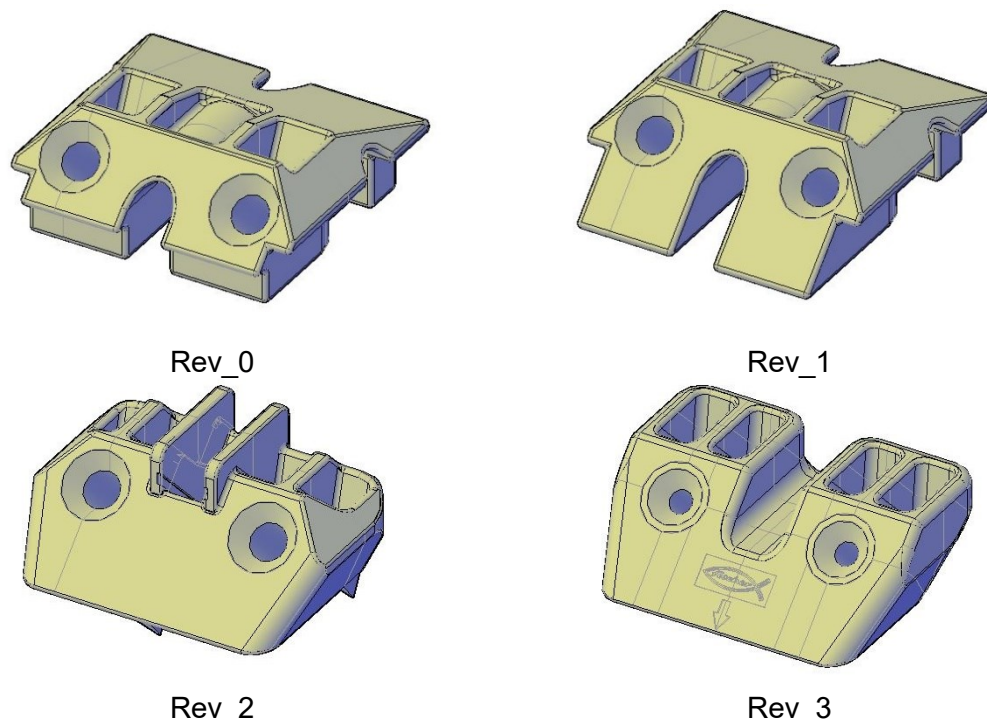


Fig. 2.10 – Evolution of the connector's shape during the design process.



Fig. 2.11 – Prototypes realized by stereolithography.

The final shape (Rev_3) consist of a hollow block of GFRP with outer dimensions of 75x60x25 mm including the following features (see Fig. 2.12):

- Sloping/undercut on all three sides to improve the clamping effect to the concrete layer; a wider surface opposing to the concrete increase the development of the concrete cone leading to a higher strength on the concrete side thus ensuring ductile failure;
- 10-mm sharp teeth at the bottom to ensure the positioning and blocking of connector during the screw insertion. The shape of the teeth were refined and tested carefully until the complete blocking of the element occurred with only a couple of rubber mallet hits;
- 12-mm wide hollow used to support the steel wire mesh comprised in the concrete layer; as usual wire diameters are between 6 and 8 mm a non-perfect alignment of connectors is allowed;
- Conical hollows suitable for countersunk head screws to reduce stress concentration transferred to the GFRP element.

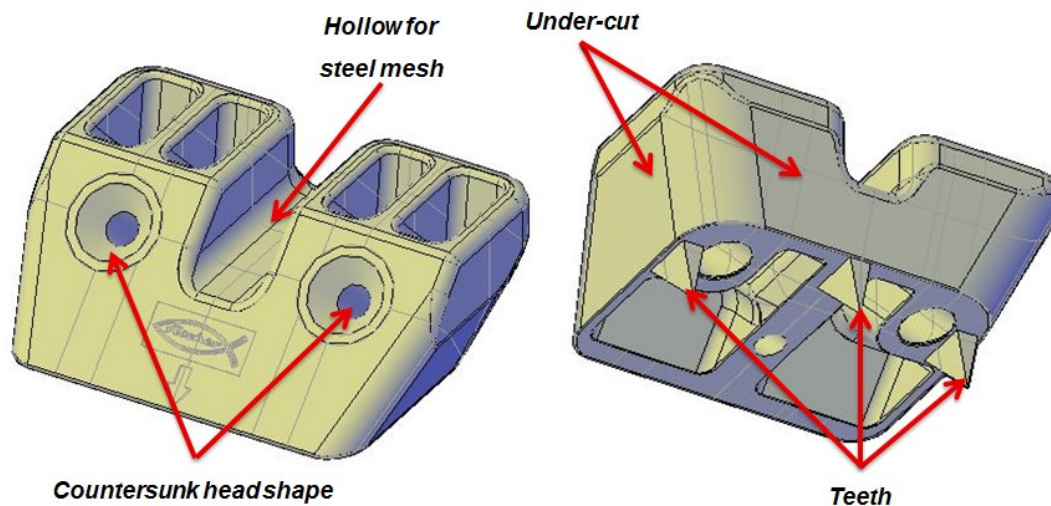


Fig. 2.12 – Main features of the GFRP connector.

In this case, the ULS model was used to predict the behaviour of the connection. Results of the numerical simulations are reported in Fig. 2.13 and are referred to the final shape. Observing the load vs. slip curves analysis, it emerges a slight decrease of the initial stiffness due to the gap present between the screw shank and the GFRP hole. Then, screw start again to work in tension and develop the same stiffness as the screw-only configuration. However, this issue should be overcome easily by employing full thread screws that avoid this initial *bending* effect. The inelastic strains at screw-to-timber and connector-to-concrete interfaces have been considerably mitigated (in comparison to

Fig. 2.8a). This ensure a much better coupling with the concrete and helps to distribute the stress concentration that affected the screw-only configuration (see Fig. 2.13d).

The higher stress in the GFRP part are localized in proximity to the screw's head and will be further examined in the evaluation of long term deformations predictions caused by creep (see section 2.3.6).

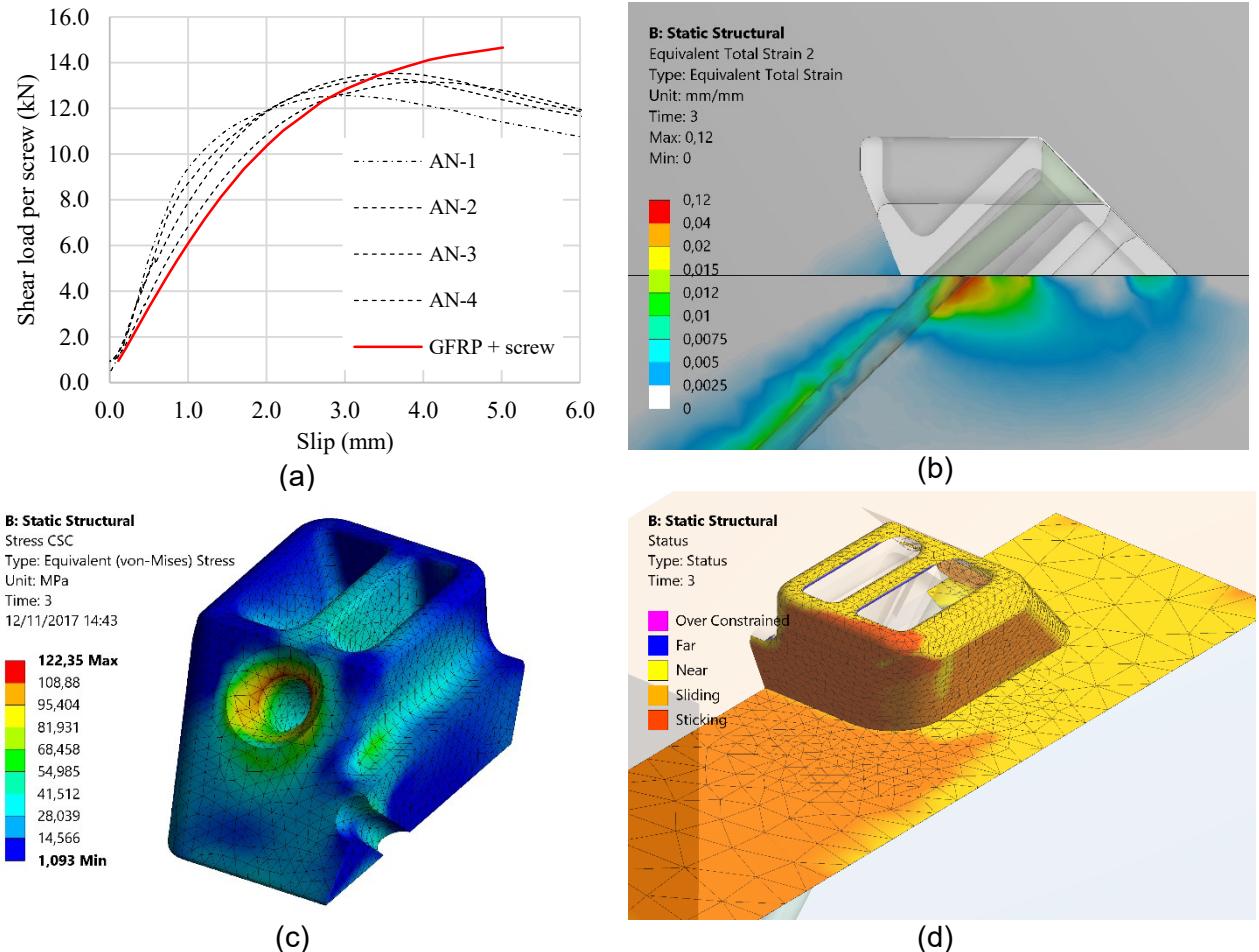
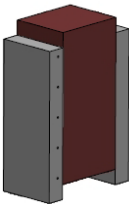
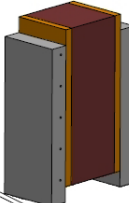


Fig. 2.13 – FE simulation results: (a) load vs. slip curve per single screw; (b) total accumulated strain; (c,d) equivalent Von Mises stress and contact status measured at 12.0 kN of shear load per screw.

2.3 Experimental tests

Experimental tests were conducted at the Construction Materials Testing Laboratory of the Department of Civil, Environmental and Architectural Engineering of the University of Padova, to assess the mechanical performance of the studied connector. Eight different configurations, each one comprising five specimens (40 specimens in total, configured according to Table 2-4), were tested varying the screw withdrawal strength, concrete type and presence of an interlayer between timber and concrete.

Table 2-4 – Summary of the tested specimen's characteristics.

ID	Presence of Interlayer	Concrete type	Screw Type	N° of connectors / N° of screws	N° of tests
NA_PT		Normal concrete	Partial thread	4 / 8	5
NA_FT			Full thread	4 / 8	5*
LA_PT		Light weight concrete	Partial thread	4 / 8	5
LA_FT			Full thread	4 / 8	5
NB_PT		Normal concrete	Partial thread	4 / 8	5
NB_FT			Full thread	4 / 8	5*
LB_PT		Light weight concrete	Partial thread	4 / 8	5
LB_FT			Full thread	4 / 8	5

* 2 of the 5 specimens used an increased length of 195 mm

2.3.1 Specimen geometry

The same push-out configuration and geometry described in Section 1.3.1 was employed for the tests. Two connectors (4 screws) were fastened on each side of the specimen. Details of the connector's arrangement and spacing are reported from Fig. 2.14 to Fig. 2.16. Spacing of the fasteners a_1 parallel to the grain was calculated to avoid any interference between the connectors. The theoretical effective number n_{ef} was calculated according to EC5 [2.14] with the following expression:

$$n_{ef} = \min \left(n ; n^{0.9} \cdot \sqrt[4]{\frac{a_1}{13 \cdot d}} \right) \quad (2.6)$$

where d correspond to the outer thread diameter.

A 6-mm thick 100x100 mm steel mesh was placed in the middle of the concrete layer to help possible anticipated failure due to concrete splitting. Such phenomenon was evidenced in preliminary test with full thread screws in which no reinforcing bars were disposed. This should underline that, for component tests of TCC high-strength joints and thin concrete topping, splitting could easily occur and anticipate the ductile failure in the timber side.

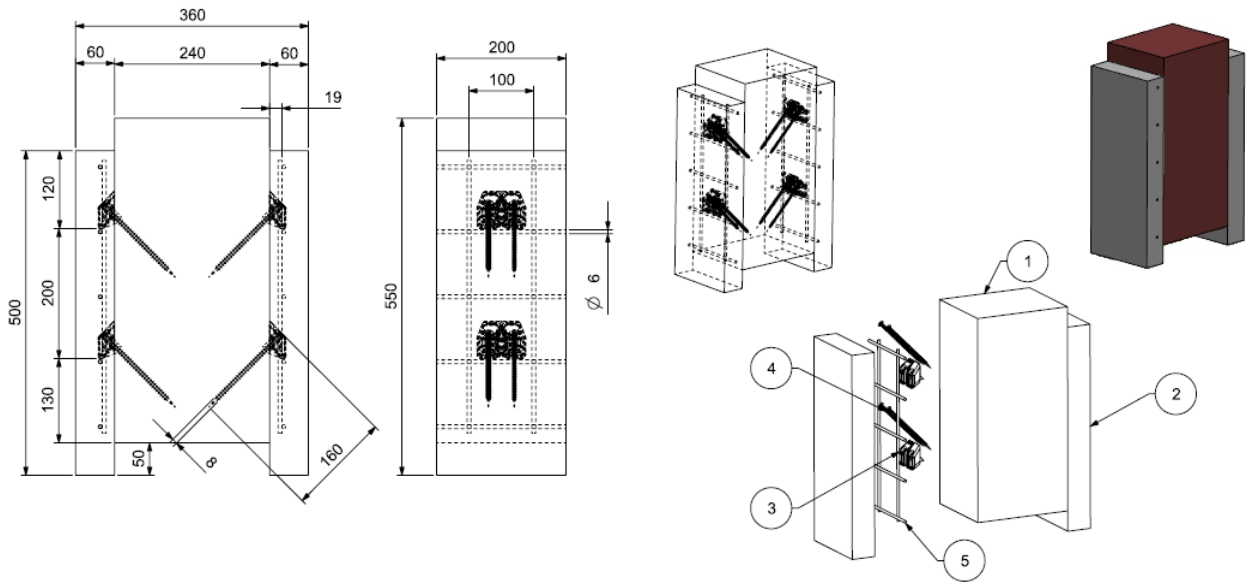


Fig. 2.14 – Geometry of specimens without interlayer.

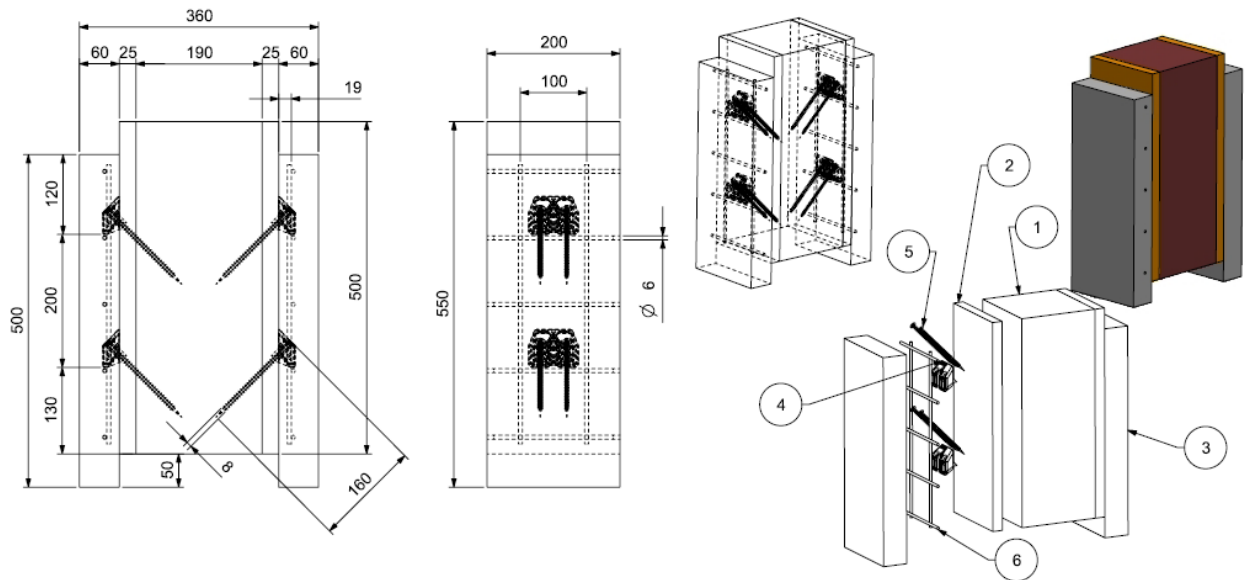


Fig. 2.15 – Geometry of specimens with a 25-mm timber planks interlayer.

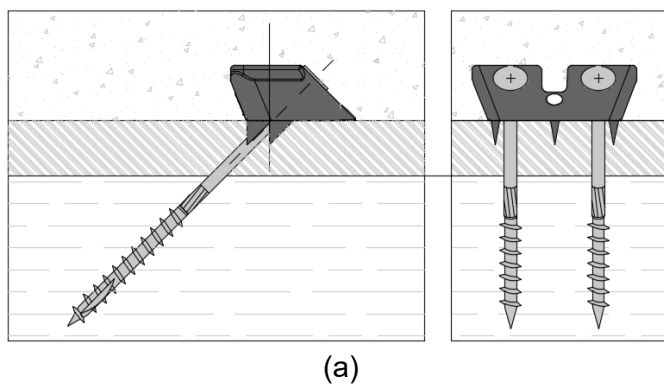


Fig. 2.16 – Detail of Connector and screw installation onto the timber beam.

2.3.2 Material and test setup

The timber used for fabricating the test specimens is spruce (*Picea abies*) glued laminated timber of strength class GL24h according to EN 14080 [2.43] with nominal characteristic and mean density values of $\rho_k = 385 \text{ kg/m}^3$ and $\rho_m = 420 \text{ kg/m}^3$ respectively. 25-mm thick timber boards were used to simulate the interlayer and nailed with small diameter nails, thus allowing slip of the layer of boards with respect to the timber beam. Moisture content was determined on each specimen with a pin-type thermo-hygrometer providing a mean value of 11.6%.

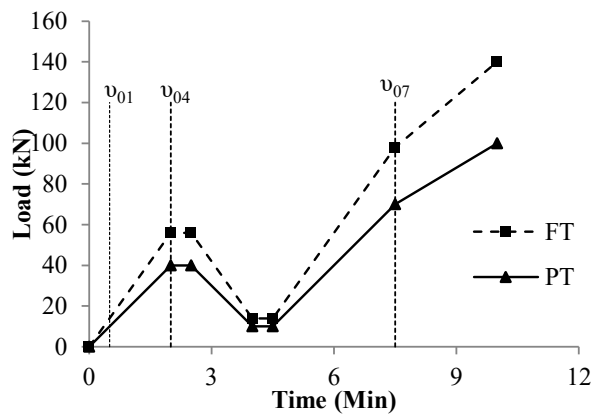
The screws used to fasten the nylon-based connector in the timber element involve a partial thread and full thread shank, henceforth named PT and FT screws respectively. Both screws have nominal diameter d equal to 8 and main geometrical parameters are reported in Table 2-5. A total length of 160 mm was suitable to allow the whole tread of the PT screws to be placed in the timber beam also for the specimens with the interlayer, thus exploiting its maximum withdrawal strength F_{ax} (see Fig. 2.16). FT screws have a shorter thread pitch from PT screws, which increases the withdrawal capacity according to its homologation document [2.49]. Checks of minimum spacing and edge distance were done according to Eurocode 5 [2.14] (calculated with $d = d_{nom}$) to avoid possible group effects.

Table 2-5 – Screw characteristics according to ETAs ([2.27];[2.49]).

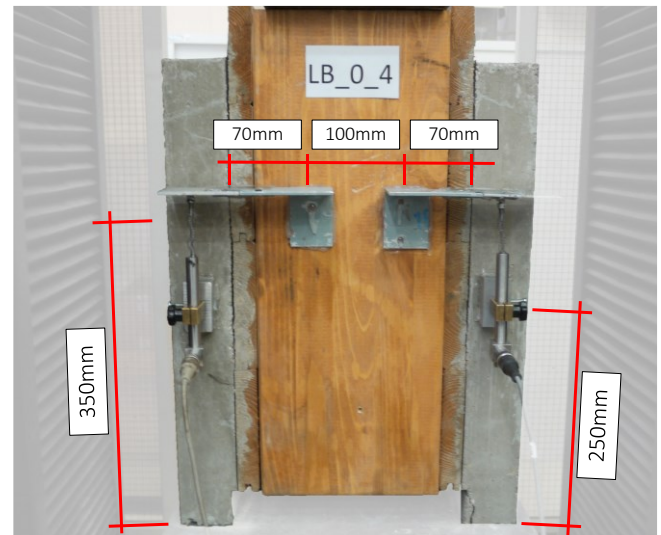
Parameter	Nominal length	Threaded length	Nominal diameter	Core diameter	Head diameter	Thread pitch
(units)	l (mm)	l _{eff} (mm)	d (mm)	d _{core} (mm)	d _{head} (mm)	p (mm)
Partial thread screws (PT)	160	80	8.0	5.4	6.0	6.0
Full thread screws (FT)	155/195	145/185	8.0	5.2	5.2	5.2

The mechanical performance were evaluated by compressive tests on cubes for each of the four groups of specimens according to EN 12390 [2.50] and the corresponding mean elastic modulus E_{cm} was calculated following Eurocode 2 provisions. For normal concrete the measured mean uniaxial compressive strength was $f_{cm} = 37.01 \text{ MPa}$ and a corresponding elastic modulus of $E_{cm} = 32.575 \text{ GPa}$ was calculated. For lightweight aggregate concrete corresponding values were $f_{cm} = 25.53 \text{ MPa}$ and $E_{cm} = 15.414 \text{ GPa}$ respectively. Characterization tests on concretes were performed just before the start of push-out tests.

EN 26891 [2.51] loading protocol was used to evaluate main mechanical parameters of the connection. The total estimated force, on which the loading procedure was calibrated (see Fig. 2.17a), was evaluated by analytical prediction using the theoretical model described in section 1.2.1.2. An $F_{v,est}$ value of 140 kN and 100 kN were calculated for full-thread and partial thread screws respectively. The vertical load was applied to the central timber beam and relative slip were measured by a couple of Linear Variable Differential Transducers (LVDTs) placed according to Fig. 2.17b.



(a)



(b)

Fig. 2.17 – (a) loading protocol calculated according to [2.51]; (b) specimen with interlayer on the testing machine and position of LVDTs.

2.3.3 Test results

Fig. 2.18 to Fig. 2.21 illustrate the force-displacement curves obtained from tests according to EN 26891 [2.51] allowing a parallel comparison between the load capacity reached with by FT and PT screws. In this case, loads are referred to the total load applied to the specimen, while plotted displacement are the mean values measured by the couple of LVDTs. A ductile failure took place in all specimens and, as expected, the connection with FT screws and absence of interlayer (NA_FT and LA_FT series) achieved the highest peak shear strength $F_{v,peak}$ due to their high withdrawal strength. In detail, a combined withdrawal of the screw and partial wood embedment phenomena near the timber-concrete interface was observed in all specimens (see Fig. 2.22). In general, wood embedment was less evident than the screw only-tests, especially when the interlayer was present (according to similar tests available in [2.52]), showing that the shear contribution became minimal in this case. It is worth noting that the composite socket was almost intact and no significant cracking effects were observed in the concrete slab (also due to presence of the reinforcing steel mesh).

Table 2-6 summarize the average values and COV of the measured shear strength $F_{v,Rk,exp}$, serviceability stiffness $K_{ser,exp}$ and the calculated conventional yielding point $F_{v,y}$, d_y (determined like in screw only tests with $F_{v,y} = 0.5F_{v,exp}$ and $d_y = d(F_{v,y})$ [2.53]). The total estimated load $F_{v,est}$ matched with the average strength values obtained in all the eight configurations. Scattering of the measured peak shear strength was always limited with a maximum COV of 6.3% and 15.2% for NA and NB series respectively. Also the average stiffness $K_{ser,exp}$ showed less dispersion than the screw-only tests and did not affect specific series with respect to other. Regarding the conventional yielding point, it emerges that FT screws manifested higher yielding strength F_y but higher yielding displacement d_y (of about $0.3 \div 0.5$ mm). This should be taken into account when designing a TCC structures that an increased relative slip must be accepted. Analysing the load vs. slip curves and the visual comparison of the mean results for strength and stiffness reported in Fig. 2.25 and Fig. 2.26, the impact of each analysed variable could be summarized as follows:

- *Concrete type*: no substantial differences were measured on the load bearing capacity between the normal concrete topping and LWAC topping when slab and timber beam were in direct contact (i.e. no interlayer was present). Only the combination of PT screws and presence of interlayer produced a noteworthy reduction of the load bearing capacity from normal to LWAC. The reduced stiffness of LWAC does not significantly affect the serviceability stiffness $K_{ser,exp}$, with respect to the screw only tests reported in the previous chapter. This should be attributed to the fact that besides from the concrete topping, the screw is in contact only with the GFRP socket, which has a lower Elastic modulus than normal concrete and closer to the one of LWAC.
- *Interlayer presence*: The interlayer presence seems not to produce any significant changes for the shear strength demonstrated by partial thread screws as all the threaded part is kept on the timber beam on both configurations. On the contrary, the decrease measured on FT screws specimens is clearly due to the lower penetration and effective threaded length l_{eff} between NA_FT and NB_FT series causing a reduction of the withdrawal capacity. Regarding stiffness $K_{ser,exp}$, the observed reduction of the mean values occurred with the interposition of the timber boards are comprised in the range of 10-15%, contrary to *traditional* connections [2.54]. The observed uniform reduction is due to the lower penetration of the screw in the timber element and perhaps to the additional eccentricity of the shear load which causes additional shear deformation to the fasteners;
- *Type of screws*: strength increases with FT screws according to the higher withdrawal parameter $f_{ax,k}$ and higher effective length l_{eff} in the timber element. Regarding the serviceability stiffness $K_{ser,exp}$, a uniform decrease was observed when PT screws were substituted with FT screws, whereas switching between the two concrete types provided negligible variations in all studied cases. As a consequence, the mean yielding displacement d_y shifted from a range of 1.4-2.0 mm to values between 2.0-2.5 mm.

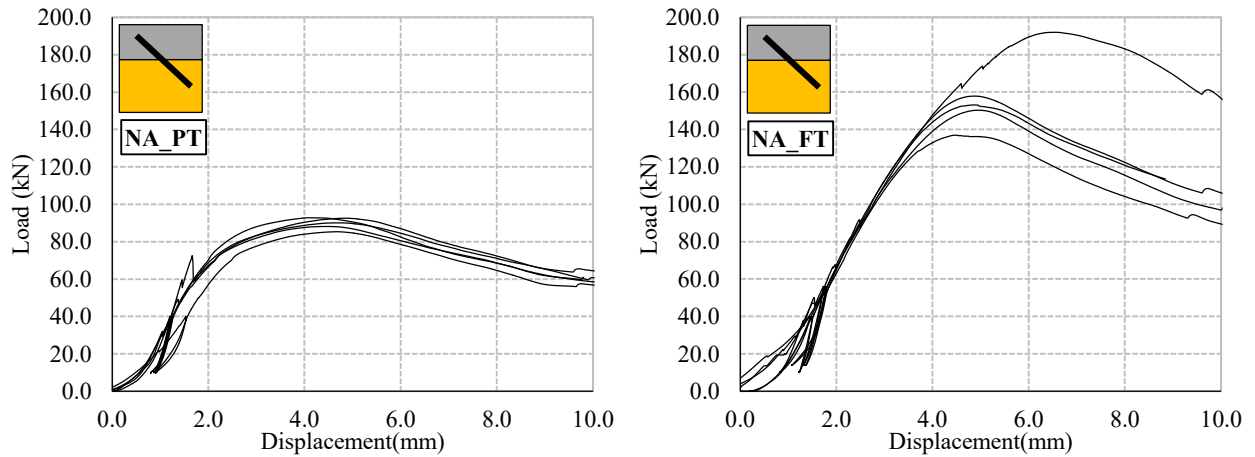


Fig. 2.18 – Experimental load vs. displacement curves for specimens without interlayer and normal concrete (NA series): PT screws and FT screws.

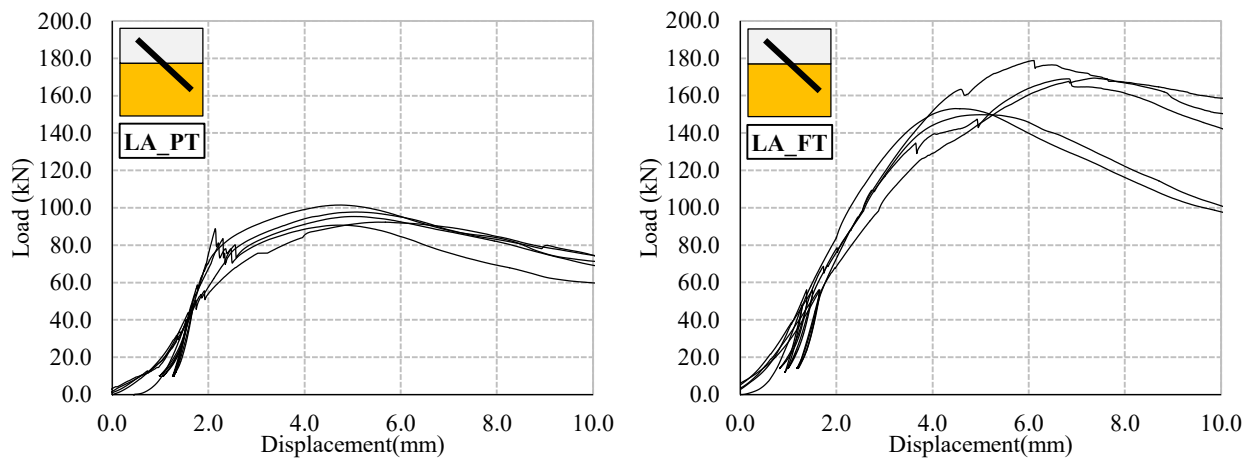


Fig. 2.19 – Experimental load vs. displacement curves for specimens without interlayer and lightweight concrete (LA series): PT screws and FT screws.

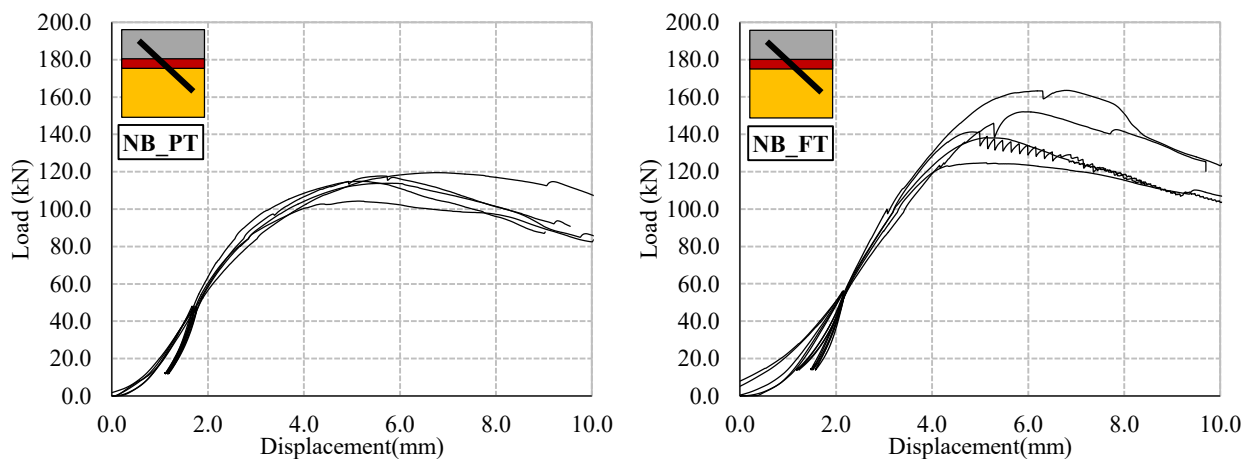


Fig. 2.20 – Experimental load vs. displacement curves for specimens with interlayer and normal concrete (NB series): PT screws and FT screws.

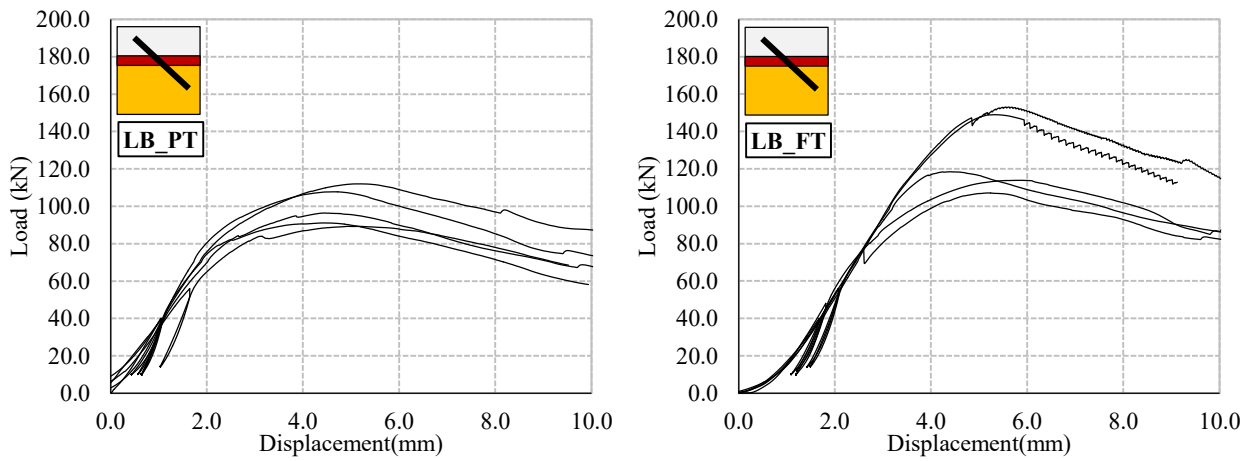


Fig. 2.21 – Experimental load vs. displacement curves for specimens without interlayer and lightweight concrete (LA series): PT screws and FT screws.



Fig. 2.22 – Investigation of connection after failure: (a) screw withdrawal with partial rotation of the plastic element; no critical failure observed in the thermoplastic connector.



Fig. 2.23 – Localized failure of a specimen with interlayer (ID:LB_FT_5) observed at large displacements.

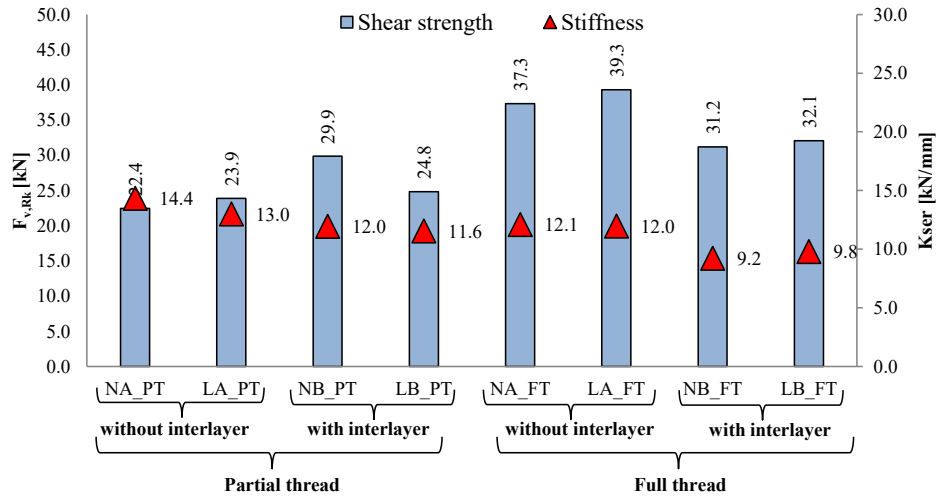


Fig. 2.24 – Mean values of load-carrying capacity and serviceability stiffness calculated per single CP.

Table 2-6 – Experimental shear strength $F_{v,exp}$, stiffness $K_{ser,exp}$ and yielding point ($F_{v,y}$; δ_y) for each specimen, average values and variation coefficient (COV).

NA Series					LA Series				
Spec. ID	$F_{v,exp}$ (kN)	$K_{ser,exp}$ (kN/mm)	$F_{v,y}$ (kN)	δ_y (mm)	Spec. ID	$F_{v,exp}$ (kN)	$K_{ser,exp}$ (kN/mm)	$F_{v,y}$ (kN)	δ_y (mm)
NA_PT_1	92,8	50,5	46,4	1,4	LA_PT_1	92,3	50,0	46,2	1,6
NA_PT_2	92,6	44,6	46,3	1,4	LA_PT_2	101,5	65,8	50,7	1,7
NA_PT_3	85,3	66,0	42,7	1,7	LA_PT_3	90,7	50,9	45,4	1,7
NA_PT_4	88,2	54,8	44,1	1,3	LA_PT_4	95,3	40,3	47,7	1,7
NA_PT_5	90,1	71,3	45,0	1,3	LA_PT_5	97,7	53,1	48,9	1,7
Average	89,8	57,4	44,9	1,4	Average	95,5	52,0	47,8	1,7
COV	3,2%	17,6%	3,2%	10,6%	COV	4,1%	16,1%	4,1%	1,6%
NA_FT_1	136,9	39,2	68,5	2,1	LA_FT_1	153,1	57,4	76,5	1,8
NA_FT_2	157,8	51,2	78,9	2,2	LA_FT_2	149,8	42,8	74,9	2,0
NA_FT_3	153,1	54,8	76,6	2,2	LA_FT_3	169,0	43,7	84,5	2,2
NA_FT_4*	191,9	38,0	96,0	2,5	LA_FT_4*	169,4	36,7	84,7	2,5
NA_FT_5*	150,3	44,7	75,1	2,2	LA_FT_5*	178,8	39,6	89,4	2,3
Average	149,3	48,4	74,6	2,2	Average	157,3	48,0	78,6	2,0
COV	6,3%	14,4%	6,3%	2,6%	COV	5,6%	14,5%	5,6%	7,3%
NB Series					LB Series				
Spec. ID	$F_{v,exp}$ (kN)	$K_{ser,exp}$ (kN/mm)	$F_{v,y}$ (kN)	δ_y (mm)	Spec. ID	$F_{v,exp}$ (kN)	$K_{ser,exp}$ (kN/mm)	$F_{v,y}$ (kN)	δ_y (mm)
NB_PT_1	113,9	50,6	56,9	2,0	LB_PT_1	96,4	37,2	48,2	1,3
NB_PT_2	104,3	52,5	52,2	1,8	LB_PT_2	107,7	55,4	53,9	1,4
NB_PT_3	114,9	44,3	57,5	1,9	LB_PT_3	91,1	46,5	45,5	1,2
NB_PT_4	117,7	48,0	58,9	2,0	LB_PT_4	89,3	39,4	44,6	1,5
NB_PT_5	119,5	43,9	59,8	2,1	LB_PT_5	112,0	52,7	56,0	1,5
Average	114,1	47,9	57,0	2,0	Average	99,3	46,2	49,7	1,4
COV	4,7%	7,3%	4,7%	5,2%	COV	9,3%	15,8%	9,3%	9,6%
NB_FT_1	163,5	45,8	81,8	2,7	LB_FT_1	153,1	38,3	76,5	2,6
NB_FT_2	152,1	30,0	76,0	2,7	LB_FT_2	118,4	40,3	59,2	2,2
NB_FT_3	141,3	37,5	70,6	2,5	LB_FT_3	148,9	40,7	74,5	2,5
NB_FT_4	138,2	33,4	69,1	2,5	LB_FT_4	107,1	38,7	53,5	2,0
NB_FT_5	124,7	38,0	62,4	2,3	LB_FT_5	113,9	38,2	56,9	2,0
Average	144,0	36,9	72,0	2,5	Average	128,3	39,2	64,1	2,3
COV	9,3%	14,7%	9,3%	5,9%	COV	15,2%	2,8%	15,2%	11,1%

* specimens with higher length of screws

** mean values and COV calculated for a sample number of 3

2.3.4 Comparison with analytical calculations

Results obtained from the experimental campaign are now compared with theoretical predictions either for the shear strength $F_{v,rk}$ and stiffness K_{ser} . The mechanical parameters accounted for the analytical calculations, extrapolated from the screws ETA documents ([2.27];[2.49]), are briefly summarized:

- Characteristic withdrawal parameter $f_{ax,k}$ equal to 10.0 N/mm² and 11.1 N/mm² for PT and PF screws;
- Characteristic yielding moment $M_{y,Rk}$ according to Eq. (1.37);
- Characteristic wood embedment capacity $f_{h,k}$ calculated according to Eurocode 5 [2.29] with $\rho_k = 385 \text{ kg/m}^3$;

Table 2-7 shows the characteristic experimental $F_{v,rk,exp}$ values calculated according to EN 14358 [2.55] assuming a coefficient $k_s = 2.48$ for all configuration with except for NA_FT and LA_FT series for which $k_s = 3.34$ was used, to account for the reduced number of samples. Values are referred to a single CP (i.e. two screws). The relative difference $\Delta F_{v,Rk} = 1 - (F_{v,Rk,th} / F_{v,Rk,exp})$ calculated with respect to theoretical provisions of Eurocode 5 [2.14] (i.e. Eq.(1.5)) shows the same trend obtained in the screw-only test campaign. An average difference of 37.1% was obtained for test involving PT screws, which increases to 42.3% for FT screws. The theoretical proposition for inclined screws formulated [2.56] (reported in Section 1.2.1.2) and calculated with a friction coefficient $\mu = 0.25$ reduces this difference to a mean value of 24.4% and 18.1%. Assuming $\mu = 0.6$ yet reduces this gap to 19.1% and 7.6%. The trend depicted for the shear strength is reflected also when analysing the calculated relative difference $\Delta K_{ser} = 1 - (K_{ser,th} / K_{ser,exp})$. Eurocode 5 shows an important safety margin, $\Delta K_{ser} = 29.6\%$ and 19.5% for PT and FT screws, given by its simplified formulation that do not account for screw inclination and withdrawal capacity contribution (see Eq.(1.33)). The alternative method shows a good fitting with experimental results thus overestimating the stiffness for LWAC or with presence of interlayer. In these cases, the hypothesis of a fully rigid behaviour of the fastener in the concrete joint may not be applied. A plausible suggestion would be to avoid including the multiplication factor of 2 in the formulation of the lateral stiffness $K_{ser,\perp}$.

Fig. 2.25 to Fig. 2.28 show a visual comparison of the values above discussed and add to the comparison a prediction of the axial/shear contribute per CP derived with Eq.(1.25).

Table 2-7 – Comparison between experimental and analytical results per CP.

Series	Shear strength $F_{v,rk}$						Stiffness K_{ser}					
	Experimental			Theoretical			Experimental			Theoretical		
	$F_{v,rk,exp}$			$F_{v,rk,th}$			$K_{ser,exp}$			$K_{ser,th}$		
	Mean	$F_{v,Rk,exp}$	$F_{v,Rk}$	$\Delta F_{v,Rk}$	$F_{v,Rk}$	$\Delta F_{v,Rk}$	Mean	K_{ser}	ΔK_{ser}	K_{ser}	ΔK_{ser}	
(kN)	(kN)	(kN)	(%)	(kN)	(%)	(kN/mm)	(kN/mm)	(%)	(kN/mm)	(%)		
NA_PT	22.4	19.8	14.2	28.3%	15.9	19.6%	14.4	8.9	38.1%	11.6	18.9%	
LA_PT	23.9	21.1	14.2	32.6%	15.9	24.4%	13.0	8.9	31.6%	11.6	10.5%	
NB_PT	29.9	25.0	12.2	51.1%	15.1	36.2%	12.0	8.9	25.7%	11.6	2.7%	
LB_PT	24.8	19.3	12.2	36.5%	15.1	17.3%	11.6	8.9	23.1%	11.6	-0.8%	
Average values				37.1%		24.4%			29.6%		7.8%	
NA_FT	37.3	29.0	16.9	41.9%	24.8	14.5%	12.1	8.6	29.3%	13.2	-9.4%	
LA_FT	39.3	31.7	16.9	46.7%	24.8	21.7%	12.0	8.6	28.6%	13.2	-10.4%	
NB_FT	31.2	27.8	14.3	48.5%	18.2	29.1%	9.2	8.6	7.3%	12.2	-31.6%	
LB_FT	32.1	21.2	14.3	32.3%	18.2	6.9%	9.8	8.6	12.7%	12.2	-23.9%	
Average values				42.3%		18.1%			19.5%		-18.8%	

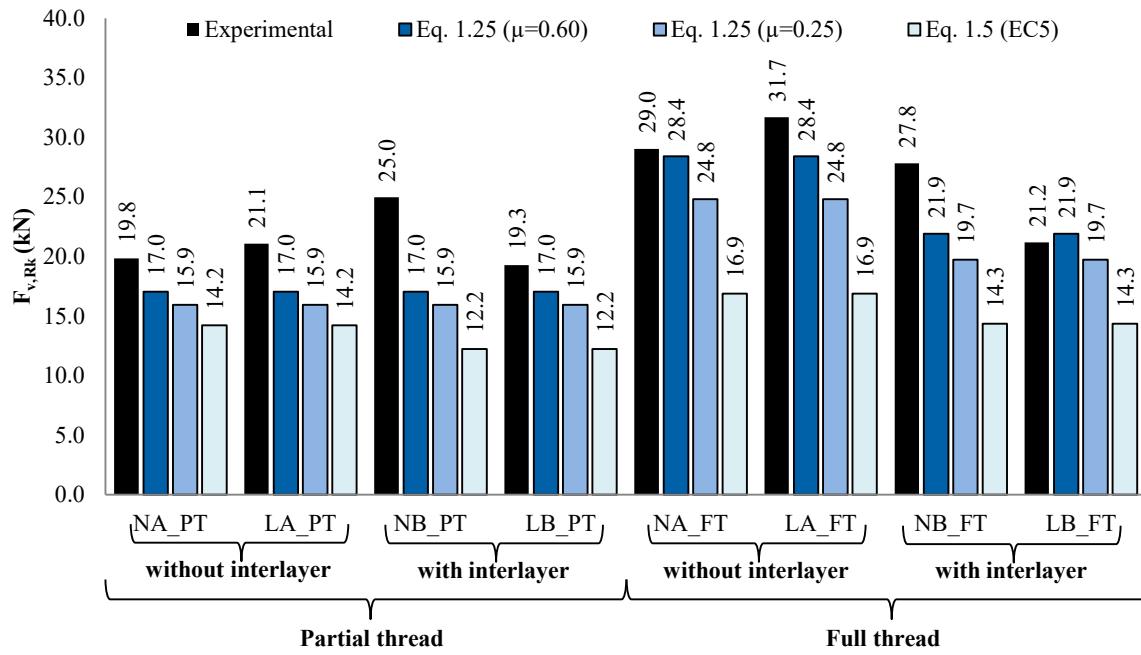


Fig. 2.25 – Characteristic shear strength $F_{v,Rk,exp}$ calculated according to EN 14358 [2.55] and analytical values.

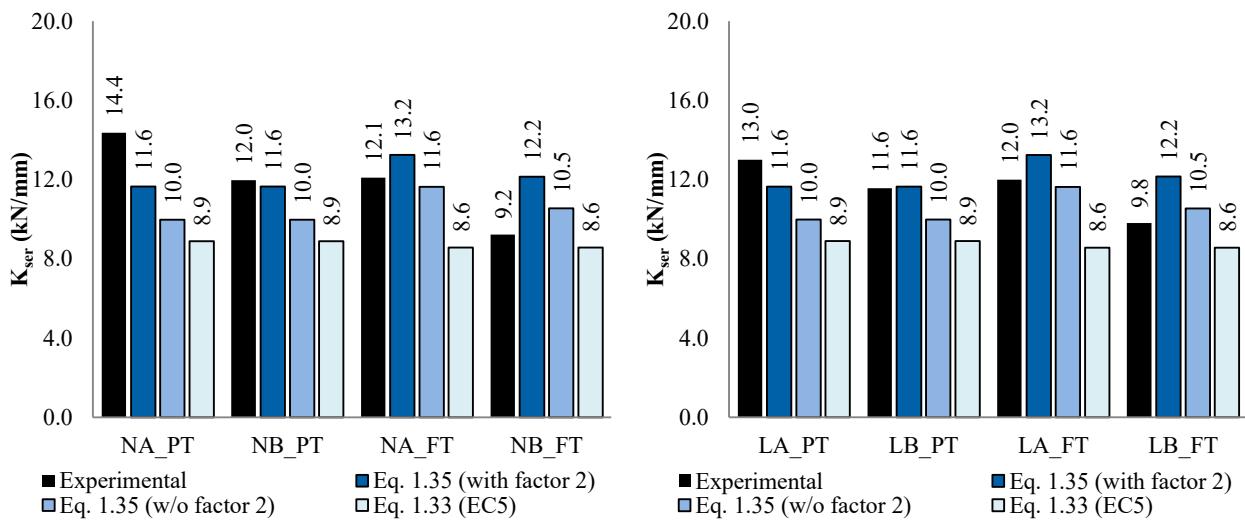


Fig. 2.26 – Mean service stiffness $K_{ser,exp}$ and analytical values $K_{ser,th}$.

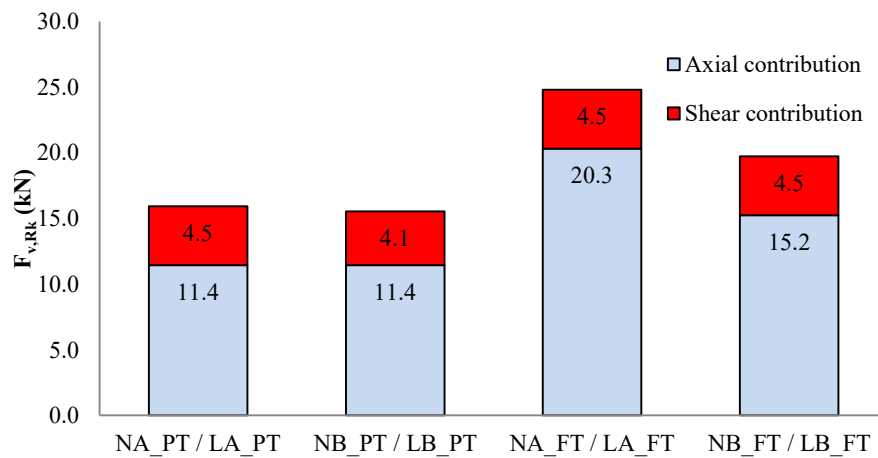


Fig. 2.27 – Axial and lateral contribution calculated for each configuration ($\mu = 0.25$).

2.3.5 Comparison with the screw only configuration

Obtained results are also compared to the screw-only configuration of the previous experimental campaign. However, a valid comparison is suitable only within the same boundary conditions: a) 8-mm partial thread screws; b) absence of interlayer; c) normal and lightweight concrete. Therefore, Fig. 2.28 shows the superposition between AN-8 and NA_PT series and AL-8 to LA_PT series. No significant difference emerges in terms of load bearing capacity with the addition of the GFRP element. Regarding the mean experimental stiffness $K_{ser,exp}$ the GFRP component produced a decrease of stiffness from 17.4 to 14.4 kN/mm for normal concrete while specimens with LWAC produced the same results (13.2 and 13.0 kN/mm respectively). This could be explained by the fact that the elastic modulus E of the GFRP part is more similar to that of LWAC than to a normal concrete.

Nevertheless, the important outcome of the GFRP socket is that for each of the 40 tests failure was localized in the timber layer and no sudden strength losses were noticed due to splitting and/or concrete cone expulsion as evidenced in several test with the screw-only configuration.

No comparison regarding the enhanced easiness of screw insertion is contemplated in this section.

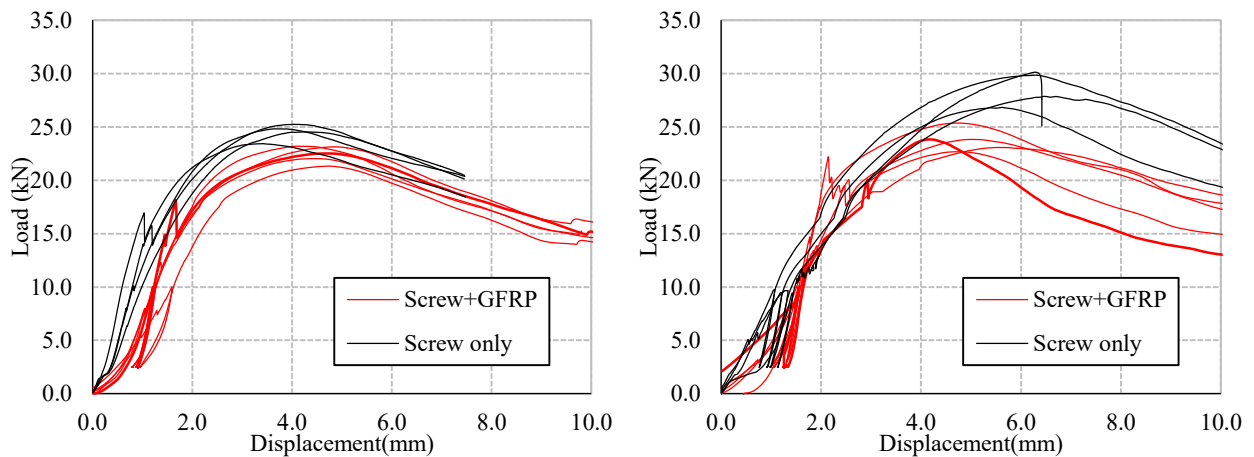


Fig. 2.28 – Experimental load vs. displacement curves with normal concrete (left) and lightweight concrete (right).

2.3.6 FE model results and considerations on the creep phenomena

Thermoplastic materials suffer from creep phenomena, which is directly connected to the level of stress constantly applied to the element. Giving a prediction on the actual stress level can be a complex task. However, a possible solution would be to apply the same considerations, already well consolidated in timber structures, to evaluate the deflections at the serviceability limit states. According to Eurocode 5 [2.14] permanent and long-term loads are responsible for the creep deformation of timber structures. More specifically, TCC structures should involve long-term tests to account for the actual contribution of the connection to the global behaviour. A literature review of such tests can be found in [2.57], explaining that difficulties in the tests setup are responsible for the shortage of information available. However, by crosschecking experimental data, numerical simulations and creep information of the materials, some preliminary precautions can be extrapolated.

In particular, by analysing the force-displacement curves and, the load range for which K_{ser} is evaluated (i.e. $0.1 \div 0.4 F_{v,est}$), eventual prediction on the quasi-permanent stress level allocated on the GFRP element can be drawn. For partial thread and full thread screws, these values for each connector are equal to 10.0 and 14.0 kN respectively. Alternatively, the highest calculated yielding strength F_y can be taken as a reference (see Fig. 2.29a), which correspond to a value of 57.0 kN (or 14.25 kN per connector). In case of FT screws this value raise to 78.4 kN (19.6 kN per connector).

Examining the numerical simulations (conducted with the SLS model), at these loads the Von Mises stress near the screw's head are contained within 70-80 MPa (see details of Fig. 2.29b). Specific creep curves that correlate the increase of deformation for a constant applied stress are not available for the adopted GFRP material, but valuable information for similar PA6 materials are available in [2.23]-[2.24]. Isochronous Stress-strain curves obtained from the mentioned resources are shown in Table 2-8. With these hypotheses, the long-term serviceability stiffness can be calculated according to Eq. (2.7) in compliance with EC5 [2.14] assuming a contribution to creep of both the screw $k_{def,w}$ and the nylon part $k_{def,GFRP}$:

$$K_{ser,fin} = \frac{K_{ser}}{(1 + \Psi_2 k_{def})} \quad (2.7)$$

$$k_{def} = 2 \sqrt{k_{def,w} k_{def,GFRP}} \quad (2.8)$$

As an initial simplification, the factor for the nylon-based part $k_{def,GFRP}$ can be extrapolated from the isochronous stress-strain curves with the following relation:

$$k_{def,GFRP} = \frac{\varepsilon_{100000h}}{\varepsilon_{10h}} - 1 \quad (2.9)$$

where ε_{10h} and $\varepsilon_{100000h}$ are the strain values at 10 and 100,000 hours respectively for a given stress level. Assuming the maximum calculated value of 0.75 for $k_{def,GFRP}$ for whatever stress level (see Table 2-8), the suggested k_{def} is equal to 1.34 for glued laminated timber and 1.55 for solid timber.

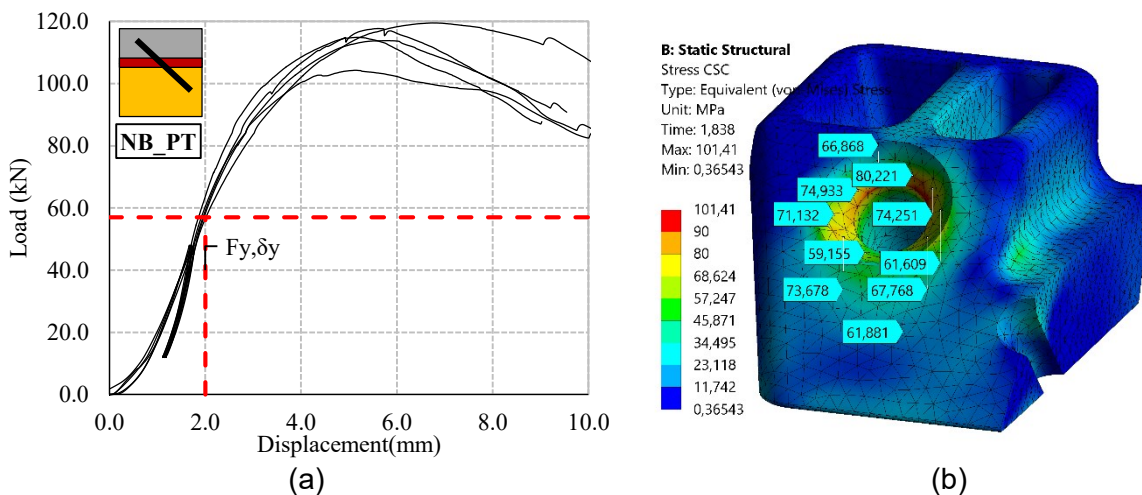
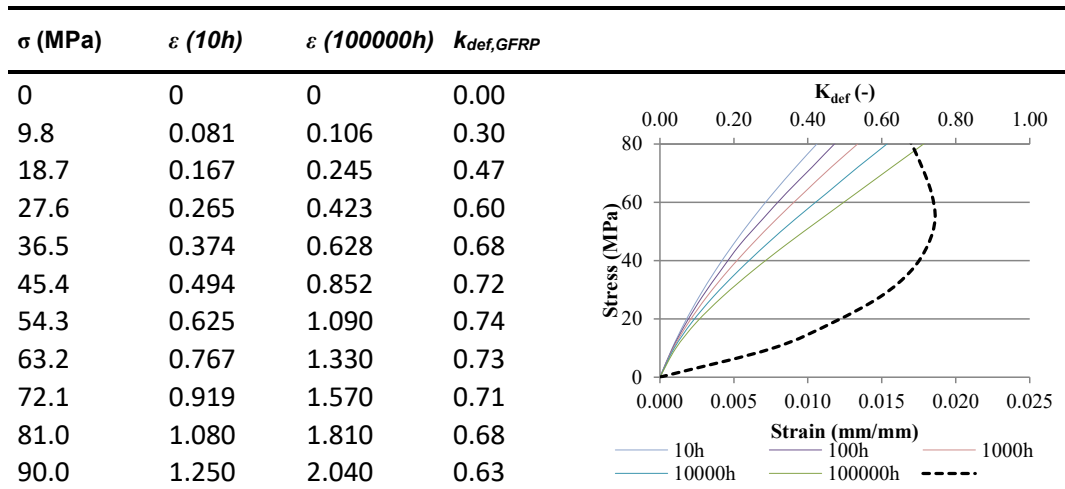


Fig. 2.29 – (a) Mean yielding point for NB_PT series; (b) Von Mises stress distribution in the GFRP element in proximity of the housing for the countersunk head screw.

Table 2-8 – Stress-strain relationship and equivalent k_{def} values.

2.4 Conclusions

This chapter presented an evolution of TCC connections employing screws inclined at 45° . The experimentation described in the Chapter 1 of the present manuscript was taken as a basis for the study of a system that would make the use of such connections more efficient. In particular the investigate solution aimed to solve two problems: a) the typical onsite issues detected during the installation of the screws into the timber beams (i.e. correctness of the screw inclination and penetration); b) the possibility to develop anticipated failure in the concrete layer observed in the previous chapter.

A finite element model of the complete timber-to-concrete connection, which followed a hybrid modelling approach, was developed to replicate the experimental results. Material non-linearities like orthotropy of timber and elastoplastic behaviour of the screw were included whereas the load transmission between screw and wood was modelled by means of equivalent springs and frictional contact elements.

The FEM model was necessary to design a GFRP socket that, coupled with two inclined screws, intended to fulfil the aforementioned functions. Additionally, the model has been used to define the state of stress to which the GFRP component should be subjected in the short and long term in order to predict analytically the deformability factor k_{def} of the complete system.

Outcomes from experimental tests were used to evaluate the mechanical behaviour of the complete system varying: withdrawal strength of screws, presence of a wood interlayer, type of concrete.

Comparisons with analytical predictions of the actual Eurocode 5 method and the approach described in the previous chapter were made. The conservative nature of Eurocode 5 provisions were confirmed also in this case. Likely, to the screw-only configuration, a better fitting was achieved with the proposed approach that have been validated also varying the screw strength and the presence of interlayer.

The contribution of the GFRP component has not lead to significant changes on the load bearing capacity while it slightly affected the stiffness if normal concrete is used. The last important outcome

is that the thermoplastic element fulfilled the protection against concrete splitting or concrete cone failure in all the tested configurations.

Further research might involve deeper analyses to evaluate the effectiveness of the simplified numerical approach in the investigation of TCC joints realized with modern screws. GFRP materials produced by injection moulding could be helpful in the continuous improvements of timber connections provided that sufficient care is taken into account in determining the actual conditions of environment and loading conditions to whom they will be subjected during their working life.

Acknowledgments

The author would like to thank the R&D office of fischer Italia for having provided its knowledge of injection moulding process and having refined the final shape of the connector. Company fischer Italia is acknowledged for supplying materials and specimens for tests and the personal of the Construction Materials Testing Laboratory of the Department of Civil, Environmental and Architectural Engineering of Padova for supervising tests.

References – Chapter 2

- [2.1] EN 26891 (1991). “Joints made with mechanical fasteners. General principle for the determination of strength and deformation characteristics”. CEN. Brussels, Belgium.
- [2.2] EN 12512 (2001). “Timber structures - test methods - cyclic testing of joints made with mechanical fasteners”. CEN. Brussels, Belgium.
- [2.3] EN 14592 (2012). “Timber structures - Dowel-type fasteners – Requirements”. CEN. Brussels, Belgium.
- [2.4] EN ISO 8970 (2010). “Timber structures - Testing of joints made with mechanical fasteners - Requirements for wood density”. CEN. Brussels, Belgium.
- [2.5] Website of Rothoblaas. Available online: <http://www.rothoblaas.com/>
- [2.6] Website of Leca. Available online: <http://www.laterlite.com/>
- [2.7] Website of Heco. Available online: <http://www.heco.it/>
- [2.8] Website of Peter Cox. Available online: www.petercoxitalia.it/
- [2.9] Website of Tecnaria. Available online: <http://www.tecnaria.com/en/>
- [2.10] Website of Wurth. Available online: <http://www.wuerth.com/>
- [2.11] Symons, D., Persaud, R., and Stanislaus, H. (2010). “Strength of inclined screw shear connections for timber and concrete composite construction”. *Structural Engineer*, **88(1)**:25-32.
- [2.12] Moshiri, F., Shrestha, R., and Crews, K. (2014). “The Predictive Model for Stiffness of Inclined Screws as Shear Connection in Timber-Concrete Composite Floor”. RILEM Bookseries. DOI: 10.1007/978-94-007-7811-5_40.

- [2.13] Steinberg, E., Selle, R., and Faust, T. (2003). "Connectors for timber-lightweight concrete composite structures". *Journal of Structural Engineering*, **129(11)**:1538-1545. ASCE.
- [2.14] EN 1995-1-1 Eurocode 5 (2009). "Design of Timber Structures, Part 1-1, General: Common Rules and Rules for Buildings". CEN. Brussels, Belgium.
- [2.15] Uddin, N. (2013). "Developments in fiber-reinforced polymer (FRP) composites for civil engineering". Elsevier. Amsterdam, Netherlands.
- [2.16] Goodship, V. (2004). "Practical guide to injection moulding". Smithers Rapra Publishing.
- [2.17] EN ISO 291 (2008). "Plastics -- Standard atmospheres for conditioning and testing". CEN. Brussels, Belgium.
- [2.18] EN ISO 1110 (1998). "Plastics - Polyamides - Accelerated conditioning of test specimens". CEN. Brussels, Belgium.
- [2.19] Pedersen, M. (2002). "Dowel type timber connections". Ph.D. Thesis Delft University of Technology, Netherlands.
- [2.20] Drake, R.D. (2003). "The advancement of structural connection techniques for timber buildings". Ph.D. Thesis. University of Bath, UK.
- [2.21] Thomson, A. (2010). "The structural performance of non-metallic timber connections". Ph.D. Thesis, University of Bath, UK.
- [2.22] Brandon, D., Ansell, M. P., Harris, R., Walker, P., and Bregulla, J. (2014). "Modelling of non-metallic timber connections at elevated temperatures". In *Materials and Joints in Timber Structures* (pp. 231-241). Springer. Dordrecht, Netherlands.
- [2.23] www.campusplastics.com
- [2.24] <http://www.materialdatacenter.com/>
- [2.25] ANSYS® Mechanical Workbench.
- [2.26] Ellingsbø, P., and Malo, K.A. (2012). "Withdrawal capacity of long self-tapping screws parallel to grain direction". In *Proceedings of the 12th World conference on Timber Engineering (WCTE)*. 15-19 July 2012, Auckland, New Zealand.
- [2.27] European Organisation for Technical Assessment (EOTA) (2016). "Self-tapping screws for use in timber structures". European Technical Approval ETA-11/0027. Charlottenlund, Denmark.
- [2.28] ANSYS® Mechanical APDL, Help System, Contact Technology Guide.
- [2.29] Dias, A.M.P.G. (2005). "Mechanical behaviour of timber-concrete joints". Ph.D. Thesis Delft University of Technology, Netherlands.
- [2.30] ANSYS® Mechanical Workbench and APDL, Help System, Theory Reference.
- [2.31] Patton-Mallory, M., Pellicane, P. J., and Smith, F. W. (1997). "Modeling bolted connections in wood". *Journal of structural engineering*, **123(8)**:1054-1062.
- [2.32] Dias, A.M.P.G., Van de Kuilen, J.W.G., Cruz, H., and Lopez, S. (2004). "Non-linear FEM models for timber-concrete joints made with dowel type fasteners". In *Proceedings of the 8th World conference on Timber Engineering (WCTE)*, 14-17 June 2004, Lahti, Finland.
- [2.33] Dias, A.M.P.G., Van de Kuilen, J.W.G., Lopes, S., and Cruz, H. (2007). "A non-linear 3D FEM model to simulate timber-concrete joints". *Advances in Engineering Software*. DOI: //doi.org/10.1016/j.advengsoft.2006.08.024.

- [2.34] Gutkowski, R., Balogh, J., and To, L.G. (2010). "Finite element modelling of short-term field response of composite wood-concrete floors/decks". *Journal of Structural Engineering*, **136(6)**:707–714. ASCE.
- [2.35] Xu, B. H., Taazount, M., Bouchaïr, A., and Racher, P. (2009). "Numerical 3D finite element modelling and experimental tests for dowel-type timber joints". *Construction and building materials*, **23(9)**:3043-3052.
- [2.36] Xu, B. H., Bouchaïr, A., Taazount, M., and Vega, E. J. (2009). "Numerical and experimental analyses of multiple-dowel steel-to-timber joints in tension perpendicular to grain". *Engineering Structures*, **31(10)**: 2357-2367.
- [2.37] Lopes, S., Jorge, L., and Cruz, H. (2012). "Evaluation of non-linear behavior of timber–concrete composite structures using FE model". *Materials and structures*, **45(5)**:653-662.
- [2.38] Oudjene, M., Meghlat, E. M., Ait-Aider, H., and Batoz, J. L. (2013). "Non-linear finite element modelling of the structural behaviour of screwed timber-to-concrete composite connections". *Composite Structures*, **102**:20-28.
- [2.39] Hassanieh, A., Valipour, H. R., Bradford, M. A., and Sandhaas, C. (2017). "Modelling of steel-timber composite connections: Validation of finite element model and parametric study". *Engineering Structures*, **138**:35-49.
- [2.40] Hill R. (1950). *The Mathematical Theory of Plasticity*. Clarendon Press. Oxford, UK.
- [2.41] Tsai, S.W., and Wu, E.M. (1971). "A general theory of strength for anisotropic materials". *Journal of composite materials*, **5(1)**:58-80.
- [2.42] Hoffman, O. (1967). "The brittle strength of orthotropic materials". *Journal of Composite Materials*, **1(2)**:200-206.
- [2.43] EN 14080 (2013). "Timber structures - Glued laminated timber and glued solid timber – Requirements". CEN. Brussels, Belgium.
- [2.44] Ross, R.J. (2010). *Wood handbook: Wood as an engineering material*.
- [2.45] Sandhaas, C. (2012). "Mechanical behaviour of timber joints with slotted-in steel plates". Ph.D. Thesis Delft University of Technology, Netherlands.
- [2.46] Sandhaas, C. (2012). "Constitutive model for wood based on continuum damage mechanics". In *Proceedings of the 12th World conference on Timber Engineering (WCTE)*. 15-19 July 2012, Auckland, New Zealand.
- [2.47] EN 1992-1-1 Eurocode 2 (2014). "Design of concrete structures, Part 1-1: General rules and rules for buildings". CEN. Brussels, Belgium.
- [2.48] General Design Principles for DuPont Engineering Polymers. 2000
- [2.49] European Organisation for Technical Assessment (EOTA) (2016). "Self-tapping screws for use in timber structures". European Technical Approval ETA-12/0073. Charlottenlund, Denmark.
- [2.50] EN 12390-3 (2009). "Testing hardened concrete - Compressive strength of test specimens". CEN. Brussels, Belgium.
- [2.51] EN 26891 (1991). "Joints made with mechanical fasteners. General principle for the determination of strength and deformation characteristics". CEN. Brussels, Belgium.
- [2.52] Jorge, L.F.C., Lopes, S.M.R., and Cruz, H.M.P. (2011). "Interlayer influence on timber-LWAC composite structures with screw connections". *Journal of Structural Engineering*. DOI: 10.1061/(ASCE)ST.1943-541X.0000299.
- [2.53] Karacabeyli, E., and Ceccotti, A. (1996). "Quasi-static reversed-cyclic testing of nailed joints". In

Proceedings of Meeting 29 of the Working Commission W18-Timber Structures, Universität Karlsruhe, Karlsruhe, Germany. Paper CIB-W18/29-7-7.

- [2.54] Gelfi, P., Giuriani, E., and Marini, A. (2002). "Stud shear connection design for composite concrete slab and wood beams". *Journal of Structural Engineering*, **128(12)**:1544-1550.
- [2.55] EN 14358 (2016). "Timber structures - Calculation and verification of characteristic values". CEN. Brussels, Belgium.
- [2.56] Marchi, L., Scotta, R., and Pozza, L. (2017). "Experimental and theoretical evaluation of TCC connections with inclined self-tapping screws". *Materials and Structures*. <http://dx.doi.org/10.1617/s11527-017-1047-1>.
- [2.57] Yeoh, D., Fragiacomio, M., De Franceschi, M., and Heng Boon, K. (2011). "State of the art on timber-concrete composite structures: literature review". *Journal of Structural Engineering*. **137(10)**:1085–1095. ASCE.
- [2.58] Tomasi, R., Crosatti, A., and Piazza, M. (2010). "Theoretical and experimental analysis of timber-to-timber joints connected with inclined screws". *Construction and Building Materials*. DOI: 10.1016/j.conbuildmat.2010.03.007.

PART II

INNOVATIVE EARTHQUAKE-RESISTANT DISSIPATIVE DEVICE FOR CLT STRUCTURES

Chapter 3 Development of an innovative high-dissipative device for CLT structures

Abstract

The need of more reliable connections for earthquake-resistant CLT shear-wall assemblies that provides well-known hysteretic behaviour, reduced pinching phenomenon (caused by the wood embedment) and strength degradation justify the continuous development of “innovative” connections. In this chapter, a newly developed connection device for CLT structures that works for both tensile and shear loads is designed and assessed, and the significant aspects of its hysteretic behaviour are discussed.

The design procedure of the connection system and preliminary experimental test that validates the numerical predictions are illustrated. Then, subsequent versions of the dissipating device are described and its experimental results reported with particular attention in describing its hysteretic response and coupled shear-tension strength domain. The application of the capacity design criteria to innovative connections is also thoroughly assessed and supported by experimental evidence.

3.1 Introduction

The seismic behaviour of CLT buildings has been studied by numerous researchers from various countries. Quasi-static tests of shear-wall systems and shake-table tests of full-scale buildings [3.1]-[3.5] showed that CLT structures are characterized by high strength and stiffness when subjected to seismic actions. However, they might exhibit low ductility and dissipative capacity if not correctly designed to prevent brittle failure or if realized with large and continuous wall elements, without vertical joints (i.e., if characterized by prevailing sliding behaviour).

The current version of European seismic code Eurocode 8 [3.6] does not consider explicitly CLT as a structural system, and the closest definition is “glued wall panels with glued diaphragms”. Therefore, CLT is classified as a low-ductility system and a behaviour factor $q_0 = 2$ is suggested for the design of CLT buildings, regardless of assembling variables.

Actually, the seismic response of CLT structures is mostly dependent on the building geometry (e.g., slenderness), number, type, arrangement and design of joints used to assemble timber panels and the capability of connections to guarantee a suitable amount of plastic work. Such dependency was demonstrated by experimental tests of different shear walls [3.3], shake-table tests of different buildings [3.2];[3.5] and numerical and analytical simulations of buildings and wall systems with different geometries. In the building practice, the adoption of large panels with few joints allows the reduction of time and costs for on-site assembling. However, the use of narrow panels allows one to optimize the use of the material and to reduce the weight and dimensions to be lifted and transported. The University of Padova [3.7]-[3.9] proved that slender and highly-jointed buildings can show higher displacement and dissipative capacity than squat and scarcely-jointed buildings. This is obtained by assuring a rocking behaviour of each panel and by using ductile fasteners. The authors also obtained different behaviour factor values, depending on building geometry and panel arrangement.

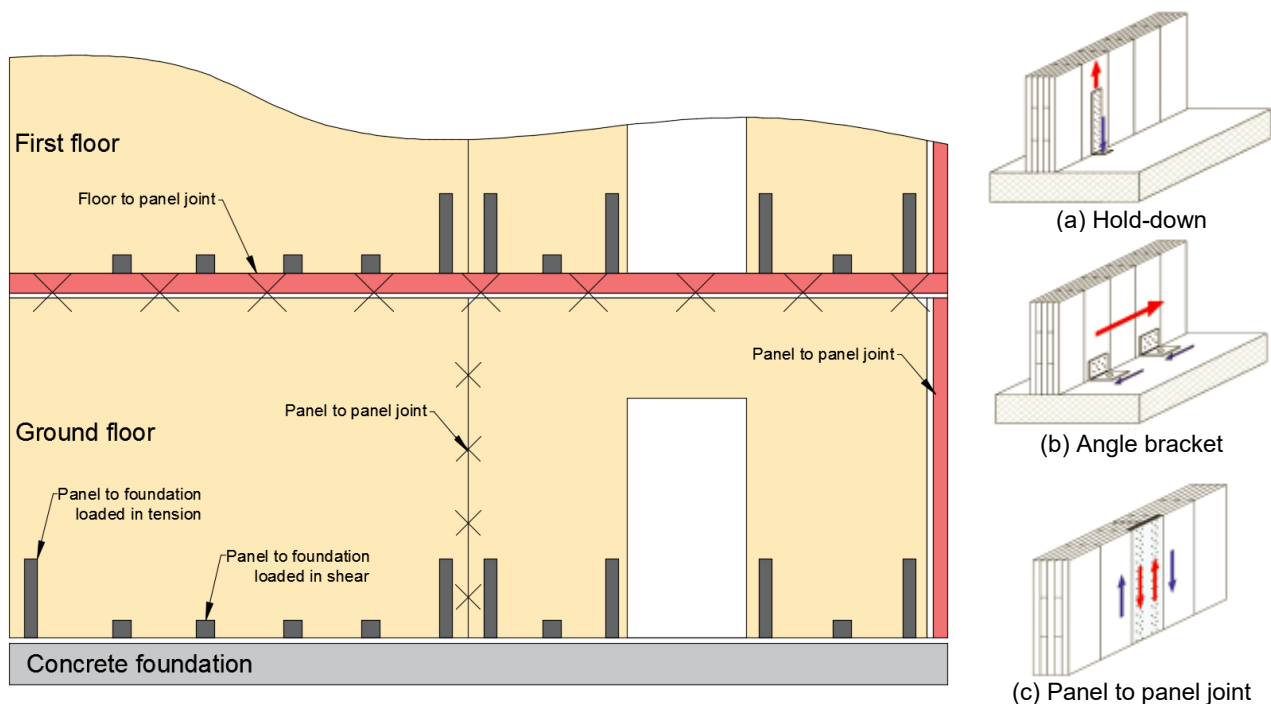


Fig. 3.1 – Traditional earthquake-resistant connections employed in CLT shear walls.

Consequently, the seismic performance of CLT buildings is strictly related to the capability of connections to perform plastic work, since timber elements have limited capability to deform

inelastically [3.10]-[3.11]. Nowadays, the use of hold-down and angle bracket connections, which were originally developed for platform-frame constructions, has been extended also to CLT buildings. Nevertheless, the dissipative capacity of light-frame buildings is mainly diffused in nailing between frames and panels, i.e., in the shear deformation of the wall [3.12]-[3.16]. This condition could be also achieved by assembling massive timber elements using ductile fasteners [3.17]. Contrariwise, in CLT walls, the dissipative contribution is exclusively assured by ductile connections at the base of the panels or by slender fasteners at vertical joints, being cross-wise layers reciprocally glued.

Eurocode 8 [3.6] commands the evaluation of the mechanical performance of timber connections according to a cyclic loading procedure (recalling EN 12512 [3.18]) and define the requirements for ductility: *“the dissipative zones shall be able to deform plastically for at least three fully reversed cycles at a static ductility ratio of 4 for ductility class M structures and at a static ductility ratio of 6 for ductility class H structures, without more than a 20% reduction of their resistance”*.

Actually, hold-downs, angle brackets and vertical joints belongs to L or M ductility class (rarely H) but they show a marked pinching behaviour due to the wood embedment phenomenon, which reduces the energy dissipation capability of connections (see Fig. 3.2). This fact, can be measured by calculating the drop of equivalent viscous damping ratio v_{eq} ([3.18];[3.19]) that occurs between the 1st and 3rd cycle. Tomasi and Sartori [3.16] performed experimental tests of *traditional* connections applied to the original intended building technique (i.e. platform-frame shear walls) obtaining v_{eq} at the third cycle under 5% for hold-down loaded in tension and a range of 10-20% for angle brackets loaded in shear. Tomasi and Smith [3.20] investigated the cyclic performance of angle brackets loaded in shear and confirmed the range of 10-20%. Gavric et al. [3.21] calculated a decrease from 8.1–8.5 % to 2.8–3.6 % for axially loaded connections and from 19.8-21.4 % to 14.6-16.1 % for connections loaded in shear.

Moreover, *traditional* connections are optimized for uniaxial loading but their resistance can be considerably weakened [3.9] when coupling effects (i.e. tension-shear interaction) are taken into account (see Fig. 3.3), leading to an undesired brittle behaviour ([3.22]-[3.24]).

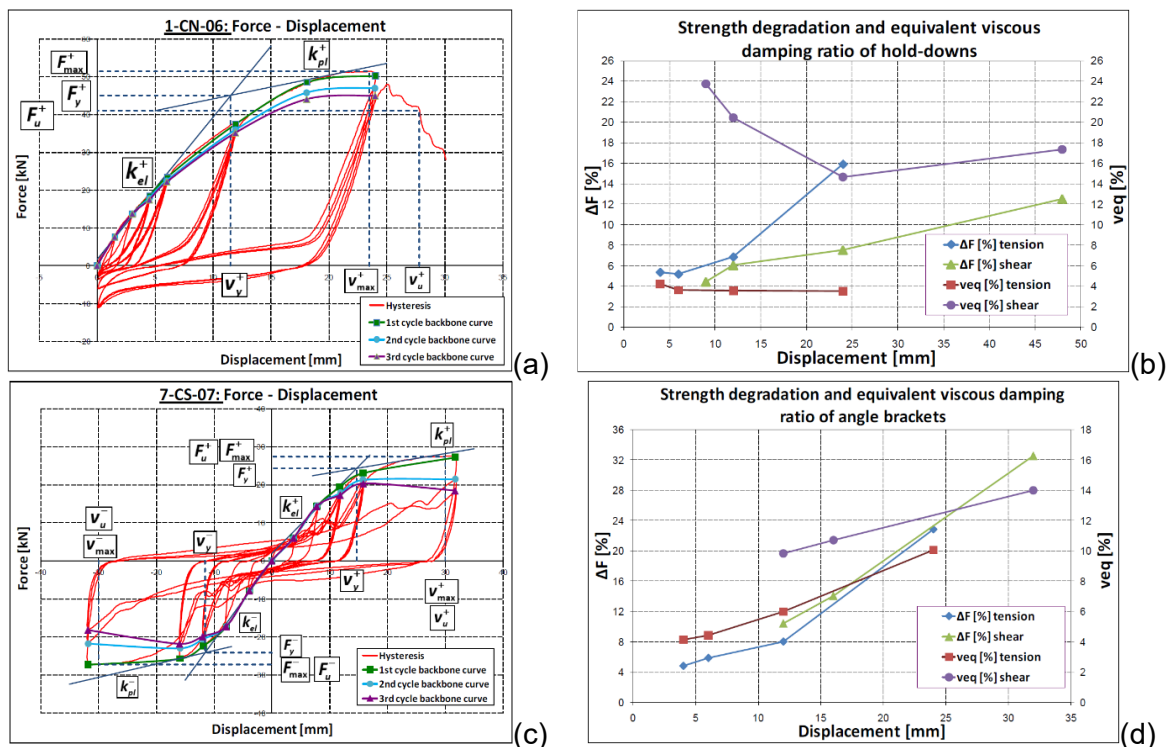


Fig. 3.2 – Typical hysteretic response of traditional CLT joint [3.23]: force vs. displacement curve, strength degradation and viscous damping of a typical hold-down in tension (a,b) and an angle bracket in shear (c,d).

Brittle failures can occur also when the capacity design approach [3.24]-[3.25] is not correctly applied (see Fig. 3.3). The application of the capacity concept to the design of hold-downs and angle brackets is not an easy task dealing with timber structures, due to the difficulty of assuring the overstrength of brittle components versus ductile ones. This is because the strength of fasteners embedded in timber members could be far greater than the design characteristic value evaluated according to Johansen's theory [3.26], as proposed in Eurocode 5 [3.27]. In fact, scattering of material strength and correspondent deviation values are sensibly greater on the timber side than on the steel side of connections. Consequently, the actual strength of nails or screws might exceed the maximum strength of connected perforated steel plates, leading to unexpected fragile behaviour. Therefore, when using CLT constructions, there is the need to shift the weakest element of the capacity design chain, toward the steel ductile components of the connection, the yielding load of which can be forecasted more reliably than for fasteners embedded in timber members.



Fig. 3.3 – Example of brittle or “less ductile” failures occurred on experimental tests ([3.21];[3.24]) and lateral yielding of an hold-down due to coupling effects [3.9].

3.1.1 State of the art on innovative connections for CLT buildings

The need of high energy-dissipating connections has been arising in parallel to the increased interest to develop CLT structures in high seismic-prone areas (e.g., New Zealand and Southern Europe). Furthermore, a considerable attention in this topic is also due to the raising attention in the study of medium to high-rise building realized with CLT monolithic panels, which require high-performance connections placed at the foundation to withstand the ever-increasing demand of strength. Lastly, innovative connection systems are also being developed in the perspective of low-damage structures, whose aim is to withstand subsequent seismic events by applying minor interventions at the structure between one event and another. In this case the fuse-like connection system must prevent the timber panel being damaged (and the whole structure as well) and should consent a fast and efficient replacement of the worn-out element.

The high efficiency of *innovative* devices in terms of hysteretic response (see Fig. 3.4) can be achieved through the following methods:

- *Yielding* of specific steel components (i.e. *fuses*) or portion of them;
- *Yielding* of specific components with displacement restrained by additional elements that limit unwanted deformations (i.e. concepts of Buckling Restrained Bracing system);
- *Friction* between sliding components, sometimes enhanced by interposing additional metal components (e.g., thin brass sheets).

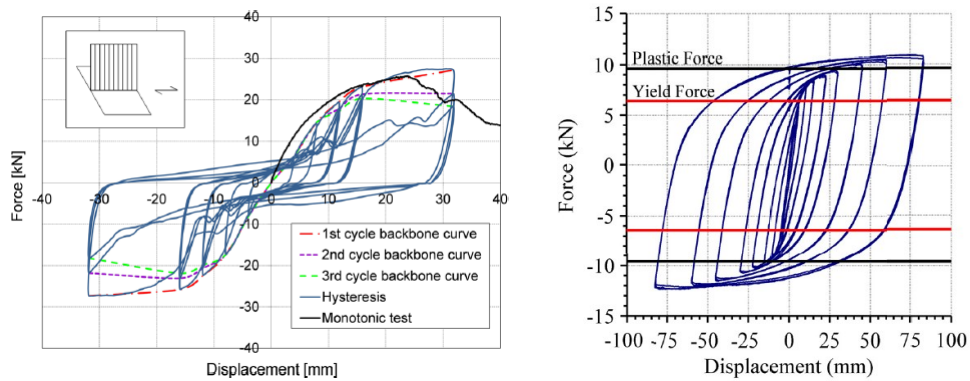


Fig. 3.4 – Typical hysteretic response of a CLT joint: traditional connection in which energy dissipation is demanded to the nails (image on the left, from [3.20]); (b) innovative connection in which energy dissipation is demanded to steel plasticization (image on the right, from [3.28]).

The study of efficient devices for CLT shear wall systems mainly started with the study of low-damage solutions employing self-centering structures. In New Zealand, dissipating devices coupled with post-tensioned shear walls were originally designed for multi-storey RC structures [3.29]. The favourable results lead to the analyses of steel connection devices capable of high relative displacement while maintaining a rather unaltered energy dissipation capacity [3.30].

Lately, this hybrid building technology have been extended to engineered timber shear walls [3.31] and referred to as Pres-Lam (Prestressed Laminated timber) system. Iqbal et al. [3.32] and Smith et al. [3.33] carried out further research studies on LVL walls. This knowledge was applied also to post-tensioned timber frames [3.34] but studies concentrated mostly in shear wall assemblies.

The UFP connector (Fig. 3.5a) originally developed in the 1970s [3.35] involved a simple U-shape realized from bending of a sufficient thick steel plate. This device was designed as a high performance vertical joint device necessary to fasten adjacent panels [3.28] and dissipate energy exploiting the rocking behaviour of high and slender CLT panels restrained at the base by post-tensioned cables.

Fused-type buckling-restrained dissipaters (Fig. 3.5b,c) concepts have also been transferred to high-strength CLT connections by Sarti et al. and Kramer et al. ([3.36]-[3.37]) and subsequently applied to a self-centering system [3.38]. In this case, the connection obviously requires more refinement than the U-shape element but can withstand higher tensile loads.

The use of slip-friction devices have been investigated by Loo et al. [3.39] where a high-performance hold-down was designed and tested. The connection system involved 12mm thick steel plates connected with bolts that slip through slotted holes. Tension was kept constant by using proper Belleville steel washers. The tension-only behaviour of the connections was assured with specifically designed shear-keys placed at the panel base to prevent any possible slip of the panel and consequent shear loading to the dissipating devices. More recently, an enhanced version was proposed by the same University of Auckland [3.40].

Innovative solutions have also been studied without coupling the topic to self-centering systems. Polastri et al. [3.41] developed a solution suitable for prefabricated CLT structures, which incorporates self-tapping wood construction screws, LVL inserts and a high strength steel device. This solution is meant to enhance CLT seismic performance and reduce meanwhile the on-site installation costs by partially fastening the joint to the CLT panel in the factory.

University of Salerno [3.42] designed and tested high-efficient angle brackets (named XL-Stubs) that concentrate energy dissipation in the knee-joint substituting traditional hold-downs while, more recently, Schmidt and Blass [3.43] presented a study on a steel plate combined with special LVL

inserts and secured into the CLT panel to realize high-ductility energy-dissipating panel-to-panel joints.

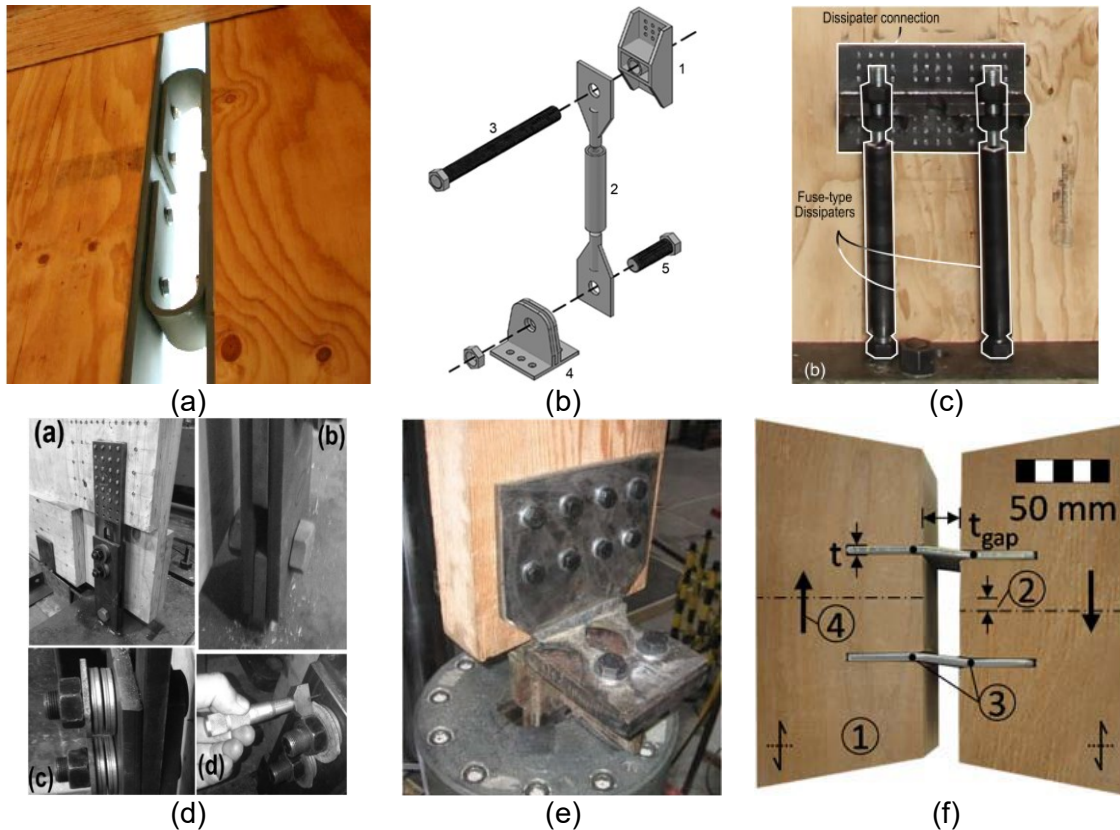


Fig. 3.5 – Examples of innovative connections for CLT structures: (a) UFP [3.28]; (b) Fuse-type dissipater [3.37]; (c) Fuse-type dissipater [3.38]; (d) Slip-friction connector [3.39]; XL-Stub [3.42]; (f) Steel plate dissipater [3.43].

It is worth noting that the term “innovative connection” used in this work does not necessarily mean a device that introduces new technologies or particular materials to the cause of CLT connections but should intend a different way of conceiving the connection. In fact, a duality characterizes traditional or innovative connections, which is sketched in Fig. 3.6. Generally, both types of connection comprise two components: a fastening system (e.g., dowel-type fasteners) to anchor the connector to the panel and the connector itself (e.g., hold-downs, steel plates). That being said, the concept of innovative connections is to switch the dissipative and usually ductile element from the fastening components to the connector. This process is governed, and must be carefully taken into account, by capacity design.

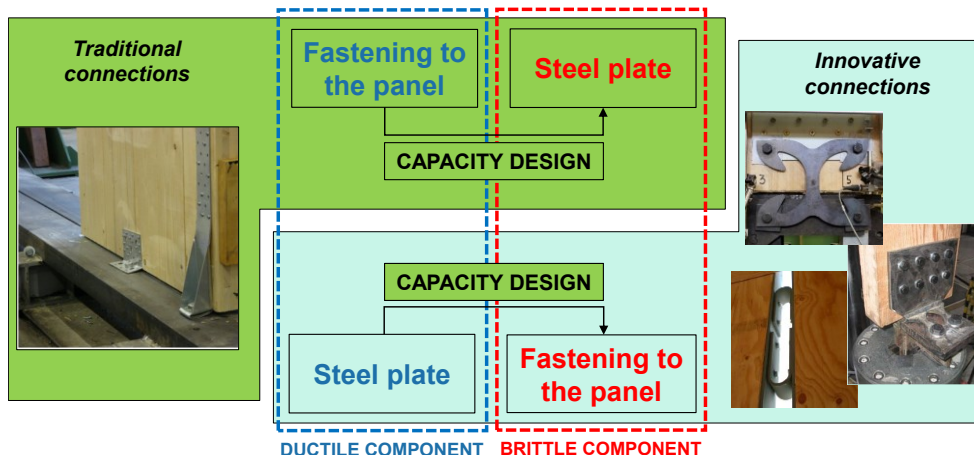


Fig. 3.6 – Duality of failure mechanisms between traditional and innovative connections.

3.1.2 Capacity design of connections for CLT structures

Research results presented in this section are partially available in the Proceedings of International Network on Timber Engineering Research (INTER), meeting 50, 28-31 August 2017, Kyoto, Japan. Paper INTER/50-15-5 [3.44].

In order to exploit completely the improved reliability of ductile *innovative* connections it is mandatory to guarantee that failures or incompatible deformations be not localized in the brittle parts of the connection. In this context, a digression in the theoretical concepts of the capacity design criteria applied either to *traditional or innovative* CLT connection and the general procedure for the robust evaluation of proper γ_{Rd} values is reported.

The capacity design approach was originally developed for RC structures [3.45]. Its extension to timber and specifically to CLT structures has been formally defined and applied ([3.24];[3.25];[3.46]-[3.48]). Capacity design needs the definition of reliable overstrength factors γ_{Rd} , which are not provided in the current version of Eurocode 8 [3.6] for timber structures. A proposal for revision of Chapter 8 of Eurocode 8 [3.6] is available in literature ([3.49]; [3.50]). In these works, a γ_{Rd} for the CLT building technology and the formulations for its application in the capacity design are proposed.

The main obstacle to apply capacity design with *traditional* connections derives from the uncertainty in evaluating the actual strength of fasteners (i.e., the ductile component of traditional connections), which often largely exceeds the corresponding characteristic load-bearing capacity provided by Codes, e.g., Eurocode 5 [3.27] or specific Technical Approvals (ETAs). This evidence and the high standard deviation values exhibited by the ductile part of such connections result in frequent events of brittle failures [3.24]. Conversely, the use of *innovative* connections, characterized by low scattering of strength properties and well-predictable yielding and peak forces, makes capacity design more accessible. In this case, the underestimation of the actual strength of dowel-type fasteners (i.e., the brittle component of innovative connections) is on the safe side in the application of the capacity design.

Fig. 3.7 shows a conceptual model according to [3.46] of the capacity design of the weakest brittle component, starting from the strength properties of the ductile element of the system. It has to be highlighted that, the component of the connection that is desirable to deform plastically and fail before the others is identified as *ductile*, whereas all the other components that are brittle or less ductile are in any case identified as *brittle*. For example, the fastening of a connection to the CLT panel will be referred as the *ductile* part of a *traditional* connection or the *brittle* part of an *innovative* connection, independently from its actual ductility.

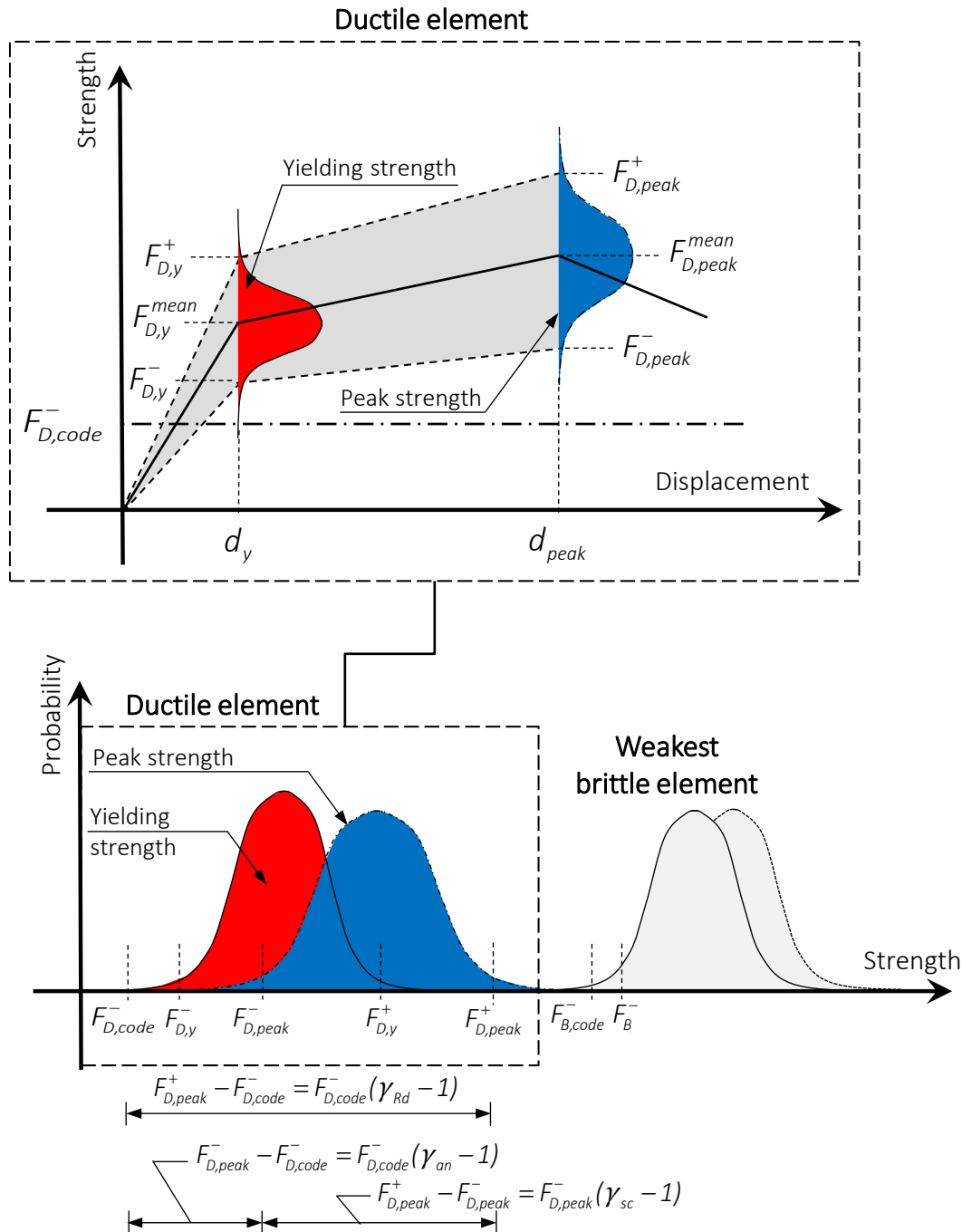


Fig. 3.7 – Yielding and peak strength of a ductile element and their statistical distribution.

This approach is based on the scattering of peak strength of the ductile part and the analytical procedures applied to evaluate such strength (i.e., rules according to a Code). The main parameters in Fig. 3.7 are:

- d_y yielding displacement;
- d_{peak} displacement corresponding to peak strength;
- F_{code}^- characteristic load-bearing capacity estimated according to Code;
- F_{peak}^- 5th percentile of the maximum strength obtained by tests;
- F_{peak}^{mean} mean value of the maximum strength obtained by tests;
- F_{peak}^+ 95th percentile of the maximum strength obtained by tests;

- F_y^- 5th percentile of the yielding strength obtained by tests;
- F_y^{mean} mean value of the yielding strength obtained by tests;
- F_y^+ 95th percentile of the yielding strength obtained by tests;
- γ_{Rd} overstrength factor;
- γ_{an} analytical overstrength ($F_{peak}^- = \gamma_{an} F_{code}^-$);
- γ_{sc} scattering of peak strength ($F_{peak}^+ = \gamma_{sc} F_{peak}^-$).
- Subscripts *B* or *D* identify brittle elements or the ductile element respectively.

The capacity design consists in fulfilling inequality (3.1), i.e., the brittle parts of the system must assure a 5th-percentile load-bearing capacity higher or equal to the 95th-percentile peak strength of the ductile part, which is expressed as the product of the overstrength factor γ_{Rd} and the Code strength $F_{D,code}^-$:

$$F_{B,code} \geq F_{D,peak}^+ = \gamma_{Rd} \cdot F_{D,code}^- \quad (3.1)$$

Hence, the overstrength factor γ_{Rd} can be defined directly as a unique term, according to Eq. (3.2), or can be split into two parts as in Eq.(3.3).

$$\gamma_{Rd} = F_{D,peak}^+ / F_{D,code}^- \quad (3.2)$$

$$\gamma_{Rd} = \gamma_{sc} \cdot \gamma_{an} = F_{D,peak}^+ / F_{D,peak}^- \cdot F_{D,peak}^- / F_{D,code}^- \quad (3.3)$$

The described conceptual model is based on the hypothesis that a set of experimental tests (at least three) is available to characterize the statistical distribution of the peak strength of the ductile component and then to compute directly $F_{D,peak}^+$. However, this experimental characterization is generally not available, and $F_{D,peak}^+$ is normally unknown by practitioners. For the same reason, in this formulation the brittle component is defined with the value $F_{B,code}^-$ and not $F_{B,y}^-$ or $F_{B,peak}^-$. Furthermore, by using $F_{B,code}^-$ (f.e., by means of the European Yielding Model [3.27]) the designer has sufficient guarantees that the brittle elements behave mostly in the pre-yielding phase, and consequently, by exploiting their highest stiffness, do not alter the stiffness of the dissipating device. Note that γ_{Rd} is code-dependent being strictly correlated to the analytical method used to compute $F_{D,code}^-$, which is the only value available to practitioners. This aspect is of utmost importance for timber connections, and specifically for CLT, for which $F_{D,code}^-$ is currently not univocally defined, depending on the chosen values of parameters in the calculation model. For instance, for a dowel-type fastener, $F_{D,code}^-$ is normally computed according to Eurocode 5 [3.27], applying the Johansen's Theory [3.26], but the resulting load-bearing capacity is not univocal, depending on the chosen values of parameters in the analytical formulations and on the special rules provided by product approvals (e.g., European Technical Approval, ETA). Therefore, γ_{Rd} values are affected not only by the statistical variability of the strength of the ductile element (γ_{sc}) but also by the analytical method to estimate its characteristic strength, according to a particular Code (γ_{an}). Therefore, it is fundamental that γ_{Rd} values proposed in a Code be consistent with the analytical methods and parameters available in the same Code.

It must be evidenced that, differently from the proposal in ([3.48]-[3.50]), the factor β_{Sd} , accounting for the strength degradation due to cyclic loading, does not appear in Eq. (3.1). According to the cited works, factor β_{Sd} (≤ 1.0) should divide $F_{D,code}^-$ to estimate the first cycle strength starting from

load-bearing capacity of the third loading cycle. However, according to the Johansen's Theory [3.26] or specific ETAs, $F_{D,code}^-$ already represents the monotonic strength of metal fasteners. Therefore, the further division of $F_{D,code}^-$ by β_{Sd} would be conceptually not consistent with the theory used to estimate the load-bearing capacity of the connector. Otherwise, the strength $F_{B,code}^-$ could be reduced by β_{Sd} when the brittle component is subjected to strength degradation, but such provision results to be excessively conservative since the application of capacity design is intended to prevent the entering of brittle components into their inelastic field.

Finally, it is worth emphasizing that, the example provided in Fig. 3.7 displays a typical connection characterized by an elastic-hardening skeleton curve with a final softening behaviour. According to standards for loading tests (e.g., EN 12512 [3.18]), the failure load F_u can be lower than the peak strength, when ultimate displacement d_u is higher than the displacement at maximum strength d_{peak} . Note that F_u is not needed for the application of the capacity design and has not to be confused with the peak strength.

3.1.2.1 Capacity design for CLT connections

As mentioned above, the application of capacity design to *traditional connections* is based on the evaluation of the strength properties of the ductile part, which is in most cases realized with small diameter nails or screws.

An exhaustive experimental research about steel-to-timber joints with ring shank nails for CLT is available in [3.48]. According to these tests and depending on the chosen parameters to compute $F_{D,code}^-$ and on the angle of the force to the face lamination of the panel, the obtained γ_{Rd} values are in the range between about 1.6 and 2.6, thus demonstrating the strict correlation between γ_{Rd} and the analytical models and parameters to compute $F_{D,code}^-$. These values may be used to apply the capacity design at connection level, to design the steel plate of the connection or the anchoring to foundation or floor.

Gavric et al. [3.21] evaluated γ_{Rd} from tests in shear or tension of angle brackets and hold-downs anchored to CLT floors or to foundation. Values of γ_{sc} and γ_{an} were given; γ_{Rd} can be obtained from their product, resulting in values in the range between about 2.0 and 3.4. These values may be useful to apply a capacity design at wall level, i.e., selected ductile connections should yield before others so assuring a rocking-type failure instead of a sliding one [3.7], or at the building level, where a "box" behaviour of the building should be assured, allowing an effective transmission of shear forces among adjacent panels [3.24].

The adoption of *innovative connections* developed to localise yielding in steel parts, and therefore with well-defined and predictable yielding and peak strength, undoubtedly would result in a more reliable application of the capacity design. No formulas are normally available to evaluate the load-bearing capacity of such connections. According to Eurocode 3 [3.51], in steel structures $F_{D,code}^-$ is normally assumed coincident with nominal $F_{D,y}^-$: this assumption can be extended to innovative connections and, according to Eq. (3.2), γ_{Rd} can be obtained directly as ratio between $F_{D,peak}^+$ and $F_{D,y}^-$. Testing of the ductile component can be handled separately from tests of brittle components. It is worth noting that for these connections, if their strength and stiffness depend only on the property of steel and not on other phenomena (e.g., friction and wood embedment), $F_{D,y}^-$ might be computed with good accuracy also by means of detailed finite-element analyses if a robust non-linear constitutive law reproducing the actual elastoplastic behaviour of steel (e.g., the Ramberg & Osgood law [3.52]) is adopted.

3.1.3 Aim of this work

The aim of this work is to develop and characterize an innovative dissipative connection, specifically developed for CLT buildings, that improves the intrinsic ductility and the cyclic behaviour of CLT wall systems.

The connector is designed to be applied with minor adaptation as a panel-to-foundation, panel-to-panel and floor-to-panel joint. The connection system exploits the aforementioned energy dissipation methods and has been designed for low to medium-rise CLT buildings and could, on the occasion, be coupled with self-centering systems.

The newly-developed connection element looks forward to apply a reliable capacity design at the joint level. In detail, the availability of results from cyclic-loading tests allows the detailed application of capacity design. Reliability of the obtained γ_{Rd} for the capacity design of the fastening of the innovative bracket to a CLT panel is demonstrated through experimental evidences. The proposed procedure for γ_{Rd} evaluation is comparatively applied also to traditional connections, for which experimental data are available in literature, to give a contribution towards the reliability of capacity design of CLT, and in general of timber buildings.

3.2 Design, testing and mechanical characterization of an innovative dissipative connection

Contents of this chapter are the results of a three-year work, which prompted a continuous improvement of the analysed system and produced subsequent versions of the dissipative device. Within each version, the investigations aimed to characterize different aspects of the connection obtaining at the end an exhaustive representation of the system (see Table 3-1). In particular, the work can be summarized in three phases, each one distinguished by a version of the connector:

- [Version 1](#): the study aimed to find the optimal shape that guarantee the best compromise between strength, ductility and dissipative capacity;
- [Version 2](#): the investigations focused on the anchoring of the device to the CLT element with particular attention to the capacity design rules;
- [Version 3](#): the analyses focused on the easiness of installation proposing an alternative anchoring system integrated into the main element;

Table 3-1 – Analysed aspect within each version.

Version Of the element	Investigated aspects			
	Cyclic performance	Capacity design	Reusability of the system	Easiness of installation
Version 1	Yes	No	No	No
Version 2	Yes	Yes	Yes	No
Version 3	Yes	Yes	No	Yes

3.2.1 Design Criteria

Currently adopted connectors for CLT panels are differentiated to prevent either sliding (angle brackets) or rocking movements (hold-downs). Conversely, the connection proposed in this work operates properly in both circumstances and has a definite behaviour when subjected to mixed axial and shear forces (deeply discussed in Chapter 4). It assures high ductility before failure and demonstrates negligible pinching behaviour, allowing one to emphasize the dissipative capacity under cyclic loading. The utilization of the proposed connection to realize both panel-to-foundation and panel-to-panel joints of shear walls is sketched in Fig. 3.8a. The usage of the bracket on different loading conditions (e.g., in in Fig. 3.8b the connection is loaded in tension/shear while in in Fig. 3.8c-d is loaded in shear only), requires a clear definition of its mechanical response in its entire shear-tensile strength domain and for each specific application. Recalling that the adequate seismic design of a specific building involves the decision about their number, position and dimensions in fulfilment of the capacity design criteria, the main mechanical parameters such as yielding and ultimate strength, displacement capacity and overstrength factors are to be defined within each possible configuration.

A practical example can be drawn analysing Fig. 3.8c and d (external and concealed panel-to-panel application) where the X-brackets are theoretically subjected to the same demand of strength and displacement capacity but shows a different post-elastic behaviour (discussed in detail in 3.2.5): *softening* for the external bracket and *hardening* for the concealed one. This lead, even for the same geometry of the bracket, to distinct values of yielding point (F_y ; $d(F_y)$) peak point (F_{peak} ; $d(F_{peak})$) and consequently, to distinct overstrength factors. As stated in Section 3.1.2.1 it emerges once again the

primary importance of the experimental characterization when analytical instruments and numerical simulations lack of precision or reliability in predicting the actual behaviour of connections.

The main objectives to be fulfilled through the parametric design of the connection's shape were: displacement capacity not less than that of alternative typically-used connections; high ductility class according to Eurocode 8 [3.6]; strength comparable to the traditional connectors [3.23]; optimized shape with minimum scraps' production in the manufacturing process.

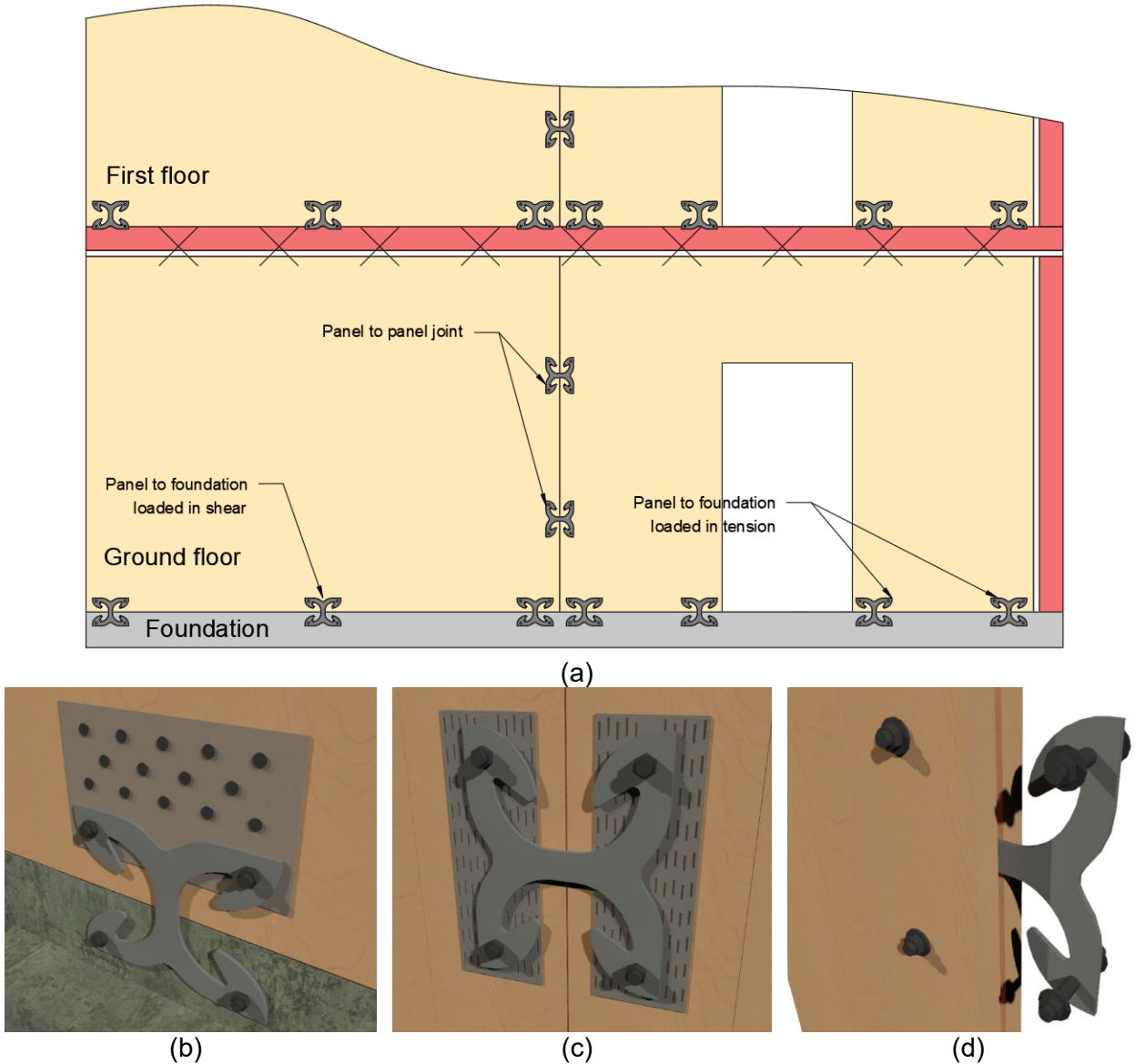


Fig. 3.8 – (a) Conceptual disposition of X-brackets in shear walls realized with CLT panels; (b) panel-to-foundation joint; (c) panel-to-panel joint; (d) concealed panel-to-panel joint.

3.2.2 Version 1

Research results presented in this section are partially available at MDPI via <http://dx.doi.org/10.3390/ma9030139> [3.53]. Journal Materials is acknowledged as the original source of publication.

3.2.2.1 Parametric Design Assisted by Numerical Modelling

Once the first-tentative “X” shape was decided, a parametric Finite-Element (FE) model with modifiable geometries was used to derive the optimal dimensions, which fulfil the design criteria listed above. A 3D FE model of the X-bracket using high-order solid elements was implemented into ANSYS Workbench [3.54]. The twelve geometrical parameters chosen as the variable in the model are evidenced with letters in Fig. 3.9a. To allow a single-cut production process, as shown in Fig. 3.9b, reciprocal constraints among geometrical properties were imposed (see the red and blue lines in Fig. 3.9a). Cylindrical hinges placed on the four fixing points allowed the rotation of the horizontal arms. The non-linear geometrical analysis option was activated to account for possible buckling phenomenon under high displacements. A compression only surface placed on the back of the bracket forced the possible out-of-plane buckling only on the opposite side (i.e. to simulate the presence of the CLT panel on its back).

An elastic-plastic constitutive law combined with a Von Mises yield criterion and a kinematic hardening model was adopted to simulate steel cyclic behaviour. In the parametric design phase, the elastic and hardening moduli of S275JR steel were set to 200,000 and 780 MPa, respectively, whereas yielding stress and ultimate stress were set to 275 MPa and 430 MPa, respectively. To minimize failure risk due to low-cyclic fatigue, a limit to the maximum strain of steel was imposed [3.55] when determining the ultimate displacement capacity for the X-brackets. Accordingly, maximum axial deformation of the X-brackets was limited between +10% and -2% (the possibility of limited compressive deformation was accounted for), while their allowable shear strain was set in the range $\pm 6\%$.

Nearly 80 different combinations of the parameters were examined. Each combination consisted of a pure tension and pure shear pushover and/or cyclic loading analysis. Part of the outcomes of the final analyses are shown in Fig. 3.10: results of each change were compared with the previous one by calculating the relative strength increment ΔF measured at a fixed displacement level and the corresponding plastic strain increment/decrement $\Delta \epsilon$. The analyses ended when changes on a single parameter produced only increments of the total accumulated plastic strains.

The parametric analyses were helpful, as modifying the length and thickness of vertical and horizontal arms allowed one to calibrate shear and tensile displacement capacity, respectively. Additionally, the variation of stiffness and strength was permitted by changing the internal curvature radius. The dimensions of the final shape listed in Table 3-2 allowed one to balance at the same time the strength, stiffness and ductility values of the connector and to assure similar performance, both in shear and in tension. The chosen thickness of 6.0 mm was found to be a balanced solution to withstand high loads, while avoiding premature triggering of local buckling phenomena. The internal curvature radius connecting vertical and horizontal arms was modified until the highest amount of plasticized area was involved. In particular, the high ductility in shear is mainly assured by the plastic deformation of the vertical arm, whereas in tension by the bending deformation of the horizontal arms. Results from tests and simulations described hereafter have confirmed the good balance among the main mechanical performances to assure an optimal seismic behaviour of the device.

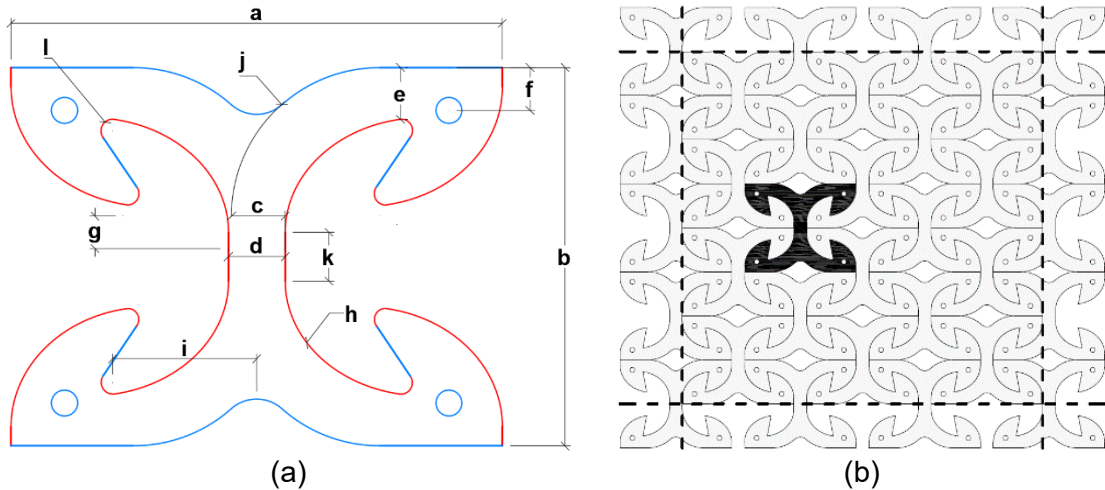


Fig. 3.9 – Shape and geometry of the connection: (a) model parameters; (b) manufacturing process from a steel plate.

Table 3-2 – Main dimensions of X-brackets relative to Fig. 3.10a.

Parameters (units)	Dimensions	Parameters (units)	Dimensions
a (mm)	303.0	h (mm)	85.0
b (mm)	233.0	i (mm)	89.0
c (mm)	33.0	j (mm)	23.5
d (mm)	35.0	k (mm)	30.0
e (mm)	31.0	l (mm)	1.0
f (mm)	33.0	Thickness (mm)	6.0
g (mm)	26.5	Hole diameter (mm)	16.0

ID	Geometrical parameters												Tensile loading					Shear loading					
	a) (mm)	b) (mm)	c) (mm)	d) (mm)	e) (mm)	f) (mm)	g) (mm)	h) (mm)	i) (mm)	j) (mm)	k) (mm)	l) (mm)	D _{1/2} (mm)	F _{1/2} (kN)	ε _{1/2} (mm/mm)	F _{1/2} Rel. diff. %	ε _{1/2} Rel. diff. %	D _{1/2} (mm)	F _{1/2} (kN)	ε _{1/2} (mm/mm)	F _{1/2} Rel. diff. %	ε _{1/2} Rel. diff. %	
V0	1	355.0	240.0	35.0	50.0	15.0	35.0	30.0		12.0	25.0	3.0	31.5	13.47	0.0624	11%	-18%	35.7	24	0.2150	0%	0%	
	2	355.0	270.0	35.0	50.0	15.0	35.0	30.0		12	25	3.0	31.7	15.24	0.0634	21%	-16%	35.7	20.16	0.1091	-18%	-97%	
	3	355.0	270.0	35.0	50.0	15.0	35.0	30.0		12	25	3.0	31.8	17.48	0.0687	31%	-7%	35.7	19.13	0.0930	-25%	-131%	
	4	355.0	300.0	35.0	50.0	8.0	35.0	30.0		50	25	3.0	31.8	17.43	0.0733	31%	-0%	35.8	19.86	0.1153	-21%	-86%	
	5	355.0	300.0	35.0	50.0	8.0	35.0	30.0		50	25	3.0	32.2	26.88	0.1194	55%	39%	35.7	20.38	0.1189	-17%	-81%	
	6	355.0	320.0	35.0	50.0	0.5	25.0	25.0		50	0.5	3.0	32.2	26.72	0.1195	55%	39%	35.9	27.50	0.1801	13%	-19%	
	7	355.0	270.0	35.0	50.0	0.5	25.0	25.0		50	0.5	3.0	32.2	26.87	0.1189	0%	0%	35.7	20.37	0.1185	0%	0%	
V0b	8	355.0	320.0	50.0	35.0		25.0	25.0		50.0	25.0	3.0	30.0	26.75	0.1170	-0%	-2%	35.7	20.37	0.1176	-0%	-1%	
	9	355.0	320.0	50.0	35.0		25.0	25.0		50.0	25.0	3.0	30.0	26.75	0.1157	-0%	-3%	35.7	20.38	0.1165	0%	-2%	
	10	355.0	320.0	50.0	35.0		25.0	25.0		50.0	25.0	3.0	25.0	24.43	0.0915	-10%	-30%	20.5	18.41	0.0608	-11%	-95%	
	11	320.0	320.0	50.0	35.0		20.0	20.0		50.0	25.0	3.0	27.5	49.08	0.1643	45%	28%	20.4	20.11	0.0705	-1%	-68%	
	12	300.0	280.0	50.0	35.0		20.0	20.0		30.0	25.0	3.0	26.9	30.65	0.1448	12%	18%	20.5	22.88	0.0954	11%	-24%	
	13	300.0	210.0	50.0	28.0		20.0	20.0		30.0	15.0	3.0	26.9	16.26	0.1018	-65%	-17%	20.8	18.08	0.0957	-13%	-24%	
	14	300.0	210.0	50.0	28.0		20.0	20.0		30.0	5.0	3.0	27.0	18.55	0.1081	-45%	-10%	20.7	20.10	0.0988	-1%	-20%	
	15	300.0	210.0	50.0	28.0		20.0	20.0		25.0	5.0	3.0	26.9	17.12	0.0995	-57%	-19%	20.8	18.44	0.0890	-10%	-35%	
	16	300.0	210.0	50.0	28.0		20.0	20.0		30.0	15.0	3.0	26.9	16.30	0.0949	-65%	-25%	20.8	17.81	0.0821	-16%	-44%	
	17	300.0	210.0	50.0	28.0		20.0	20.0		30.0	15.0	3.0	26.9	16.45	0.0946	-63%	-25%	20.8	17.81	0.0811	-16%	-46%	
	18	300.0	210.0	50.0	28.0		20.0	20.0		30.0	10.0	3.0	27.8	27.89	0.1781	3%	33%	20.8	20.48	0.1241	1%	5%	
	19	245.0	210.0	37.0	28.0		18.0	18.0		30.0	10.0	3.0	27.8	18.40	0.1948	-46%	39%	20.8	13.84	0.1248	-49%	5%	
	20	245.0	210.0	37.0	28.0		18.0	18.0		30.0	10.0	3.0	27.5	24.18	0.1582	-11%	25%	20.8	17.79	0.1098	-15%	-8%	
	21	245.0	210.0	30.0	27.0		18.0	18.0		55.0	10.0	3.0	27.5	24.19	0.1589	-11%	24%	20.8	15.50	0.1245	-10%	5%	
	22	245.0	210.0	30.0	27.0		18.0	18.0		45.0	30.0	1.0	3.0	27.8	27.95	0.1765	4%	33%	20.7	19.98	0.1166	-2%	-2%
V0c	23	245.0	210.0	30.0	30.0	28.0	40.0	20.0	89.0	85.0	40.0	5.0	7.0	27.9	28.53	0.1693	2%	-4%	20.8	22.54	0.1118	11%	-4%
	24	245.0	210.0	30.0	30.0	28.0	40.0	20.0	89.0	85.0	40.0	5.0	7.0	27.7	30.35	0.1561	8%	-13%	20.8	27.39	0.1076	27%	-8%
	25	245.0	210.0	30.0	30.0	28.0	40.0	40.0	89.0	85.0	40.0	5.0	7.0	27.7	20.20	0.1624	-38%	-9%	20.8	18.25	0.1082	-9%	-8%
	26	245.0	210.0	30.0	30.0	28.0	40.0	20.0	89.0	85.0	40.0	5.0	7.0	27.9	28.94	0.1702	3%	-4%	20.8	25.14	0.1131	21%	-3%
	27	245.0	210.0	30.0	30.0	28.0	40.0	20.0	89.0	85.0	40.0	5.0	7.0	27.8	29.44	0.1857	5%	-7%	20.7	25.48	0.1000	22%	-17%
	28	245.0	210.0	30.0	30.0	28.0	40.0	30.0	89.0	85.0	40.0	5.0	7.0	27.7	30.98	0.1573	10%	-12%	20.5	28.27	0.1580	29%	26%
	29	245.0	210.0	30.0	30.0	28.0	40.0	50.0	89.0	85.0	40.0	5.0	7.0	27.7	30.92	0.1505	10%	-17%	20.5	28.08	0.1452	29%	20%
	30	245.0	210.0	30.0	30.0	28.0	40.0	50.0	89.0	85.0	30.0	5.0	7.0	27.6	24.51	0.1519	-14%	-16%	20.8	23.59	0.1105	15%	-6%
	31	245.0	210.0	30.0	30.0	28.0	40.0	50.0	89.0	70.0	30.0	5.0	7.0	27.7	30.35	0.1540	8%	-15%	20.6	27.37	0.1068	27%	-9%
	32	245.0	210.0	30.0	30.0	28.0	40.0	40.0	89.0	85.0	30.0	5.0	10.0	27.7	30.29	0.1571	8%	-12%	20.8	27.37	0.1082	27%	-10%
	33	245.0	210.0	30.0	30.0	28.0	40.0	40.0	89.0	85.0	30.0	5.0	7.0	27.7	30.49	0.1351	8%	-31%	20.8	26.98	0.0888	25%	-26%
V0d	34	245.0	210.0	30.0	30.0	28.0	18.0	18.0	85.0	89.0	40.0	5.0	7.0	28.1	30.87	0.2109	9%	16%	20.8	27.01	0.0902	39%	-24%
	35	245.0	210.0	30.0	30.0	28.0	18.0	18.0	85.0	83.0	40.0	5.0	3.0	28.0	27.60	0.1278	-1%	-38%	20.8	26.19	0.0723	25%	-39%
	36	255.0	210.0	30.0	30.0	28.0	18.0	18.0	85.0	89.0	40.0	5.0	3.0	27.7	30.24	0.1368	8%	-29%	20.8	26.97	0.0894	27%	-27%
	37	245.0	210.0	30.0	30.0	28.0	18.0	18.0	85.0	89.0	40.0	5.0	2.0	32.9	19.87	0.0792	-41%	-123%	21.1	23.24	0.1190	12%	2%
	38	280.0	210.0	30.0	30.0	28.0	25.0	25.0	85.0	89.0	40.0	5.0	3.0	38.5	20.95	0.0978	-33%	-81%	21.1	23.28	0.1004	12%	-11%
	39	280.0	210.0	30.0	30.0	28.0	25.0	25.0	85.0	89.0	40.0	5.0	3.0	28.0	27.58	0.1279	-1%	-38%	20.8	26.19	0.0723	26%	-40%
	40	270.0	210.0	30.0	30.0	28.0	23.0	20.0	85.0	89.0	40.0	5.0	3.0	32.9	25.80	0.1332	-8%	-33%	20.5	26.16	0.1512	24%	48%
V1	41	303.0	233.0	35.0	33.0	31.0	33.0	26.5	85.0	89.0	23.5	15.0	2.0	32.9	25.79	0.1585	-8%	-11%	20.5	26.15	0.1548	23%	43%
	42	303.0	233.0	35.0	33.0	31.0	33.0	26.5	85.0	89.0	23.5	15.0	1.0	33.7	26.06	0.1325	1%	-20%	20.4	26.11	0.1035	-0%	-33%
	43	303.0	233.0	33.0	35.0	31.0	31.0	25.0	85.0	89.0	30.5	15.0	6.0	33.7	26.17	0.1200	1%	-32%	20.4	26.15	0.1080	-0%	-30%
	44	303.0	233.0	33.0	35.0	31.0	31.0	25.0	85.0	89.0	30.5	15.0	6.0	33.7	25.99	0.1669	1%	-1%	20.4	24.74	0.0691	-5%	-55%
V2	45	303.0	243.0	33.0	35.0	31.0	31.0	25.0	85.0	89.0	30.5	15.0	7.5	33.7	25.92	0.1558	1%	-2%	20.4	24.74	0.0691	-5%	-55%

Fig. 3.10 – Excerpt from the parametric analyses results. Final parameters of version 1 and 2 are highlighted in green.

Fig. 3.11 shows the deformation at maximum imposed displacements, in pure tension and pure shear loading. The grey contour shows plastic regions in which the yielding stress has been exceeded. The position and extension of yielded areas vary with the loading type; however, the spread of yielding is well evident for both tests.

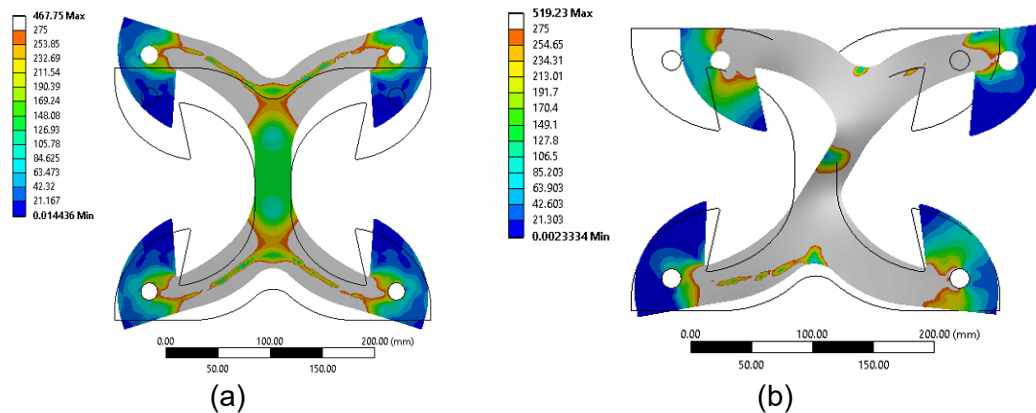


Fig. 3.11 – Numerical model: equivalent Von Mises stress contour on deformed geometry of X-brackets: (a) tension loading; (b) shear loading. Plastic regions are evidenced in grey colour.

3.2.2.2 Experimental tests of prototypes

After the design and optimization phases, preliminary experimental tests on prototypes have been conducted to obtain the actual cyclic behaviour of X-brackets. Three tests were performed in pure tension (T1, T2, T3) and as many in pure shear (S1, S2, S3). A couple of X-brackets was placed into a rigid portal in every test. Therefore, a total of twelve equal X-brackets were tested.

Tests were performed at the Laboratory of Construction and Materials, Department of Civil, Environmental and Architectural Engineering (ICEA) of the University of Padova.

Two specific setups were designed for tension and shear tests (Fig. 3.12). In order to evaluate exclusively the behaviour of the X-brackets, suitable rigid steel frames were realized to transmit load from the actuators. The couple of X-brackets were fixed externally on both sides of the supporting frame without any buckling restraining elements. This arrangement allows the local buckling phenomenon for large cycles, permitting the connector to work properly, but avoids unrealistic global out-of-plane deformation. As concerns the tension configuration (see Fig. 3.12), the two lower fixing points were connected to a rectangular 20 mm-thick steel plate rigidly fixed to the portal. The two upper fixing points were connected to another rectangular 20 mm-thick plate fixed to the hydraulic jack through an eyebolt mechanism. The pure shear loading was obtained with an unbraced steel truss, in which the X-brackets operated as the cross-bracing element (see Fig. 3.12). 15mm-thick angle-shaped steel plates were used for the steel truss. The whole assembly was positioned in a rotated configuration, in order to keep the loading direction as close as possible to the virtual diagonal line. In actual applications, friction might occur between the X-bracket and connected elements, so increasing the apparent strength and dissipative capacity of the connections. The unreliability of the friction effects imposes that they must be disregarded. Therefore, in all of experimental tests, polytetrafluoroethylene (Teflon - PTFE) sheets were interposed between contact surfaces to minimize friction and to determine purely the connection capacities assured by the X-bracket.

Cyclic tests were performed according to the quasi-static loading protocol recommended by EN 12512 [3.18]. The cyclic procedure was stopped after reaching a relative displacement of 30 mm; then the specimens were loaded monotonically until their failure. Tests were conducted under displacement control with a deformation rate of 0.02 mm/s.

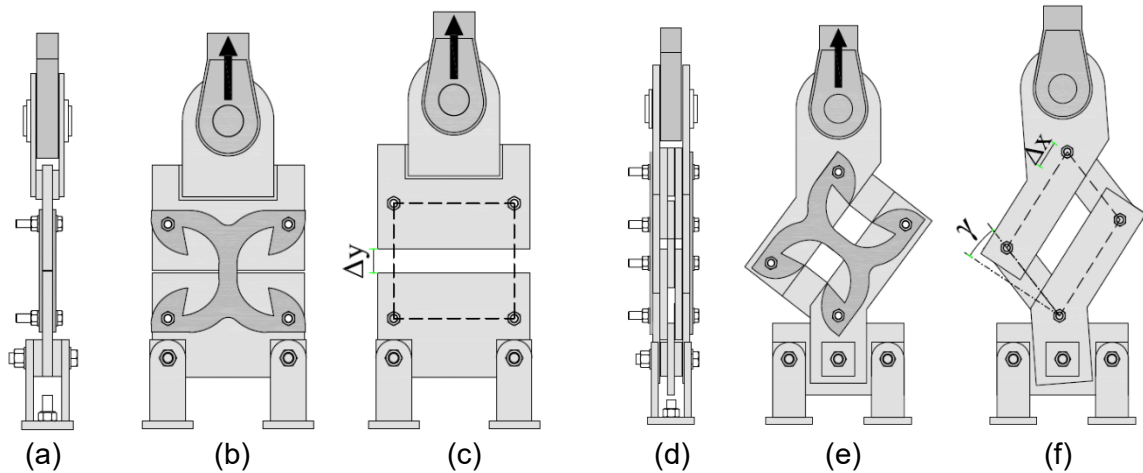


Fig. 3.12 – Setup and imposed deformations: (a,b,c) rigid frame for tension tests; (d,e,f) unbraced steel truss for shear tests.

Experimental tension and shear tests on X-brackets were reproduced with the same FE model adopted in the parametric design phase. Mean steel parameters introduced in the numerical models exposed later have been derived from tensile tests according to EN ISO 6892-1 [3.56] on specimens obtained from the same steel sheet with which the X-brackets were produced. Fig. 3.13 plots the results of the experimental tests in comparison with those from numerical analyses for a single bracket. Displacement were measured by means of one LVDT directly fixed on each side of the supporting steel plates. For tension tests, the transducer measured directly the relative displacement Δy of the two rigid plates (see Fig. 3.12c), while the shear deformation was measured by converting the virtual diagonal elongation (see Fig. 3.12f) into the actual shear displacement Δx . This was possible by the absence of gaps in the 16-mm holes of every steel component.

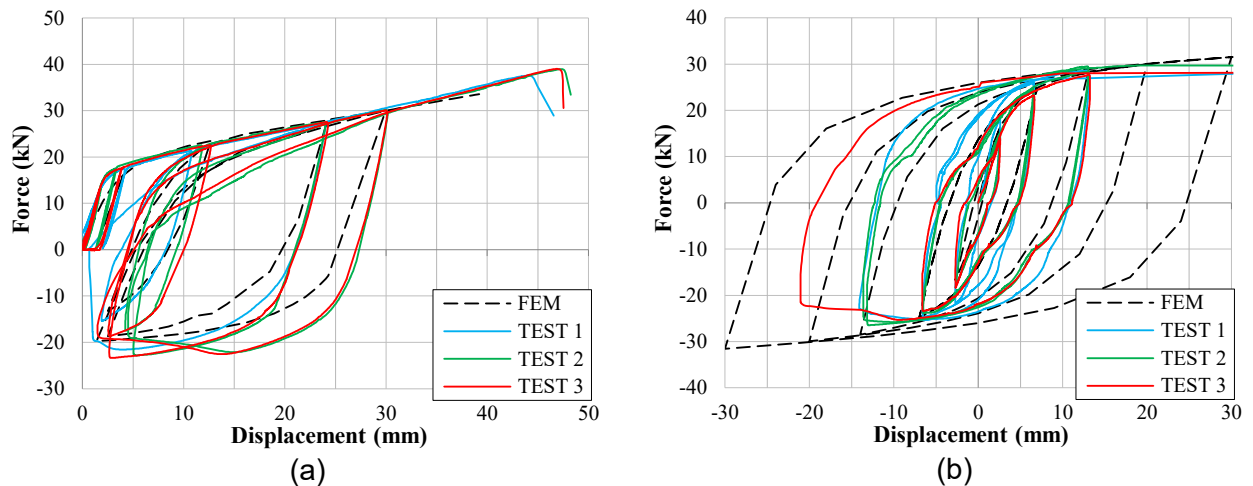


Fig. 3.13 – Experimental cycles in comparison to FEM results per bracket: (a) Tension tests; (b) shear tests.

On the 30 mm cycle of the tension test (Fig. 3.13a), the reloading path decreased gradually due to the instability phenomenon. For the same reason, the maximum compression force measured during unloading was lower than the tension one, but still maintained a wide hysteresis area and, consequently, an appropriate dissipative capacity. The numerical model tolerably underestimated force and stiffness for the unloading sequences.

Results from the shear tests are plotted in terms of force-displacement curves in Fig. 3.13b. The progressive rotation of the steel frame was accounted for the correct evaluation of the shear component of the applied force. The experimental hysteresis loops are perfectly centered on the origin of the axis, thus demonstrating the suitability of the setup configuration. The experimental cyclic shear tests were stopped at about ± 15 mm due to the limitations of the test setup. Then, X-

brackets were deformed monotonically up to 50, 58 and 80 mm in Tests S1, S2 and S3, respectively. In general, no noticeable strength degradation was observed in the experimental tests, and cracks induced by oligo-cyclic fatigue were not observed. Some differences appear between the experimental curves of Specimens S1, S2 and S3. They are mainly in the un-loading branches, when buckling of the web portion (clearly evidenced in Fig. 3.14) strongly affects the response of the brackets. Perhaps, such differences are within the normal scattering of the experimental tests.

Numerical simulations of cyclic shear tests were extended up to ± 30 mm. In the range ± 15 mm, the numerical results are in good agreement with the experiments, even if the numerical predictions slightly over-estimate shear force at higher displacements. This was possible as the numerical model permitted large deformations and considered out-of-plane buckling of the X-brackets, as shown in Fig. 3.14.

Fig. 3.15 shows the tested specimens subjected to very large displacement (35 mm in the tension test, 50 mm in the shear test). The main evidence is that X-brackets are able to experience large plastic deformations before failure, in both loading configurations. Instability phenomena of limited parts of the specimen occurred during both shear and axial tests without impairing significantly the mechanical performance of the connectors. A direct comparison between deformed geometries in Fig. 3.11 and Fig. 3.15 again shows the consistency between numerical analysis and experimental validation. Specimens failed for very large displacements due to stress concentration in fillet "j" in Fig. 3.9a. Therefore, the ductility of X-brackets could be further improved with a proper modification of this detail.

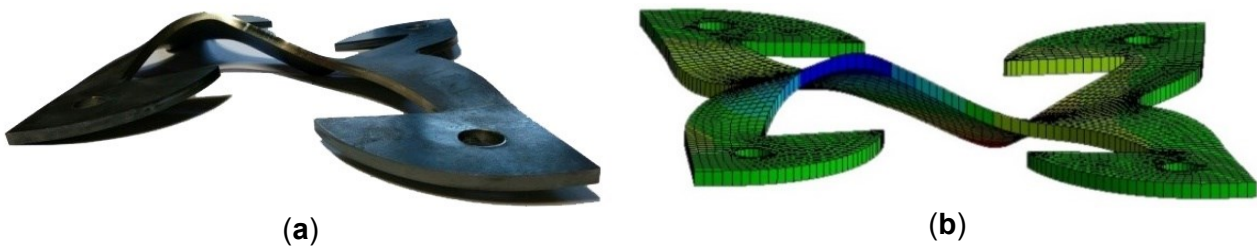


Fig. 3.14 – Plate buckling under shear loading: (a) Experimental evidence; (b) numerical prediction.

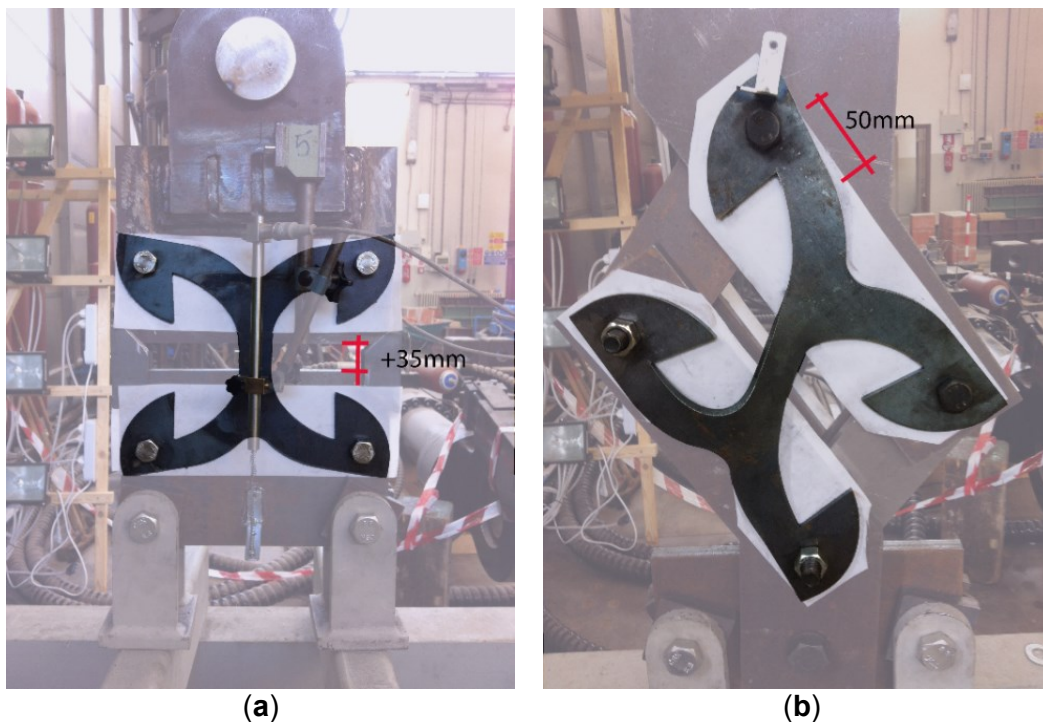


Fig. 3.15 – Deformed specimens: (a) Axial test; (b) shear test.

3.2.2.3 Analysis of Test Results

The performed cyclic tests allowed one to define the main mechanical parameters for a proper characterization of the tested elements. Various methods were proposed to compute these parameters ([3.18];[3.57]). In this work, the envelope of the hysteresis curves was fitted using the analytical formulation proposed by Foschi and Bonac [3.58]. Then, Method (a) of EN 12512 [3.18] was chosen for both axial and shear tests, in order to obtain the best linear fitting of the envelope curve. This method is suitable to interpolate data with two well-defined linear branches, and the yielding point is defined by the intersection of these two lines. Moreover, also the equivalent elastic-plastic energy (EEEE) method [3.59] was used to analyse the results of the shear test, because of the almost elastic perfectly plastic behaviour. From the bi-linear curves, it was then possible to obtain the elastic and post-elastic stiffness (k_{el}, k_{pl}), yielding point (d_y, F_y), failure condition (d_u, F_u), and ductility ratio μ and to classify the proposed connection into the appropriate ductility class, according to Eurocode 8 [3.6], i.e., low (L), medium (M) or high (H) ductility class. Table 3-3 and Table 3-4 list the obtained results referring to a single bracket, i.e., each of them represents the mean result between the couple of X-brackets contemporarily tested. Therefore, average values, standard deviations (SD) and 5th and 95th characteristic values (k^-, k^+), were computed considering a sample of six elements for both tension and shear tests.

Results show that the proposed connection is characterized by a high initial stiffness and adequate strength for both tension and shear loads. However, the most valuable result is the very high value of ductility obtained, coupled with almost the null strength degradation and limited pinching effect.

High values of ductility are the consequences of a combination of large displacement capability d_u , similar or greater than typically used connections, and an early yielding condition d_y . The highest values were obtained for the axial configuration. However, ductility for the shear configuration was computed assuming d_y as 50 mm, although in Test 3, failure of the specimen occurred for a displacement equal to 80 mm, whereas Tests 1 and 2 were stopped before failure. If the ultimate displacement capacity of 80 mm was assumed, ductility values in shear tests would become higher and comparable to those from axial tests. It must be highlighted that these steel connection have evidently a different displacement capacity if the load is applied monotonically or cyclically, due to the accumulation of plastic strain and consequent failure due to oligocyclic fatigue typical of steel elements. Analysing values of initial stiffness and of yielding and ultimate forces from the two configurations, it can be observed that the connection shows a similar response when subjected to shear or axial loads.

Table 3-4 lists the 5th and the 95th percentile of the ultimate and yielding force (k^-, k^+), computed according to EN 1990 [3.60]. According to the capacity design criteria the ratio described in Eq. (3.2) is fundamental for the estimation of the overstrength factor to be used in the capacity design approach. Since only steel from a single sheet has been used for the realization of the tested X-brackets, the obtained values should be further amplified to account for the typical randomness of steel properties. Furthermore, characteristic values were obtained from a limited number of tests; therefore, the actual dispersion of the parameters may be different, resulting in slightly different overstrength values. Nevertheless, it can be stated qualitatively that the proposed connection assures limited values of γ_{Rd} , which are lower than those shown by traditional connections failing on the timber side (ductile failure). This indicates that the adoption of capacity design rules would become less onerous in designing CLT structures with innovative connections. This topic will be better examined in the Section 3.2.3.3.2 where an example of application to a CLT panel is investigated in deep.

Table 3-3 – Tension tests: main mechanical parameters according to EN 12512 method a [3.18].

Parameters (units)	Test T1	Test T2	Test T3	Mean	SD	COV	k ⁻	k ⁺
F_y (kN)	17.55	18.37	17.99	17.97	0.36	2.03%	17.18	18.76
d_y (mm)	1.89	2.01	1.98	1.96	0.06	3.02%	1.83	2.09
F_{max} (kN)	37.18	37.84	38.25	37.76	0.48	1.28%	36.70	38.81
d_u (mm)	44.30	47.30	47.00	46.20	1.48	3.20%	-	-
k_{el} (kN/mm)	9.31	9.12	9.08	9.17	0.11	1.17%	8.94	9.40
k_{pl} (kN/mm)	0.46	0.43	0.45	0.45	0.01	3.30%	0.42	0.48
μ (V_u) (-)	23.49	23.49	23.72	23.57	0.12	0.52%	23.30	-
Ductility Class	H	H	H	-	-	-	-	-

Table 3-4 – Shear tests: main mechanical parameters according to EN 12512 method a [3.18] and EEEP method [3.59]).

Parameters (units)	Test S1		Test S2		Test S3		Mean		SD		k ⁻		k ⁺	
	EN	EEEE	EN	EEEE	EN	EEEE	EN	EEEE	EN	EEEE	EN	EEEE	EN	EEEE
F_y (kN)	26.71	27.41	29.41	28.88	28.14	27.83	28.09	28.04	1.21	0.68	25.46	26.56	30.71	29.52
d_y (mm)	2.38	2.60	4.00	4.45	4.02	4.53	3.46	3.86	0.84	0.98	1.63	1.73	5.30	5.99
F_{max} (kN)	29.00	27.41	29.70	28.88	28.40	27.83	29.03	28.04	0.58	0.68	27.76	26.56	30.30	29.52
d_u (mm)	50.00*	50.00*	58.00*	58.00*	50.00	50.00	-	-	-	-	-	-	-	-
k_{el} (kN/mm)	11.24	10.55	7.36	6.49	7.00	6.14	8.53	7.73	2.10	2.19	3.95	2.95	13.12	12.50
k_{pl} (kN/mm)	0.05	0.00	0.01	0.00	0.00	0.00	-	-	-	-	-	-	-	-
μ ($d_u=50$ mm)	21.04	19.24	12.51	11.24	12.44	11.03	-	-	-	-	-	-	-	-
Ductility Class	H	H	H	H	H	H	-	-	-	-	-	-	-	-

* Tests 1 and 2 were stopped before the ultimate displacement.

3.2.3 Version 2

After the encouraging results obtained with the *version 1* of the X-bracket, a second prototype was conceived applying minor shape adjustments, involving fillet radius and hole spacing, with the aim to further improve the connection's strength. Geometry of the zones subjected to yielding, which is responsible of the actual hysteretic behaviour, was not modified. A 6-mm thick steel plate, with strength corresponding to a S450 steel grade according to EN 10025-2 [3.61], was chosen to realize the latest specimens cyclically tested in the laboratory of construction material testing of Department ICEA of the University of Padova.

3.2.3.1 Experimental tests

Six mechanical tests (three in tension and three in shear) were performed according to the quasi-static cyclic-loading protocol of EN 12512 [3.18], imposing a yielding displacement $d_{y,est}$ equal to 4mm, calculated according to initial numerical simulations and preliminary monotonic tests. The same symmetric test procedure of the *version 1* was followed, by anchoring a couple of X-brackets to a rigid steel frame, with M16 8.8-class steel bolts (Fig. 3.16). Therefore, six brackets were tested in tension and six in shear. Two LVDTs According to EN 12512 [3.18] the cyclic procedure should be stopped at 30 mm of relative displacement. However, for the tension tests the X-brackets were

cyclically loaded up to their actual failure, which occurred at 48mm, i.e., $12d_{y,est}$, due to the strength degradation recorded at that cycle amplitude (see Fig. 3.17b).

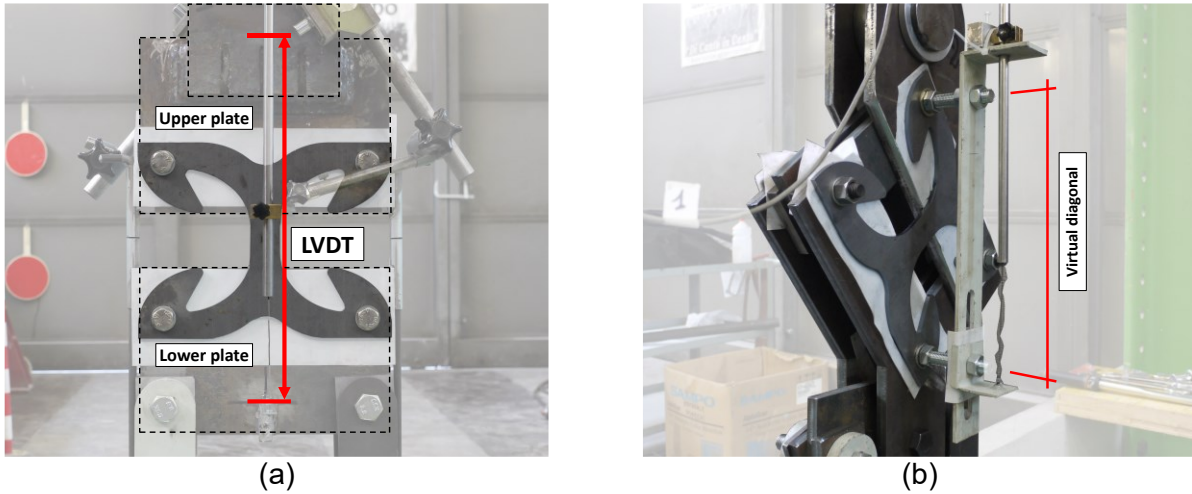


Fig. 3.16 – Test setup of version 2 and positioning of LVDTs for tensile (a) and shear (b) tests.

Obtained results show that the proposed connector is characterized by large ductility resulting from a combination of high elastic stiffness and elevated displacement capacity. These properties confer to a CLT structure realized with these connections, a low-damage rigid behaviour for low-intensity earthquakes, and high displacement capacity for high seismic shocks. In tension tests, failure occurred due to large amount of plastic deformations of the vertical web, which is subjected to out-of-plane buckling during the unloading phase and consequent strength degradation during the reloading (see Fig. 3.17a). This phenomenon starts from the 24mm cycles, whereas up to this deformation, no instability or strength degradation occurred. Moreover, for the subsequent 32, 40 and 48mm cycles, the hysteretic response was still very acceptable and all the three repeated cycles were successfully completed (see Fig. 3.17b). Also for shear tests, failure was located in the vertical web, which is subjected to repeated load inversions and consequent out of plane buckling phenomena for large deformations (i.e. ± 16 mm cycles in Fig. 3.18a). However also for shear tests, all three ± 32 mm cycles were completed without showing excessive strength degradation (see Fig. 3.18b).

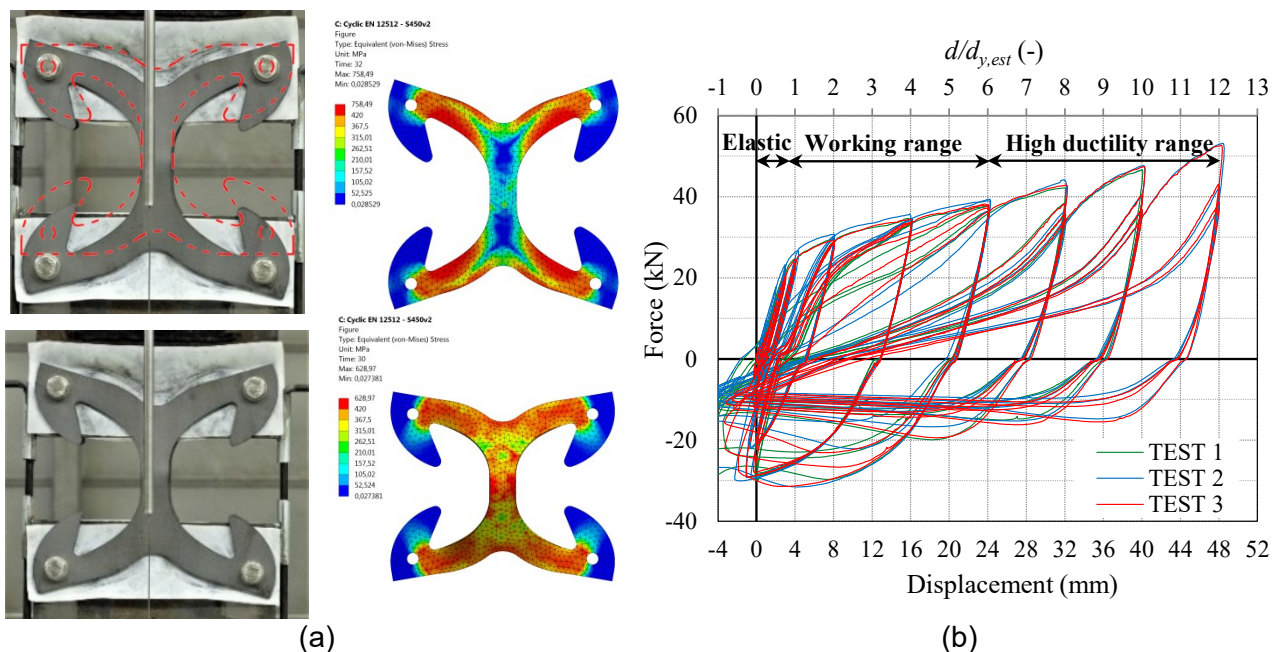


Fig. 3.17 – Axial tests of the X-brackets: photos of non-deformed and deformed specimens (a) and force-displacement curves for a single bracket (b) (ductility evaluated as $d_u/d_{y,est}$ according to the loading procedure).

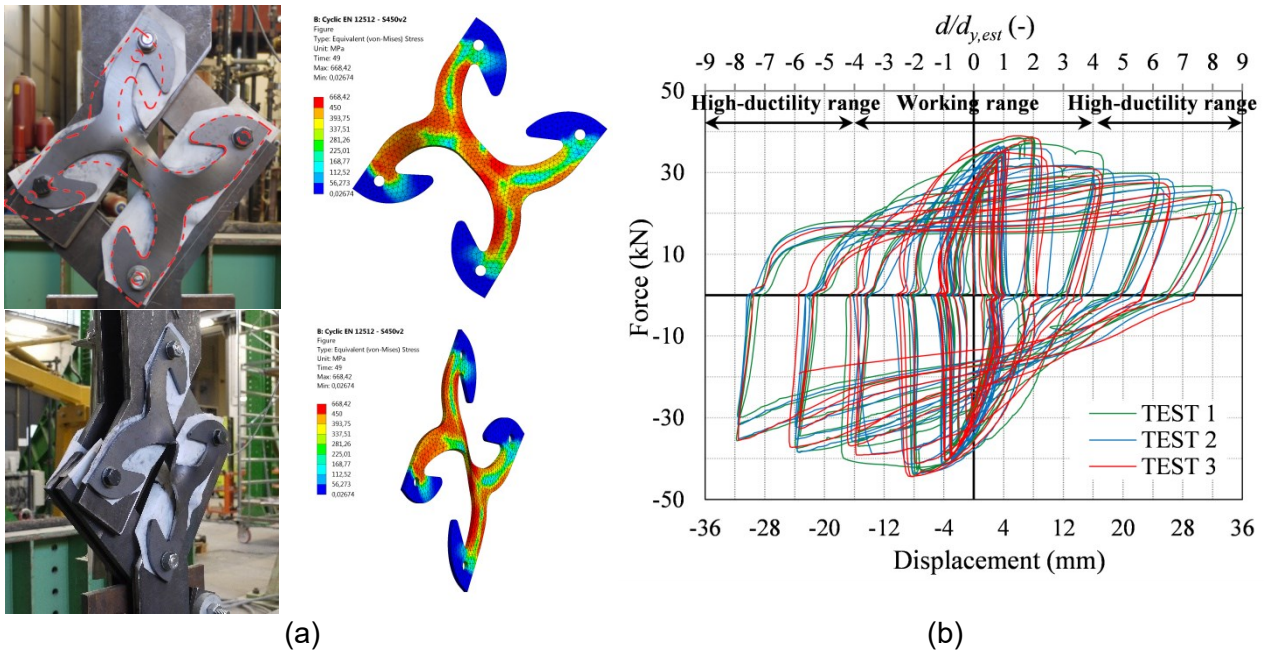


Fig. 3.18 – Shear tests of the X-brackets: photos of non-deformed and deformed specimens (a) and force-displacement curves for a single bracket (b) (ductility evaluated as $d_u/d_{y,est}$ according to the loading procedure).

3.2.3.2 Analysis of Test Results

Mechanical parameters and ductility

The performed cyclic tests allowed defining the main mechanical parameters as the previous version, by fitting the envelope of the hysteresis curves using the analytical formulation proposed by Foschi and Bonac [3.58] and applying proper bi-linearization methods. In particular, similarly to *version 1*, due to the different post-elastic behaviour of the connector, method (a) of EN 12512 [3.18] was chosen for tensile tests results while the EEEP method [3.59] was considered suitable for pure shear tests.

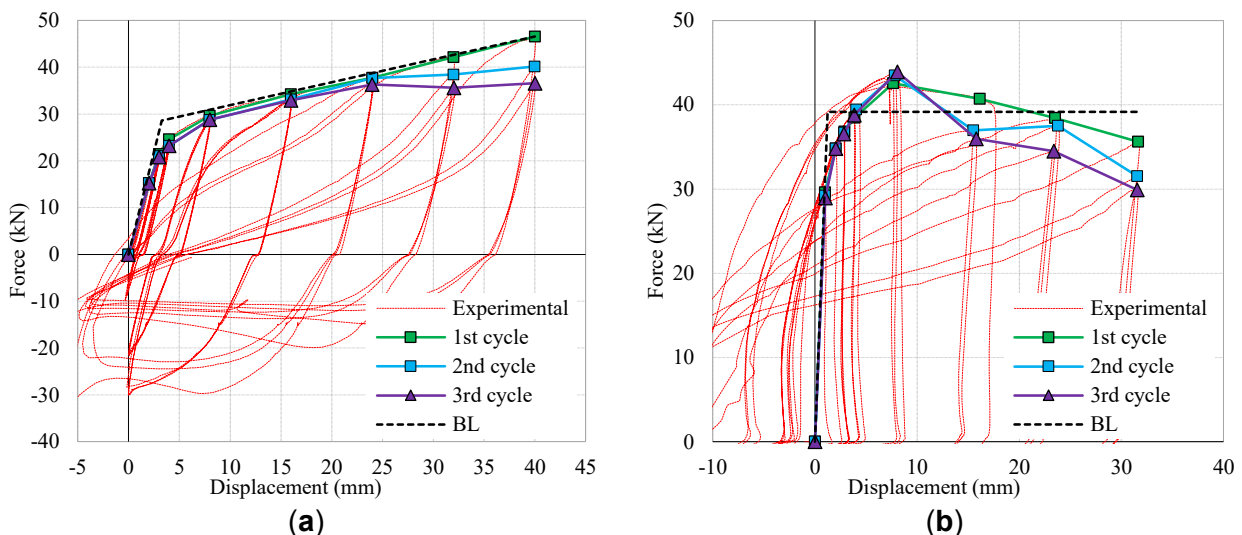


Fig. 3.19 – Envelope of cycles and bi-linearization of tension (a) and shear (b) tests of the X-brackets.

From the obtained bi-linear curves (see Fig. 3.19), it was possible to classify the proposed connection into the appropriate ductility class (Low (L), Medium (M) and High (H), according to Eurocode 8 [3.6]. These values are listed in Table 3-5, whereas the equivalent viscous damping v_{eq} and strength degradation ΔF are discussed in the next subsection. Characteristic 5th percentile and

95th percentile values were calculated assuming a normal distribution according to EN 1990 [3.60] and EN 14358 [3.62]. The upgrade of the steel strength produced an increment of strength and stiffness with respect to *version 1* compatible with the difference between an S275 and S455 [3.61]. The higher amount of cycles performed on both configurations with respect to *version 1* showed a reduced ultimate displacement capacity of the X-bracket, especially in shear configuration. However, the slighter re

Table 3-5 – Tension tests: main mechanical parameters according to EN 12512 method a [3.18].

Parameter (units)	TEST T1	TEST T2	TEST T3	Mean	SD	COV	EN 1990		EN 14358	
							k ⁻	k ⁺	k ⁻	k ⁺
F_y (kN)	28.59	29.51	28.16	28.75	0.62	2.14%	27.41	30.09	25.39	32.11
d_y (mm)	3.26	3.08	3.21	3.18	0.08	2.53%	3.01	3.36	2.81	3.55
F_{max} (kN)	46.60	47.60	47.30	47.17	0.46	0.97%	46.17	48.17	41.65	52.68
d_u (mm)	40.00	40.00	40.00	40.00	0.00	0.00%	-	-	-	-
k_{el} (kN/mm)	8.78	9.57	8.77	9.04	0.41	4.57%	8.14	9.94	7.98	10.10
k_{pl} (kN/mm)	0.49	0.49	0.52	0.50	0.02	3.12%	0.47	0.53	0.44	0.56
μ (d_u) (-)	12.29	12.98	12.46	12.58	0.32	2.56%	11.87	-	11.10	0.00
Ductility Class	H	H	H	-	-	-	-	-	-	-

Table 3-6 – Shear tests: main mechanical parameters according to EEEP method [3.59].

Parameter (units)	TEST 1	TEST 2	TEST 3	Mean	SD	COV	EN 1990		EN 14358	
							k ⁻	k ⁺	k ⁻	k ⁺
F_y (kN)	39.15	39.51	39.84	39.50	0.31	0.78%	38.83	40.17	34.88	44.12
d_y (mm)	1.24	1.26	1.25	1.25	0.01	0.97%	1.23	1.28	1.11	1.40
F_{max} (kN)	43.91	43.59	44.45	43.98	0.39	0.88%	43.14	44.83	38.84	49.13
d_u (mm)	32.00	32.00	24.00	-	-	-	-	-	-	-
k_{el} (kN/mm)	31.64	31.25	31.75	31.55	0.23	0.74%	31.03	32.06	27.85	35.24
k_{pl} (kN/mm)	0.00	0.00	0.00	0.00	-	-	-	-	-	-
μ (V_u) (-)	25.86	25.31	19.13	23.43	3.34	14.27%	16.14	-	15.61	0.00
Ductility Class	H	H	H	-	-	-	-	-	-	-

Hysteretic response

With reference to the hysteretic loops of Fig. 3.17b and Fig. 3.18b, three different displacement ranges can be identified to clarify the usage of the connector for high-ductility CLT buildings:

- The *elastic range*, which is characterized by high elastic stiffness and therefore high strength vs. low displacement, which is favourable for static lateral loads (e.g., wind action) or low-intensity earthquakes (i.e., damage limitation state - DLS)
- The *working range*, which comprises an optimal behaviour of the X-bracket in terms of high dissipation capacity, limited instability phenomena, no pinching behaviour and low strength degradation, all conditions that are favourable for high-intensity earthquakes (i.e., ultimate limit state - ULS). In this displacement range the response of this connector is much better than *traditional* connections ([3.20]-[3.21]) and the hysteretic property of the structural steel is entirely employed;
- The *high-ductility range*, which is characterized by instability phenomena during unloading, lower dissipative capacity and higher strength degradation than the working range. However,

this range is useful to assure the high ductility, i.e., to avoid failure even if the working range is exceeded during the earthquake guaranteeing a wide safety margin. This displacement range is not reached by *traditional* connections, which normally fail for displacements lower or equal than 30mm ([3.21];[3.23]).

Fig. 3.20 and Fig. 3.21 show the calculated equivalent viscous damping ratio v_{eq} within each half cycle and the corresponding maximum strength. Tension tests shows that the calculated v_{eq} at the 3rd cycle is comprised between 6 and 15% in the working range. These values are much higher than traditional connections (see section 3.1). The measured strength degradation ΔF becomes significant only for very high ductility values ($d/d_y > 6$) where the accumulated plastic strains are leading to the failure of the vertical web. With reference to shear tests, the device is characterized by an early yielding displacement d_y resulting in a high inelastic working range with viscous damping ratio always higher than 30%. Also registered strength degradation ΔF within 1st and 3rd cycle is negligible up to ductility values μ equal to 8 (that is $d = \pm 16\text{mm}$). Even if the high ductility range is characterized by a pinching behaviour due to buckling phenomena described in the previous section, v_{eq} values are still much higher than *traditional* angle brackets [3.20]. The slight dispersion of v_{eq} measured in the $\mu=4$ cycles is due to an earlier out-of-plane buckling initiation of the web occurred in test 2.

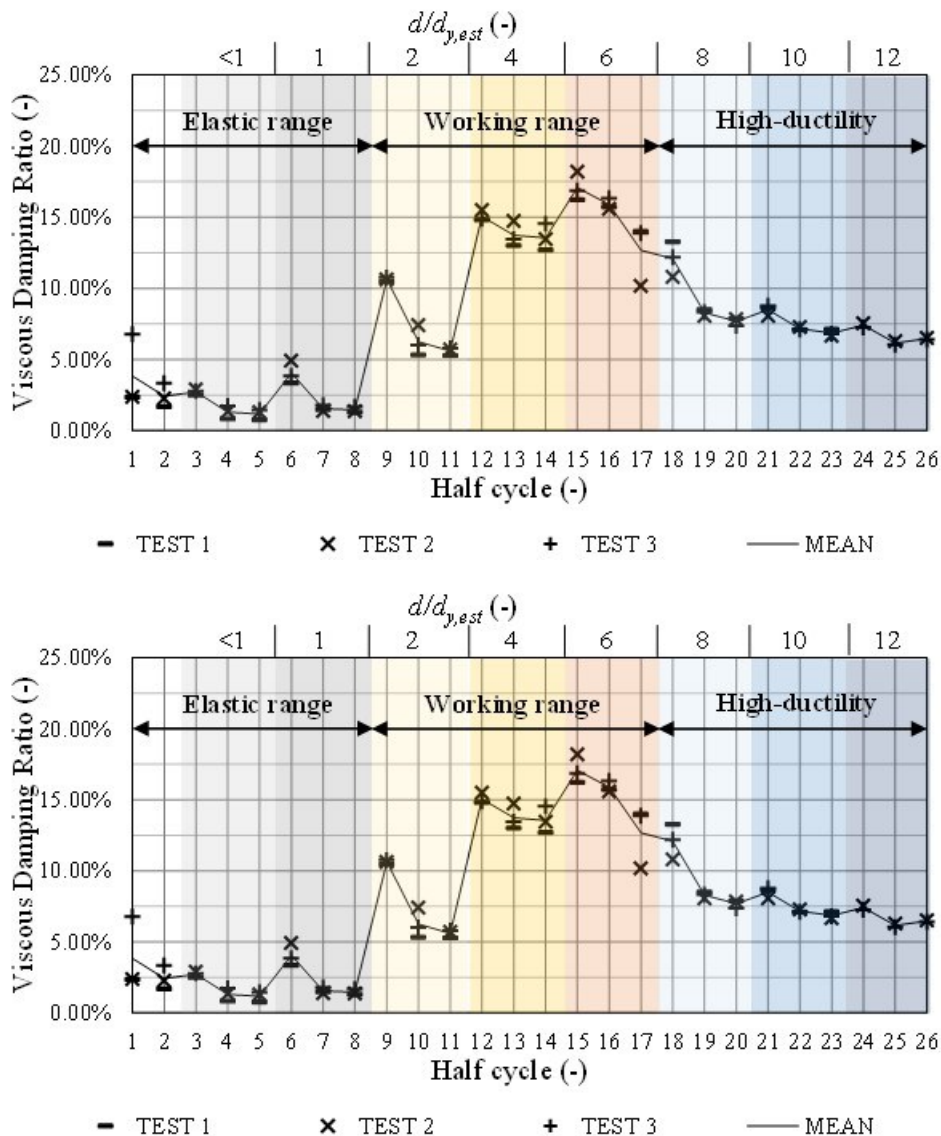


Fig. 3.20 – Progress of viscous damping ratio and strength during the cyclic tests for tensile tests.

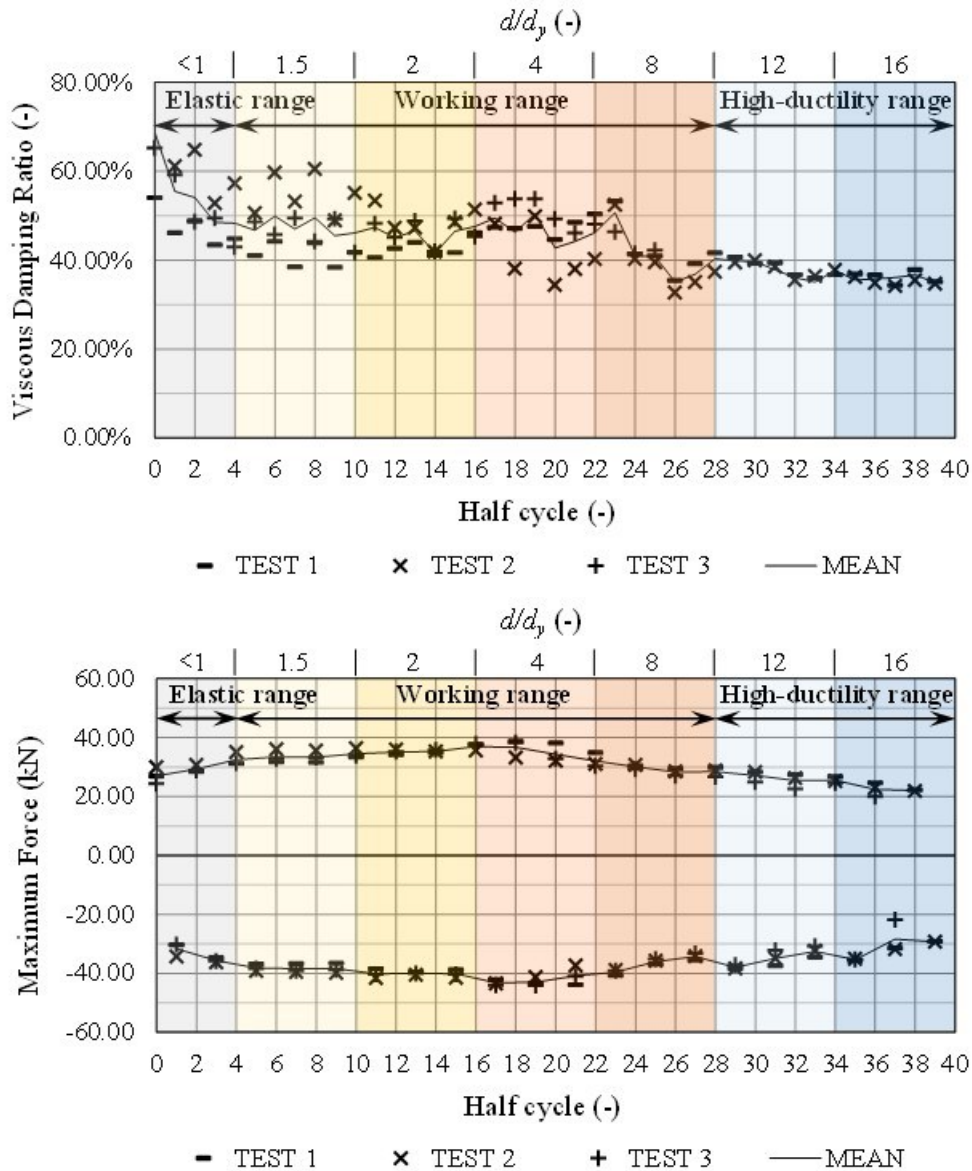


Fig. 3.21 – Progress of viscous damping ratio and strength during the cyclic tests for shear tests.

3.2.3.3 Application of the capacity design

3.2.3.3.1 Overstrength factors

The tension tests of the X-bracket and the bi-linearization method (a) of EN 12512 [3.18] returned $F_{D,y}^-$ and $F_{D,peak}^+$ values $F_{D,code}^-$ of 27.41 kN and 48.17 kN respectively, according to EN 1990 [3.60]. Therefore, the resulting overstrength factor γ_{Rd} for the X-bracket loaded in tension, according to the conceptual model presented in section 3.1.2 and assuming $F_{D,code}^- = F_{D,y}^-$, is equal to 1.76. In shear loading conditions, γ_{Rd} is equal to 1.15, resulting from $F_{D,y}^-$ and $F_{D,peak}^+$ values of 38.83 kN and 44.83 kN respectively. This lower value for the shear tests is mainly due to the perfectly plastic behaviour.

Table 3-7 shows a comparison of γ_{Rd} values for traditional hold-downs, angle brackets and for steel-to-timber joints with ring shank nails laterally loaded in parallel or perpendicular to face lamination of the CLT panel. These values have been extrapolated from literature ([3.21];[3.48]), assuming as

$F_{D,code}^-$ the characteristic load-bearing capacities evaluated according to Eurocode 5 [3.27], which are available in the same research works. It is worth noting that the obtained γ_{Rd} for the X-bracket is mostly due to the post-elastic stiffness and the high displacement capacity of the connector and not to the dispersion of results. Therefore, if lower ultimate displacement levels are reached during an earthquake a wide safety margin is assured applying such value.

Table 3-7 – Comparison of overstrength factors for the innovative bracket, steel-to-timber nails and standard hold-downs and angle brackets.

Connector / Fastener	γ_{sc}	γ_{an}	γ_{Rd}
X-bracket Version 2 in tension	1.04	1.68	1.76
X-bracket Version 2 in shear	1.04	1.11	1.15
Nails loaded parallel to face lamination*	1.27	1.61	2.04
Nails loaded perpendicular to face lamination*	1.53	1.69	2.59
Hold-down in tension**	1.30	2.60	3.38
Hold-down in shear**	1.38	-	-
Angle bracket in tension**	1.23	2.80	3.44
Angle bracket in shear**	1.16	1.70	1.97

*Values extrapolated from [3.48]; **Values extrapolated from [3.21]

3.2.3.3.2 Anchoring to the CLT panel

The anchoring of the X-bracket to a CLT panel subjected to tensile loads was designed, referring to the mechanical properties of the bracket in tension and γ_{Rd} evaluated in the previous section. The timber element is a 120mm thick CLT panel composed by 5 layers of C24 timber boards. The two 16mm diameter upper fixing points of the X-bracket are supposed to be fastened to the panel with two 16x200mm 8.8-class calibrated bolts, to allow the horizontal arms to rotate and to dissipate energy due to steel plasticization. These two cylindrical restraints are subjected to high concentrated forces, which would result in predominant wood embedment, compromising the dissipative properties of the connection. Several techniques are available both to improve strength and stiffness of dowel-type joints and to reduce the pinching phenomenon (e.g., punched steel plates, toothed plate connectors, hollow steel tubes) [3.63]. In this application, a technique similar to punched metal plates [3.64] has been chosen, using a thin steel plate placed between the bracket and the panel with two 16mm diameter holes in correspondence to the fixing points of the bracket. A rectangular S275JR steel plate with dimensions of 330x200x3mm, was designed and fastened to the panel with fourteen 8x100mm self-tapping partially threaded screws. The characteristic load-bearing capacity of the screws $F_{B,code}^-$ was computed according to Eurocode 5 [3.27]. In detail, a total shear strength $F_{B,code}^- = 52.86$ kN was obtained for the effective number of screws, evaluating the characteristic embedment strength in the timber member $f_{h,k}$ according to Eurocode 5 formulation [3.27], assuming the fastener yield moment $M_{y,Rk}$ and withdrawal capacity $f_{ax,k}$ according to ETA [3.65] and a the characteristic value of panel density ρ_k equal to 385 kN/m³. This value of $F_{B,code}^-$ is higher than $\gamma_{Rd} \cdot F_{D,code}^- = 48.24$ kN (assuming again $F_{D,code}^- = F_{D,y}^-$), thus fulfilling Eq. (3.3) and complying with the capacity design. In addition, the other brittle mechanisms of the complete connections were verified according to the capacity design, i.e., shear failure of bolts, steel plate embedment and plug-shear failure of the CLT panel. Spacing and edge distance of fasteners were verified according to Eurocode 5 [3.27].

A cyclic-loading test of the complete connection was conducted following the same cyclic-loading procedure and setup adopted for the bracket, in order to obtain a direct comparison between the

hysteretic behaviour of the X-bracket and of the complete connection. The experimental test of the complete connection was conducted only in tension. However, by changing the plate dimensions and the position of the screws, it is possible to realize the same over-resistant connection in case of shear loading conditions.

It is worth noting that the symmetric disposition was intentionally made to simulate the actual conditions of anchoring the CLT panel to the concrete foundation: it should imply two external X-brackets for each connection point whereas a one-sided application, and its consequent load eccentricity, could anticipate the out-of-plane buckling of the web and reduce the load bearing capacity, especially with mainly tensile loading conditions. Fig. 3.22 shows the photos of a non-deformed and a deformed specimen. Displacement were measured with a couple of LVDTs per side. In particular, one instrument (LVDT_1) measured the relative displacement (uplift) between the steel frame (lower fixing point of the X-bracket and the CLT panel while the second (LVDT_2) measured the relative slip between the steel plate and the CLT panel. In these tests, the external bracket was not in contact with the CLT panel (due to the 3-mm steel plate) and any secondary frictional effects were avoided by the insertion of PTFE sheets in correspondence of the 16-mm steel bolts (see Fig. 3.22). However, the possible frictional effects induced by an adherence of the X-bracket and the CLT panel, for example by adopting a different anchoring system, should not be relevant for the rather small contact surface between the arms of the bracket and the timber element.

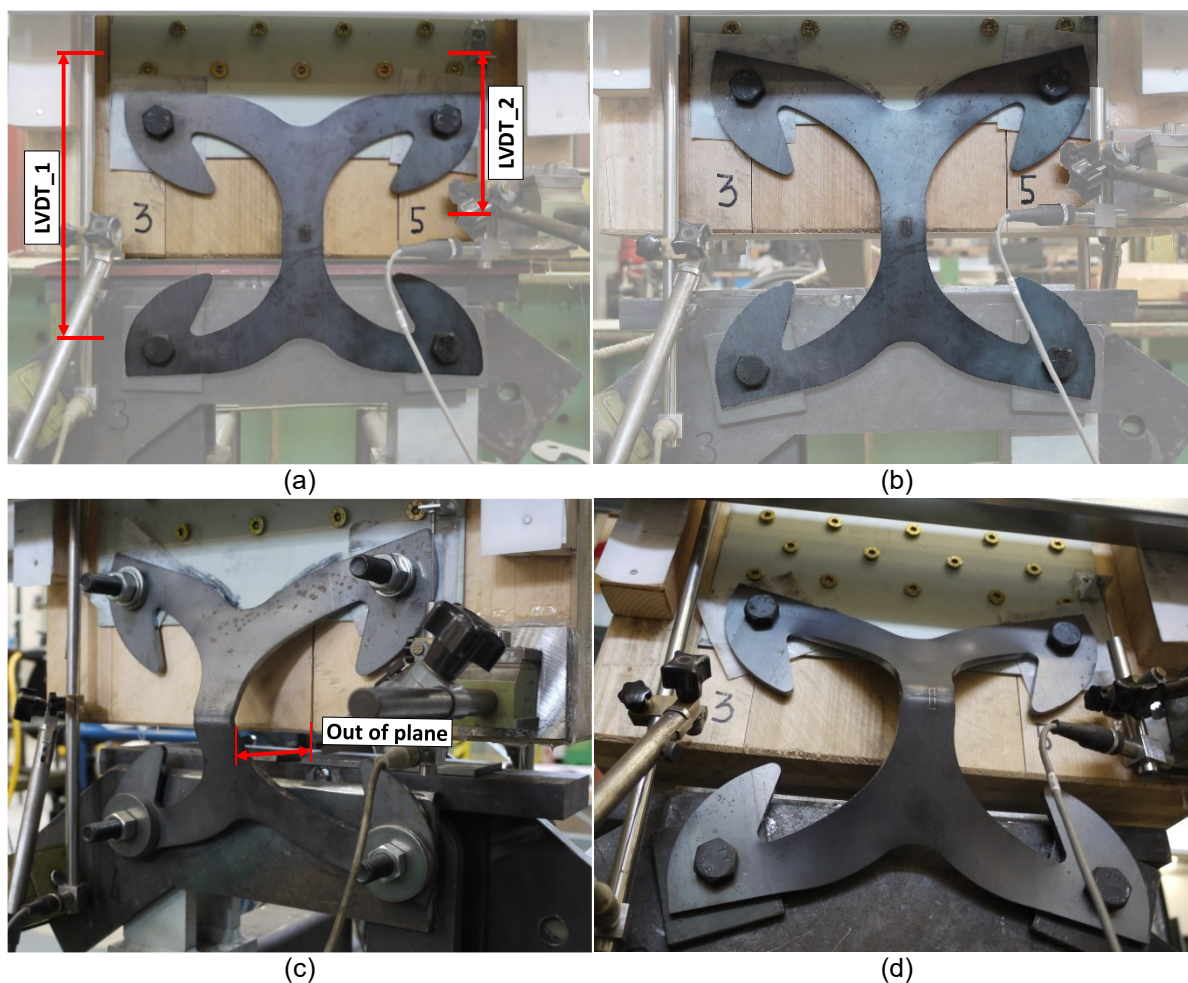
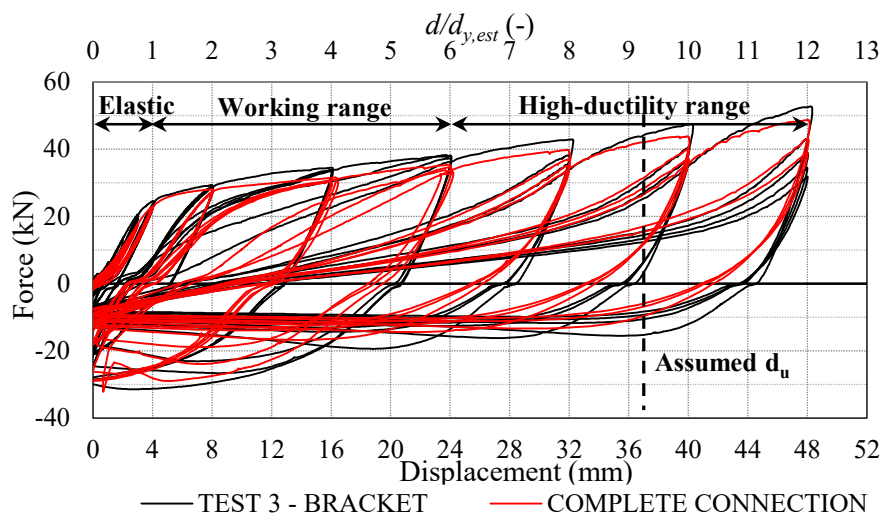


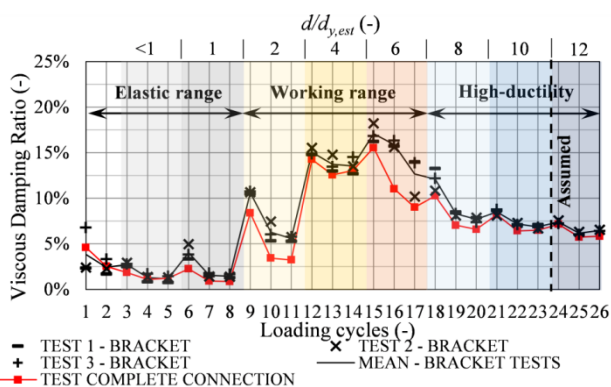
Fig. 3.22 – Test of the complete connection: (a) photo of the non-deformed specimen; (b) specimen at maximum vertical displacement of 48m; (c,d) failure due to accumulated plastic work in the connector's web.

From the superimposition of the results recorded for the X-bracket and the test of the complete connection, a very similar hysteresis behaviour (Fig. 3.23a) and a negligible decrease of dissipative capacity and strength was evidenced (Fig. 3.23b-c). The maximum relative slip of the 3-mm steel

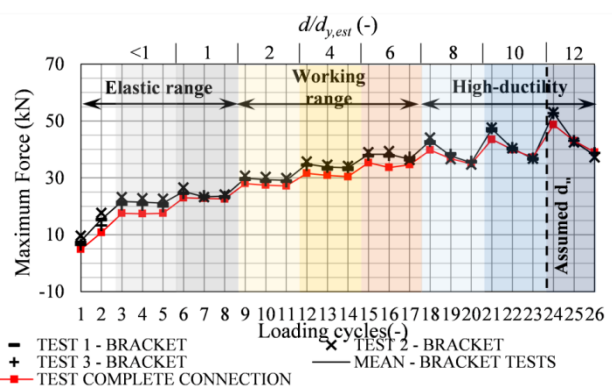
plate is contained within 0.4mm, negligible with respect to the displacement amplitude of the bracket. The reduction of strength and dissipative capacity (in terms of viscous damping ratio v_{eq} [3.18]) for the complete connection with respect to the mean value from the three tests of the X-bracket can be quantified from a comparison of the red and the black lines in Fig. 3.23b-c for all the loading cycles. It can be noted that no relevant strength reduction was recorded: a mean difference in strength equal to 2.75 kN (about 8.0%) was obtained in the working range and lower value in the high-ductility range. This proves that in the high-ductility range, characterized by the highest tensile loads, the proposed connection system is still able of withstanding the imposed loads and the hardening behaviour of the X-bracket (included in $\gamma_{Rd} = 1.76$) is completely exploited, in compliance with the capacity design approach. A slight decrease of viscous damping ratio was recorded in the working range. However, the resulting values show again the high dissipation capability of the X-bracket also considering the slight reduction of performances due to the low elastic deformation of the fastening system. The recorded viscous damping ratios both in the working and in the high-ductility range are substantially higher than traditional hold-downs, having v_{eq} of about 3 due to marked pinching behaviour [3.20].



(a)



(b)



(c)

Fig. 3.23 – Comparison among tests of brackets and of the complete connection in tension: (a) hysteresis cycles; (b) Equivalent viscous damping; (c) Maximum force per loading cycle ($d_{y,est} = 4.00$ mm).

3.2.3.3.3 Repeated test of the anchoring to the CLT panel (low damage design)

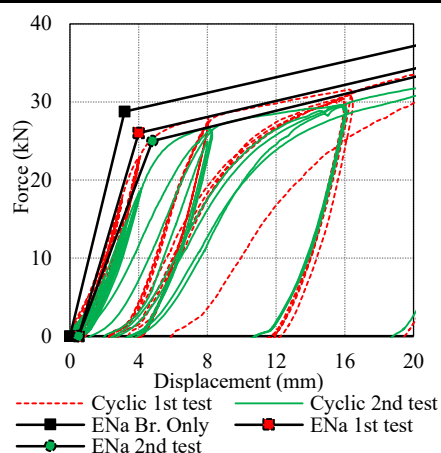
Low-damage design is gaining more and more interests ([3.36];[3.66]), especially in high seismic zones, where multiple earthquakes could affect the life of a building. Such technique is being investigated in several research works, in particular for multi-storey timber buildings but might be applied also to low-rise structures with specific DLS and ULS requirements (for example, structures of high importance class [3.6]).

The aim of this test was to give a preliminary evaluation of the possibility to use the investigated connection as “fuse” that is to be easily replaced after a medium intensity seismic shock. The analysis of the self-centering system is not part of this work, but examples can be found in ([3.36];[3.39]). For this purpose, the tested anchoring system described in the previous section was reused with a new dissipative element.

The failed connection was dismantled from the anchoring system. Negligible damage was observed in the steel plates, where only minor steel embedment and slight plastic deformations were experienced by the 16-mm dowels. Then, a new X-bracket was anchored to the panel with new steel bolts while the self-tapping screws that fastened the rectangular plate were not replaced. The same loading procedure [3.18] was applied to the specimen. An initial gap of about 1mm was observed and affected the resulting elastic stiffness k_{el} while the hardening branch presented the same inclination, i.e. the same post-elastic stiffness k_{pl} (see Table 4-1). Results show that the device can withstand another cyclic loading procedure without significant losses in terms of strength and, more important, dissipative capability. This is the result of the damage-free design criteria used to design the anchoring element at both strength and stiffness level. Fig. 3.24 evidences that the dissipative capacity is almost fully exploited and neglecting the elastic phase, the mean strength loss ΔF measured on each cycle was of about 2.5%.

Table 3-8 – Test results: main mechanical parameters according to EN 12512 method a [3.18].

Parameter	BRACKET ONLY(mean)	BRACKET + CLT_1	BRACKET + CLT_2
F_y (kN)	28.75	26.17	24.93
d_y (mm)	3.18	4.69	5.77
$F_{u(40mm)}$ (kN)	47.17	48.64	53.85
d_u (mm)	40.00	47.99	54.98
k_{el} (kN/mm)	9.04	5.36	7.49
k_{pl} (kN/mm)	0.50	0.57	0.66
μ (d_u) (-)	12.58	10.22	19.86
Ductility Class	H	H	H



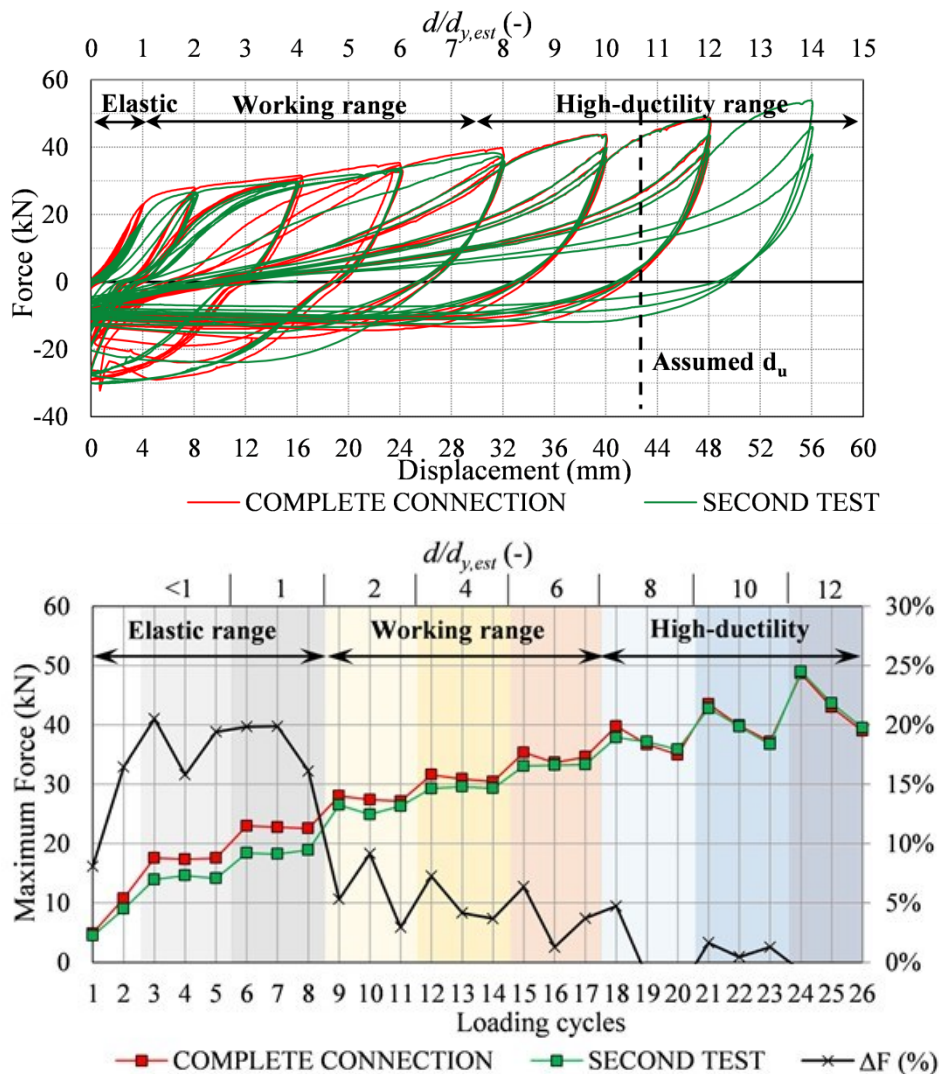


Fig. 3.24 – Comparison among first and second test of the complete connection in tension: (a) hysteresis cycles; (b) Maximum force and relative difference per loading cycle ($d_{y,est} = 4.00$ mm).

3.2.4 Version 3

Since the experimental results of the X-bracket connected to the CLT confirmed the possibility to exploit its dissipative capacity without significant energy losses, a further step into the refinement of the device was handled with the third version. The key-point of this design phase was to obtain a version that incorporates the elements necessary to fix rigidly the device to the CLT panel. For this reason a new *concealed* version was designed, starting from the same concept used for the concealed joist hangers commonly designed to support timber beams.

The possibility to realize multiple elements from a single cut (see Fig. 3.9) was sacrificed by the integration, into the bracket's shape, of a supporting element that restrains the main element and avoid the concentration of forces on the four dowels that block the connector. The main shape of the connector (i.e. thickness and curvature radius of the arms) was not modified with except of the area near the four fixings. This to maintain unaltered the hysteretic behaviour of the In this zone, the characteristic outline of the X-brackets was transformed into round shapes to let the arms rotate into a housing created into a steel counter plate and deform according to the different modes evidenced in *version 1 and 2* (see Fig. 3.11). The shape of the counter plate was designed to withstand the

reaction of the plates when subjected to shear and tension load: the lower part (near the edge of the panel) work as a cantilever beam and the outline was carefully designed to avoid possible skidding of the bracket from its housing. The whole assembly is meant to be concealed in an appropriate milling realized in the middle layer of the CLT wall. Milling can be localized (see Fig. 3.25b) or continuous along the whole panel edge. The fastening of this version exploit the same 16-mm steel bolts for the main fixings, whereas the counter plate is to be fastened with self-drilling steel dowels. Position of these dowels was designed through FEM simulations in order to find the disposition that better distributes the shear forces among the fasteners. Edge distance and spacing were also checked.

It is worth noting that a higher level of prefabrication can be achieved with this version. First, the central milling of the CLT panel is to be prepared in factory. The holes that houses the 16-mm steel bolts, with their correct edge distance and spacing, might be replicated in the CLT side by means of a portable drilling template. The self-drilling dowels might also be installed with a drilling guide in their correct position. Also the 16mm holes might be realized in factory, but that requires a much higher precision in placing the X-bracket in the correct position otherwise the dowels might not be aligned with the holes.

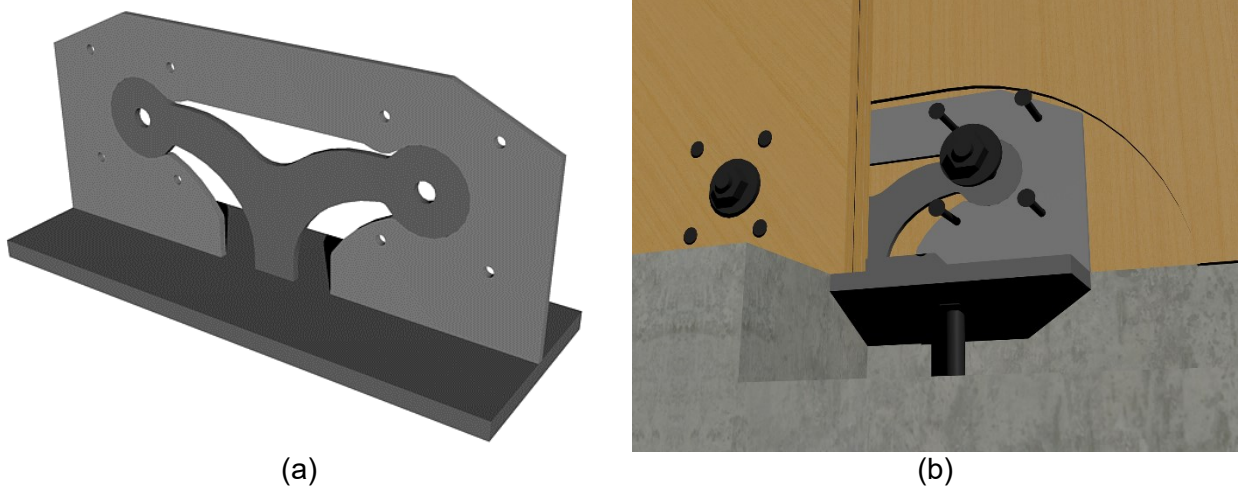


Fig. 3.25 – 3D model of the X-bracket version 3 (a) and example of application as a hold-down (b).

3.2.4.1 Capacity design

It is worth noting the importance of a correct capacity design approach in order to exploit the maximum amount of energy that the connector is capable to dissipate. As previously assessed for the fastening of *version 2* bracket, it is mandatory to ensure that failure of the bracket $F_{D, peak}^+$ occurs before the shear reaction acting on the dowels becomes bigger than the shear strength $F_{B, code}^-$ calculated according to EC5 [3.27]. As the dowel-type connections (i.e. 8 self-drilling dowels and 2 calibrated bolts) are working in parallel, the total force transmitted by the brackets is distributed among the dowels proportionally to their stiffness (i.e. the fastener diameter). The mechanical properties and characteristic shear strength of fasteners calculated according to EC5 [3.27] are reported in Table 3-9.

Fasteners to CLT were schematized through equivalent linear springs with stiffness equal to the lateral stiffness of dowel type fasteners K_{ser} calculated according to table 3.1 of EN 1995-1-1 [3.27]. Table 3-9 lists the mechanical properties of dowels for a GL24h class timber. In detail, for a mean density ρ_m of 410 kg/m³, K_{ser} were set equal to 9.02 kN/mm and 23.1 kN/mm for the self-drilling dowels and the calibrated bolts respectively, providing a total stiffness of the fastening of 127.05

kN/mm. Monotonic tensile and shear loading conditions were replicated assuming a maximum working uplift of 20mm and slip of ± 24 mm.

Table 3-9 – Mechanical parameters of dowels.

Type of fastener	d (mm)	N° (-)	$M_{y,Rk}$ (kNmm)	K_{ser} (kN/mm)	$F_{v,Rk}$ (kN)
16-mm 8.8 class steel bolts	16	2	324.3	23.1	36.1
7-mm self-drilling bolts	7	8	30.9	10.1	9.2

According to tests provided by the producer of the designed self-drilling dowels [3.67], an overstrength factor γ_{Rd} of almost 1.6 further improves that reliability of capacity design. Fig. 3.26 displays the position for the 7-mm dowels. Fig. 3.27 and Fig. 3.28a show the numerical predictions of the load slip curves for the connector used as a hold-down, as a panel-to-panel joint thus subjected to only positive displacements. Fig. 3.28b shows the absolute resulting shear force acting on the dowels during the cyclic loading and confirms that dowels should accomplish mainly elastic deformations and satisfy the equation $F_{v, fem}^- < F_{v, code}^-$ with $F_{v, code}^- = F_{v, Rk}$. The only apparent issue was concentrated on dowels M6 and M7 (see Fig. 3.26) for the bracket subjected to tensile loads. Consequently, these dowels were shifted as much as possible from the M16 dowels, yet meeting the minimum requirements for the edge distance according to Eurocode 5 [3.27]. The same outputs for the X-bracket *version 3* loaded in shear are reported in Fig. 3.29 and Fig. 3.30.

Lastly, buckling of the bracket was included in the model although the CLT panel is supposed to restrain possible out-of-plane deformations. This because, preliminary analyses implied that for high amplitude cycles, compression strength of CLT orthogonal to the fibre might not be sufficient to avoid crushing of the timber boards.

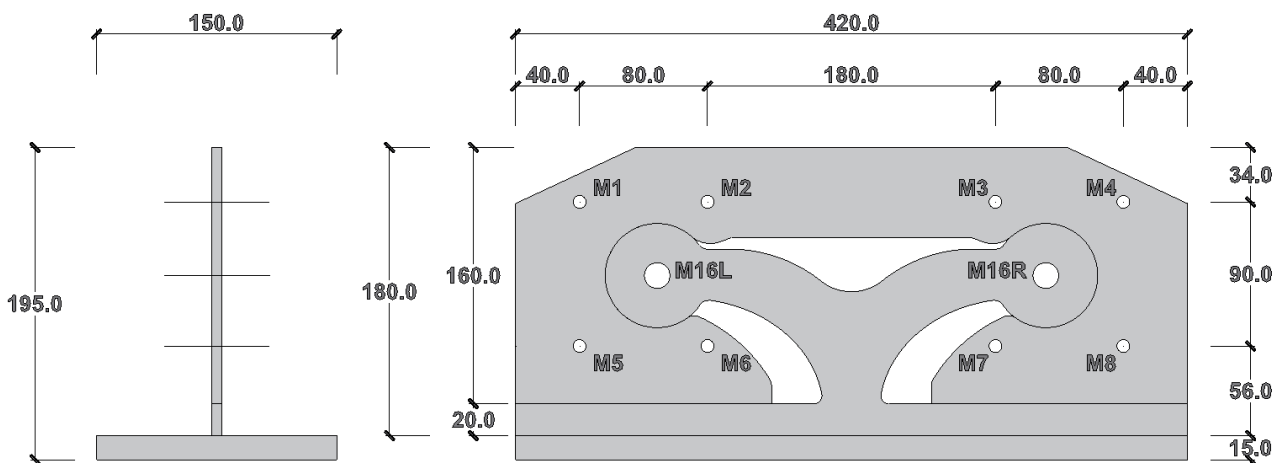


Fig. 3.26 – Dimensions of version 3 and position of 7-mm self-drilling dowels (M1 to M8) and 16-mm dowels.

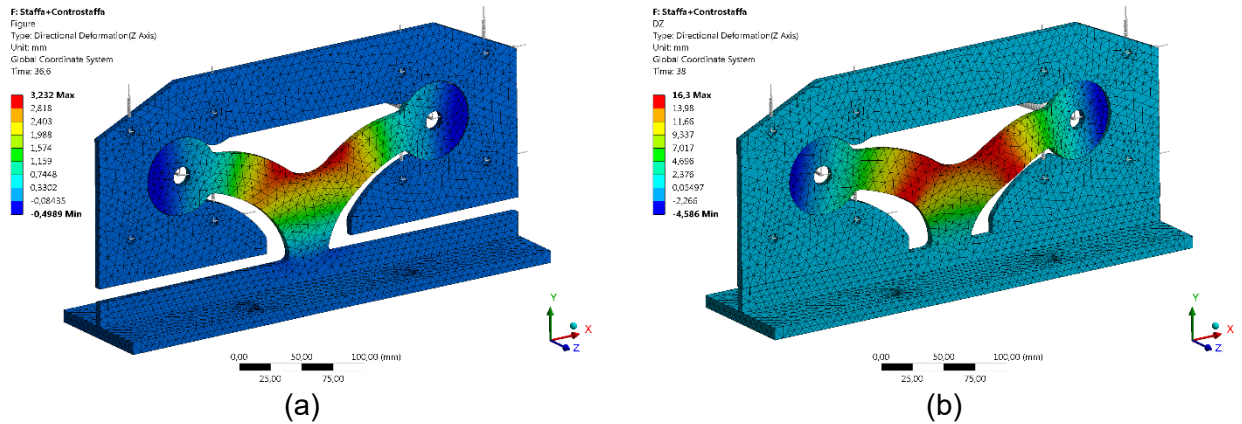


Fig. 3.27 – Out-of-plane deformations: (a) at vertical uplift of 20 mm; (b) residual deformation after the complete cyclic loading procedure.

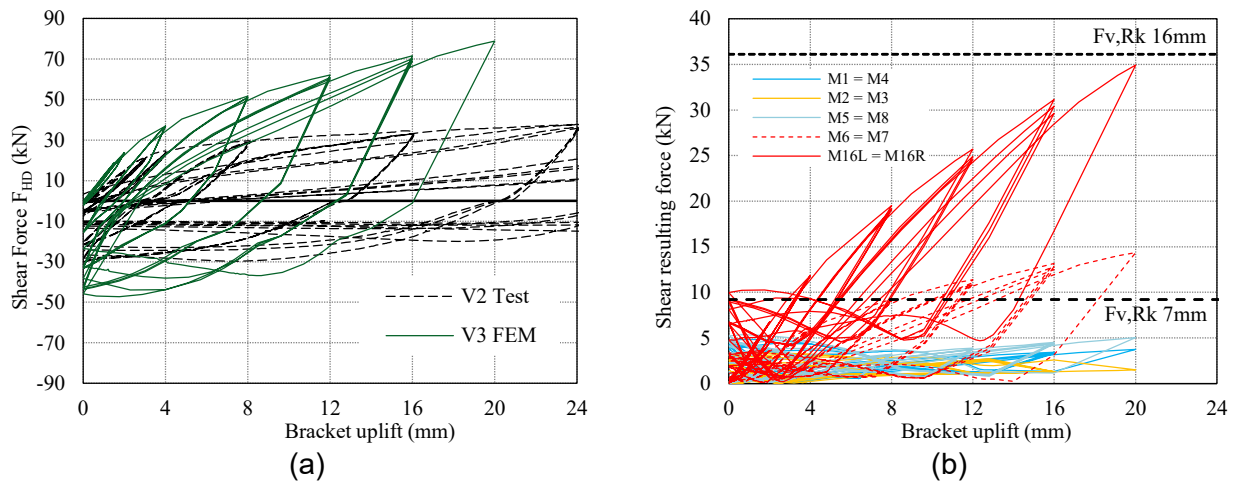


Fig. 3.28 – Numerical simulation results: (a) hysteretic response of bracket for cyclic tensile loading; (b) total absolute shear reaction of dowels vs. bracket uplift.

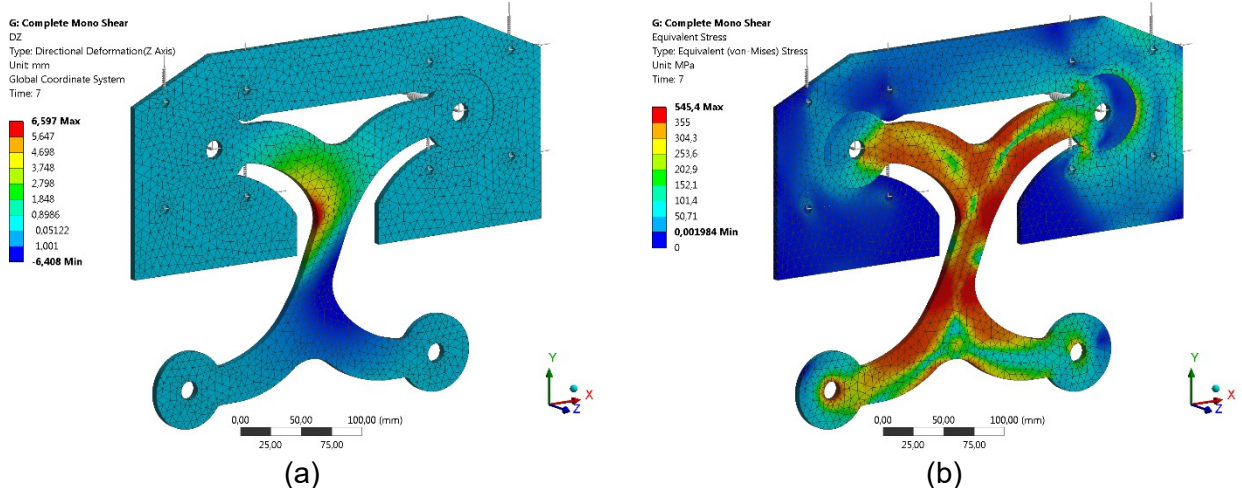


Fig. 3.29 – Out-of-plane buckling at a 24mm of horizontal slip: (a) out-of-plane displacements; (b) Von Mises stress distribution (post-yielding zones in red).

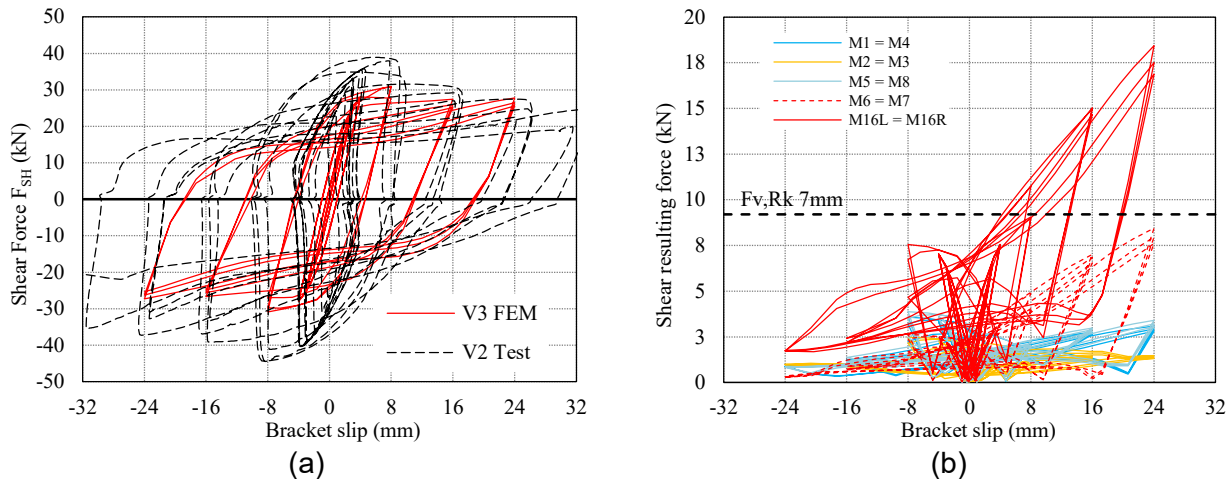


Fig. 3.30 – Numerical simulation results: (a) hysteretic response of bracket for cyclic shear loading; (b) total absolute shear reaction of dowels vs. bracket slip.

3.2.4.2 Experimental tests

Test of the third version of the bracket were conducted tested in the laboratory of construction material testing of Department ICEA of the University of Padova.

The cyclic performance of the bracket only (i.e., hysteretic behaviour of the steel element) must logically be the same obtained with *version 2*, therefore tests directly aimed to analyse the bracket anchored to the CLT wall. A test setup was designed to investigate the X-bracket behaviour working as an hold-down (henceforth called V3_{HD}) or as shear connection (henceforth called V3_{SH}) for a panel-to-panel joint (see Fig. 3.31 and Fig. 3.32). In particular:

- For tension tests, a single bracket was anchored to a 5-layered CLT panel with a thickness of 100mm (20-20-20-20-20) and dimensions of 1300x1000mm. The panel was secured to an HEA 140 steel beam by means of four M24 steel rods, and welded to an eyebolt mechanism, in order to apply the vertical displacement with an hydraulic actuator. The base plate of the bracket was fixed to the rigid frame with four 16-mm 5.8 class steel rods. Although the investigation focus primary on the fastening to the CLT wall, spacing of the four rods were designed following a preliminary design of the anchoring to the concrete foundation by means of chemical resins. Two UNP profiles with additional timber elements protected with PTFE sheets were placed on each side of the portal to avoid possible out-of-plane displacements of the whole assembly. The vertical uplift of the concealed bracket was monitored with two LVDTs that measured the relative displacement between mid-point of the horizontal steel baseplate and the CLT panel (see Fig. 3.33a).
- For shear tests, a symmetrical solution was designed. The same central CLT panel of the tension tests was attached by means of the investigated brackets to two lateral CLT rectangular elements with the same thickness and dimensions of 1300x600mm each. These elements were restrained to the rigid portal by means of M24 steel rods. Also in this case out-of-plane displacements were restrained with UNP profiles. No frictionless material was interposed between the panel edges to simulate the actual conditions of a CLT assembly. The panel-to-panel slip was measured with two LVDTs, for each bracket, on each side of the panel in proximity of the fixing points (see Fig. 3.33b).

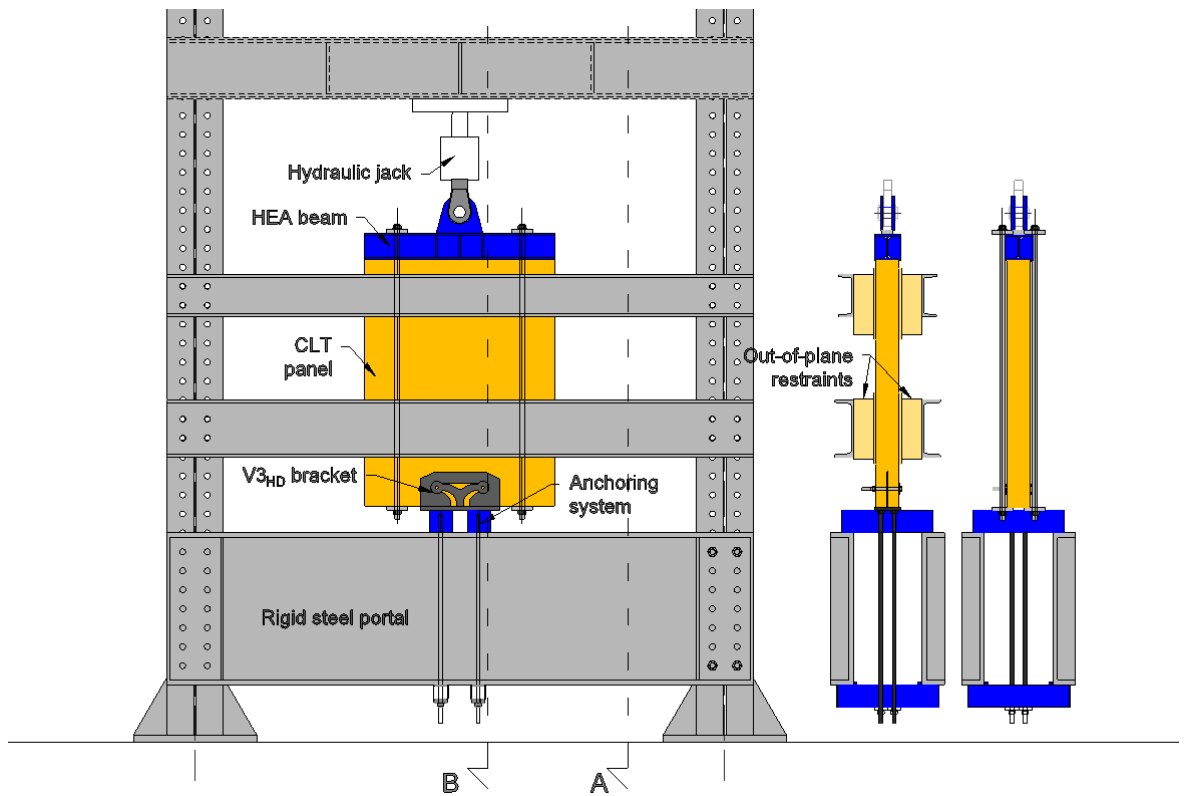


Fig. 3.31 – Test setup for X-bracket V3_{HD}.

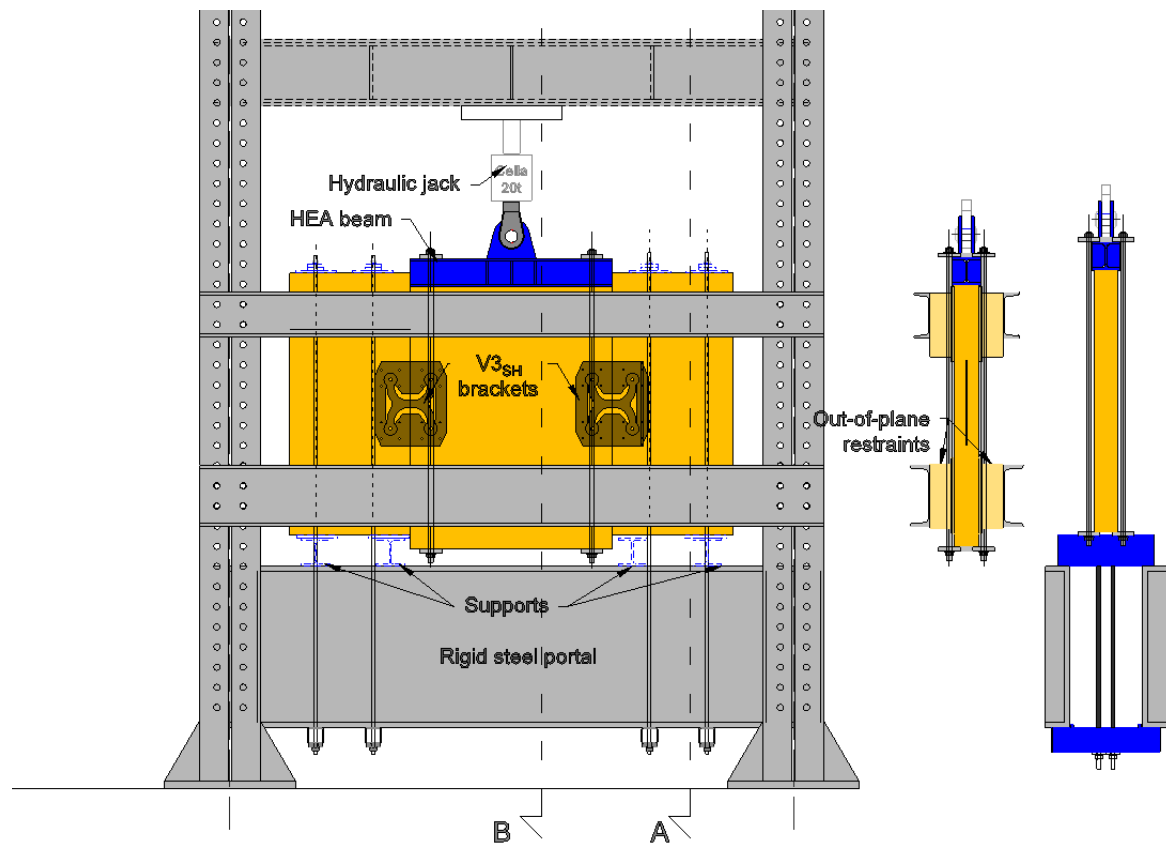


Fig. 3.32 – Test setup for bracket V3_{SH}.



Fig. 3.33 – Position of LVDTs to assess displacements of each bracket for tension tests (a) and shear test (b).

3.2.4.3 Test Results

A total of three tests were performed in this phase: two for tensile loading conditions and one for shear loading conditions. The EN 12512 cyclic loading protocol [3.18] was adopted in all tests imposing a $d_{y,est}$ of 2 mm for both shear and tension tests ($V3_{HD}$ bracket has only two arms subjected to deformations compared to *version 1 and 2*, and consequently has half of the displacement capacity). Fig. 3.34a and b shows the obtained force vs. displacement loops and the comparison with the numerical predictions. Regarding tension tests (Fig. 3.35a), the bracket succeeded in all the 20-mm amplitude cycles but failed at an uplift of 24 mm (Fig. 3.35b) due to the accumulated plastic work in proximity of the horizontal arms (Fig. 3.35c). No damage was evidenced either in the dowel-type fasteners or in the CLT panel (Fig. 3.35d). Frictional effects are confirmed to be responsible for the higher manifested strength F_{SH} with respect to *version 2* (see FEM comparison in Fig. 3.34a): the predicted strength increment due to friction ($\mu = 0.60$) measured at 20 mm is of 51.2%. The fact that the web is welded to the lower base does significantly reduce the buckling phenomena during compression. The shear test (Fig. 3.36) showed a hysteretic response typical of cyclically loaded steel connectors with a more “stable” behaviour than *version 2*. Failure occurred in the steel component (see Fig. 3.37a) after the completion of the 24-mm cycles Fig. 3.37b), but it is worth noting the important confinement effect demonstrated by the CLT panel with respect to the out-of-plane buckling of the central web.

The device worked with the same principle of Buckling-restrained bracings (BRB) where the steel fuses are confined into a grout of concrete. In particular, only at large deformations (near failure conditions) the pushing of the web caused failure of the inner CLT boards layers due to compression orthogonal to the grain allowing the rotation of the vertical web (see Fig. 3.37c).

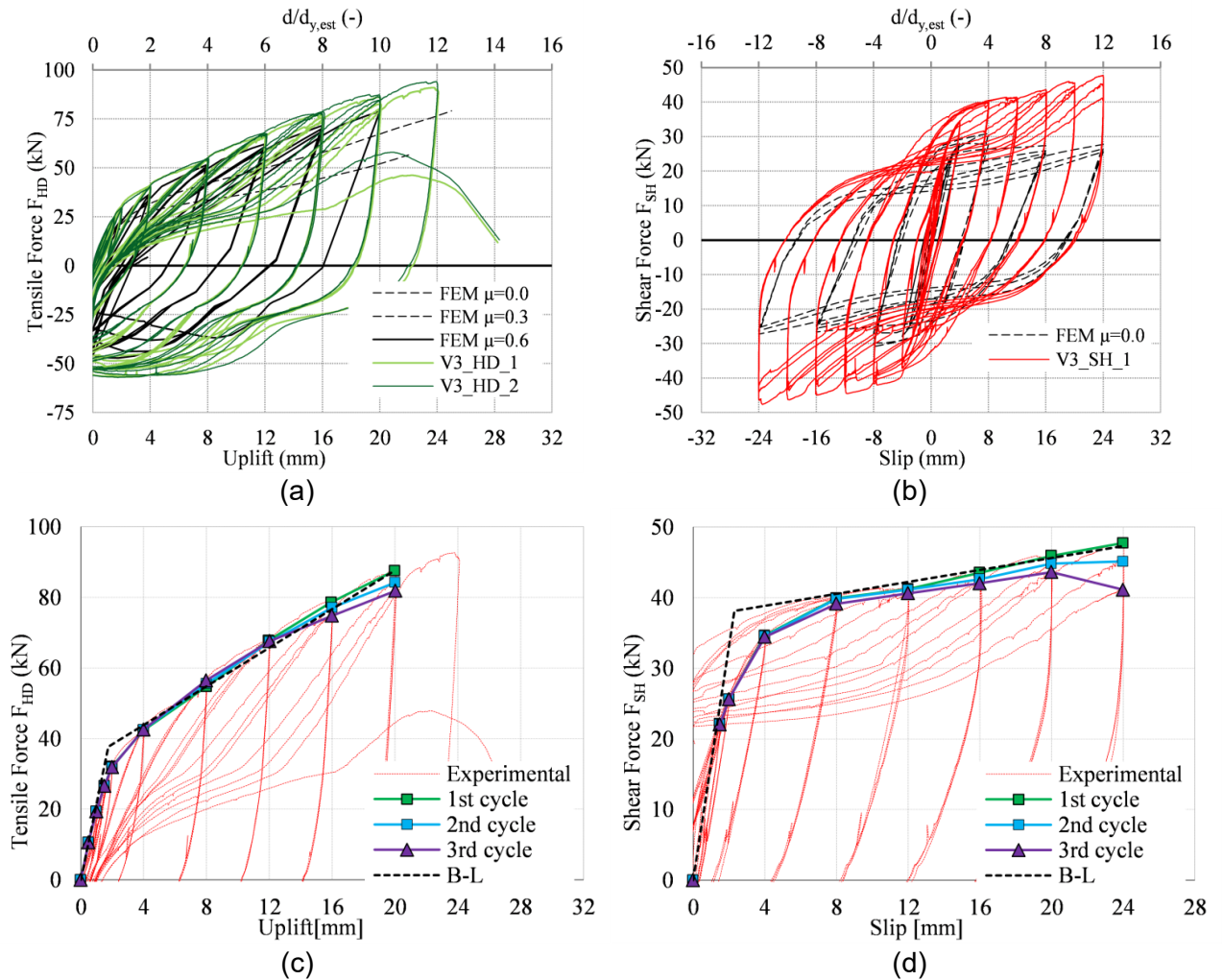


Fig. 3.34 – Hysteresis loops and backbone curves of tension tests (a,c) and shear tests (b,d).

Bi-linearization of the envelope curves were accomplished with the EN 12512 method a [3.18] on both loading conditions and the corresponding mechanical parameters are reported in Table 3-10. It emerges the similar yielding conditions (F_y, d_y) and ductility either in tension or in shear, but also the very different post-elastic behaviour. As already mentioned, the latter fact has to be taken into account when designing the anchoring to the CLT panel. Further details on the comparison with *version 2* are given in the following subsection.

Table 3-10 – Mechanical parameters and hysteretic loops for V3_{HD} and V3_{SH} bracket.

Parameter	V3_HD_1	V3_HD_2	V3_SH_1	BI-LINEARIZATION
F_y (kN)	37.75	36.64	41.70	
d_y (mm)	1.76	1.71	2.39	
F_{max} (kN)	87.57	88.19	47.50	
d_u (mm)	20.00	20.00	24.00	
k_{el} (kN/mm)	21.43	21.43	17.43	
k_{pl} (kN/mm)	2.22	2.22	0.27	
$\mu(V_u)$ (-)	11.34	11.68	10.03	
Ductility Class	H	H	H	

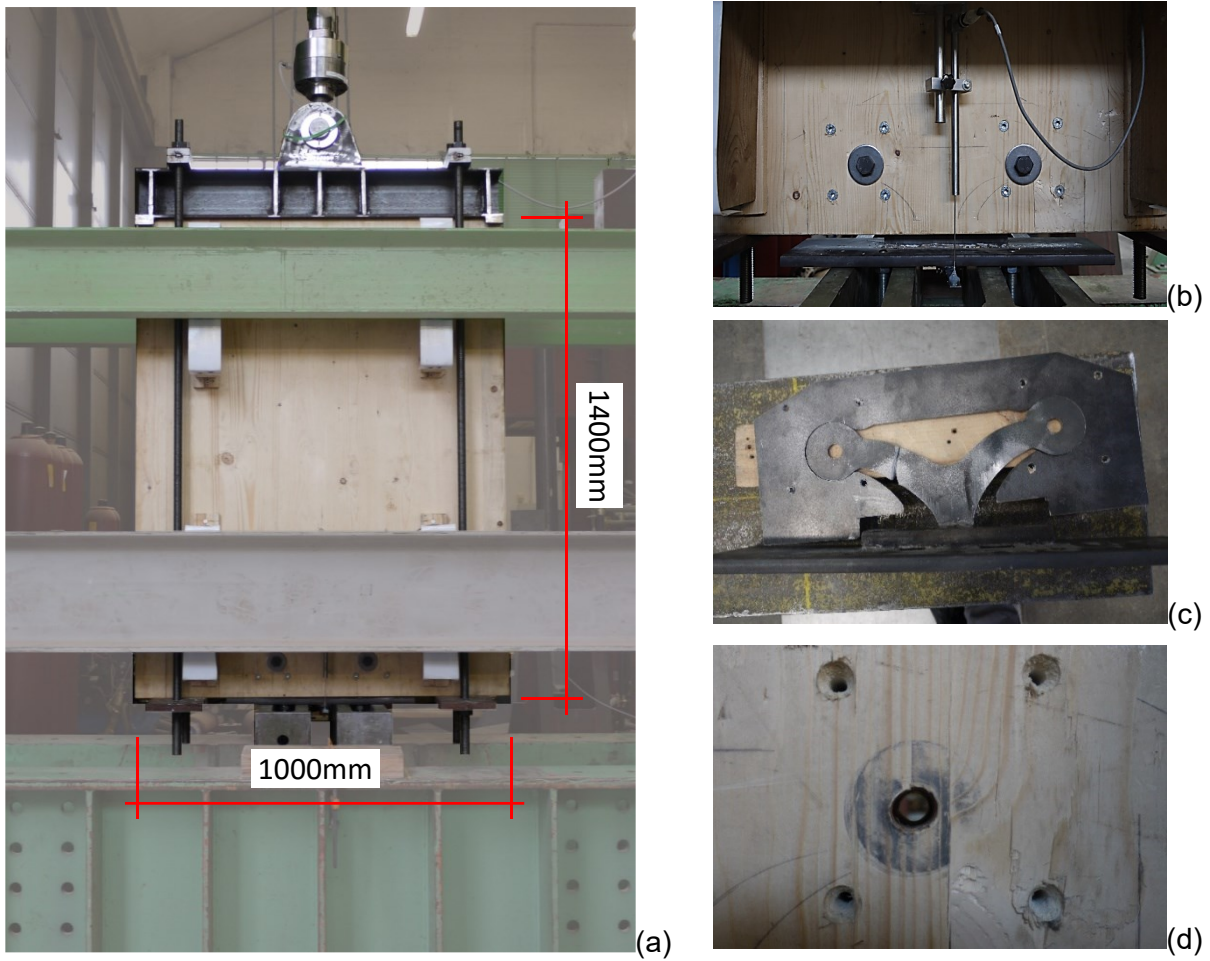


Fig. 3.35 – V3_{HD} test: (a) test setup; (b) specimen at max uplift of 24mm; (c) failure of the X-bracket; (d) holes in timber panel after test.

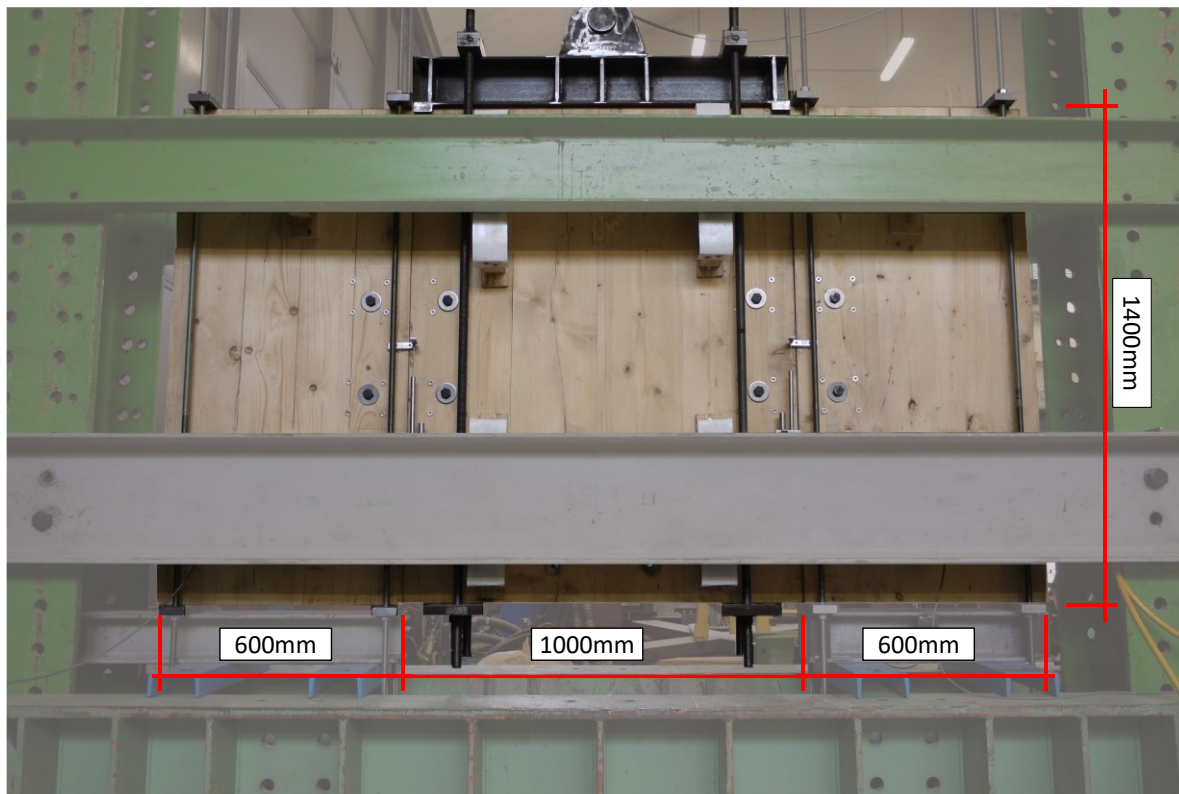


Fig. 3.36 – V3_{SH} test setup.

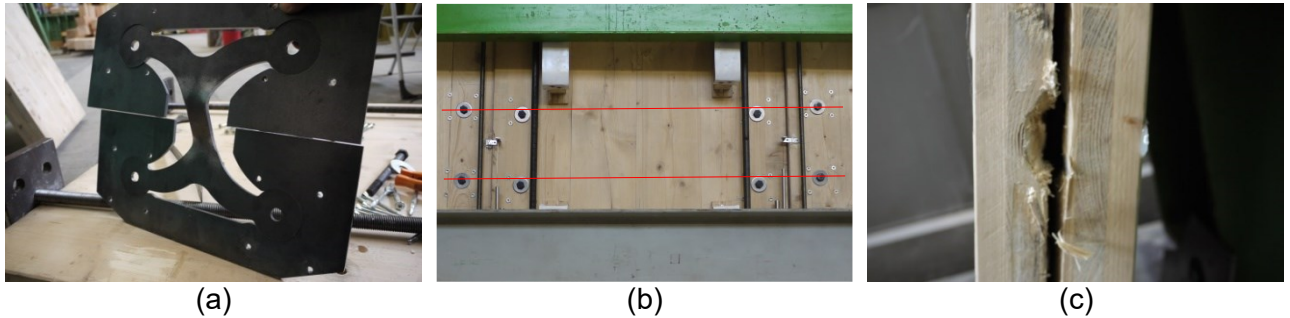


Fig. 3.37 – $V3_{SH}$ test: (a) failure of the X-bracket; (b) specimen at 24mm of slip; (c) damaged inner layers.

3.2.5 Comparison between the investigated versions

In this section the hysteretic response of the tested versions are analysed in deep but, as X-brackets *version 1* and *2* differ only by the type of steel employed and some minor shape changes, the comparison of the hysteretic behaviour is given only between X-brackets V2 and V3.

From a functional point of view, each of the brackets has its own advantages and disadvantages:

- *Version 1 and 2*: do not require any particular woodworking of the CLT panel as it is fixed externally. The buckling of the connector, that becomes relevant for high displacement, induces pinching phenomenon and partial loss of dissipating capability. Fire-protection has to be addressed like *traditional* connections.
- *Version 3*: does implicitly satisfy the capacity design if fasteners that fix the counter plate are placed according to the tested configuration. Fire-protection is given by the presence of the CLT layers. Main drawbacks are that it does require a partial milling of the panel edge; Dimensions may become relevant for panels with a short base-length.

Regarding the mechanical performances, they have been increasing within each version (see Table 3-11). The change of steel grade from *version 1* to *version 2* produced a yielding strength increment for tensile loading ΔF_{HD} and shear loading conditions ΔF_{SH} of nearly 60.0% and 40.6% respectively. Switching to *version 3* provide more interesting results. Although steel was downgraded to an S355 the tensile yielding strength increased of an additional 29.4%, reaching a similar load bearing capacity to when loaded in shear, which on the contrary did not change considerably. This was caused by two different effects: 1) the increased vertical spacing of the M16 bolts allowed the horizontal arms to work more in tension than the previous versions; 2) the frictional effect of the plate rotating over the housing of the counter-plate produced a considerable strength increment (see previous section). The higher vertical spacing affected the response to shear loading with a limited increase of shear strength F_{SH} and a reduction of elastic stiffness of 44.8%. In conclusion, X-bracket *version 3* has demonstrated to be a more balanced solution from a designer point of view in term of load bearing and displacement capacity.

The different hysteretic response between *version 2* and *version 3* (see Fig. 3.38) is highlighted through the computation of the equivalent viscous damping ratio ν and the total amount of dissipated energy. In Fig. 3.38a the displacement of *version 2* were divided by a factor 2 allowing to evaluate better the strength increment obtained with *version 3*. Fig. 3.38c-d show the change of post-elastic behaviour of the brackets. It clearly emerges that each application had to be tested in order to assess its mechanical parameters and determine the correct overstrength factor to be chosen within each version.

Table 3-11 – Comparison of the three tested versions (mean values).

Parameter	Version 1		Version 2		Version 3	
	Tension	Shear	Tension	Shear	Tension	Shear (*)
Steel (-)	S275JR		S450JR		S355JR	
Dimensions B x H (mm x mm)	303 x 233		303 x 233		420 x 360 (**)	
Spacing of fixings (mm x mm)	237 x 180		243 x 185		243 x 200	
F_y (kN)	17.97	28.09	28.75	39.5	37.19	41.70
d_y (mm)	1.96	3.46	3.18	1.25	1.74	2.39
F_u (kN)	37.76	29.03	47.17	43.98	87.88	47.50
d_u (mm)	46.20	50.00	40.00	24.00	20.00	24.00
k_{el} (kN/mm)	9.17	8.53	9.04	31.55	21.43	17.43
k_{pl} (kN/mm)	0.45	-	0.50	-	2.22	0.27
μ (d_u) (-)	23.57	14.45	12.58	23.43	11.51	10.03
Ductility Class	H	H	H	H	H	H

* one test only

** including counter plate

*** value for monotonic load

In Fig. 3.39a,b the comparison is given on the basis of an equivalent ductility level (i.e. $d_i/d_{y,est}$) to account for the different displacement capacity between the two versions. The calculated damping at the 1st and 3rd cycle is comparable up to $d/d_{y,est} = 6$ but *version 3* shows values in the range of 12-15% also for high displacements ($6 < d/d_{y,est} \leq 10$). Additionally, the reduced pinching phenomena is confirmed by the minor damping losses measured from the 1st to the 3rd cycles. Typical values for *traditional* connections (i.e. hold-downs) are in the range between 9% (1st cycle) and 3% (third cycle) [3.21]. Lastly, the combination of higher strength and dissipative capacity translate into an increment of total cumulated energy ΔE_d dissipated by the connector of 54.0%.

Comparison on shear cyclic loading responses are presented for the same cyclic amplitude (Fig. 3.39c,d). A reduction of the equivalent viscous damping ratio was measured for all the displacement amplitudes, but still high values were computed if compared to *traditional* connections (angle brackets) ([3.20];[3.21]). Also in this case, the dissipative capacity did not vary significantly between the 1st and 3rd cycle. Furthermore, the softening-to-hardening post-elastic change occurred with V3 produced an amount of cumulated dissipated energy nearly equal to V2 with at a lower number of cycles and lower displacement amplitude.

Unfortunately, very limited information regarding the energy dissipation capabilities of *traditional* connectors are available in literature. It is therefore not possible to make a direct comparison in terms of dissipated energy for a given strength or displacement level. However, in the following Chapter (section 4.4.4), the replication of experimental tests of CLT panel assemblies taken from literature will allow to give some preliminary prediction also in these terms.

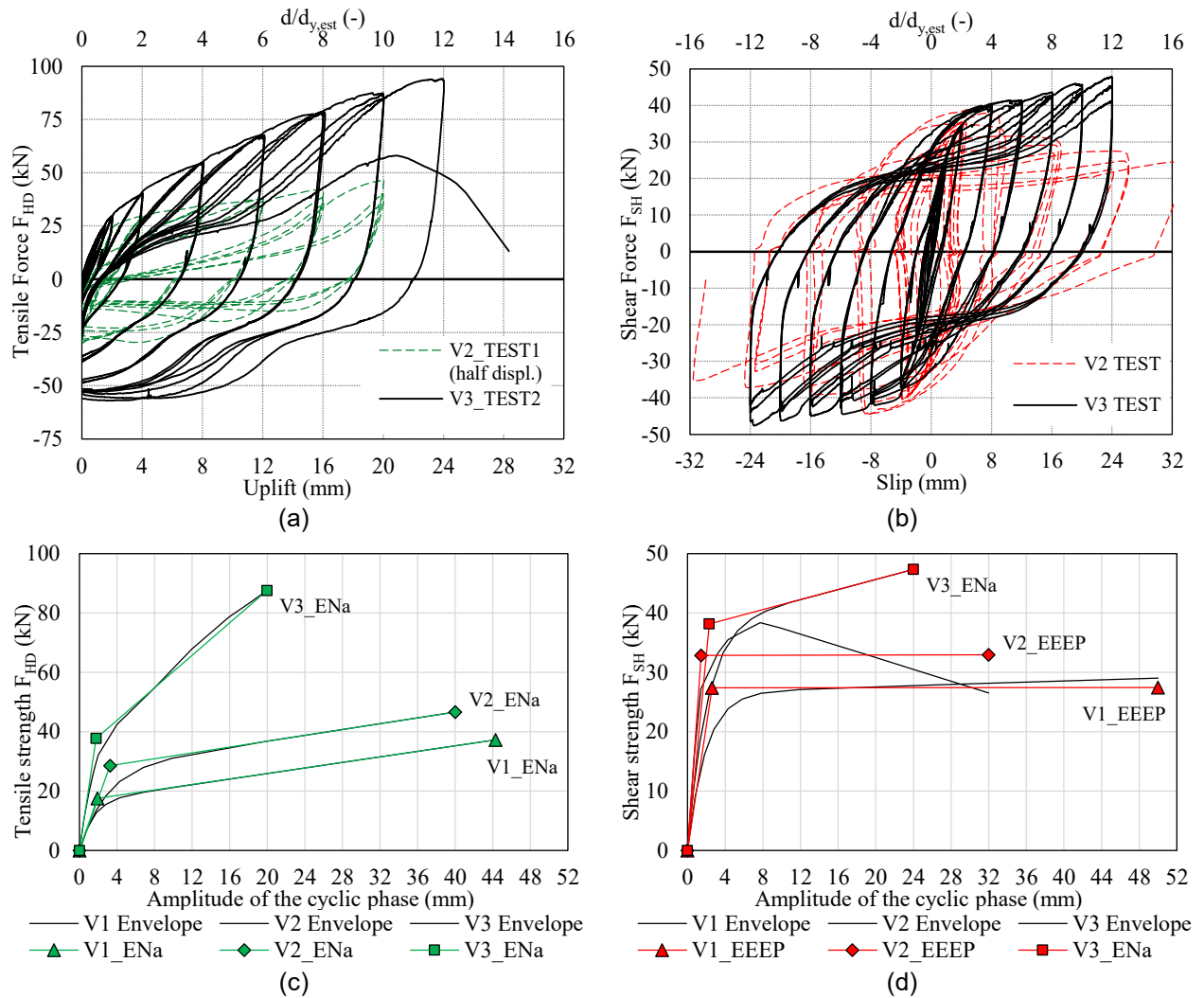


Fig. 3.38 – Comparison of load vs. displacement cycles, envelope curves and bi-linearization of version 2 and 3 on tension (a,c) and shear (b,d).

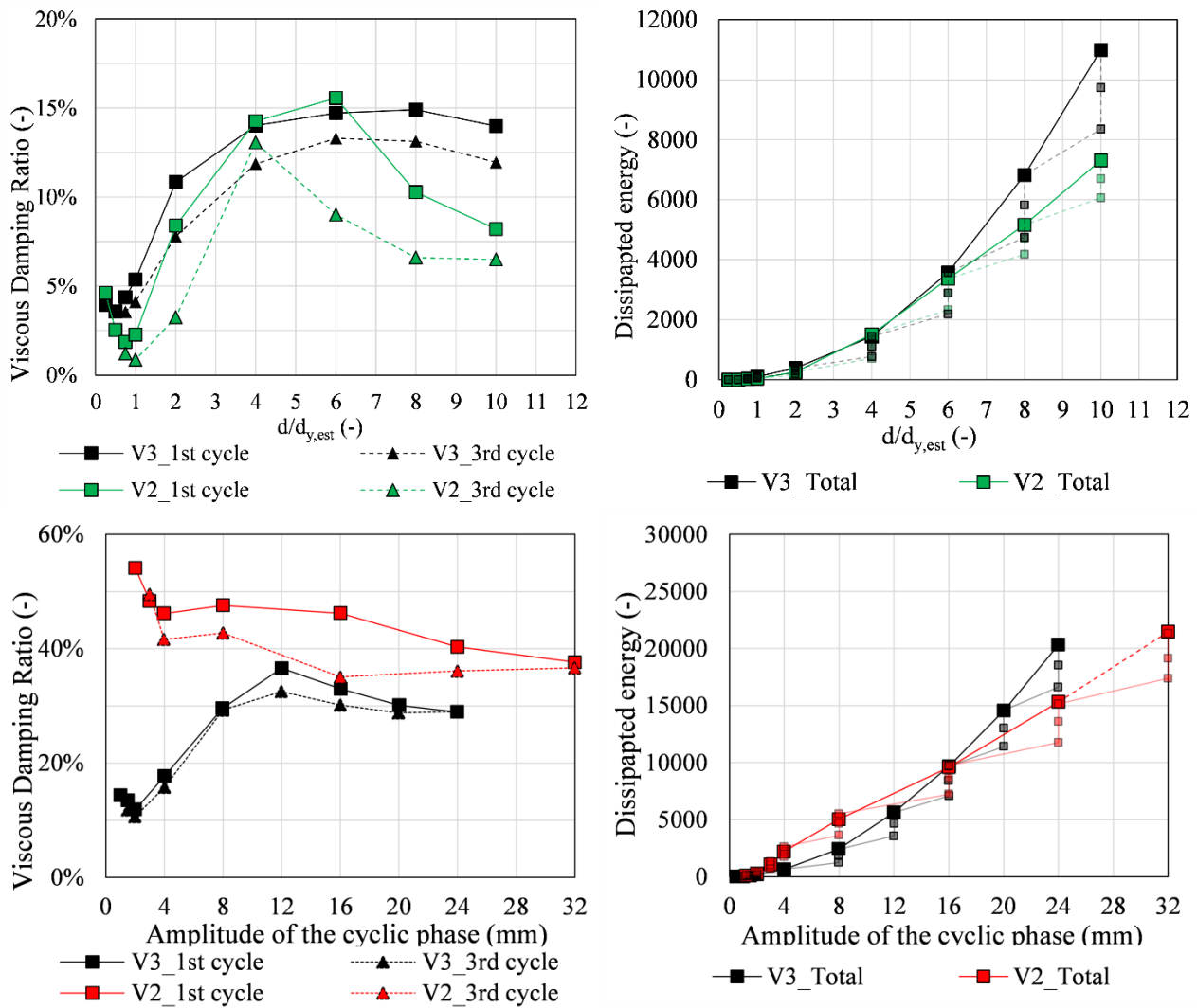


Fig. 3.39 – Viscous damping ratio and dissipated energy for the X-brackets loaded in tension (a,b) and in shear (c,d).

3.3 Conclusions

This chapter presented the development of an innovative highly dissipative connection system for Cross-laminated Timber structures. The concept on which the research have been based was to shift the dissipating element from the usual dowel-type fasteners employed in traditional connections to the steel element meanwhile preserving the fasteners from behaving inelastically.

The design phases of each connection were described in detail, and the prediction of the FE models have been confirmed each time by means of proper experimental tests. These tests involved the imposition of cyclic loading conditions at increasing displacement both in tension and in shear according to the standardised procedure of EN 12512.

Version 1 and 2 of the device focused the energy dissipation in the development of plastic strains. A significant increase of the total dissipative capacity and load bearing capacity was achieved by introducing friction phenomena and reducing out-of-plane buckling effects with Version 3. This modifications allowed the device to performed as an hybrid device that exploited the same principle

of Buckling-Restrained Bracing fuses typical of steel structures and slip-friction connection systems demonstrating the highest mechanical performance.

Obtained results allowed determining the main mechanical parameters. The high ductility class according to Eurocode 8 [3.6] was achieved with the combination of a high elastic stiffness and a displacement capacity comparable or even higher than traditional connections. The calculated equivalent viscous damping ratio was approximately double than traditional connections either in shear or in tension. Lastly, strength degradation became relevant only for very high displacement and ductility values ($\mu \geq 6$).

Particular care was given to the determination of a correct capacity design procedure. The theoretical definitions of the capacity design rules available in literature were extended to the field of innovative connections for CLT structures. Further experimental tests allowed to assess the presented procedure and to express the whole dissipative capacity of the element without incurring into unwanted brittle failures.

Acknowledgments

The author would like to thank the personal of the Construction Materials Testing Laboratory of the Department of Civil, Environmental and Architectural Engineering of Padova for supervising tests.

References – Chapter 3

- [3.1] Ceccotti, A. (2008). “New technologies for construction of medium-rise buildings in seismic regions: The XLAM case”. *Structural Engineering International*, **18(2)**:156-165.
- [3.2] Ceccotti, A., Sandhaas, C., Okabe, M., Yasumura, M., Minowa, C. and Kawai, N. (2013). “SOFIE project—3D shaking table test on a seven-storey full-scale cross-laminated timber building”. *Earthquake Engineering and Structural Dynamics*, **42(13)**:2003–2021.
- [3.3] Gavric, I., Fragiaco, M. and Ceccotti, A. (2015). “Cyclic behavior of CLT wall systems: Experimental tests and analytical prediction models”. *Journal of Structural Engineering*. DOI:10.1061/(ASCE)ST.1943-541X.0001246.
- [3.4] Popovski, M., and Gavric, I. (2015). “Performance of a 2-story CLT house subjected to lateral loads”. *Journal of Structural Engineering*. DOI:10.1061/(ASCE)ST.1943-541X.0001315.
- [3.5] Flatscher, G., and Schickhofer, G. (2015). “Shaking-table test of a cross-laminated timber structure”. *Proceedings of the ICE – Structures and Buildings*, **168(11)**:878–888.
- [3.6] EN 1998-1-1 Eurocode 8 (2004). “Design of structures for earthquake resistance, part 1: general rules, seismic actions and rules for buildings”. CEN. Brussels, Belgium.
- [3.7] Pozza, L., Scotta, R., Trutalli, D., Ceccotti, A., and Polastri, A. (2013). “Analytical formulation based on extensive numerical simulations of behavior factor q for CLT buildings”. In *Proceedings of the Meeting 46 of the Working Commission W18-Timber Structures*, CIB, Vancouver, BC, Canada, paper CIB-W18/46-15-5.
- [3.8] Pozza, L., and Scotta, R. (2015). “Influence of wall assembly on behaviour of cross-laminated timber buildings”. *Proceedings of the ICE – Structures and Buildings*, **168(4)**:275-286.

- [3.9] Pozza, L., Scotta, R., Trutalli, D., Polastri, and A., Smith, I. (2016). "Experimentally based q-factor estimation of cross-laminated timber walls". Proceedings of the ICE – Structures and Buildings. DOI:10.1680/jstbu.15.00009.
- [3.10] Smith, I., Landis, E., and Gong, M. (2003). "Fracture and Fatigue in Wood". John Wiley & Sons: Chichester, UK.
- [3.11] Piazza, M., Polastri, A., and Tomasi, R. (2011). "Ductility of Joints in Timber Structures". Proceedings of the ICE – Structures and Buildings, **164(2)**:79–90.
- [3.12] Germano, F., Metelli, G., and Giuriani, E. (2015). "Experimental results on the role of sheathing-to-frame and base connections of a European timber framed shear wall". Construction and Building Materials, **80**:315–328.
- [3.13] Gattesco, N., Dudine, A., and Franceschinis, R. (2012). "Experimental investigation on the seismic behavior of timber shear walls with particle boards". In Proceedings of the 12th World conference on Timber Engineering (WCTE). 15-19 July 2012, Auckland, New Zealand.
- [3.14] Gattesco, N.; and Boem, I. (2015). "Seismic performances and behavior factor of post-and-beam timber buildings braced with nailed shear walls". Engineering Structures, **100**:674–685.
- [3.15] Sartori, T., Piazza, M., Tomasi, R., and Grossi, P. (2012). "Characterization of the mechanical behavior of light-frame shear walls through full-scale tests". In Proceedings of the 12th World conference on Timber Engineering (WCTE). 15-19 July 2012, Auckland, New Zealand.
- [3.16] Tomasi, R., and Sartori, T. (2013). "Mechanical behavior of connections between wood framed shear walls and foundations under monotonic and cyclic load". Construction and Building Materials, **44**:682–690.
- [3.17] Pozza, L., Scotta, R., Trutalli, D. and Polastri, A. (2015). "Behaviour factor for innovative massive timber shear walls". Bulletin of Earthquake Engineering, **13(11)**:3449-3469.
- [3.18] EN 12512 (2001). "Timber structures—test methods—cyclic testing of joints made with mechanical fasteners". CEN. Brussels, Belgium.
- [3.19] Chopra, A. K. (1995). Dynamics of structures (Vol. 3, p. 339). Prentice hall, New Jersey.
- [3.20] Tomasi, R., and Smith, I. (2014). "Experimental characterization of monotonic and cyclic loading responses of CLT panel-to-foundation angle bracket connections". Journal of Materials in Civil Engineering, 27(6), 04014189.
- [3.21] Gavric, I., Fragiaco, M., and Ceccotti, A. (2015). "Cyclic behaviour of typical metal connectors for cross-laminated (CLT) structures". Materials and structures, **48(6)**:1841-1857.
- [3.22] Sandhaas, C., Boukes, J., Van de Kuilen, J.W.G. and Ceccotti, A. (2009). "Analysis of X-lam panel-to-panel connections under monotonic and cyclic loading". In Proceedings of the Meeting 42 of the Working Commission W18-Timber Structures, CIB, Dübendorf, Switzerland, paper CIB-W18/42-12-2.
- [3.23] Gavric, I., Ceccotti, A., and Fragiaco, M. (2011). "Experimental cyclic tests on cross-laminated timber panels and typical connections". In Proceedings of the XIV ANIDIS, Bari, Italy, 18-22 September 2011.
- [3.24] Gavric, I., Fragiaco, M., and Ceccotti, A. (2013). "Capacity seismic design of X-LAM wall system based on connection mechanical properties". In Proceedings of the Meeting 46 of the Working Commission W18-Timber Structures, CIB, Vancouver, BC, Canada, 26-29 August 2013, paper CIB-W18/46-15-2.
- [3.25] Fragiaco, M., Dujic, B., and Sustersic, I. (2011). "Elastic and ductile design of multi-storey crosslam massive wooden buildings under seismic actions". Engineering Structures, **33**:3043–3053.
- [3.26] Johansen, K.W. (1949). "Theory of timber connections". International Association of bridge and

- structural Engineering, Bern, pp. 249-262.
- [3.27] EN 1995-1-1 Eurocode 5 (2004). "Design of timber structures, Part 1-1, General: Common rules and rules for buildings". CEN. Brussels, Belgium.
- [3.28] Baird, A., Smith, T., Palermo, A., and Pampanin, S. (2014). "Experimental and numerical study of U-shape flexural plate (UFP) dissipators". In New Zealand Society for Earthquake Engineering Conference, Auckland, New Zealand.
- [3.29] Priestley, M. N., Sritharan, S., Conley, J. R., and Pampanin, S. (1999). "Preliminary results and conclusions from the PRESSS five-story precast concrete test building". PCI journal, **44(6)**:42-67.
- [3.30] Henry, R. S., Aaleti, S., Sritharan, S., and Ingham, J. M. (2009). "Concept and finite-element modeling of new steel shear connectors for self-centering wall systems". Journal of Engineering Mechanics, **136(2)**:220-229. ASCE.
- [3.31] Palermo, A., Pampanin, S., and Buchanan, A. H. (2006). "Experimental investigations on LVL seismic resistant wall and frame subassemblies".
- [3.32] Iqbal, A., Pampanin, S., Buchanan, A., and Palermo, A. (2007). Improved seismic performance of LVL post-tensioned walls coupled with UFP devices. In Proceedings of the 8th Pacific Conference on Earthquake Engineering.
- [3.33] Smith, T., Ludwig, F., Pampanin, S., Fragiaco, M., Buchanan, A., Deam, B., and Palermo, A. (2007). Seismic response of hybrid-LVL coupled walls under quasi-static and pseudo-dynamic testing. In 2007 New Zealand Society for Earthquake Engineering Conference, Palmerston North, New Zealand (Vol. 8).
- [3.34] Iqbal, A., Pampanin, S., and Buchanan, A. H. (2010). Seismic performance of prestressed timber beam-column sub-assemblies. In Proceedings of the New Zealand society for Earthquake Engineering annual conference, Wellington, New Zealand.
- [3.35] Kelly, J. M., Skinner, R. I., and Heine, A. J. (1972). "Mechanisms of energy absorption in special devices for use in earthquake resistant structures". Bulletin of NZ Society for Earthquake Engineering, **5(3)**:63-88.
- [3.36] Sarti, F. (2015). "Seismic Design of Low-Damage Post-Tensioned Timber Wall Systems". Ph.D. Thesis. University of Canterbury, Christchurch, New Zealand.
- [3.37] Kramer, A., Barbosa, A.R., and Sinha, A. (2015). "Performance of steel energy dissipators connected to cross-laminated timber wall panels subjected to tension and cyclic loading". Journal of Structural Engineering, **142(4)**:E4015013.
- [3.38] Sarti, F., Palermo, A., and Pampanin, S., (2015). "Quasi-static cyclic testing of two-thirds scale unbonded posttensioned rocking dissipative timber walls". Journal of Structural Engineering. DOI:10.1061/(ASCE)ST.1943-541X.0001291.
- [3.39] Loo, W. Y., Kun, C., Quenneville, P., and Chouw, N. (2014). "Experimental testing of a rocking timber shear wall with slip-friction connectors". Earthquake Engineering and Structural Dynamics, **43(11)**: 1621-1639.
- [3.40] Hashemi, A., Zarnani, P., Masoudnia, R., and Quenneville, P. (2017). "Seismic resistant rocking coupled walls with innovative Resilient Slip Friction (RSF) joints". Journal of Constructional Steel Research, **129**:215-226.
- [3.41] Polastri, A., Angeli, A., and Dal Ri, G. (2014). "A new construction system for CLT structures". In Proceedings of the World Conference on Timber Engineering (WCTE), 10-14 August 2014, Quebec City, QC, Canada.
- [3.42] Latour, M., and Rizzano, G. (2015). "Cyclic behavior and modeling of a dissipative connector for cross-laminated timber panel buildings". Journal of Earthquake Engineering, **19(1)**:137-171.

- [3.43] Schmidt, T., and Blaas, H.J., (2017). "Dissipative joints for CLT shear walls". In Proceedings of International Network on Timber Engineering Research (INTER), meeting 50, 28-31 August 2017, Kyoto, Japan. Paper INTER/50-15-2.
- [3.44] Scotta, R., Trutalli, D., Marchi, L., and Pozza, L. (2017). "Capacity design of CLT structures with traditional or innovative seismic-resistant brackets". In Proceedings of International Network on Timber Engineering Research (INTER), meeting 50, 28-31 August 2017, Kyoto, Japan. Paper INTER/50-15-5.
- [3.45] Paulay, T., and Priestley, M.J.N. (1992). Seismic design of reinforced concrete and masonry buildings. Wiley, New York.
- [3.46] Jorissen, A., and Fragiaco, M., (2011). "General notes on ductility in timber structures". Engineering Structures, **33(11)**:2987-2997.
- [3.47] Sustersic, I., Fragiaco, M., and Dujic, B. (2011). "Influence of connection properties on the ductility and seismic resistance of multi-storey cross-lam buildings". In Proceedings of the Meeting 44 of the Working Commission W18-Timber Structures, CIB, Alghero, Italy.
- [3.48] Izzi, M., Flatscher, G., Fragiaco, M., and Schickhofer, G. (2016). „Experimental investigations and design provisions of steel-to-timber joints with annular-ringed shank nails for Cross-Laminated Timber structures". Construction and Building Materials, **122**:446-457.
- [3.49] Follesa, M., Fragiaco, M., Vassallo, D., Piazza, M., Tomasi, R., Rossi, S., and Casagrande, D. (2015). "A proposal for a new Background Document of Chapter 8 of Eurocode 8". In Proceedings of International Network on Timber Engineering Research (INTER), meeting 49, Šibenik, Croatia.
- [3.50] Follesa, M., Fragiaco, M., Casagrande, D., Tomasi, R., Piazza, M., Vassallo, D., and Rossi, S. (2016). "The new version of Chapter 8 of Eurocode 8". Proceedings of the 14th World Conference on Timber Engineering (WCTE), 22-25 August 2016, Vienna, Austria.
- [3.51] EN 1993-1-1 Eurocode 3 (2005). "Design of steel structures, Part 1-1: General rules and rules for buildings". CEN. Brussels, Belgium.
- [3.52] Ramberg, W., and Osgood, W.R. (1943). "Description of stress-strain curves by three parameters". NACA, TN-902.
- [3.53] Scotta, R., Marchi, L., Trutalli, D., and Pozza, L. (2016). "A dissipative connector for CLT buildings: concept, design and testing". Materials, MDPI. DOI:10.3390/ma9030139.
- [3.54] ANSYS® Mechanical Workbench.
- [3.55] Priestley, M.J.N.; Seible, F.; Calvi, G.M. Seismic Design and Retrofit of Bridges; Wiley: New York, NY, USA, 1996.
- [3.56] EN ISO 6892-1 (2009). "Metallic Materials - Tensile Testing - Part 1: Method of Test at Room Temperature". CEN: Brussels, Belgium.
- [3.57] Muñoz, W., Mohammad, M., Salenikovich, A., and Quenneville, P. (2008). "Need for a harmonized approach for calculations of ductility of timber assemblies". In Proceedings of the Meeting 41 of the Working Commission W18-Timber Structures, CIB, St. Andrews, NB, Canada, 25-28 August 2008.
- [3.58] Foschi, R.O., and Bonac, T., (1977). "Load slip characteristic for connections with common nails". Wood Science Technology, **9(3)**:118–123.
- [3.59] Foliente, G.C. (1996). "Issues in seismic performance testing and evaluation of timber structural systems". In Proceedings of International Wood Engineering Conference, New Orleans, United States, Vol.1, pp.29-36.
- [3.60] EN 1990 (2002). "Basis of structural design". CEN. Brussels, Belgium.

- [3.61] EN 10025-2 (2004). "Hot rolled products of structural steels. Technical delivery conditions for non-alloy structural steels". CEN. Brussels, Belgium.
- [3.62] EN 14358 (2016) "Timber structures - Calculation and verification of characteristic values". CEN. Brussels, Belgium.
- [3.63] Rodd, P.D., and Leijten, A.J.M. (2003). "High-performance dowel-type joints for timber structures". *Progress in Structural Engineering and Materials*, **5(2)**:77-89.
- [3.64] Blass, H.J., Schmid, M., Litze, H., and Wagner, B. (2000). "Nail plate reinforced joints with dowel-type fasteners". In *Proceedings of the World Conference on Timber Engineering (WCTE)*, July 31-August 3 2000, Whistler Resort, British Columbia, Canada.
- [3.65] European Organisation for Technical Assessment (EOTA) (2016). "Self-tapping screws for use in timber structures". European Technical Approval ETA-11/0027. Charlottenlund, Denmark.
- [3.66] Massari, M. (2017). "Seismic Behavior of Cross laminated Timber (CLT) Structural Systems: from Traditional Steel Connections to Low-Damage Solutions" Ph.D. Thesis, University of Bologna, Italy.
- [3.67] Heco Italia S.r.l. (2016). "Tests to determine the influence of self drilling dowel type fasteners on the mechanical behaviour of fitch plate connections". Lignum Test Center, Graz, Austria.

Chapter 4 Development of a Macro-element model to simulate the hysteretic behaviour of the dissipative device

Abstract

In this last chapter, the numerical procedure used to evaluate the seismic performance of CLT shear wall assemblies adopting the investigated device is reported. The experimental data collected through the cyclic loading tests have proven the correctness of the detailed numerical model. Such results allowed to extend the analysis with detailed models and to define the complete strength-domain that describes the shear-tensile interaction on the connection element. Moreover, a macro-element model approach realized with a second numerical code allowed to compute NLDAs of a case-study CLT building with reduced computational effort. The obtained results concluded in the evaluation of a plausible behaviour factor that could characterize a CLT shear wall assembly that employ the investigated connections.

4.1 Introduction

A fundamental issue in the seismic design of complex CLT shear-wall assemblies is the definition of suitable values of the stiffness and distribution of connections, which influence the building fundamental period, the distribution of seismic forces and the displacement and drift of each storey [4.1]. The vibration period depends on the mass distribution and on the global stiffness of the building, which is highly sensitive to deformability of the connection elements. The distribution of seismic forces is function of stiffness of the shear-walls, which on its own depends on stiffness of seismic-resisting connections. Displacements and inter-storey drifts depend on the deformation of the shear walls, which can be a rocking, sliding and/or shear deformation. Consequently, for a precise modelling of a building the definition of the strength and stiffness of each connection is crucial. As an example, in platform-frame buildings the correct modelling of panel-to-frame connections or of equivalent shear stiffness of each shear wall is fundamental (predominant shear behaviour). Conversely, in CLT buildings the most important elements to be modelled are angle brackets, hold-downs and panel-to-panel joints (predominant rocking and sliding mechanisms).

Even in a linear-elastic design process, engineers are therefore required to solve an iterative scheme [4.1]. In detail, the connection stiffness influences the fundamental period of the building, the distribution of forces and drifts and meanwhile, the external force in each connection induced by earthquake is a function of the period and of the connection stiffness. Therefore, the load bearing capacity of the connections has to be compatible with the external force (Ultimate Limit State verification – ULS [4.2]) and the drift of each storey has to be compatible with the limitation of damage of non-structural elements (Damage Limitation State verification – DLS [4.2]). It is therefore clear how even in a simplified analysis that is a linear elastic analysis requires precise information on the connection's behaviour when subjected to tension, shear or a combination of them.

In this context, Trutalli [4.1] and Pozza et al. [4.3] analysed the behaviour of a series of cyclic loading experimental tests on CLT shear-walls anchored with different arrangements of shear-resisting connections. The main outcomes confirmed that mechanical parameters and seismic capacity (e.g., strength, ductility, and behaviour factor) were considerably worsened with respect to the case of no axial-shear interaction within each connection. Such result was also demonstrated by Izzi et al. [4.4] with a numerical approach. More recently, deeper experimental tests were performed to investigate the strength domain of traditional connections in a rocking CLT shear wall system ([4.5];[4.6]). Additionally, once experimental tests confirm the reliability of the connections, Non-linear dynamic simulations are to be performed in order to predict the actual response of a CLT structures (i.e. the response of each connection/device that link adjacent panels or the whole structure to the foundation).

4.1.1 Numerical approaches to simulate CLT structures

With regard to numerical models, various approaches for simulating CLT structures are available in literature, which can be subdivided in two main categories [4.7]. The first one considers the building as an assembly of single wall elements, disregarding the hysteretic behaviour of single connections and concentrating the non-linear behaviour in the wall macro-elements, e.g., [4.8]-[4.10]. With the second methodology, the building is modelled as an assembly of CLT panels and connection elements ([4.7]; [4.11]-[4.15]). This “component approach” is proven to be more accurate, but it requires the use of numerical models capable of reproducing the actual behaviour of all the connection elements used to fasten each other the CLT panels and the foundations. However, the

majority of the models is calibrated through uniaxial experimental tests accomplished for a single connection element.

With both modelling approaches, elements capable of representing the non-linear behaviour of an entire CLT shear wall or a single connection, are needed in order to reproduce faithfully the response of CLT structures. Several examples are available in literature, starting from the hysteretic model proposed by Ceccotti and Vignoli [4.16], implemented into the non-linear dynamic analysis program Drain-2DX [4.17], used to reproduce the shaking table tests carried out on the well-known SOFIE project [4.8]. More recently, the hysteretic model proposed in origin to reproduce the behaviour of reinforced concrete beam-column joints [4.18] was profitably adopted to reproduce the response of CLT assemblies accounting for pinching behaviour of timber connections. However, such hysteretic models are suitable for reproducing the uniaxial behaviour of the connection elements, but are not capable to account for a combined application of axial and shear forces.

An important attempt to account for axial-shear coupling in CLT connections was presented in Rinaldin et al. [4.15]. where shear-tension coupling was dealt with by defining an elliptical strength domain for yielding axial and shear strengths of the connection system without specific reference to experimental tests on axial-shear coupled interaction. In their model uncoupled (axial and shear) tests are used to calibrate the hysteretic law and the axial-shear interaction is taken into account only once, modifying the backbone envelope curve when the domain yielding surface is first reached. More recently, Pozza et al. [4.6] developed a potential solution to analyse this topic basing its numerical model on significant experimental tests that reproduced the behaviour of hold-downs subjected to axial loading when a lateral force is already acting and partially compromising its response.

4.1.2 Aim of this work

In this concluding chapter, the procedure used to evaluate the seismic performance of CLT shear wall assemblies by means of numerical simulations is reported step-by-step (see Fig. 4.1). The experimental data collected through the cyclic loading tests and elaborated were correctly reproduced by the numerical simulations. Such results allowed extending the analysis of the connection to the definition of a complete strength domain, which describes the shear-tensile interaction effect on the connection element. This characterization was carried out with non-linear pushover analyses (NLSA) conducted with the 3D model (see 3.2.2.1), from now on named *detailed* model. The next step involved the implementation of a 2D numerical model, exploiting a macro-element approach, which allowed replicating the cyclic behaviour of the bracket with a much lower computational effort. The calibration of the Macro-Element model (MEM), otherwise referred as *simplified* model, was carried out from the cyclic loading test ran in pure shear and pure tension. The cyclic response of the MEM, when mixed tension/shear loading conditions occur, was evaluated comparing the results from non-linear cyclic analyses of case study CLT walls anchored with the investigated devices and performed with both *detailed* and *simplified* modelling approaches. It is implicitly assumed that the detailed model is able to reproduce the actual hysteretic behaviour of the steel element on all loading conditions. Comparison in terms of base shear strength, displacement capacity and total dissipated energy confirmed the respectable outcomes of the MEM approach in all the possible working conditions (i.e. using the X-bracket as hold-down, angle bracket or vertical joint). The last step consisted of running NLDA of a case-study CLT building for which *traditional* connections were substituted with the investigated connections. Then, by adopting an hypothetical design procedure, well described in the respective section, the performance of the bracket were measured in terms of potential behaviour factor demonstrated by the analysed building. The

described procedure is summarized in the following diagram. It must be emphasized that also in this case, innovative dissipative connections that bypass the issue of reproducing the hysteretic response of traditional fasteners are easier to be reproduced numerically. In conclusion, this fact make even more reliable the outcomes from numerical analyses of CLT structures that employ innovative connection systems.

Lastly, all the procedure reported in this chapter was based on the experimental data collected for the Version 2 of the X-bracket. It is clear that the following approach is meant to be valid also for the other tested versions but, more important, it could be hypothetically applied to whatever innovative connection or device is characterized by a well-known hysteretic behaviour that have been assessed through detailed experimental tests.

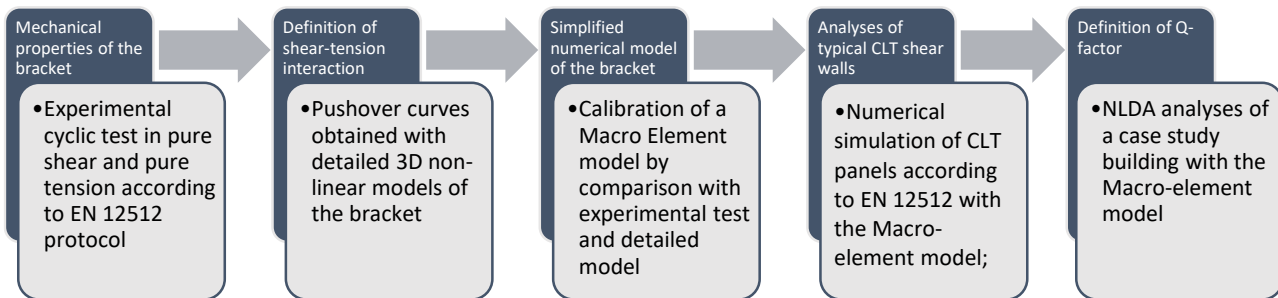


Fig. 4.1 – Work-flow adopted in this work to evaluate the seismic response of a CLT building employing the studied devices by means of a MEM approach.

4.2 Definition of the strength domain

Research results presented in this section are partially available Marchi, L., Trutalli, D., Scotta, R., Pozza, L., and Ceccotti, A. (2016). “A new dissipative connection for CLT buildings”. In *Proceedings of the Third International Conference ICSA, 27-29 July 2016, Guimaraes, Portugal. Structures and Architecture 17:169-177*. DOI: <http://dx.doi.org/10.1201/b20891-20>

Since the X-bracket can be used as a hold-down or an angle bracket, and consequently be subjected to combined loadings, it is mandatory that its shear-tensile strength domain has to be predicted. To this aim, displacement-controlled pushover analyses have been conducted, with 10 intermediate angles α between pure shear condition ($\alpha = 0^\circ$) and pure tension condition ($\alpha = 90^\circ$). Obtained curves (see Fig. 4.2) are linear (i.e., forces proportional to deformations) in the initial elastic phase, and deviated when entering the plastic phase. The yielding limits shown in Fig. 4.3 were evaluated applying method “a” of EN 12512 [4.19] to the resulting inclined force F_{TOT} and decomposing the obtained values in tension and shear components, F_{HD} and F_{SH} respectively (Method 1). The peak strength was fixed at achievement of the ultimate steel strain.

ENa method was applied also after the decomposition of the inclined force to the single components (Method 2). In particular the bi-linearization was applied to F_{SH} for angles $\alpha \leq 45^\circ$ and to F_{HD} for $45 < \alpha \leq 90^\circ$. The latter method can be considered more reliable, because the yielding limits are evaluated on the “principal” component for angles $\alpha < 30^\circ$ and $\alpha > 55^\circ$ and, lower values are provided at the highest level of coupling (i.e., the range $30^\circ \leq \alpha \leq 55^\circ$) (see Fig. 4.4). A simple linear law can be used to fit the failure strength, although it can be seen that for lower angles ($\leq 30^\circ$) the shear

force is not impaired by tension loads, suggesting that shear bracket might work respond well to shear loads even if the panels causes tension forces (e.g., due to rocking behaviour).

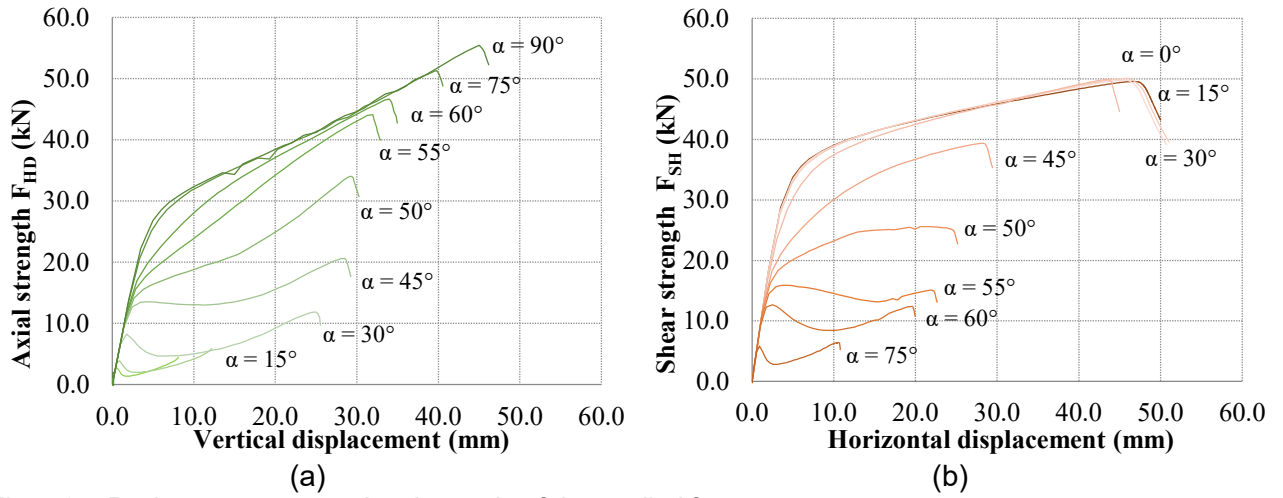


Fig. 4.2 – Pushover curves varying the angle of the applied force.

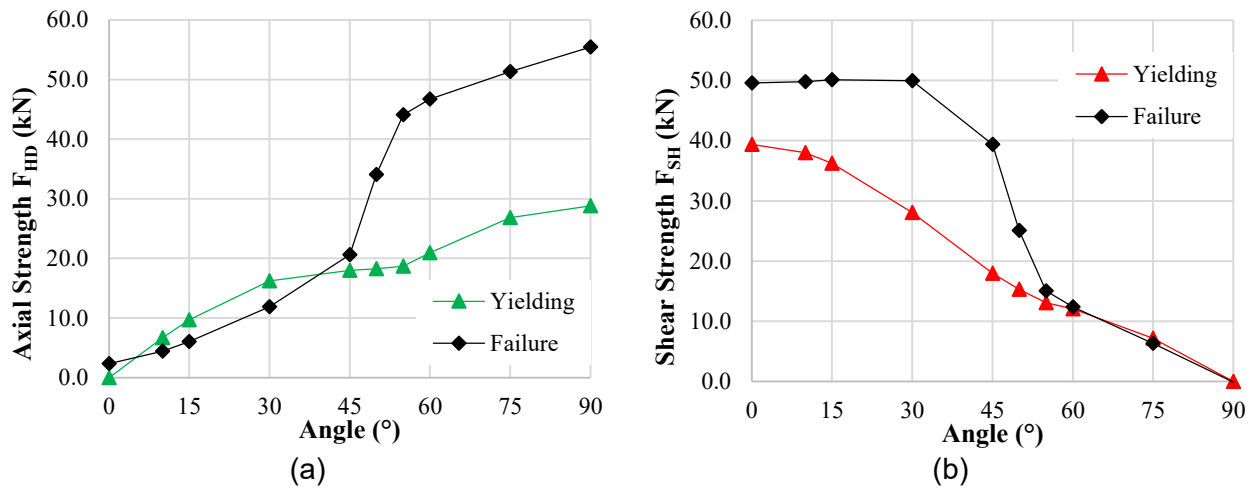


Fig. 4.3 – Strength at yielding and failure obtained from the analyses for the bracket working mainly in tension F_{HD} (a) and mainly in shear F_{SH} (b).

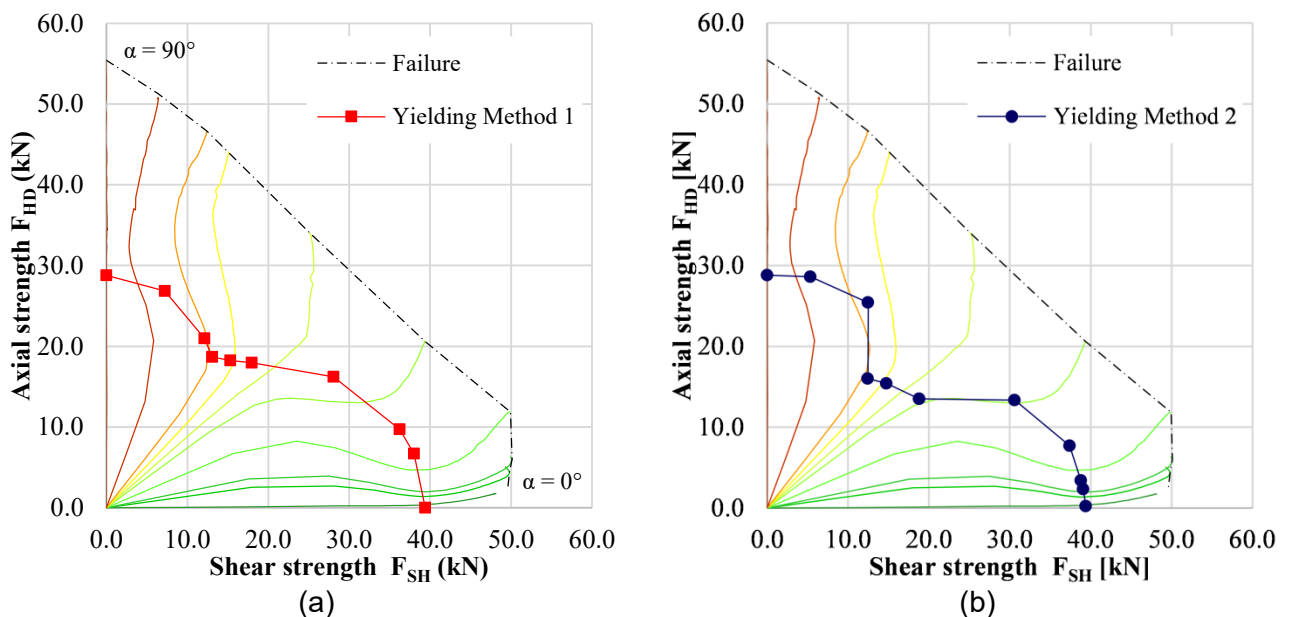


Fig. 4.4 – Strength domain definition with 10 axial/shear deformation ratios: (a) method 1; (b) method 2.

4.2.1 Abacus of strength

The need to dispose of sufficient strength and stiffness at every connection point of the building has led to investigate one last aspect of the studied bracket: the changes of its main mechanical properties (i.e. represented by yielding and failure limits) varying the bracket thickness and form-factor. This requisite could be explained by analysing the case of a multi-storey building, for which the maximum dissipative capacity shall be reached. This coincides to the condition for which all the employed connections do plastic work and consequently dissipate energy. In fact it can easily be expected that, for a multi-storey regular building (in plane and in elevation), the request of strength at the foundation level is much higher than the one demanded at the second floor. Consequently, the design method for CLT connections structures require iterative procedure to obtain the “optimal” solution. This procedure aims to define the proper disposition and strength of the brackets all along the building. For *traditional* connections (i.e. hold-downs and angle brackets), the number of nails can be changed to adapt at each demand, while for the X-bracket, three solutions are available:

- Change of steel grade;
- Increase number of bracket placed at each point;
- Change the aspect ratio of the bracket.

The first solution allows determining the actual design strength of the X-bracket by introducing a multiplying factor equal to $f_{y,k}/f_{y,test}$ where $f_{y,k}$ is the yielding strength of the chosen grade and $f_{y,test}$ the yielding test obtained for experimental test (450MPa). The second choice has obvious limits that are “more practical”. In particular number of brackets is limited to two for the external version, ore only one for the concealed solution. The third possibility is investigated in this section taking into account the possible changes of thickness t or form factor, henceforth noted as λ .

To this purpose, an analytical procedure supported by numerical simulation was adopted, by exploiting the same 3D model and parametric analysis described in Section 3.2.2.1. Further pushover curves were conducted varying ratios between axial and shear deformations α , the thickness t between 4 and 10 mm and the form factor between $0.75 \leq \lambda \leq 1.125$ and for each combinations yielding point (F_y, d_y) and failure (F_u, d_u) were defined. Results of the numerical simulations are reported in Fig. 4.5 and Table 4-1. It is worth noting that some combinations are missing: this is due to the unfavourable combination where thickness is small and form factor high and vice versa. Analysing Fig. 4.5a,c it emerges that varying the thickness t , at a given forma factor, produces proportional variations in strength, whereas does not significantly affect both yielding and ultimate displacements (d_y, d_u) . However, a clear proportionality of strength with respect to t and λ is visible in all cases.

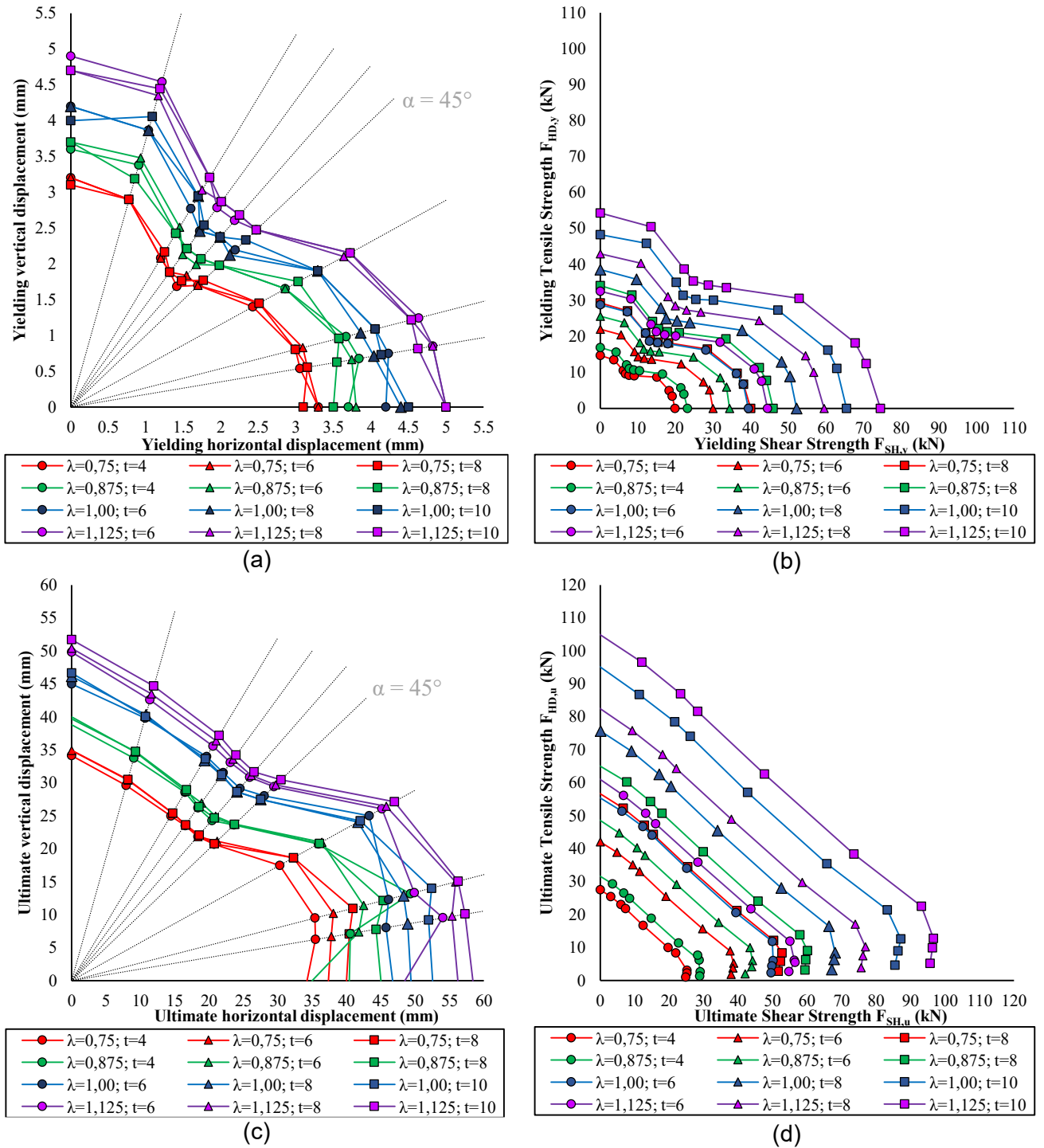


Fig. 4.5 – Shear-tension domains of the varying t and λ : yielding (a,b) and ultimate (c,d) conditions.

Table 4-1 – Results from parametric analyses in terms of yielding point (F_y, d_y), ultimate failure (F_u, d_u) and ductility μ .

		$\lambda = 0.75$		$\lambda = 0.875$		$\lambda = 1.00$		$\lambda = 1.125$	
		HD	SH	HD	SH	HD	SH	HD	SH
t= 4	F_y	14.7	19.9	16.9	23.2				
	d_y	3.2	3.3	3.6	3.7				
	F_u	27.6	24.8	31.8	28.8				
	d_u	34.1	34.3	38.8	40.4				
	μ	10.7	10.4	10.8	10.9				
t= 6	F_y	22.0	30.0	25.6	34.4	28.8	39.4	32.6	44.5
	d_y	3.2	3.3	3.7	3.8	4.2	4.2	4.9	5.0
	F_u	42.1	38.0	48.7	42.0	55.5	49.6	61.2	54.8
	d_u	34.9	37.4	40.0	35.0	45.0	46.7	49.8	48.5
	μ	10.9	11.3	10.8	9.2	10.7	11.1	10.2	9.7
t= 8	F_y	29.3	40.0	34.1	46.0	38.6	52.2	43.0	59.5
	d_y	3.1	3.1	3.7	3.5	4.2	4.4	4.7	5.0
	F_u	56.8	51.6	65.2	59.4	75.7	67.2	82.7	75.7
	d_u	35.0	40.0	39.7	45.0	46.2	49.4	50.4	56.2
	μ	11.3	12.9	10.7	12.9	11.0	11.2	10.7	11.2
t=10	F_y					48.3	65.5	54.3	74.5
	d_y					4.0	4.5	4.7	5.0
	F_u					95.4	85.5	105.3	95.7
	d_u					46.7	52.6	51.7	58.4
	μ					11.7	11.7	11.0	11.7

The numerical simulations confirmed that the strength at failure due to pure shear $F_{SH,u}$ and pure tension $F_{HD,u}$ are similar for each combination. It was therefore possible to propose analytical formulas for the computation of the strength F with suitable correlation between t and λ . The first formulation correlates the strength values with t and λ by means of four coefficients, as shown by Eq. (4.1):

$$F(\lambda, t) = k_1 \cdot t^{k_2} + k_3 \cdot \lambda^{k_4} \quad (4.1)$$

$$F(\lambda, t) = (k_1 + k_2 \cdot t) \lambda^{k_3} \quad (4.2)$$

$$F(\lambda, t) = (k_1 + k_2 \cdot \lambda) t^{k_3} \quad (4.3)$$

where $F(\lambda, t)$ can be either F_{HD} or F_{SH} .

The second and third formulation propose a function according to Eq. (4.2) and Eq. (4.3), have the same proposition where t and λ were exchanged.

Two separate formulation could be defined, one for tension and one for shear, due to the different post-elastic behaviour of the bracket (hardening for tension and perfect plastic for shear). However, a unique solution for both cases was searched in order to simplify the final proposition. By calculating the mean value μ_F and the difference δ_F of the tension and shear strength, it was observed that the ratio $\Delta = \delta_F / \mu_F$ is almost constant for all the combinations of t and λ (see Table 4-2).

Table 4-2 – Mean value μ_F and difference δ_F between tension and shear strength.

	$\lambda = 0.75$					$\lambda = 0.875$					$\lambda = 1.00$					$\lambda = 1.125$					
	F_{HD}	F_{SH}	μ_F	δ_F	Δ (%)	F_{HD}	F_{SH}	μ_F	δ_F	Δ (%)	F_{HD}	F_{SH}	μ_F	δ_F	Δ (%)	F_{HD}	F_{SH}	μ_F	δ_F	Δ (%)	
t=4	F_y	14.7	19.9	17.3	5.2	30.1	16.9	23.2	20.1	6.3	31.4										
	F_u	27.6	24.8	26.2	-2.7	-10.5	31.8	28.8	30.3	-2.9	-9.6										
t=6	F_y	22.0	30.0	26.0	8.0	30.8	25.6	34.4	30.0	8.8	29.3	28.8	39.4	34.1	10.6	31.1	32.6	44.5	38.6	11.9	30.9
	F_u	42.1	38.0	40.0	-4.1	-10.3	48.7	42.0	45.4	-6.8	-14.9	55.5	49.6	52.5	-5.9	-11.2	61.2	54.8	58.0	-6.4	-11.1
t=8	F_y	29.3	40.0	34.7	10.7	30.9	34.1	46.0	40.1	11.9	29.7	38.6	52.2	45.4	13.6	30.0	43.0	59.5	51.3	16.5	32.2
	F_u	56.8	51.6	54.2	-5.2	-9.6	65.2	59.4	62.3	-5.9	-9.4	75.7	67.2	71.4	-8.5	-11.9	82.7	75.7	79.2	-7.0	-8.9
t=10	F_y										48.3	65.5	56.9	17.2	30.2	54.3	74.5	64.4	20.2	31.4	
	F_u										95.4	85.5	90.4	-9.9	-10.9	#####	95.7	#####	-9.7	-9.6	

It is therefore convenient to: 1) calibrate the analytical formulation by using as interpolating magnitude the mean force μ_F ; 2) evaluate to the analytical values of F_{HD} and F_{SH} thanks to the mean value of Δ extrapolated from all the numerical predictions (noted as $\bar{\Delta}$). As a result:

$$\{F_{HD}(\lambda, t) ; F_{SH}(\lambda, t)\} = \beta \cdot \mu_F(\lambda, t) \tag{4.4}$$

where β is equal to $1 \pm (\bar{\Delta}/2)/100$ and μ_F is calculated according to one of the previous polynomial formulations. Fitting of results returned a value of β equal to 0.945 for tension and 1.055 for shear. The evaluation of the parameters k_i was performed via the *solver* subroutine included in Microsoft Excel using the *Generalized Reduced Gradient method*.

By observing the residual plots it can be stated that the third proposition demonstrates a proper fitting of the results either for yielding and ultimate strength, which translates into the following equations:

$$\{F_{HD,y}; F_{SH,y}\} = (1 \mp 0.155) \cdot (0.13 + 5.62 \cdot t) \lambda^{0.9} \tag{4.5}$$

$$\{F_{HD,u}; F_{SH,u}\} = (1 \mp 0.055) \cdot (0.45 + 7.29 \cdot t) \lambda^{1.065} \tag{4.6}$$

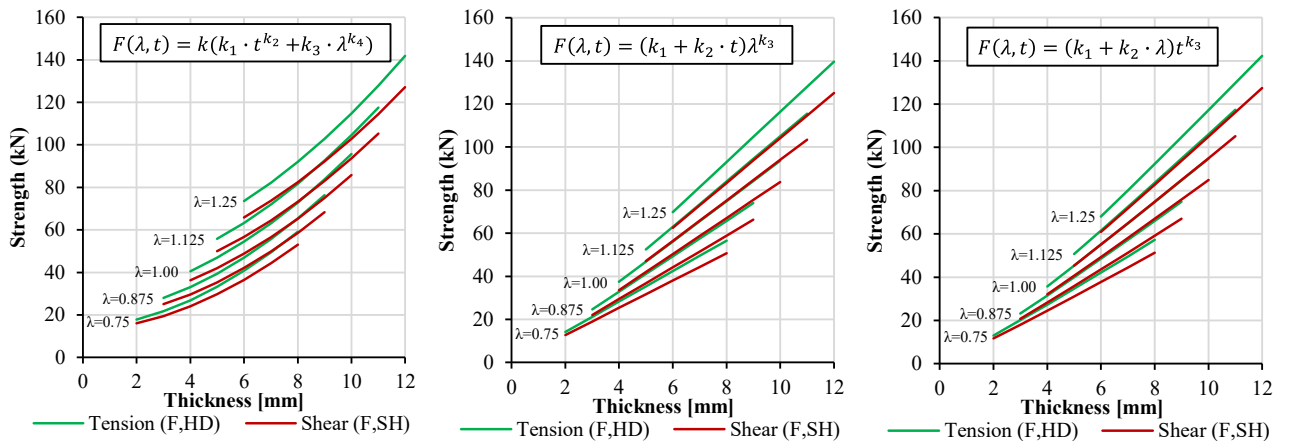


Fig. 4.6 – Abacus representation for the strength estimation with the three formulations.

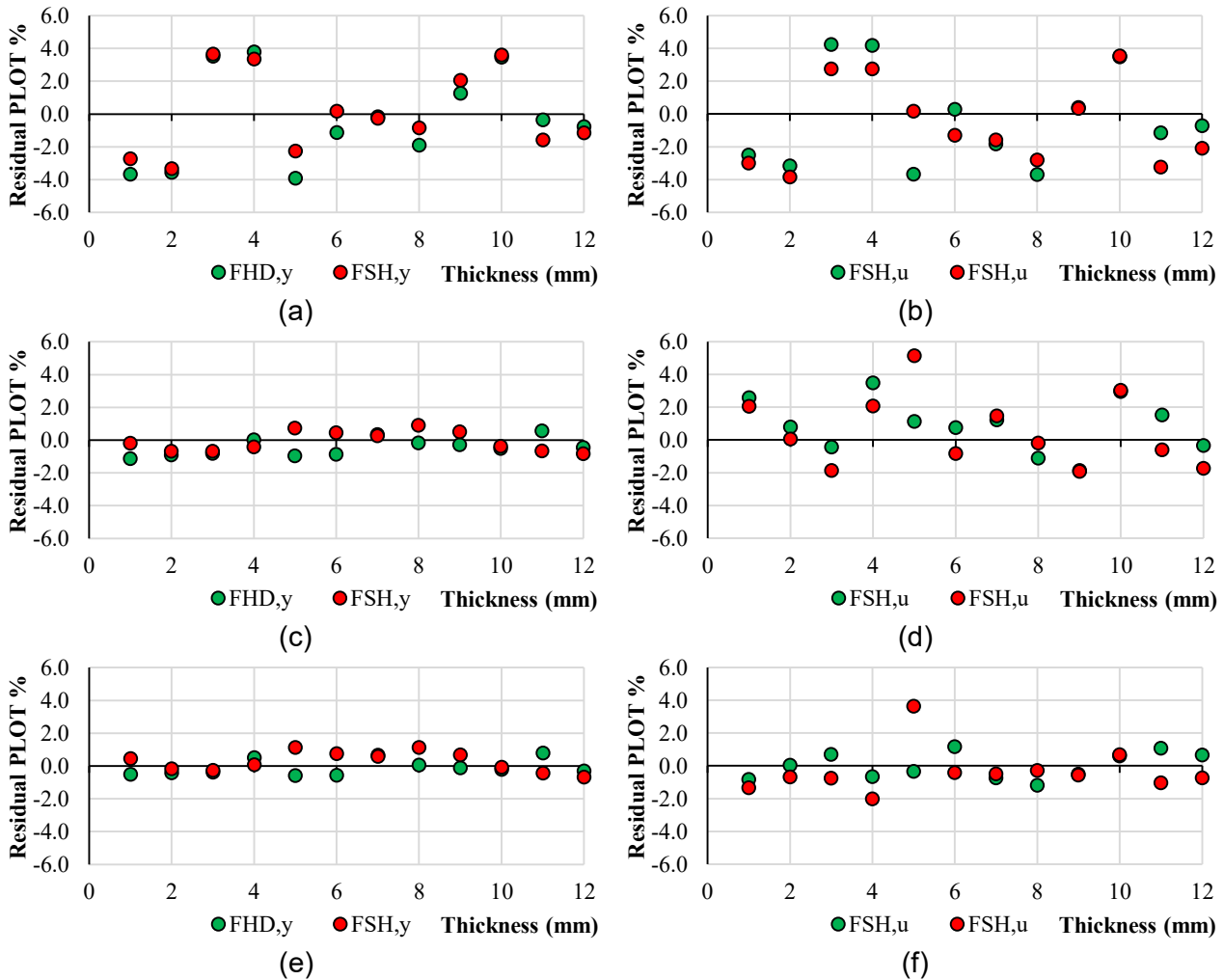


Fig. 4.7 – Residual plots obtained with the first (a,b), second (c,d) and third (e,f) analytical formulations.

4.3 Macro-element model

Research results presented in this section are partially available Marchi, L., Trutalli, D., Scotta, R., and Pozza, L. (2017). “Numerical simulation of the coupled tension-shear response of an innovative dissipative connection for CLT buildings”. In *Proceedings of the 6th ECCOMAS Thematic Conference on Computational Methods in Structural Dynamics and Earthquake Engineering (COMPdyn)*, 15-17 June 2017, Rhodes Island, Greece

A numerical model was implemented within the open-source research FEM code “Open System for Earthquake Engineering Simulation–OpenSees” [4.20] with the aim to perform analyses currently characterized by several non-linearities with a relatively low computational effort if compared to *detailed* 3D models (described in the Chapter 3). In the proposed solution, the complex connector’s shape was simplified into a Macro-Element composed by few sub-elements each one incorporating specific mechanical parameters according to the material models available in the OpenSees library [4.20]. Fig. 4.8 shows a superposition between the outline of the X-bracket and the 6-nodes ME.

With regard to Fig. 4.8, the model is composed by:

- Six *nodes*, represented in figure by the six black dots. Nodes 1 to 4 have spacing equal to the actual spacing of the X-bracket's fixing points while the two additional nodes, 5 and 6, are placed exactly between node 1 and 2 and nodes 3 and 4 respectively;
- Four elastic *beam element*, represented by the black lines, connect the two upper fixing point nodes with node 5 and the two lower ones with node 6. They simulate the connectors' flanges having a common node in the flange-web intersection;
- One *beam element* representing the web of the connector, connects nodes 5 and 6 thus linking the four horizontal arms (flanges) of the X-bracket;
- One *column element* (that works only in compression) placed in parallel to the previous element;
- Six *hinge elements*, represented by the red and green dots, are responsible for the inelastic response of the element and calibrated through a moment/curvature relationship;

Each beam element has a cross-section dimension similar to the actual *version 2* of the X-bracket with yielding moment/curvature parameters M_y and θ_y derived on the hypothesis of an S450 steel grade. This choice is arbitrarily chosen in order to try giving a physical justification to the chosen parameters. It is worth noting that the main goal is to try reproducing the hysteretic behaviour of the element, and whatever combination of dimensions and yielding conditions may be chosen, should lead to the same results.

The need to decouple the behaviour of the MEM in case of pure tension or pure shear loads, forces to distinguish the non-linear moment/curvature law of the flanges with respect to the web (Fig. 4.8b). Regarding the flanges, plasticity is concentrated on one end of the element only (red dots in Fig. 4.8a). On the contrary, the web incorporates two hinges at its ends (green dots on element 15 in Fig. 4.8a). In fact, beams and non-linear hinges are modelled exploiting *beamWithHinges* elements [4.20] which considers plasticity concentrated over a specified length from the end nodes. Lastly, a *Hysteretic material model* is applied to the 2D elements, and calibrated through additional parameters in order to reproduce the hysteretic response of the beams (see Fig. 4.8b and section 4.3.1). As the X-brackets is characterized by some pinching phenomenon due to buckling phenomena occurring at high displacement, the *column element* is necessary to simulate the different secant stiffness that characterizes the unloading phase. The flowchart of the model implemented in OpenSees is depicted in Fig. 4.9 whereas an example of the numerical code is available in 0.1.

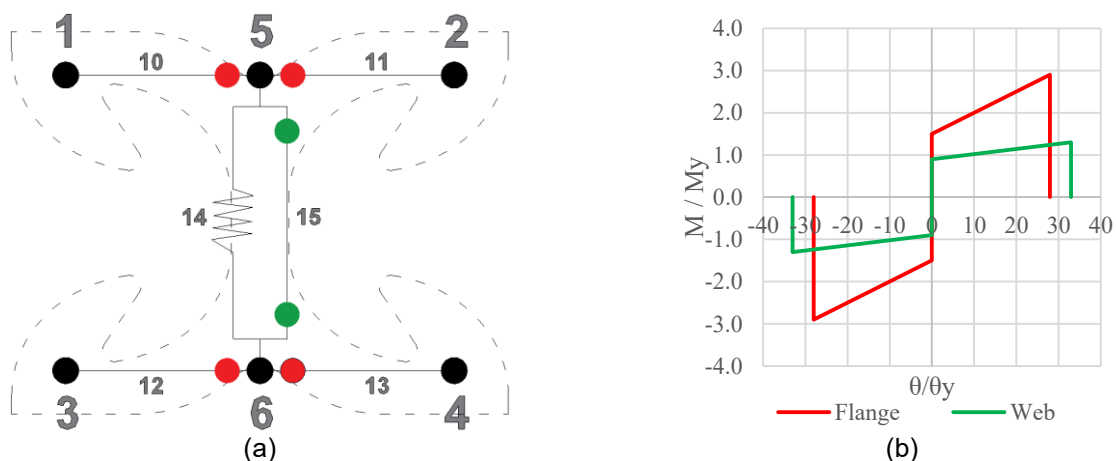


Fig. 4.8 – Macro element Model of the X-bracket (a) and Moment/curvature law applied to the hinges (b).

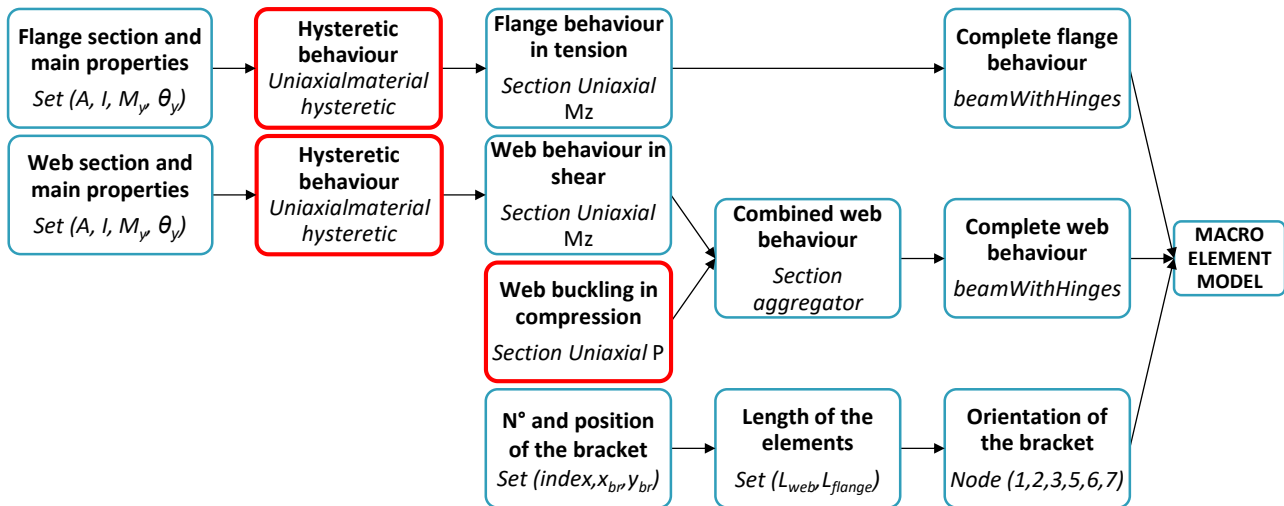


Fig. 4.9 – Flowchart of the intended Macro element Model.

4.3.1 Calibration of the MEM model

Fig. 4.10 shows a comparison between experimental evidence of X-bracket *version 2*, reported in section 3.2.3, and numerical prediction of the 3D model (*detailed*) and the MEM (*simplified*). Analysing the cyclic tensile results (see Fig. 4.10a,b) the detailed model almost overlaps the experimental hysteretic loops which translate into a good matching of the elastic K_{el} and post-elastic stiffness K_{pl} and dissipated energy. Within high displacements, the overestimation of the peak compression force in the unloading phase is (energetically) balanced by an underestimation of the stiffness during 2nd and 3rd reloading cycles. The shear response (see Fig. 4.10c and d) of the detailed model is almost identical in the range ± 12 mm. However, high amplitude cycles are difficultly replicated by the detailed model due to particular buckling phenomena (and localized plastic strain) occurring in the X-bracket web for repeated reversed cycles.

As for the MEM, the hysteretic response to tensile loading conditions is correctly captured. In detail, the lower dissipated energy, emerging from low-amplitude cycles, is mainly due to the lower the absence of buckling phenomena observed in the experimental test, while the column element is always active in all the displacement range. However, the dissipated energy measured for high displacement cycles is very well replicated from the model (see Fig. 4.10b) and demonstrated by the equal gradient of the experimental and numerical curves. As an anticipation, the model is being further enhanced by adding a threshold level to the column element up to which the buckling remains inactive. This, to reduce the underestimation of 21% that is left at the end of the cyclic procedure. Lastly, the MEM is also faithfully reproducing the shear loading conditions where, apart from low amplitude range (-4mm, +4mm), is capable to reproduce both loading and unloading stiffness and strength degradation.

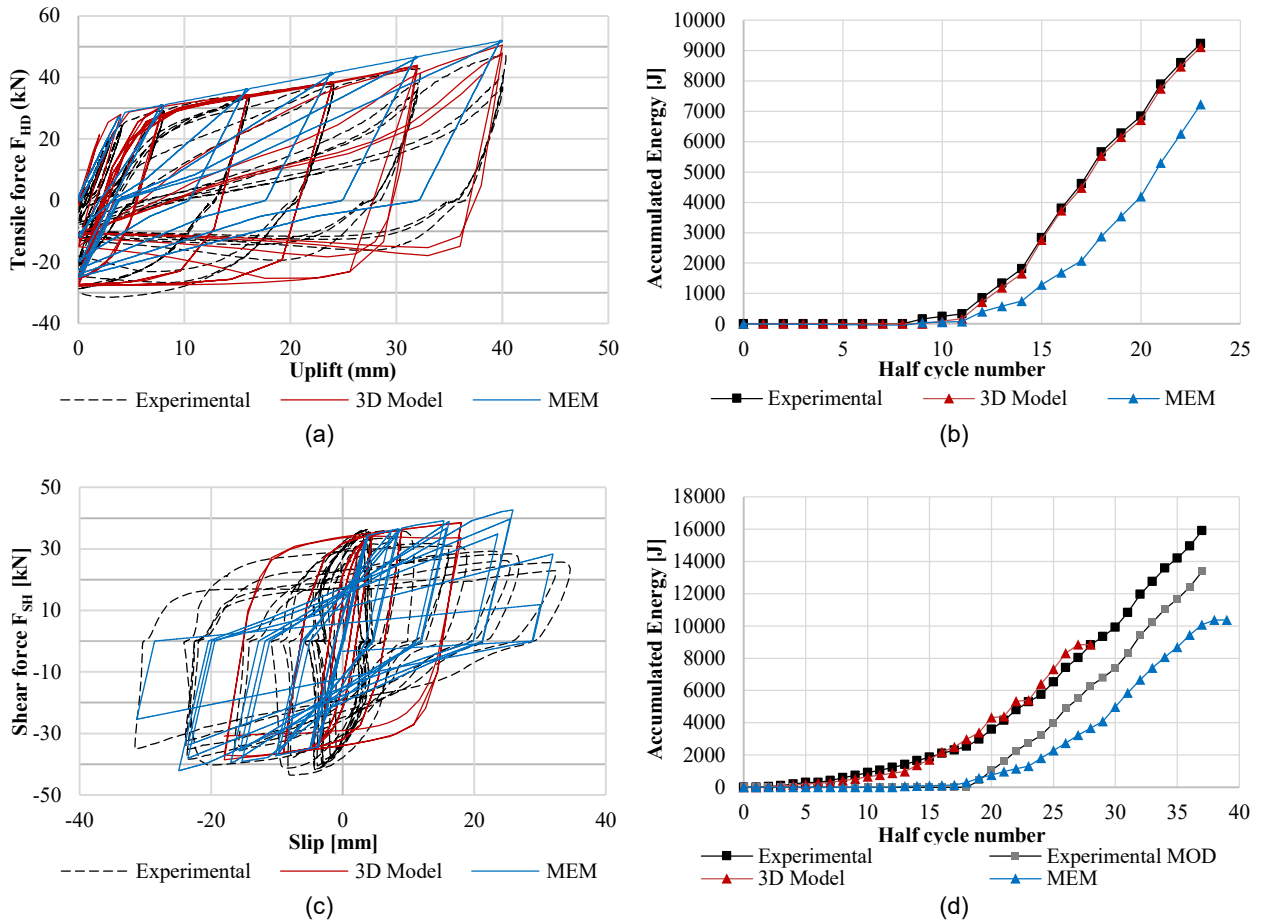


Fig. 4.10 – Comparison of cyclic loading tests: Pure tension test hysteretic loops and respective cumulated energy for pure tension (a,b) and pure shear (c,d) loading.

4.4 MEM application to Case-study CLT shear walls

The evaluation of the combined shear-tensile interaction was given by the numerical simulation of full-scale CLT shear-walls adopting various configuration of wall geometry and number and position of the brackets. FE simulations of typical CLT shear walls fastened with the investigated device were realized with both models. Quasi-static cyclic-loading tests were simulated according to EN 12512 protocol 4) with increasing amplitude taking as a reference an horizontal top-displacement at yielding d_y equal to 10 mm. The four chosen walls have exactly reproduced the CLT specimens (dimension of 2.95 x 2.95 m, aspect ratio 1:1 and vertical distributed load 18.5 kN/m) tested at CNR-IVALSA laboratory within the SOFIE project [4.21]. These configurations were chosen to allow a direct comparison with shear-walls representative of the CLT technology and anchored using *traditional* connection system. Wall I.1 is anchored with two hold-downs and two angle brackets whereas wall I.2 exploited two hold-downs and four angle brackets. Wall 2.4 and 3.1 have the same height but are composed by two panels jointed together. The vertical joint is realized in the first case (wall 2.4) with a half-lap joint fastened with ten 8x100mm self-tapping screws. The second wall have two lines of 20 screws in a LVL spline joint [4.21].

Fig. 4.11 shows the geometry and connection arrangement of the modelled CLT shear walls employing the newly developed connection:

- Wall A simulates the condition of the minimum number of brackets necessary to anchor a single panel at the base. The connection placed at the corner act mainly as hold-downs, thus are mainly subjected to tensile loading condition;
- Wall B presents the normally designed condition of a typical panel where an additional bracket is placed in the middle to absorb mainly shear loads;
- Wall D.1 has four brackets placed at the base and a single bracket acting as vertical joint;
- Wall D.2 have the same configuration of D.1 but two brackets are placed as element connecting the two panels.

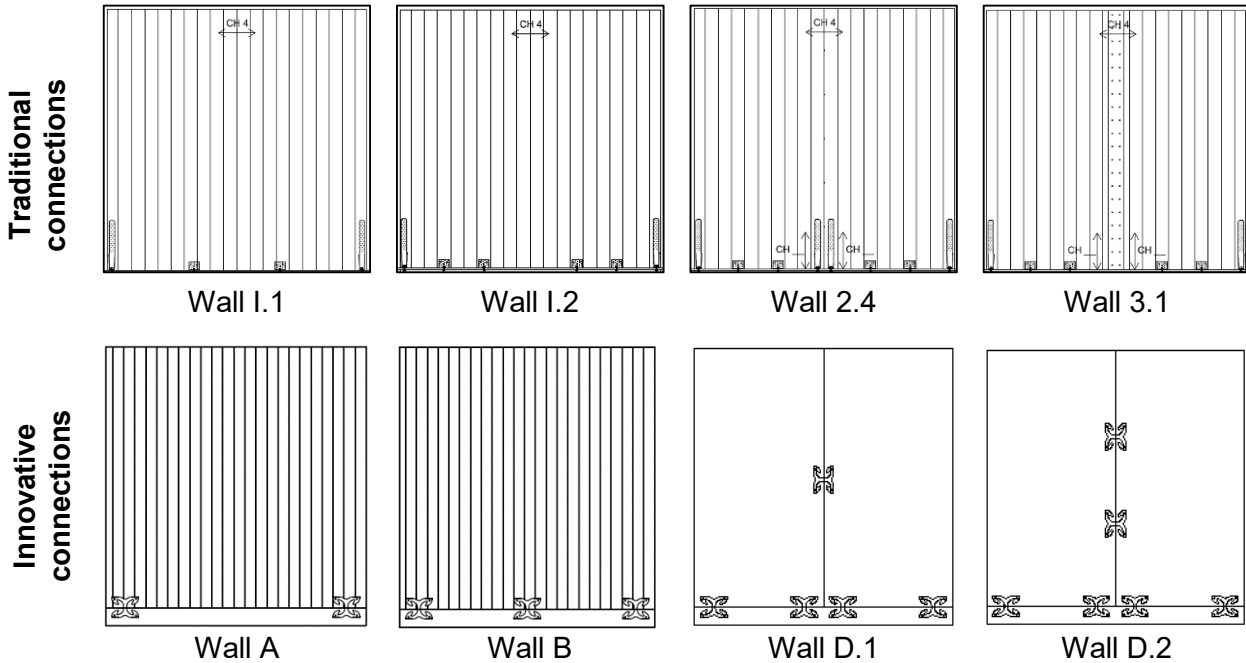


Fig. 4.11 – Geometry and connection arrangement of the investigated walls: tested walls with traditional connections (first row); simulated walls with innovative connections (second row).

4.4.1 Detailed model

Linear elastic membrane elements with thickness of 85 mm (5 layers of 17-mm thick timber boards) were used to simulate the timber panels (see Fig. 4.12). The panel orthotropy was included by calculating equivalent Elastic moduli in the horizontal $E_{Eq,x}$ and vertical directions $E_{Eq,y}$ and shear Moduli G according to [4.22]. The innovative brackets were modelled with the same FE non-linear model already validated in Section 3.2.2.1, assuming that it is able to reproduce the behaviour of X-brackets under combined tension and shear loads. The mesh thickness of the X-bracket was partially condensed by reducing the total number of tetrahedral elements for each connection from ~15.000 to ~5.000, to reduce the computational effort while maintaining enough accuracy of the overall cyclic response. This was possible by strongly reducing the number of elements in all the areas where plastic strains do not take place (e.g., zones near the fixing points). The preservation of reliability of the 3D model can be evaluated by examining the correctness of the cyclic response of each X-bracket, reported in Appendix A.2. Steel and CLT mechanical properties adopted in the numerical models are listed in Table 4-3. Coupling constraint equations were applied in correspondence of the fixing points to avoid relative displacements between panels and X-brackets and permit exclusively the relative rotation (*hinge connections*). No gap elements were introduced at this stage to account for possible wood embedment phenomenon. Frictionless only-compression contact elements were

placed along the interface between wall and supporting elastic curb, so disregarding the contribution of friction effects to shear strength and dissipation. Constant distributed vertical load was distributed along the top edge, whereas imposed cyclic horizontal displacement of increasing magnitude was imposed to the top corner of the CLT wall.

Table 4-3 – Main parameters used in the detailed 3D model.

Steel connectors (mean values from tensile test, see Section 3.2.3)			Timber panel (typical mean values for CLT panels)		
Parameter		Value	Parameter		Value
Elastic Modulus	E (MPa)	210000.0	Eq. Elastic modulus	$E_{Eq,x}$ (MPa)	5040.0
Tangent Modulus	E_T (MPa)	957.0	Eq. Elastic modulus	$E_{Eq,y}$ (MPa)	7360.0
Yielding stress	σ_y (MPa)	450.0	Shear modulus	G_{xy} (MPa)	450.0
Ultimate true stress	σ_u (MPa)	700.0	Shear modulus	G_{yz} (MPa)	76.8
Poisson's ratio	ν (-)	0.25	Shear modulus	G_{xz} (MPa)	115.2
Mesh size range	(mm)	5.0-8.0	Mesh size range	(mm)	30.0÷200.0
Thickness	t (mm)	6.0	Thickness	t (mm)	85.0

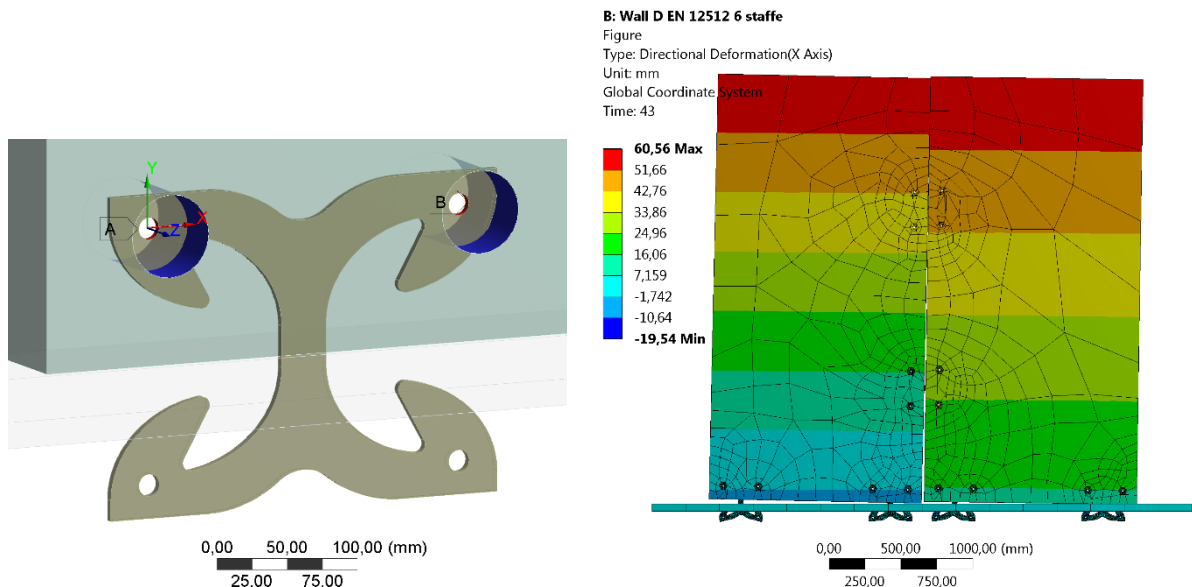


Fig. 4.12 – Detailed numerical model: Adopted constraints and example of the FE model of Wall D.2

4.4.2 Macro-element model

The CLT walls were modelled using 4-node quadrilateral element (*ShellMITC4*) already available in OpenSees [4.20]. Like in the detailed FE model, the mesh size reflects a balance between speed and accuracy, and carry the same orthotropic material model properties. The concrete curb was modelled by including elastic *no-tension truss* elements fixed to the nodes of the panel base. Each bracket, modelled with the described MEM, was connected to the mesh by using *equalDOF* commands, which construct a multi-point constraint between chosen nodes. In detail, nodes 1 and 2 of Fig. 4.8 were connected to the panel edge nodes. Actually, the MEM was not yet implemented as an independent external subroutine (i.e. each X-bracket have to be built and recalled separately) however this feature will be developed in the future to further reduce the computational effort necessary to carry out NLDAs.

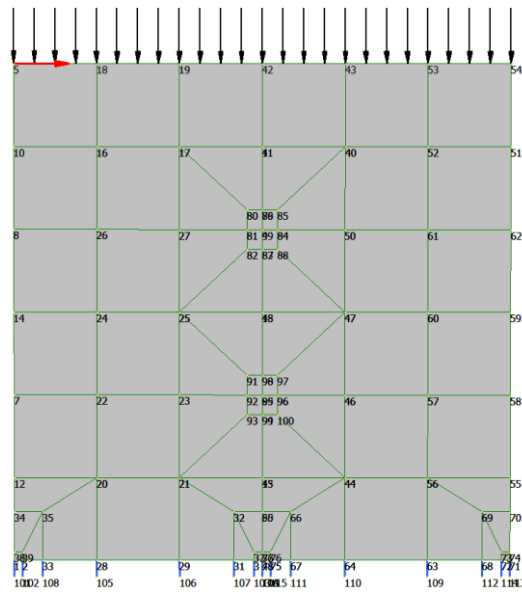


Fig. 4.13 – Simplified mesh of wall D.2 implemented into OpenSees.

4.4.3 Main results

Results from the two modelling methods are directly compared at both the single connection level and to the overall behaviour of the shear walls. In this instance, it is implicitly assumed that the detailed model accurately reproduce the brackets behaviour and consequently the actual cyclic behaviour of the CLT walls in the studied configurations. From a first look at the comparison of the force vs. displacement hysteretic loops (see Fig. 4.14) within all the configurations, the MEM is confirmed to reproduce correctly the cyclic behaviour of the brackets. Varying disposition and, consequently, the possible shear-tension interaction does not introduce any noteworthy issues in the results. Fig. 4.15 shows the total amount of dissipated energy by the system (i.e., the totality of the X-brackets). It is again confirmed the suitability of the Macro-Element approach. The only emerging differences are relative to the vertically jointed walls. In this case, the MEM seems to over-estimate the total base shear force. This is because in the 3D model the vertical joint was realized by means of the X-Brackets only and the input cyclic shear force, applied to the top left corner of the wall conveyed as an axial force from one panel to the other only through the bracket. Conversely, with the ME model the horizontal load was applied directly on the upper edge of both panels. This can easily be ascertained by analysing the force vs. displacement curve registered for each connection and in particular for the brackets placed as panel-to-panel joints (see Appendix A).

One final assumption is that the Macro-element model does reproduce the X-bracket cyclic behaviour within the entire displacement domain and not only on pure shear or pure tension loading.

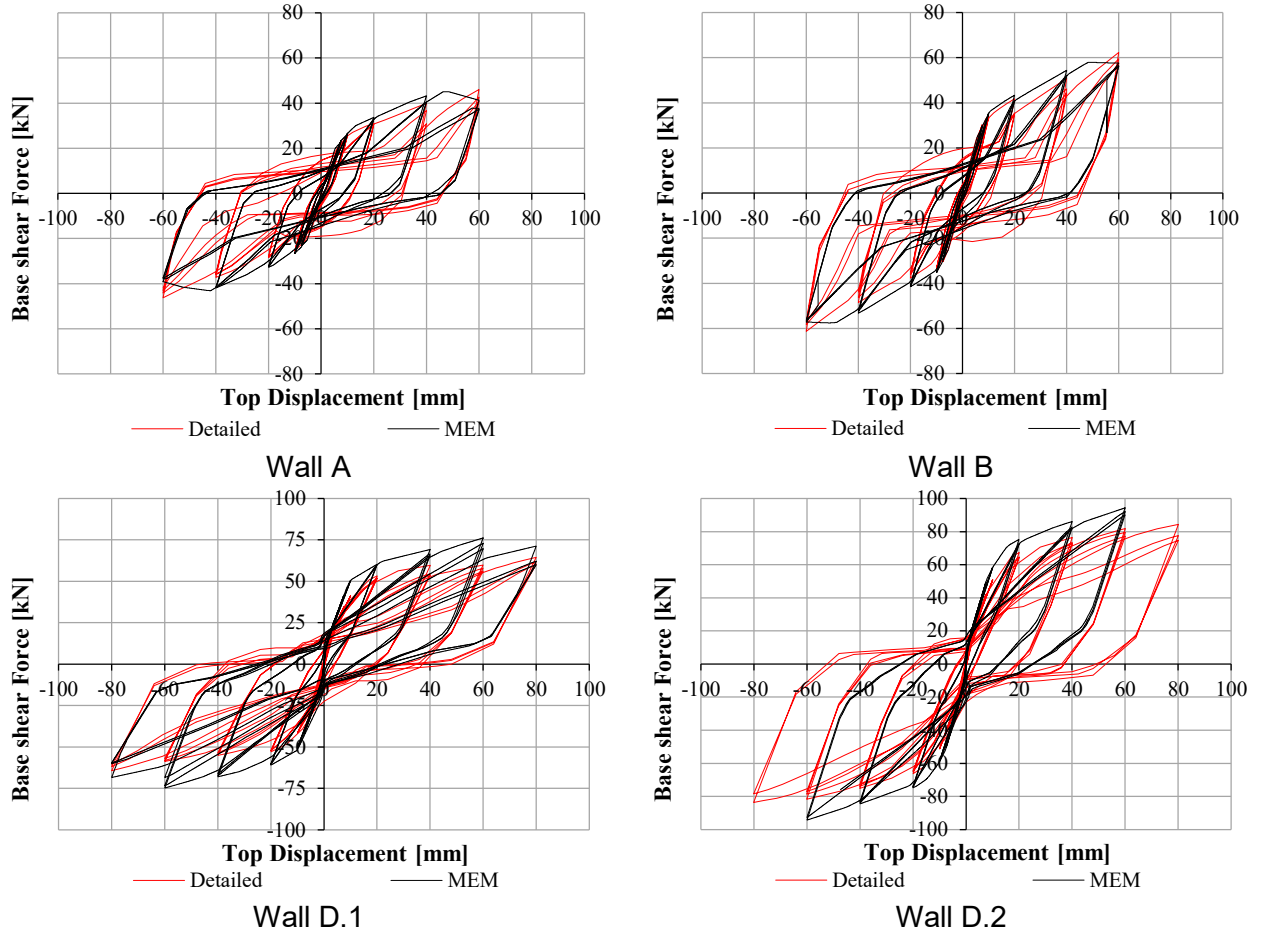


Fig. 4.14 – Force vs. top displacement loops: comparison between detailed and Macro-Element model.

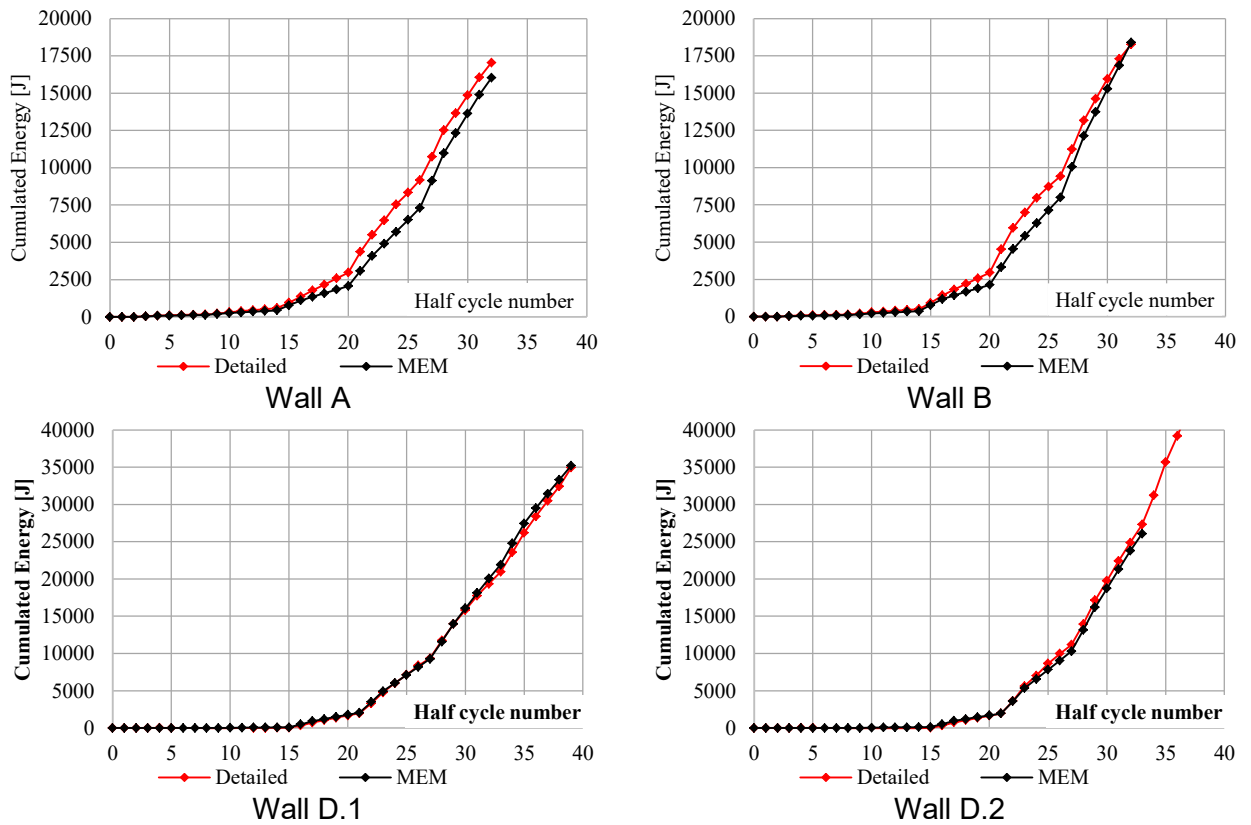


Fig. 4.15 – Total dissipated energy evaluated at the peak points: comparison between detailed model and MEM.

4.4.4 Prediction of the mechanical properties

As a supplement to the analyses, the mechanical parameters of the investigated walls are reported in Table 4-4. Either in Wall A and in wall B, failure in tension occurs for the brackets at the opposite corners but the contribution of a single bracket placed as angular bracket (from wall A to wall B) produces a conspicuous amount of base shear strength (roughly 39.9% at yielding and of 36.6% at failure). The calculated ductility values are remarkable for a CLT shear wall system. As already mentioned this is mostly due to the combination of high elastic stiffness and good displacement capacity. As expected, splitting the wall into two panels let the complete assembly take advantage of all the dissipative capacity procured by the innovative devices. Yielding strength doubles from Wall A to D.1 and from Wall B to D.2. A significant improvement is to be highlighted when an additional bracket is placed as vertical joint (wall D.1 to D.2). In fact, Wall D.1 fails in the panel-to-panel joint while in Wall D.2 the brackets at the corners are responsible for failure. Lastly, both jointed panel express the highest displacement capability (up to 80mm or 2.7% of drift). The calculated equivalent viscous damping ratio [4.19] on the 1st and 3rd cycles are mostly in the range of 15-20% with peaks up to 25-30% (see Fig. 4.16). One last noteworthy result is that the obtained total dissipated energy at the end of the cyclic procedure, even in the scarcely jointed condition of Wall A, is much higher than the one obtained with traditional connections [4.21].

Table 4-4 – Main parameters according to EN 12512 method a [4.19].

Parameter	WALL A	WALL B	WALL D.1	WALL D.2	Bi-linearization
F_y (kN)	25.34	35.28	55.39	70.62	
d_y (mm)	4.96	5.59	8.82	9.11	
F_{max} (kN)	45.70	62.50	64.60	84.40	
d_u (mm)	60.00	60.00	80.00	80.00	
k_{el} (kN/mm)	5.11	6.31	6.28	7.75	
k_{pl} (kN/mm)	0.37	0.50	0.13	0.19	
μ (V_u) (-)	12.10	10.73	9.07	8.78	
v_{eq} 1 st (%) at 60mm	19.4	17.0	20.5	18.0	
v_{eq} 3 rd (%) at 60mm	16.0	12.8	15.0	16.9	
E_d (kJ)	34.1	36.5	34.9	45.9	
Ductility Class	H	H	H	H	

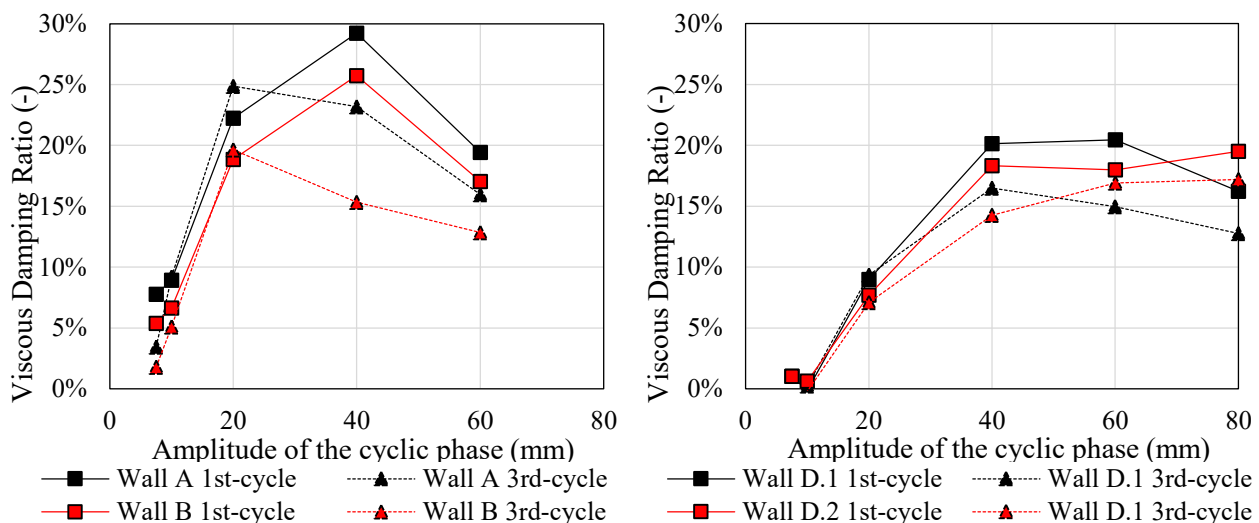


Fig. 4.16 – Equivalent viscous damping ratio of the four examined walls.

4.5 MEM application to a Case-study CLT building and computation of q-factor

In this final step, (according to Fig. 4.1) the MEM was put to the test in carrying NLDAs to assess the results, in terms of behaviour factor q , that employing proper connections designed for CLT structures can achieve on a case-study building. Part of the same numerical analyses conducted by Trutalli and Pozza [4.23] were carried out by substituting traditional angle brackets and hold-downs with the proposed connections.

The behaviour factor q was computed according to the Peak Ground Acceleration (PGA) approach ([4.8];[4.24]). According to this method, the q -factor is calculated through the ratio between PGA_d and PGA_u . The first term is the value of PGA at design condition derived through via analytical or numerical calculations. The second term is the PGA value corresponding to the near-collapse conditions and is derived through NLDAs. Additionally, the q -factor can be expressed as the multiplication of two sub-factors: the intrinsic q_0 and design over-strength Ω [4.9]. The former factor q_0 expresses the ductility, hysteresis dissipation and all the other intrinsic over-resistances (e.g., obtained from a post-elastic hardening behaviour). The latter takes into account the difference between the actual necessary strength of a component or a complete system and the strength actually required by them. Linking this concept, to the PGA approach above reported, allows a clear method of calculation of the terms q_0 and Ω . The q_0 -factor can be defined as the ratio between PGA_u and PGA_y , obtained directly from the yielding force of the building. Ω -factor can be computed in addition, as ratio between yielding and design force (see section 1.3).

4.5.1 Assumed design hypotheses and building specifications

A realistic case-study building was designed with the aim to obtain the most suitable estimation of the intrinsic behaviour factor q_0 . The following design hypotheses were made:

- The connections were designed according to Equivalent Linear Static Analysis, with the following data, according to Eurocode 8 [4.25]: type 1 elastic response spectra with type A soil, behaviour factor $q=1$, design PGA equal to 0.35g (the highest value for Italian territory) with a building importance factor of 1 and maximum spectral amplification factor equal to 2.5;
- The design value of the resistance of the brackets was assumed equal to yielding conditions obtained in the experimental tests (see Section 3.2.3.2). In particular, $F_{HD,d}$ and $F_{SH,d}$ were set equal to 27.41 kN and 38.83 kN. To take into account the shear-tensile interaction the shear strength was multiplied by a factor of 0.8 obtaining an $F_{SH,d}$ of 31.6 kN. To switch from experimental resistance to the design no other partial resistance coefficient γ_m or load duration coefficient k_{mod} were used;
- The rounding on number of connectors, i.e. the difference between the required and the actual strength was necessarily taken into account. Contrary to nailed connection, it is not possible to avoid this step (for example by calculating the exact number of nails for traditional connections). The design overstrength Ω was therefore calculated as specified (coherently with design assumption). A way to reduce this factor would be to exploit the abacus of strength provided in Section 4.2.1 and calculate the parameters (i.e. t and λ) that produces the desired design strength, however this procedure was not accounted at this stage;

- The shear-tension strength domain defined in Section 4.2 was used to evaluate the near-collapse condition of the connections for the computation of $PGA_{u,i}$ with NLDAs;

The case-study building involved a three-storey CLT structure with a total base length of 8.75 m, regular in plan and in elevation. The chosen façade was taken from a real application (Progetto Case, L'Aquila, Italy, see Fig. 4.17).

The total mass of the building M consisted in 60 t distributed as 24 t for the first two storeys and 12 t at the upper one. A resulting design shear force $F_{h,d}$ of 203 kN was calculated assuming the site conditions described above. The studied building was calculated with three different panel assemblies Fig. 4.17. In detail, the first condition assumed that no vertical joints were present and each floor was built with a singular massive squat panel. The second configuration added only one vertical joint that split the façade into two parts. The last arrangement provided the maximum amount of vertical joint possible (i.e. joints every 1.25m)



Fig. 4.17 – Case study building façade.

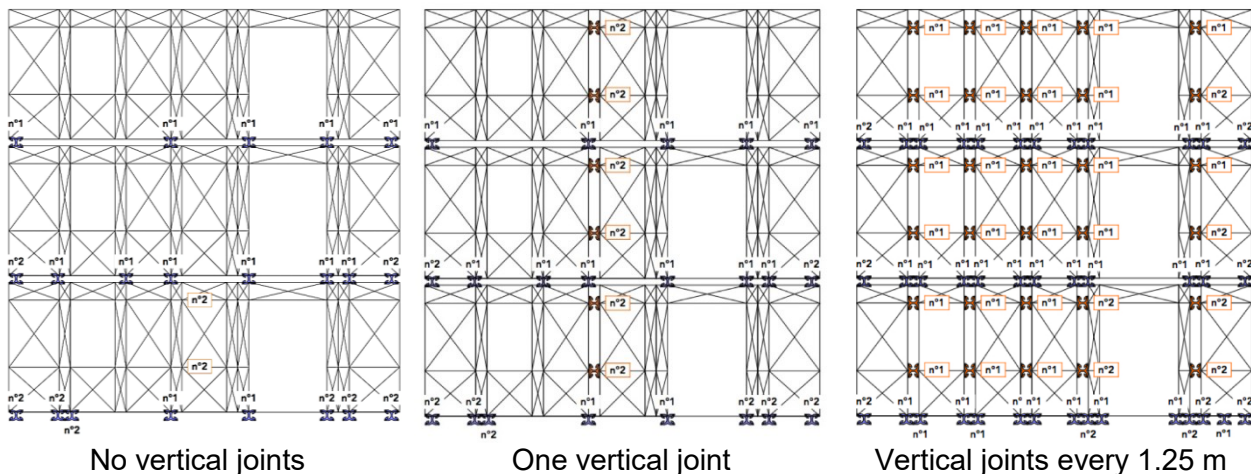


Fig. 4.18 – Bracket disposition and consequent vertical fragmentation of panels.

The design of the X-bracket disposition was provided by imposing equivalence between the horizontal force applied to each storey and the shear resistance of the brackets and the equilibrium to possible overturning of the building. Pushover analyses (NLSA) were conducted to predict the overstrength sub-factor Ω that was implicitly assumed within each of the three analysed configurations. This was done by applying a bi-linearization method to the pushover curves obtained for each of the three connections arrangements.

The NLDA were carried out for each case study with increasing PGA levels, starting from the design value, to define the failure value corresponding to the near-collapse condition. The NLDA were performed considering 3 earthquakes, artificially generated with SIMQKE_GR [4.26], so as to respect the spectrum compatibility requirement according to the design elastic spectrum. The application of various seismic signals had the aim of defining the influence of the frequency content of the earthquakes on the building response. The dynamic equilibrium equations were integrated with a time step of 0.01s, by adopting an equivalent viscous damping of 2%, according to the Rayleigh model. The choice of this damping coefficient was made according to Ceccotti [4.8]. The assumed near-collapse condition for the evaluation of the $PGA_{u,i}$ corresponds to the first failure of a connector, defined as maximum admissible displacement reached by the MEM during the applied earthquake. The values of ultimate displacements were assumed according to the strength domain of the connection. The displacement domain (see Fig. 4.5c,d) was partially simplified by assuming as an ultimate displacement $d_u = (d_{x,u}^2 + d_{y,u}^2)^{1/2}$ a value of 38 mm.

Fig. 4.19 shows pushover curves, used to design the building, overlapping the NLDA results increasing PGA, i.e., the points representing the maximum base shear vs. corresponding top displacements. Two horizontal force distributions were examined in the NLSAs: one proportional to that of the first modal shape of the building (NLSA_1) and the other proportional to storey masses (NLSA_2). As Fig. 4.19 shows, there is a good fit between NLSAs and NLDA. The interval between the curves defines the range of possible responses of the building during an earthquake.

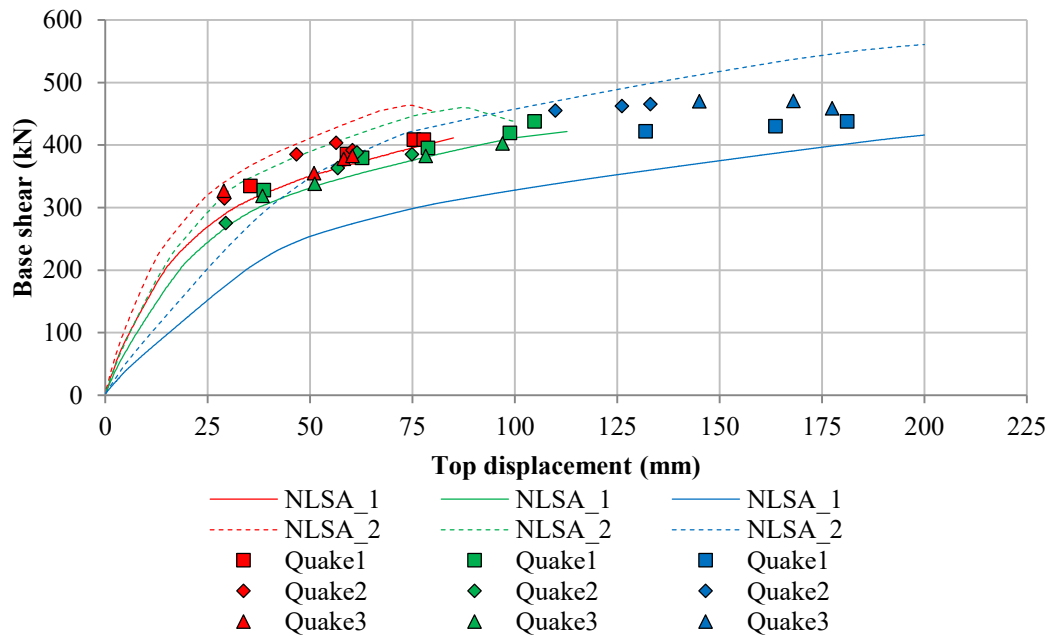


Fig. 4.19 – Comparison of results from NLSA and NLDA for the three building configurations. No joints in red, one joint in green and five joints in blue.

Fig. 4.20 plots the maximum displacement registered by the brackets at the base floor. There is a clear transition between failure due to combined rocking-sliding behaviour of the panels, observed in the case of no vertical joints, to a pure rocking failure obtained for the highly-jointed solution. From this plots emerges also that all connections entered the post-elastic phase (i.e. $d > d_y \approx 4\text{mm}$) but part of them did not exploited the whole dissipative capacity. A perfect design condition would guarantee that each connection element develops the highest plastic deformations before reaching the near-collapse condition due to the diffused failure of all connections in the building. In this way, the maximum base shear force and the maximum ductility might be reached together.

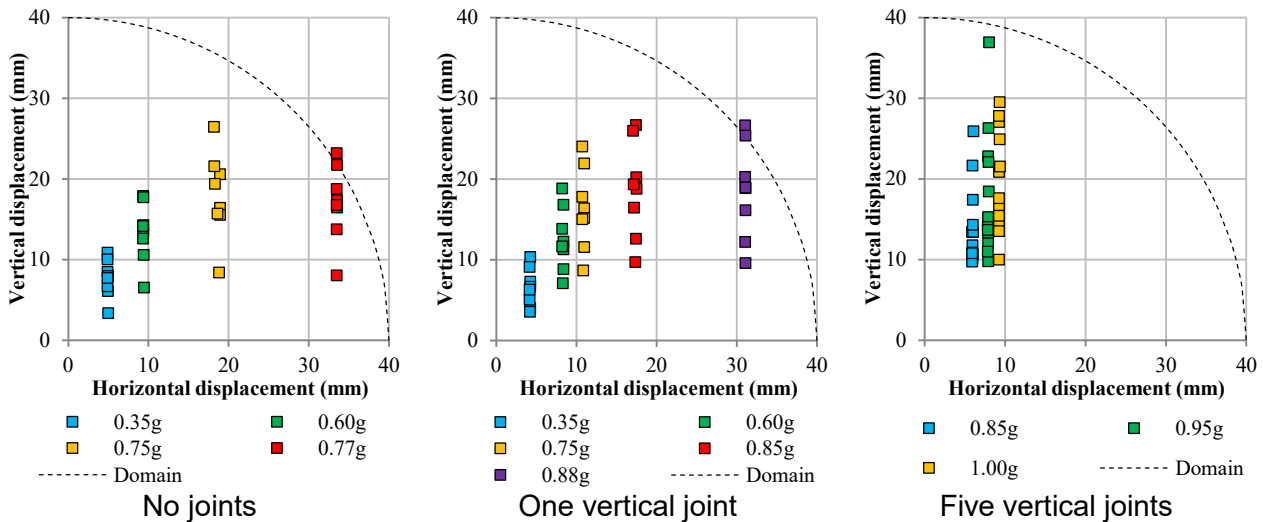


Fig. 4.20 – Maximum displacements of the base brackets for the three buildings.

Lastly, Table 4-5 reports the outcomes obtained from the PGA approach:

- In general, high values of q-factor are achieved within all panel arrangements. Even with a predominant sliding failure of the panels high ductility and dissipative capacity can be achieved;
- As expected, the higher is the number of joints, the higher will be the resulting intrinsic behaviour factor q_0 ;
- The base shear at PGA_y reduces at the increasing of joints thanks to the different post elastic behaviour that the structures assumes. In fact, the rocking behaviour is related to a pronounced hardening behaviour of the X-brackets, i.e., when they are subjected to predominant tensile loads. This translates into a reduction of the Ω -factor for the chosen bi-linearization method;
- Higher ductility means higher displacements. In highly-jointed configurations the DLS conditions could prevail on the USL condition thus reducing the actual behaviour factor for this particular case.
- From a brief comparison with the analyses conducted for the same building and seismic conditions, but employing traditional connections [4.23], it clearly emerges the improvements on ductility and dissipative capacity obtained with the studied connections. Traditional connections produced a q-factor equal to 3.41, 3.48 and 3.63 respectively for the case of no vertical joints, one joint and five vertical joints. In that study the design Ω -factor was equal to 1 so $q_0 = q$.

It must be highlighted that these outcomes are taken from a restricted amount of analyses. A larger set of earthquakes and building configurations must be analysed in order to validate and extend these results.

Table 4-5 – Evaluation of q-factor for the three analysed building configurations.

Case study	Top displ. at PGA_u (mm)	Base shear at PGA_y (kN)	Max base shear (kN)	PGA_u (g)	PGA_d (g)	q_0	Ω	q
No joints	78	263	408.7	0.77	0.33	3.7	1.3	4.7
One joint	105	244	437.9	0.88	0.33	4.5	1.2	5.4
Joints every 1.25m	181	220	438.0	1.00	0.33	5.7	1.1	6.2

4.6 Conclusions

This chapter described the numerical reproduction of the hysteretic behaviour of the innovative bracket by means of a Macro-element approach. The model was developed to simulate thoroughly the cyclic behaviour of the bracket that has been derived experimentally with a more computationally efficient solution. The proposed Macro-element, exploiting few non-linear elements, has proven to be capable of replicating the X-bracket behaviour when subjected to either tension or shear loads or a combination of them.

The model was successfully tested by conducting numerical simulations of full-scale CLT shear walls anchored at the base with the investigated devices. Four different bracket dispositions were simulated and a comparison between a detailed 3D model employing contact formulations and other non-linearities was made. The Macro-element approach reproduced correctly the shear-tension interaction that identify the bracket and allowed providing valid estimations of the energy dissipated by the complete system.

The Macro-element was then put to the test to perform non-linear dynamic analyses, with the aim of evaluating the performance of CLT structures that employ specifically designed connections. Obtained results confirmed that high behaviour factors are possibly achieved also with CLT structures once *innovative* connections are employed.

The innovative joint proved to be modelled more easily and reliably in comparison to traditional joints. This is a natural consequence of the stable and well-known hysteretic behaviour that characterizes the inelastic response of steel elements.

Further studies should concentrate in the extension of the analyses to further case-study configurations and possibly apply this modelling approach to a complete 3D model. Additionally, simplified design rules should be investigated in order to reduce as much as possible the Ω -factor.

References – Chapter 4

- [4.1] Trutalli, D. (2016). “Insight into seismic behaviour of timber shear-wall systems”. Ph.D. Thesis, University of Padova, Italy.
- [4.2] EN 1998-1-1 Eurocode 8 (2004). “Design of structures for earthquake resistance, part 1: general rules, seismic actions and rules for buildings”. CEN. Brussels, Belgium.
- [4.3] Pozza, L., Scotta, R., Trutalli, D., Polastri, and A., Smith, I. (2016). “Experimentally based q-factor estimation of cross-laminated timber walls”. Proceedings of the ICE – Structures and Buildings. DOI:10.1680/jstbu.15.00009.
- [4.4] Izzi, M., Polastri, A., and Fragiaco, M. (2016). “Advanced modelling of CLT wall systems for earthquake resistant timber structures” In International Network on Timber Engineering Research (INTER), meeting 49, Graz, Austria, Paper INTER/49-15-6.
- [4.5] Liu, J., and Lam, F. (2016). “Experimental test of cross laminated timber connections under bi-directional loading”. In Proceedings of the 14th World Conference on Timber Engineering (WCTE), 22nd- 25th August, Vienna University of Technology, Austria.
- [4.6] Pozza, L., Saetta, A., Savoia, M., and Talledo, D. (2016) “Coupled axial-shear numerical model for CLT connections”. Construction and Building Material Journal. In press.

- [4.7] Pozza, L., and Scotta, R. (2015). "Influence of wall assembly on behaviour of cross-laminated timber buildings". *Proceedings of the ICE – Structures and Buildings*, **168(4)**:275-286.
- [4.8] Ceccotti, A. (2008). "New technologies for construction of medium-rise buildings in seismic regions: the XLAM case". *Structural Engineering International*. DOI: 10.2749/101686608784218680.
- [4.9] Pozza, L., Scotta, R., Trutalli, D., and Polastri, A. (2015). "Behaviour factor for innovative massive timber shear walls". *Bulletin of Earthquake Engineering*. DOI: 10.1007/s10518-015-9765-7.
- [4.10] B. Dujic, K. Strus, R. Zarnic, A. Ceccotti. (2010). "Prediction of dynamic response of a 7-storey massive X-lam wooden building tested on a shaking table". In *Proceedings of the 11th World Conference on Timber Engineering WCTE*, Riva del Garda, Italy.
- [4.11] Fragiaco, M., Dujic, B., Sustersic, I. (2011). "Elastic and ductile design of multi-storey crosslam massive wooden buildings under seismic actions" *Engineering Structures*, **33(11)**:3043–3053.
- [4.12] Gavric, I., Rinaldin, G., Amadio, C., Fragiaco, M., and Ceccotti, A. (2012). "Experimental and numerical analyses of the seismic behaviour of cross-laminated wall systems". In *Proceedings of the 15th World Conference on Earthquake Engineering*, September 24-28, Lisbon, Portugal.
- [4.13] Pei, S., van de Lindt, J. W., & Popovski, M. (2012). "Approximate R-factor for cross-laminated timber walls in multistory buildings". *Journal of Architectural Engineering*, **19(4)**:245-255.
- [4.14] Popovski, M., Pei, S., Van de Lindt, J. W., & Karacabeyli, E. (2014). "Force modification factors for CLT structures for NBCC". In *Materials and Joints in Timber Structures* (pp. 543–553). Springer. Dordrecht, Netherlands.
- [4.15] Rinaldin, G., Amadio, C., and Fragiaco, M. (2013). "A component approach for the hysteretic behaviour of connections in cross-laminated wooden structures". *Earthquake Engineering and Structural Dynamics*, **42(13)**:2023-2042.
- [4.16] Ceccotti, A., and Vignoli, A. (1990). "Engineered timber structures: An evaluation of their seismic behaviour". In *Proceedings of the International Timber Engineering Conference*, Tokyo, Japan (pp. 946-953).
- [4.17] Prakash, V., Powell, G. H., and Campbell, S. (1993). "DRAIN-2DX Base Program Description and User Guide, Version 141". Report. UCB/SEMM-93/17, University of California, at Berkeley, Berkeley, CA.
- [4.18] Lowes, L. N., Mitra, N., and Altoontash, A. (2003). "A beam-column joint model for simulating the earthquake response of reinforced concrete frames". *Pacific Earthquake Engineering Research Center, Report 2003/10*.
- [4.19] EN 12512 (2001). "Timber structures—test methods—cyclic testing of joints made with mechanical fasteners". CEN. Brussels, Belgium.
- [4.20] "OpenSees. Open System for Earthquake Engineering Simulation" (2009). Pacific Earthquake Engineering Research Center, University of California, Berkeley. Available at <http://opensees.berkeley.edu>.
- [4.21] Gavric, I., Fragiaco, M., Ceccotti, A. (2015). "Cyclic behavior of CLT wall systems: Experimental tests and analytical prediction models". *Journal of structural engineering*. DOI: 10.1061/(ASCE)ST.1943-541X.0001246.
- [4.22] Thiel, A., "ULS and SLS design of CLT and its implementation in the CLTdesigner", In: Harris, R., Ringhofer, A., and Schickhofer, G. (eds.), *Focus solid timber solutions - European conference on cross laminated timber (CLT)*, 2013, The University of Bath, Bath.
- [4.23] Trutalli, D., and Pozza, L. (2017). "Seismic design of floor–wall joints of multi-storey CLT buildings to comply with regularity in elevation". *Bulletin of Earthquake Engineering*, 1-19.

- [4.24] Ceccotti, A., and Sandhaas, C. (2010). "A proposal for a standard procedure to establish the seismic behaviour factor q of timber buildings." In Proceedings of the 11th World Conference on Timber Engineering WCTE, Riva del Garda, Italy.
- [4.25] EN 1998-1-1 Eurocode 8 (2004). "Design of structures for earthquake resistance, part 1: general rules, seismic actions and rules for buildings". CEN. Brussels, Belgium.
- [4.26] Gelfi, P. (2012). "SIMQKE_GR", Version 2.7. University of Brescia, Italy. Available online: <http://dicata.ing.unibs.it/gelfi>.

Chapter 5 Conclusions and future works

The outcomes of this thesis lead to the following remarks.

In particular, main original outcomes from the analyses of TCC joints made with modern fasteners are:

- The use of modern self-tapping screws as TCC connections placed at an angle of 45° with respect to the grain provides suitable levels of load bearing capacity. This is valid for connection points realized with either a single inclined screw or a pair of crossed screws. Experimental results show that in its evaluation, Eurocode 5 method underestimates load capacity of inclined screws resulting more reliable for crossed screw respect to inclined screws TCC joints.
- The equilibrium equations originally developed in the Johansen's theory model for dowel-type fasteners loaded in shear, rewritten taking into account the contribution of the withdrawal capacity (enhanced by the screw inclination), leads to a better correspondence with experimental evidence. Furthermore, frictional effects could affect the resulting shear force obtained from push-out tests used to evaluate TCC connections performances in case of direct contact between timber and concrete. When single inclined screws are employed, a frictional value of 0.6 could be used;
- According to the alternative approach to Eurocode 5, crossed screws in TCC connection might lead to a special failure condition with the expulsion of concrete cover, hence precautions when estimating the total shear-strength must be taken. Moreover, the efficiency level, calculated as ratio between load bearing capacity and number of screws (in analogy with the effective number of screws), proved to be lower for a crossed screw configuration.
- As concerning the stiffness estimations, the comparison between the experimental results and the analytical formulas shows that Eurocode 5 method provide more conservative values respect to those provided by the proposed model. Moreover results demonstrate that the proposed formulation lead to more reliable estimation of the CP stiffness than simply neglecting the contribution of the shear-compressed screw as proposed by Eurocode 5;
- The hybrid FE approach chosen to simulate the experimented complete timber-to-concrete connection proves to reproduce faithfully the load exchanges occurring between timber and concrete layers through the inclined fastener. This technique requires the calibration of a single parameter, i.e., the friction coefficient between the screw shank and the timber, once the main mechanical properties of the materials are known;
- This modelling technique proves to be useful in the design of a GFRP socket that, coupled with two inclined screws, overcomes the critical installation issues of TCC joints. Additionally, the model turned to be a helpful tool in the definition of the state of stress to which the GFRP component should be subjected in the short and long term in order to predict analytically the deformability factor k_{def} of the complete system;
- The conservative nature of Eurocode 5 provisions, analysed through additional experimental tests of TCC joints with the GFRP socket, are confirmed also in this case. Likely, to the screw-only configuration, a better fitting is achieved with the proposed approach that has been validated also varying the screw strength and the presence of interlayer;

- The contribution of the GFRP component does not lead to significant changes on the load bearing capacity while it slightly affects the stiffness if normal concrete is used. The thermoplastic element fulfilled the protection against concrete splitting or concrete cone failure in all the tested configurations. This is proven valid also in the most critical combination of lightweight concrete and screws with high withdrawal capacity;
- GFRP materials produced by injection moulding could be helpful in the continuous improvements of timber connections once provided that sufficient care is taken into account in determining the actual conditions of environment and loading conditions to whom they will be subjected during their working life.

Further researches are needed before the relationships proposed in this work could be incorporated in a code revision. They should focus on the evaluation of the actual contribute of friction and of a plausible μ value for timber-concrete connections. Finally, a more extensive and detailed experimental campaign should be conducted in order to better validate the proposed model and verify the reliability of the standard methods proposed by Eurocode 5.

Regarding the experimentation provided in the field of novel connections for CLT structures:

- The concept of innovative connections is based on the idea to shift the dissipating element from the usual dowel-type fasteners employed in traditional connections to a properly designed steel element meanwhile preserving the fasteners from behaving inelastically. The high efficiency of innovative devices in terms of hysteretic response can be achieved through the combination of yielding of specific components, restraining of unwanted displacements and friction between sliding parts.
- The experimental characterization of the investigated device confirmed the significant mechanical performance achieved with respect to traditional connections. High ductility class can be achieved with the combination of a high elastic stiffness and a displacement capacity comparable or even higher than traditional connections. The calculated equivalent viscous damping ratio with the innovative device is approximately double than traditional connections either in shear or in tension due to the reduced pinching phenomenon.
- A correct capacity design procedure is of utmost importance to take all benefits that characterize innovative CLT connections. The theoretical definitions of the capacity design rules available in literature can be more reliably extended to the design of innovative connections. Experimental tests are a priority to assess the actual behaviour of the connector procedure and to evaluate the intrinsic overstrength of the connection in order to design its anchoring to the panel and express the whole dissipative capacity of the element without incurring into unwanted brittle failures.
- Capacity design applied to innovative connection allows the design of damage-free joints or, more precisely, fuse-like joints that can be easily substituted immediately after a seismic event in order to restore as much as possible the safety of the structure.
- The axial-shear interaction is a relevant topic in CLT connections and the evaluation of their strength and displacement domain is more easily comprehensible for connections that concentrate energy dissipation in specific components or mechanisms.
- Innovative joints can be more reliably modelled in comparison to traditional joints. This is a natural consequence of a stable and well-known hysteretic behaviour that characterizes the elastic-plastic cyclic response of steel elements. This was proven with the definition of numerical macro-element able to macroscopically reproduce the tension and shear

combined behaviour of the innovative joints. Such macro-model was used to perform non-linear dynamic analyses, with the aim to evaluate the performance of CLT structures that employ specifically designed connections. Obtained results confirm that high behaviour factors are possibly achieved also with CLT structures when innovative connection are employed.

Additional studies should focus on the extension of the numerical analyses to further case-study configurations or the application of this modelling approach to a 3D case study building.

Appendix A Macro-element model details

A.1 Numerical code of the MEM

The following code have been implemented in OpenSees to simulate the X-bracket *Version 2* geometry realized in S450 steel grade. The code does reproduce the bracket-only condition and neglects any effects derived from the hypothetical anchoring system of the bracket. This assumption have been proven valid if capacity design criteria is correctly fulfilled.

```

proc xbracket {index xst yst} {

model BasicBuilder -ndm 3 -ndf 6; # Define the model builder, ndm=#dimension, ndf=#dofs

#####
#           Define Section Properties and Elements           #
#####

# define material properties
set Es          134166;          # steel Young's modulus

# define web section
set A_w         474.0 ;          # cross-sectional area
set I_w         142200.0;        # moment of inertia
set My_w        3434130.0;      # yield moment
set tetay_w     5.367E-03;

# define flange section
set A_f         247.0;          #cross-sectional area (full section properties)
set I_f         29722.33;       # moment of inertia (full section properties)
set My_f        1133359.5;      # yield moment
set tetay_f     5.579e-03;

# set up geometric transformations of element
geomTransf Linear 1 0 0 -1

# Set hysteretic Material
set s1p_f       [expr 1.5*$My_f]
set e1p_f       0.0001
set s2p_f       [expr 2.9*$My_f]
set e2p_f       [expr 28*$tetay_f]
set s3p_f       0
set e3p_f       [expr 100*$tetay_f]
set s1n_f       [expr -$s1p_f]
set e1n_f       [expr -$e1p_f]
set s2n_f       [expr -$s2p_f]
set e2n_f       [expr -$e2p_f]

```

```

set s3n_f      [expr -$s3p_f]
set e3n_f      [expr -$e3p_f]
set pinchX_f   0.28
set pinchY_f   0.18
set damage1_f  0
set damage2_f  0
uniaxialMaterial Hysteretic 100 $s1p_f $e1p_f $s2p_f $e2p_f $s3p_f $e3p_f $s1n_f $e1n_f
$s2n_f $e2n_f $s3n_f $e3n_f $pinchX_f $pinchY_f $damage1_f $damage2_f

set s1p_w      [expr 0.9*$My_w]
set e1p_w      0.0001
set s2p_w      [expr 1.3*$My_w]
set e2p_w      [expr 33*$tetay_w]
set s3p_w      0
set e3p_w      [expr 100*$teta_w]
set s1n_w      [expr -$s1p_w]
set e1n_w      [expr -$e1p_w]
set s2n_w      [expr -$s2p_w]
set e2n_w      [expr -$e2p_w]
set s3n_w      [expr -$s3p_w]
set e3n_w      [expr -$e3p_w]
set pinchX_w   0.0001
set pinchY_w   0.001
set damage1_w  0.000039
set damage2_w  0.295
uniaxialMaterial Hysteretic 200 $s1p_w $e1p_w $s2p_w $e2p_w $s3p_w $e3p_w $s1n_w $e1n_w
$s2n_w $e2n_w $s3n_w $e3n_w $pinchX_w $pinchY_w $damage1_w $damage2_w

#####
#                               Limitation to compression                               #
#####

set epsyP      1
set epsyN      -0.3
uniaxialMaterial ElasticPP 300 $Es $epsyP $epsyN

#Set BeamwithHinges Element
section Uniaxial 1 100 Mz #section flange
section Uniaxial 2 200 Mz #section web
section Uniaxial 3 300 P
section Aggregator 23 200 Mz 300 P
set Lpi_f      1
set Lpi_w      1

#####
#                               Creation of nodes                               #
#####

# nodal coordinates:
set l_f        118.5;
set l_w        90.0;

# node      tag      xCrd      yCrd      ndf
node [expr $index*i+1] [expr -1.*$l_f+$xst] $yst 0;
node [expr $index*i+2] $xst $yst 0;
node [expr $index*i+3] [expr $l_f+$xst] $yst 0;
node [expr $index*i+5] $xst [expr -2.*$l_w+$yst] 0;
node [expr $index*i+6] [expr -1.*$l_f+$xst] [expr -2.*$l_w+$yst] 0;
node [expr $index*i+7] [expr $l_f+$xst] [expr -2.*$l_w+$yst] 0;

fix [expr $index*i+6] 1 1 1 0 0 0;
fix [expr $index*i+7] 1 1 1 0 0 0;

#####
#                               Creation of elements                               #
#####
# element beamWithHinges $eleTag $iNode $jNode $secTagI $Lpi $secTagJ $Lpj $E $A $Iz $Iy
$G $J $stransfTag
element beamWithHinges [expr $index*i+10] [expr $index*i+1] [expr $index*i+2]
1 0 1 $Lpi_f

```

Appendix

```

$Es      $Af      $If      10e7
10e7     10e7     1
element beamWithHinges [expr $index*i+11] [expr $index*i+3]
1        $Lpi_f   1        0
$Es      $Af      $If      10e7
10e7     10e7     1
element beamWithHinges [expr $index*i+14] [expr $index*i+5] [expr $index*i+6]
1        $Lpi_f   1        0
$Es      $Af      $If      10e7
10e7     10e7     1
element beamWithHinges [expr $index*i+15] [expr $index*i+5] [expr $index*i+7]
1        $Lpi_f   1        0
$Es      $Af      $If      10e7
10e7     10e7     1
element beamWithHinges [expr $index*i+12] [expr $index*i+2] [expr $index*i+5]
2        $Lpi_w   23       $Lpi_w
$Es      $Aw      $Iw      10e7
10e7     10e7     1

equalDOF [expr $index*10000+1] [expr $index*10000+3] 1 2
}

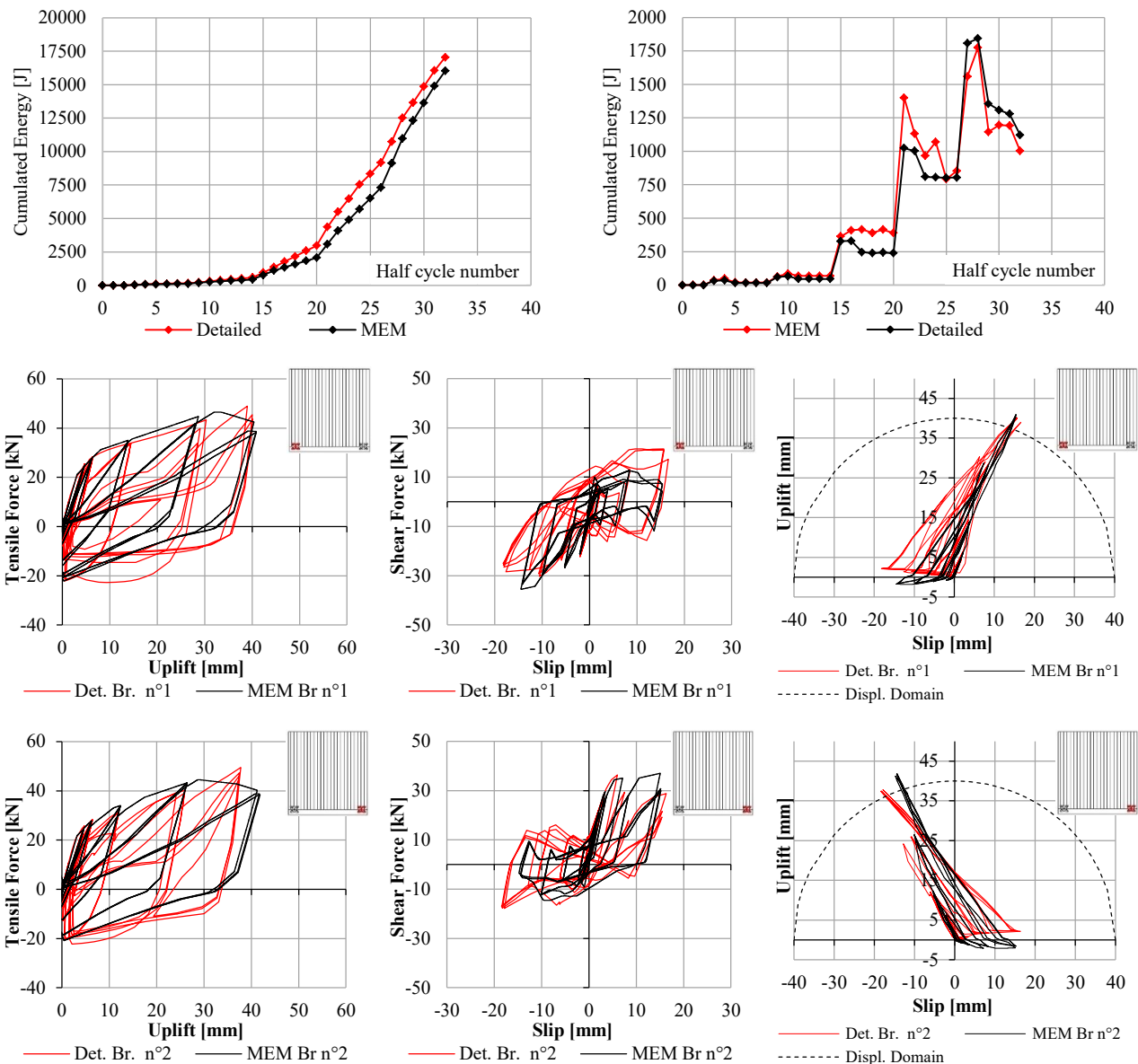
```


A.2 Detailed results of case-study CLT shear walls

This section reports the detailed outcomes from the analysed case-study CLT shear walls anchored with the investigated bracket. For each of the four investigated walls are plotted in sequence: the cumulated dissipated energy by the system, the dissipated energy within each half-cycle and the tensile force vs. uplift, shear force vs. slip and uplift vs. slip curves for each bracket. It is worth noting that the plotted circular displacement domain underestimates the displacement capacity for predominant tension conditions. Therefore, the cycles exceeding the limit of 38 mm in mostly uplift are yet taken as valid in the estimation of the mechanical parameters of the shear wall.

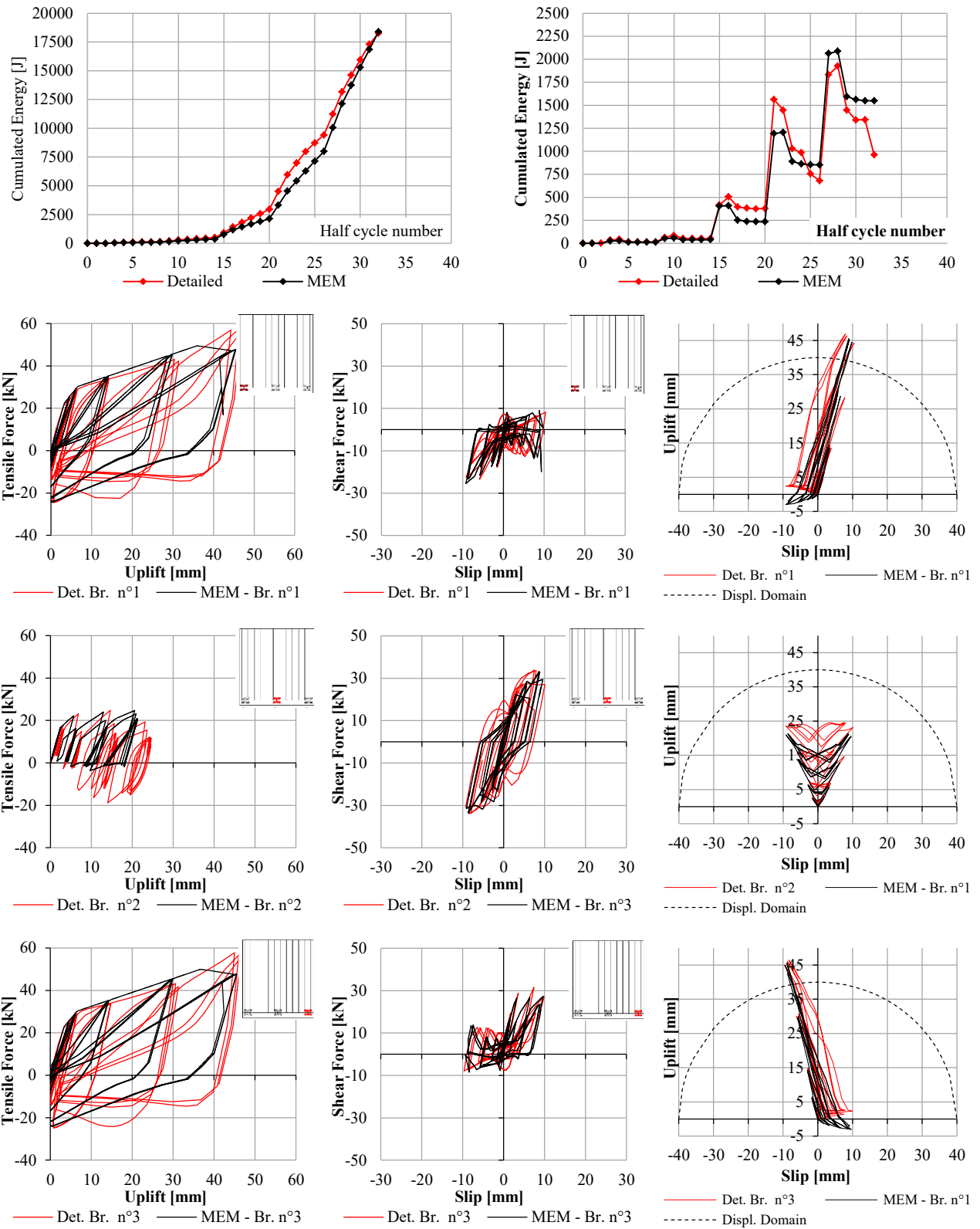
A.2.1 Wall A

Detailed results obtained with either the 3D model or Macro-element model.



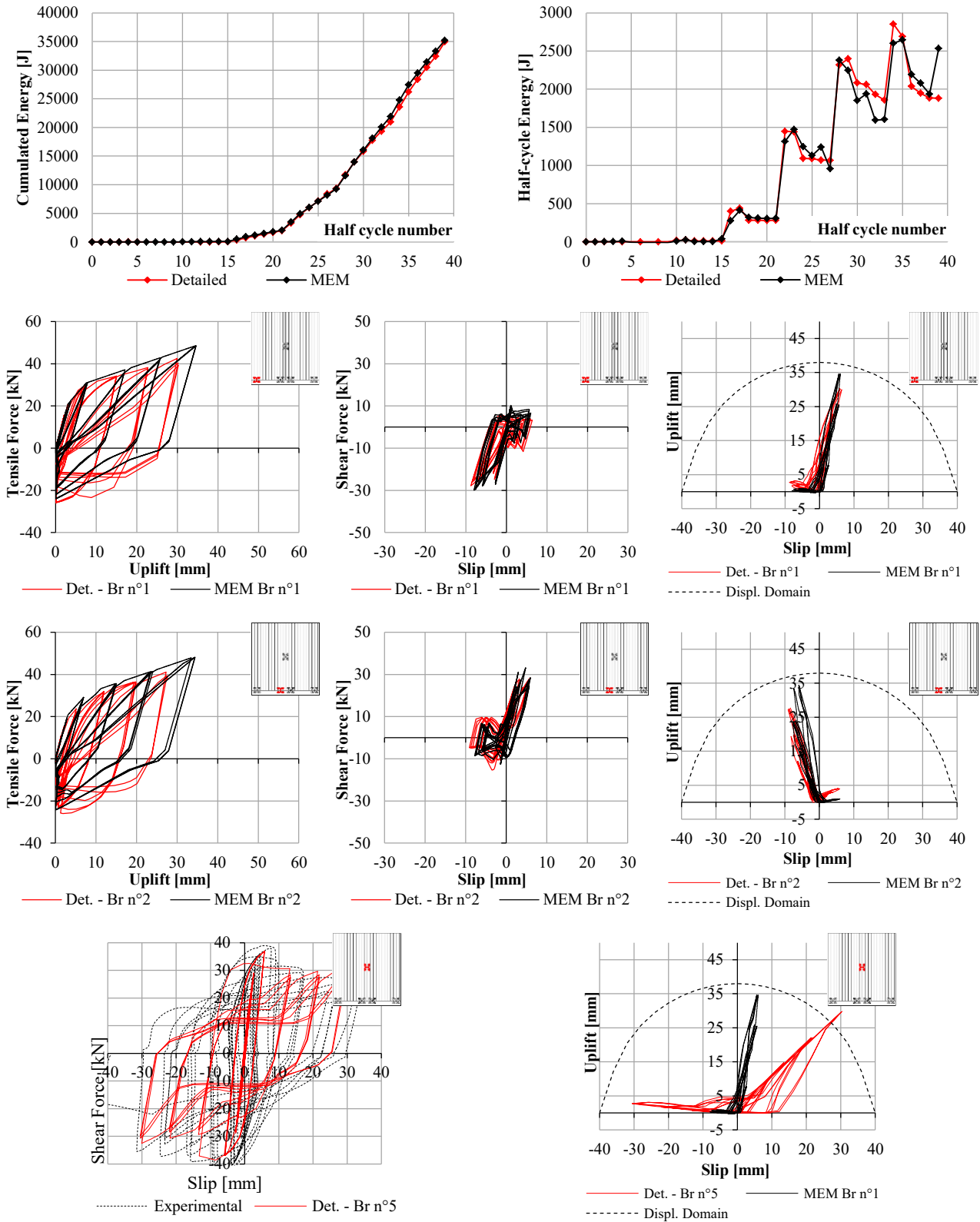
A.2.2 Wall B

Detailed results obtained with either the 3D model or Macro-element model.



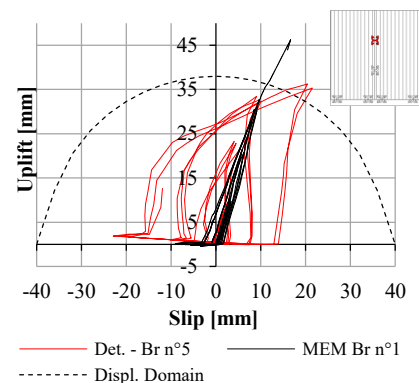
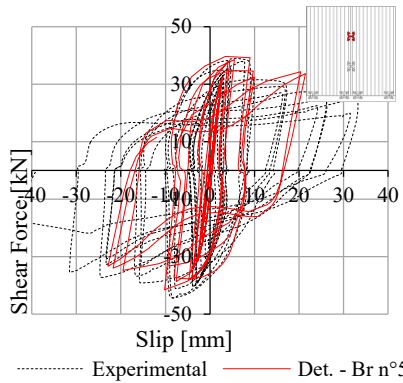
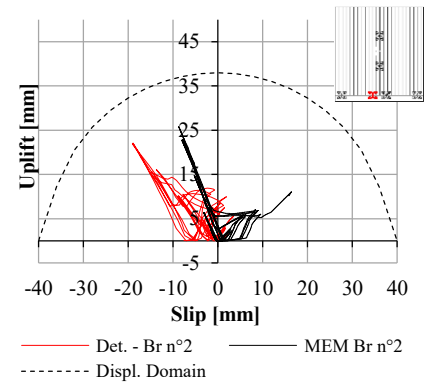
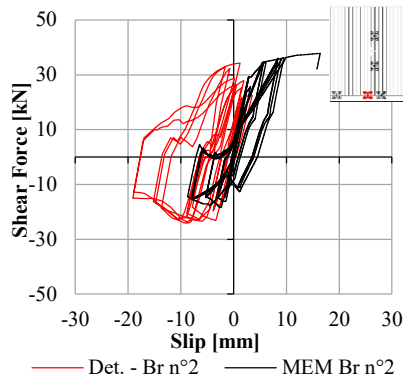
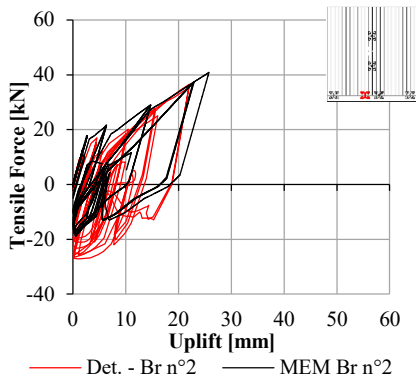
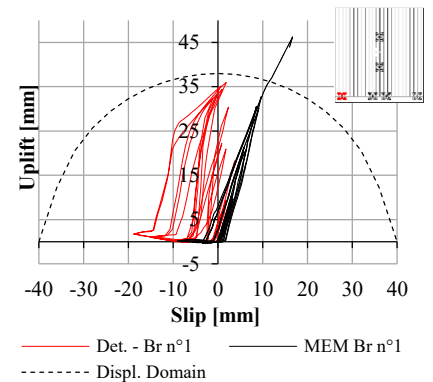
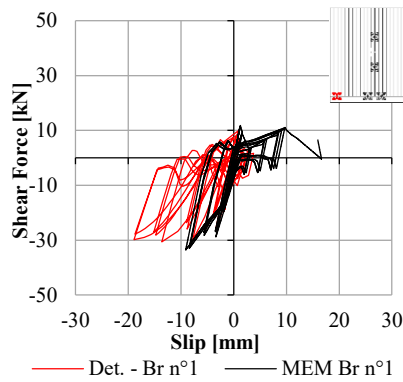
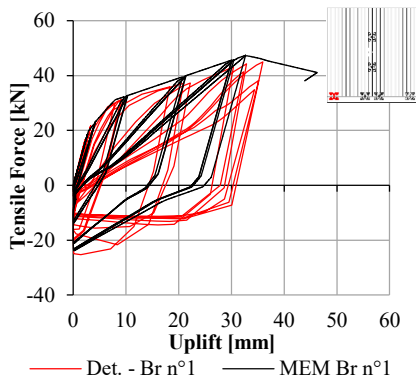
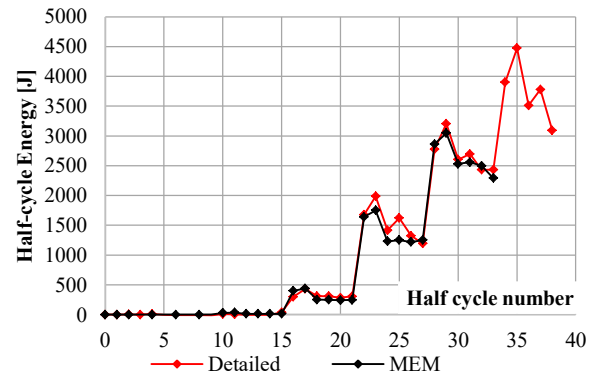
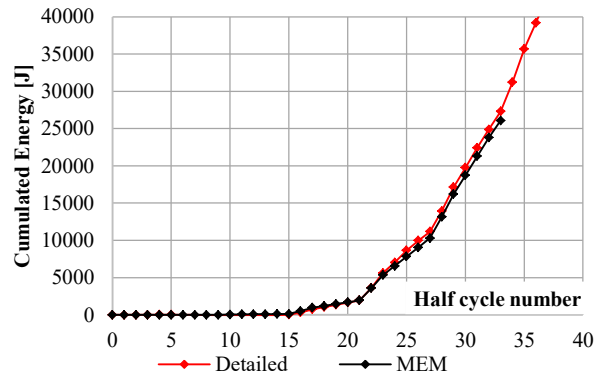
A.2.3 Wall C

Detailed results obtained with either the 3D model or Macro-element model.



A.2.4 Wall D

Detailed results obtained with either the 3D model or Macro-element model.



List of Figures

Fig. 1.1 – Inelastic behaviour of several type of joints [1.3]. The stiffest joint is glued joint (a) followed by punched metal plate fastener (f), split ring (b), double-sided toothed-plate (c), 14-mm dowel (d), 14-mm bolt (e), 4.4 mm nail (g).....	2
Fig. 1.2 – Loading procedure according to EN 26891 [1.6]	3
Fig. 1.3 – Typical hysteresis behaviour of a connection with metal fasteners [1.17]	4
Fig. 1.4 – Loading procedure according to EN 12512 [1.19]	5
Fig. 1.5 – Organization of the present work.....	6
Fig. 1.1 – TCC bridge deck in Finland on the right [1.5] and TCC prefabricated floor on the left [1.6].	14
Fig. 1.2 – Renovation of existing timber floors with mechanical connectors before realization of the concrete slab.	15
Fig. 1.3 – Example of TCC connections: (a) Notch with steel screw [1.2]; (b) Glued-in Rebar at 45° [1.30]; (c) Glued-in Rebar at 90°; (d) folded steel plate [1.29]; (e) HSB® connection [1.31]; (e) Tecnaria connector [1.27];	17
Fig. 1.4 – Load vs. slip behaviour of a connection: (a) according to standard procedure [1.17]; (b) comparison of different categories of connectors from Yeoh et al. [1.8].	17
Fig. 1.5 – Timber screws: (a) traditional 16x120 mm DIN 571 screw; (b) 10x160 mm self-tapping screw.....	19
Fig. 1.6 – Loading models for screws according to Eurocode 5: (a) inclined screw; (b) couple of crossed screws.	20
Fig. 1.7 – Mechanical models of the different failure modes for an inclined screw subjected to shear-tension stress extrapolated from [1.45] and adapted to the proposed modifications.	22
Fig. 1.8 – Failure models in the concrete layer for different loading conditions of an inclined screw subjected to shear-tension or shear-compression stress: (a) theoretical model; (b) experimental evidence.	25
Fig. 1.9 – Analytical load bearing capacity of an inclined self-tapping screw varying the angle α with respect to the grain: (a) comparison between Eurocode 5 and the proposed approach; (b) axial and lateral contribution for failure mode 3, expressed by Eq.(1.28).	25
Fig. 1.10 – Specimen geometry: (a) AN and AL series; (b) XN and XL series.	27
Fig. 1.11 – (a) Loading procedure according to EN 26891 calibrated on $F_{v,est}$ values; (b) clean specimen before tests. ...	29
Fig. 1.12 – Experimental load vs. displacement curves for 8 mm screws. Symbols stay for: inclined screws (A series) or crossed screws (X series), normal (N) or lightweight (L) concrete.....	29
Fig. 1.13 – Experimental load vs. displacement curves for 10 mm screws. Symbols stay for: inclined screws (A series) or crossed screws (X series), normal (N) or lightweight (L) concrete.....	30
Fig. 1.14 – Experimental load vs. displacement curves for 12 mm screws. Symbols stay for: inclined screws (A series) or crossed screws (X series), normal (N) or lightweight (L) concrete.....	30
Fig. 1.15 – Qualitative comparison of the load–displacement for a CP realized with one or two screws for the same fastener diameter.	32
Fig. 1.16 – Experimental mean values of the shear capacity $F_{v,exp}$ (a) and service stiffness K_{ser} (b) varying screw diameter, screw configuration and concrete type (values are referred to a single CP).....	33
Fig. 1.17 – Failure mode of fasteners: (a) wood embedment for inclined screw configuration; (b) wood embedment with crossed screw configuration; (c) detail of concrete expulsion.....	33
Fig. 1.18 – Experimental values of average shear strength $F_{v,exp}$ (dots) and 5% characteristic extrapolations (continuous lines) compared with theoretical predictions: (a) inclined screw series; (b) crossed screws series. Values are referred to a single CP. Filled area highlights the theoretical contribution of each screws in the global strength	35
Fig. 1.19 – Experimental values of slip modulus K_{ser} compared with theoretical predictions: (a) inclined screws series; (b) crossed screws series. Values are referred to a single CP.	36
Fig. 2.1 – Issues that might occur throughout the installation of many screws with an angle respect to the grain.	46

Fig. 2.2 – (a) capacity design applied to a TCC connection; (b) intended reinforcing effect of the GFRP element.....	48
Fig. 2.3 – FE model: example of the 3D mesh (left) and load transmission model between screw and timber (right).	50
Fig. 2.4 – Stress vs. strain relations employed for the steel (left) and concrete (right).....	53
Fig. 2.5 – Domamid® A1-005-V50-B technical datasheet.	54
Fig. 2.6 – Stress vs. strain relations on DAM (dashed line) and conditioned state (continuous line) of GFRP.	54
Fig. 2.7 – Excerpt of the material model calibration on the tested conditioned brackets made with GFRP.	55
Fig. 2.8 – Inclined screw results: (a) total accumulated strains at 12.0 kN of shear load; (b) load vs. slip curves.	56
Fig. 2.9 – Crossed screws results: (a) double hinges development (displacement x5 times); (b) load vs. slip curves.....	56
Fig. 2.10 – Evolution of the connector’s shape during the design process.	57
Fig. 2.11 – Prototypes realized by stereolithography.	58
Fig. 2.12 – Main features of the GFRP connector.....	58
Fig. 2.13 – FE simulation results: (a) load vs. slip curve per single screw; (b) total accumulated strain; (c,d) equivalent Von Mises stress and contact status measured at 12.0 kN of shear load per screw.....	59
Fig. 2.14 – Geometry of specimens without interlayer.	61
Fig. 2.15 – Geometry of specimens with a 25-mm timber planks interlayer.....	61
Fig. 2.16 – Detail of Connector and screw installation onto the timber beam.	61
Fig. 2.17 – (a) loading protocol calculated according to [2.51]; (b) specimen with interlayer on the testing machine and position of LVDTs.	63
Fig. 2.18 – Experimental load vs. displacement curves for specimens without interlayer and normal concrete (NA series): PT screws and FT screws.....	65
Fig. 2.19 – Experimental load vs. displacement curves for specimens without interlayer and lightweight concrete (LA series): PT screws and FT screws.....	65
Fig. 2.20 – Experimental load vs. displacement curves for specimens with interlayer and normal concrete (LA series): PT screws and FT screws.	65
Fig. 2.21 – Experimental load vs. displacement curves for specimens without interlayer and lightweight concrete (LA series): PT screws and FT screws.....	66
Fig. 2.22 – Investigation of connection after failure: (a) screw withdrawal with partial rotation of the plastic element; no critical failure observed in the thermoplastic connector.	66
Fig. 2.23 – Localized failure of a specimen with interlayer (ID:LB_FT_5) observed at large displacements.....	66
Fig. 2.24 – Mean values of load-carrying capacity and serviceability stiffness calculated per single CP.....	67
Fig. 2.25 – Characteristic shear strength $F_{v,Rk,exp}$ calculated according to EN 14358 [2.55] and analytical values.	70
Fig. 2.26 – Mean service stiffness $K_{ser,exp}$ and analytical values $K_{ser,th}$	70
Fig. 2.27 – Axial and lateral contribution calculated for each configuration ($\mu = 0.25$).	70
Fig. 2.28 – Experimental load vs. displacement curves with normal concrete (left) and lightweight concrete (right).	71
Fig. 2.29 – (a) Mean yielding point for NB_PT series; (b) Von Mises stress distribution in the GFRP element in proximity of the housing for the countersunk head screw.	72
Fig. 3.1 – Traditional earthquake-resistant connections employed in CLT shear walls.....	82
Fig. 3.2 – Typical hysteretic response of traditional CLT joint [3.24]: force vs. displacement curve, strength degradation and viscous damping of a typical hold-down in tension (a,b) and an angle bracket in shear (c,d).....	83
Fig. 3.3 – Example of brittle ore “less ductile” failures occurred on experimental tests ([3.22];[3.25]) and lateral yielding of an hold-down due to coupling effects [3.9].	84
Fig. 3.4 – Typical hysteretic response of a CLT joint: traditional connection in which energy dissipation is demanded to the nails (image on the left, from [3.20]); (b) innovative connection in which energy dissipation is demanded to steel plasticization (image on the right, from [3.29]).	85
Fig. 3.5 – Examples of innovative connections for CLT structures: (a) UFP [3.29]; (b) Fuse-type dissipater [3.38]; (c) Fuse-type dissipater [3.39]; (d) Slip-friction connector [3.40]; XL-Stub [3.43]; (f) Steel plate dissipater [3.44].	86
Fig. 3.6 – Duality of failure mechanisms between traditional and innovative connections.	86
Fig. 3.7 – Yielding and peak strength of a ductile element and their statistical distribution.....	88
Fig. 3.8 – (a) Conceptual disposition of X-brackets in shear walls realized with CLT panels; (b) panel-to-foundation joint; (c) panel-to-panel joint; (d) concealed panel-to-panel joint.	93
Fig. 3.9 – Shape and geometry of the connection: (a) model parameters; (b) manufacturing process from a steel plate.	95
Fig. 3.10 – Excerpt from the parametric analyses results. Final parameters of version 1 and 2 are highlighted in green.	95
Fig. 3.11 – Numerical model: equivalent Von Mises stress contour on deformed geometry of X-brackets: (a) tension loading; (b) shear loading. Plastic regions are evidenced in grey colour.....	96
Fig. 3.12 – Setup and imposed deformations: (a,b,c) rigid frame for tension tests; (d,e,f) unbraced steel truss for shear tests.....	97
Fig. 3.13 – Experimental cycles in comparison to FEM results per bracket: (a) Tension tests; (b) shear tests.....	97
Fig. 3.14 – Plate buckling under shear loading: (a) Experimental evidence; (b) numerical prediction.	98
Fig. 3.15 – Deformed specimens: (a) Axial test; (b) shear test.	98
Fig. 3.16 – Test setup of version 2 and positioning of LVDTs for tensile (a) and shear (b) tests.	101

List of Figures

Fig. 3.17 – Axial tests of the X-brackets: photos of non-deformed and deformed specimens (a) and force-displacement curves for a single bracket (b) (ductility evaluated as d_u/d_{y_est} according to the loading procedure).	101
Fig. 3.18 – Shear tests of the X-brackets: photos of non-deformed and deformed specimens (a) and force-displacement curves for a single bracket (b) (ductility evaluated as d_u/d_{y_est} according to the loading procedure).	102
Fig. 3.19 – Envelope of cycles and bi-linearization of tension (a) and shear (b) tests of the X-brackets.	102
Fig. 3.20 – Progress of viscous damping ratio and strength during the cyclic tests for tensile tests.	104
Fig. 3.21 – Progress of viscous damping ratio and strength during the cyclic tests for shear tests.	105
Fig. 3.22 – Test of the complete connection: (a) photo of the non-deformed specimen; (b) specimen at maximum vertical displacement of 48m; (c,d) failure due to accumulated plastic work in the connector’s web.	107
Fig. 3.23 – Comparison among tests of brackets and of the complete connection in tension: (a) hysteresis cycles; (b) Equivalent viscous damping; (c) Maximum force per loading cycle ($d_{y,est} = 4.00$ mm).....	108
Fig. 3.24 – Comparison among first and second test of the complete connection in tension: (a) hysteresis cycles; (b) Maximum force and relative difference per loading cycle ($d_{y,est} = 4.00$ mm).....	110
Fig. 3.25 – 3D model of the X-bracket version 3 (a) and example of application as a hold-down (b).	111
Fig. 3.26 – Dimensions of version 3 and position of 7-mm self-drilling dowels (M1 to M8) and 16-mm dowels.	112
Fig. 3.27 – Out-of-plane deformations: (a) at vertical uplift of 20 mm; (b) residual deformation after the complete cyclic loading procedure.	113
Fig. 3.28 – Numerical simulation results: (a) hysteretic response of bracket for cyclic tensile loading; (b) total absolute shear reaction of dowels vs. bracket uplift.	113
Fig. 3.29 – Out-of-plane buckling at a 24mm of horizontal slip: (a) out-of-plane displacements; (b) Von Mises stress distribution (post-yielding zones in red).	113
Fig. 3.30 – Numerical simulation results: (a) hysteretic response of bracket for cyclic shear loading; (b) total absolute shear reaction of dowels vs. bracket slip.	114
Fig. 3.31 – Test setup for X-bracket V3 _{HD}	115
Fig. 3.32 – Test setup for bracket V3 _{SH}	115
Fig. 3.33 – Position of LVDTs to assess displacements of each bracket for tension tests (a) and shear test (b).	116
Fig. 3.34 – Hysteresis loops and backbone curves of tension tests (a,c) and shear tests (b,d).	117
Fig. 3.35 – V3 _{HD} test: (a) test setup; (b) specimen at max uplift of 24mm; (c) failure of the X-bracket; (d) holes in timber panel after test.	118
Fig. 3.36 – V3 _{SH} test setup.	118
Fig. 3.37 – V3 _{SH} test: (a) failure of the X-bracket; (b) specimen at 24mm of slip; (c) damaged inner layers.	119
Fig. 3.38 – Comparison of load vs. displacement cycles, envelope curves and bi-linearization of version 2 and 3 on tension (a,c) and shear (b,d).	121
Fig. 3.39 – Viscous damping ratio and dissipated energy for the X-brackets loaded in tension (a,b) and in shear (c,d).	122
Fig. 4.1 – Work-flow adopted in this work to evaluate the seismic response of a CLT building employing the studied devices by means of a MEM approach.	132
Fig. 4.2 – Pushover curves varying the angle of the applied force.	133
Fig. 4.3 – Strength at yielding and failure obtained from the analyses for the bracket working mainly in tension F_{HD} (a) and mainly in shear F_{SH} (b).	133
Fig. 4.4 – Strength domain definition with 10 axial/shear deformation ratios: (a) method 1; (b) method 2.	133
Fig. 4.5 – Shear-tension domains of the varying t and λ : yielding (a,b) and ultimate (c,d) conditions.	135
Fig. 4.6 – Abacus representation for the strength estimation with the three formulations.	137
Fig. 4.7 – Residual plots obtained with the first (a,b), second (c,d) and third (e,f) analytical formulations.	138
Fig. 4.8 – Macro element Model of the X-bracket (a) and Moment/curvature law applied to the hinges (b).	139
Fig. 4.9 – Flowchart of the intended Macro element Model.	140
Fig. 4.10 – Comparison of cyclic loading tests: Pure tension test hysteretic loops and respective cumulated energy for pure tension (a,b) and pure shear (c,d) loading.	141
Fig. 4.11 – Geometry and connection arrangement of the investigated walls: tested walls with traditional connections (first row); simulated walls with innovative connections (second row).	142
Fig. 4.12 – Detailed numerical model: Adopted constraints and example of the FE model of Wall D.2.	143
Fig. 4.13 – Simplified mesh of wall D.2 implemented into OpenSees.	144
Fig. 4.14 – Force vs. top displacement loops: comparison between detailed and Macro-Element model.	145
Fig. 4.15 – Total dissipated energy evaluated at the peak points: comparison between detailed model and MEM.	145
Fig. 4.16 – Equivalent viscous damping ratio of the four examined walls.	146
Fig. 4.17 – Case study building façade.	148
Fig. 4.18 – Bracket disposition and consequent vertical fragmentation of panels.	148
Fig. 4.19 – Comparison of results from NLSA and NLDA for the three building configurations. No joints in red, one joint in green and five joints in blue.	149
Fig. 4.20 – Maximum displacements of the base brackets for the three buildings.	150

List of Tables

Table 1-1 – Nomenclature and geometries of the specimens.	28
Table 1-2 – Experimental strength $F_{v,exp}$ and stiffness $K_{ser,exp}$ and yielding points ($F_{v,y}$; δ_y) for each specimen, average values and variation coefficient (COV). Values are referred to 6 CPs for A-series and to 4 CPs for X-series.	32
Table 1-3 – Summary of experimental and theoretical results of F_v (with $\mu=0.25$) and K_{ser} , relative differences $\Delta F_{v,Rk}$ and ΔK_{ser} (calculated for each CP).	34
Table 2-1 – Examples of available products within the Italian market.	45
Table 2-2 – Orthotropic material properties chosen for GL24h.	52
Table 2-3 – Calibration of frictional parameter μ_s of the stiffness K_{ser} (in kN/mm) between experimental evidence and numerical simulations.	55
Table 2-4 – Summary of the tested specimen’s characteristics.	60
Table 2-5 – Screw characteristics according to ETAs ([2.27];[2.49]).	62
Table 2-6 – Experimental shear strength $F_{v,exp}$, stiffness $K_{ser,exp}$ and yielding point ($F_{v,y}$; δ_y) for each specimen, average values and variation coefficient (COV).	68
Table 2-7 – Comparison between experimental and analytical results per CP.	69
Table 2-8 – Stress-strain relationship and equivalent k_{def} values.	73
Table 3-1 – Analysed aspect within each version.	92
Table 3-2 – Main dimensions of X-brackets relative to Fig. 3.10a.	95
Table 3-3 – Tension tests: main mechanical parameters according to EN 12512 method a [3.18].	100
Table 3-4 – Shear tests: main mechanical parameters according to EN 12512 method a [3.18] and EEEP method [3.60].	100
Table 3-5 – Tension tests: main mechanical parameters according to EN 12512 method a [3.18].	103
Table 3-6 – Shear tests: main mechanical parameters according to EEEP method [3.60].	103
Table 3-7 – Comparison of overstrength factors for the innovative bracket, steel-to-timber nails and standard hold-downs and angle brackets.	106
Table 3-8 – Test results: main mechanical parameters according to EN 12512 method a [3.18].	109
Table 3-9 – Mechanical parameters of dowels.	112
Table 3-10 – Mechanical parameters and hysteretic loops for V3 _{HD} and V3 _{SH} bracket.	117
Table 3-11 – Comparison of the three tested versions (mean values).	120
Table 4-1 – Results from parametric analyses in terms of yielding point (F_y, d_y), ultimate failure (F_u, d_u) and ductility μ	136
Table 4-2 – Mean value μF and difference δF between tension and shear strength.	137
Table 4-3 – Main parameters used in the detailed 3D model.	143
Table 4-4 – Main parameters according to EN 12512 method a [4.19].	146
Table 4-5 – Evaluation of q-factor for the three analysed building configurations.	150
Table 1-1 – Nomenclature and geometries of the specimens.	28
Table 1-2 – Experimental strength $F_{v,exp}$ and stiffness $K_{ser,exp}$ and yielding points ($F_{v,y}$; δ_y) for each specimen, average values and variation coefficient (COV). Values are referred to 6 CPs for A-series and to 4 CPs for X-series.	32

Table 1-3 – Summary of experimental and theoretical results of F_v (with $\mu=0.25$) and K_{ser} , relative differences $\Delta F_{v,Rk}$ and ΔK_{ser} (calculated for each CP).....	34
Table 2-1 – Examples of available products within the Italian market.....	45
Table 2-2 – Orthotropic material properties chosen for GL24h.....	52
Table 2-3 – Calibration of frictional parameter μ_s of the stiffness K_{ser} (in kN/mm) between experimental evidence and numerical simulations.....	55
Table 2-4 – Summary of the tested specimen’s characteristics.....	60
Table 2-5 – Screw characteristics according to ETAs ([2.27];[2.49]).....	62
Table 2-6 – Experimental shear strength $F_{v,exp}$, stiffness $K_{ser,exp}$ and yielding point ($F_{v,y}$; δ_y) for each specimen, average values and variation coefficient (COV).....	68
Table 2-7 – Comparison between experimental and analytical results per CP.....	69
Table 2-8 – Stress-strain relationship and equivalent k_{def} values.....	73
Table 3-1 – Analysed aspect within each version.....	92
Table 3-2 – Main dimensions of X-brackets relative to Fig. 3.10a.....	95
Table 3-3 – Tension tests: main mechanical parameters according to EN 12512 method a [3.18].....	100
Table 3-4 – Shear tests: main mechanical parameters according to EN 12512 method a [3.18] and EEEP method [3.59]).....	100
Table 3-5 – Tension tests: main mechanical parameters according to EN 12512 method a [3.18].....	103
Table 3-6 – Shear tests: main mechanical parameters according to EEEP method [3.59].....	103
Table 3-7 – Comparison of overstrength factors for the innovative bracket, steel-to-timber nails and standard hold-downs and angle brackets.....	106
Table 3-8 – Test results: main mechanical parameters according to EN 12512 method a [3.18].....	109
Table 3-9 – Mechanical parameters of dowels.....	112
Table 3-10 – Mechanical parameters and hysteretic loops for V3 _{HD} and V3 _{SH} bracket.....	117
Table 3-11 – Comparison of the three tested versions (mean values).....	120
Table 4-1 – Results from parametric analyses in terms of yielding point (F_y, δ_y), ultimate failure (F_u, δ_u) and ductility μ	136
Table 4-2 – Mean value μF and difference δF between tension and shear strength.....	137
Table 4-3 – Main parameters used in the detailed 3D model.....	143
Table 4-4 – Main parameters according to EN 12512 method a [4.19].....	146
Table 4-5 – Evaluation of q-factor for the three analysed building configurations.....	150

List of Publications

International journals

Marchi, L., Scotta, R., Pozza, L. (2017). "Experimental and theoretical evaluation of TCC connections with inclined self-tapping screws". *Materials and Structures*. <http://dx.doi.org/10.1617/s11527-017-1047-1>.

Scotta, R., Marchi, L., Trutalli, D., and Pozza, L. (2017). "Engineered aluminium beams for anchoring timber buildings to foundation". *Structural Engineering International*, 27(2):158-164. IABSE <http://dx.doi.org/10.2749/101686617X14881932435736>

Trutalli, D., Marchi, L., Scotta, R., Pozza, L., and De Stefani, L. (2017). "Seismic response of a platform-frame system with steel columns". *Buildings* 7(2):33. MDPI. <http://dx.doi.org/10.3390/buildings7020033>

Scotta, R., Marchi, L., Trutalli, D., and Pozza, L. (2016). "A dissipative connector for CLT buildings: concept, design and testing". *Materials*, 9(3), 139. MDPI. <http://dx.doi.org/10.3390/ma9030139>

Scotta, R., Trutalli, D., Fiorin, L., Pozza, L., Marchi, L., and De Stefani, L. (2015). "Light steel-timber frame with composite and plaster bracing panels". *Materials*, 8(11):7354-7370. MDPI. DOI 10.3390/ma8115386. Available online: <http://dx.doi.org/10.3390/ma8115386>.

Conference Proceedings

Scotta, R., Trutalli, D., Marchi, L., and Pozza, L. (2017). "Capacity design of CLT structures with traditional or innovative seismic-resistant brackets". In *Proceedings of International Network on Timber Engineering Research (INTER), meeting 50, 28-31 August 2017, Kyoto, Japan*. Paper INTER/50-15-5

Marchi, L., Trutalli, D., Scotta, R., and Pozza, L. (2017). "Numerical simulation of the coupled tension-shear response of an innovative dissipative connection for CLT buildings". In *Proceedings of the 6th ECCOMAS Thematic Conference on Computational Methods in Structural Dynamics and Earthquake Engineering (COMPDYN), 15-17 June 2017, Rhodes Island, Greece*

Marchi, L., Trutalli, D., Scotta, R., Pozza, L., and Ceccotti, A. (2016). "A new dissipative connection for CLT buildings". In *Proceedings of the Third International Conference ICSEA, 27-29 July 2016, Guimaraes, Portugal*. *Structures and Architecture* 17:169-177. Print ISBN: 978-1-138-02651-3, DOI: <http://dx.doi.org/10.1201/b20891-20>

Scotta, R., Pozza, L., Trutalli, D., Marchi, L. and Ceccotti, A. (2015). "Dissipative connections for squat or scarcely jointed CLT buildings. Experimental tests and numerical validation". In *Proceedings of International Network on Timber Engineering Research (INTER), meeting 48, 24-27 August 2015, Šibenik, Croatia*. Paper INTER/48-15-4. ISSN 2199-9740